



**UNIVERSITÀ
DI TORINO**

Università degli Studi di Torino

PhD Programme in Biological Sciences
and Applied Biotechnologies

**Pre-symbiotic signaling and symbiosis
enhancement in arbuscular mycorrhizas**

**Tutor:
Andrea Genre**

**Candidate:
Andrea Crosino**

XXXV° Cycle: 2019 /2023

Contents

CHAPTER 1: The arbuscular mycorrhizal symbiosis.....	5
Agriculture and sustainable practices	6
Mycorrhizas	8
Signaling molecules in arbuscular mycorrhizas	11
Perception of signal molecules in AM symbiosis.....	20
Extraction and application of signal molecules	28
Aim of the work.....	36
References	37
CHAPTER 2: The impact of long-term CO application on <i>Medicago truncatula</i> roots	47
Prologue.....	48
The AMforQuality project.....	49
References	50
Long-lasting impact of chitooligosaccharide application on strigolactone biosynthesis and fungal accommodation promotes arbuscular mycorrhiza in <i>Medicago truncatula</i>	51
CHAPTER 3: Production and application of exogenous COs	69
Prologue.....	70
The fungal cell wall	71
References	73
Extraction of short chain chitooligosaccharides from fungal biomass and their use as promoters of arbuscular mycorrhizal symbiosis.....	74
CHAPTER 4: Role of clathrin-mediated endocytosis during CO perception in arbuscular mycorrhizas	88
Introduction	89
Aim of this work.....	92
Materials and methods.....	93
Results	96
Discussion.....	102
References	106

CHAPTER 5: Quantifying AM root colonization using automated image segmentation and machine learning approaches	113
Prologue.....	114
Introduction	115
Materials and methods.....	117
Results	121
Discussion.....	125
Perspectives and conclusions	127
References	129
CHAPTER 6: Unlocking the multiphasic nature of CO-triggered intracellular calcium signatures in <i>Lotus japonicus</i> roots	132
Prologue.....	133
Introduction	134
Materials and Methods	138
Results	142
Discussion.....	154
References	161
CHAPTER 7: General conclusions	166
References	170
ACKNOWLEDGEMENTS	172

CHAPTER 1

The arbuscular mycorrhizal symbiosis

Agriculture and sustainable practices

Since the beginning of the industrial revolution, the society caused a significant transformation of the earth surface, modifying the surrounding natural environment through increasing intensive agricultural practices, urbanization and soil erosion with the purpose of developing the modern production systems which we still use today (Vitousek et al., 1997). Nevertheless, the accidental or deliberate introduction of exotic species contributed to substantially impair the composition of several natural biological communities, compromising ecosystem functionality (Rapport et al., 1998; Smitha et al., 1999). Since the Green Revolution, intensive application of agrochemicals has increased productivity in agriculture, at a great cost in terms of problems. In fact, agriculture is considered one of the most polluting human activities, involving a misuse of pesticides and chemical fertilizers, aiming to combat pests and to feed the growing human population. Such phytochemical treatments are causing a great range of drawbacks, including water pollution, loss of soil fertility and biodiversity, as well as food poisoning, leading to several detrimental effects on human health (Vassilev et al. 2015). In addition, recent studies indicate that the excessive use of fertilizers may be responsible for the partial recalcitrance of cultivated species towards beneficial biotrophic interactions (Duhamel & Vandenkoornhuysen, 2013). On this line, farmers have mostly selected and bred crop varieties focusing on the aerial parts of the plant, without taking into account the underground portion and its interactions. All of such practices led to a significant reduction in the inclination of crop roots to form beneficial interactions, with the consequent depletion in biodiversity of plant growth promoting microbial consortia within agronomic fields. A change of paradigm, which puts plant beneficial interactions at its heart, in order to optimize production with less waste of soils and resources, is ever more needed and led by public awareness.

In this scenario, beneficial symbioses are raising increasing interest. Among them, arbuscular mycorrhizal (AM) symbiosis is one of the most widespread (around 72% of plant species), moreover, it involves the majority of crops (Gutjahr and Parniske 2013). AM symbiosis improves plant mineral absorption (namely phosphorus and nitrogen), tolerance to biotic and abiotic stresses and overall fitness, while fungi are rewarded with

carbon compounds derived from the photosynthetic process, such as sugars and lipids (Rich et al. 2017). During the early stages of interaction, AM fungi recognize host plants through the perception of root-secreted strigolactones (SLs; Akiyama et al. 2005; Boyno and Demir 2022). SLs boost spore germination, hyphal growth and branching (Akiyama et al. 2005; Besserer et al. 2006), mitochondrial activity in the presymbiotic mycelium (Besserer et al. 2006), expression of effector genes (Tsuzuki et al. 2016), as well as the release of plant-directed chemical signals (Genre et al. 2013), known as Myc-factors (Boyno and Demir 2022). Currently characterized Myc-factors are chitin-derived molecules: chito-oligosaccharides (COs; Genre et al. 2013) and lipo-chitooligosaccharides (LCOs; Maillet et al. 2011). Myc-factor perception activates plant symbiotic responses, including a massive cell structural reorganization, in order to favor the subsequent fungal accommodation (Gutjahr and Parniske 2013). Recent works have demonstrated that exogenous CO application in *Oryza sativa* and *Medicago truncatula* induced AM symbiosis signaling, stimulated lateral root branching and AM symbiosis development (Oldroyd 2013; Feng et al. 2019; Volpe et al. 2020; Crosino et al. 2021), leading the way to the applicative use of such treatments in sustainable agriculture (Lanfranco et al. 2016).

Mycorrhizas

Mycorrhizal fungi are a heterogeneous group of different taxa associated with the roots of over 90% of all plant species. They are divided in two wide groups, based on the anatomical localization of the fungus inside the host plant tissues: ectomycorrhizas and endomycorrhizas (Smith & Read, 2008).

Ectomycorrhizas, which are predominantly found in temperate forests, mainly concern Basidiomycetes and Ascomycetes fungi. In this symbiosis, the fungus always remains outside of the host cells, only developing within the root apoplast. Outside the root, fungal hyphae run along the epidermis and envelope the root, forming a structure called “mantle”. From there, hyphae penetrate between epidermal cell apoplast where they develop a network, the Hartig net. This is where the reciprocal exchange of nutrients takes place (Bonfante and Genre, 2010).

As opposed to the previous group, endomycorrhizas reach an even deeper relationship between the two partners, since the exchange interface is localized inside the lumen of living plant cells. Fungal hyphae, in fact, penetrate the cell wall and differentiate into specialized exchange structures that are always enveloped by an extension of the plant plasma membrane.

In ericoid mycorrhizas, which develop between members of Ericales order and Ascomycetes, intracellular colonization is limited to the root epidermis, where the fungus develops the so-called “coils”, branched and twisted hyphal structures which fill most of the cellular lumen.

Orchid mycorrhizas are formed by Orchidiaceae and a few Basidiomycetes, which provide the plant with carbon compounds needed to allow the growth of non-photosynthetic seedling during their first stages of development.

Beside orchid and ericoid mycorrhizas, the most widespread type of endomycorrhizas are arbuscular mycorrhizas (Smith & Read, 2008; Bonfante & Genre, 2010).

Arbuscular mycorrhizas

Arbuscular mycorrhizas (AM) are characterized by the formation of structure called “arbuscules” within the plant root cortical cells (Figure 1). The reciprocal exchange of nutrients takes place in these structures (Harrison 2012).

AM symbiosis is probably the most widespread plant symbiosis in the world, as well as one of the most ancient. In fact, AM fungi have existed and coevolved with plants for at least 450 million years (Redecker et al., 2000), as evidenced by fossils with AM fungi in the earliest land plants (Remy et al., 1994; Strullu-Derrien et al., 2018). These discoveries, together with their importance in nutrient transfer, support the hypothesis that AM fungi may have played a crucial role during land colonization by plants, since in terrestrial environment AM fungi may have made available mineral nutrients and water, more limited than in the aquatic environment (Bonfante and Genre 2008; Humphreys et al., 2010). This trophic advantage is the basis of the AM symbiosis wide spread, reaching almost 72% of land plants, including most cultivated species (Spatafora et al., 2016).

AM development requires a sequence of several fundamental phases. A complex chemical dialogue mediates plant-fungus recognition where AM fungi perceive root-secreted strigolactones, which promote spore germination, hyphal growth, branching and metabolism (Akiyama et al. 2005; Besserer et al. 2006). In turn, host roots recognize their symbionts through chitin-derived molecules (Genre et al. 2013), known as Myc-factors. Currently characterized Myc-factors are composed by chito-oligosaccharides (COs; Genre et al. 2013) and lipo-chitooligosaccharides (LCOs; Maillet et al. 2011). Myc-factor perception activates plant symbiotic responses, including a massive cell structural reorganization, in order to favor the subsequent fungal accommodation (Gutjahr and Parniske 2013). Once contacted the root surface, fungal hyphae form the so called hyphopodia, adhesion structures which mark the initiation of the symbiotic phase. In reply to such chemical and mechanical solicitation, the contacted root epidermal cell develops an intracellular accommodation structure, called the prepenetration apparatus (PPA), which drives the hypha through the epidermal layer, towards the root cortex (Genre et al., 2005). Penetrating single cells of the inner root

cortex, AM fungi develop the distinctive structure of this association: the arbuscule, which results from reiterated branching of a single hypha (Bonfante P., 1984), guaranteeing an impressive surface-volume ratio. Due to this, arbuscules are considered the major site of nutrient exchange (Gutjahr C, Parniske M., 2013). Outside the host root, the extensive hyphal network can reach a density of 100 m/cm^3 (Miller RM, 1995) and extend in a volume of soil that is inaccessible to roots alone (Smith SE, 2011); here, AM fungi can absorb water and mineral nutrients with great efficiency. These elements are subsequently transferred to plants in exchange for up to 20% of the carbon produced with photosynthesis (Bago et al., 2000). Interestingly, the carbon flow from the plant to the fungus seems to be proportional to the amount of phosphate that the fungus returns to its host (Kiers et al., 2011). Accordingly, while the beneficial effects of AM fungi become evident when the nutrient and water supply are limited, root colonization diminishes in soils with abundant nutrients (Liu et al., 2016).

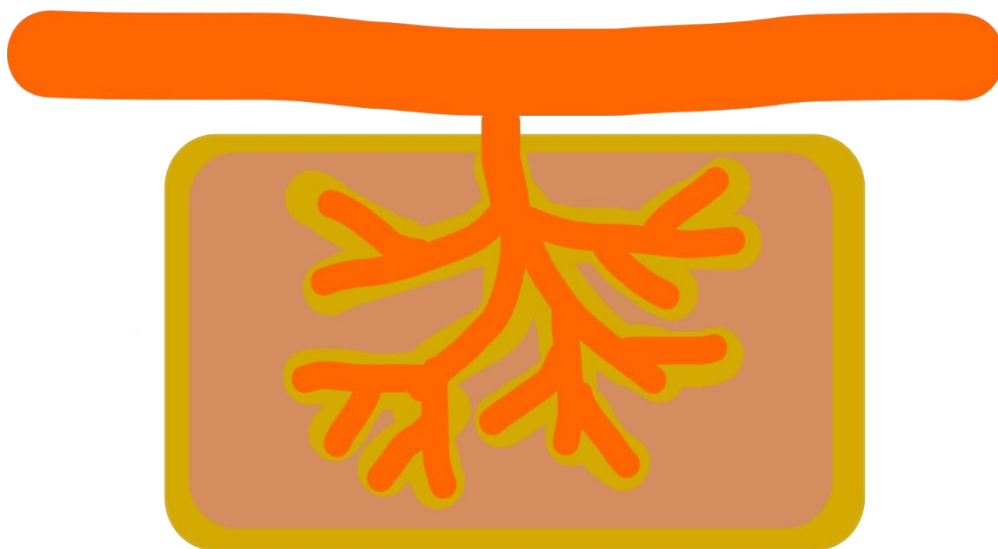


Figure 1 The scheme represents an arbuscule within a cortical cell (light brown). The arbuscule is surrounded by a plant-derived membrane (yellow), which is never penetrated by the fungus (orange) and represents the nutrient exchange area between the two organisms.

Signaling molecules in arbuscular mycorrhizas

Strigolactones, structure and biosynthesis

Strigolactones (SLs) are a small group of molecules released by roots of different plants, stimulating seed germination in weeds of *Striga* (also known as witchweeds), a genus composed by hemiparasite plants (Al-Babili and Bouwmeester 2015). The first natural SLs were isolated from cotton root exudates (*Gossypium hirsutum*), strigol and strigyl acetate, able to stimulate seed germination in the hemi-parasitic plant *Striga lutea* (Cook et al. 1966). Since then, over 20 SLs have been characterized in root exudates of several plants, including maize (*Zea mays*), red clover (*Trifolium pratense*) and sorghum (*Sorghum bicolor*) (Hauck et al. 1992; Müller et al. 1992; Siame et al. 1993; Yokota et al. 1998; Xie et al. 2013). These molecules are known to induce germination in different genera of parasitic weeds besides *Striga*, such as *Orobanche*, *Alectra*, and *Phelipanche* (Yoneyama et al. 2013). The estimated damage caused by parasitic weeds for rice crops in Africa alone is around 200 million USD, increasing by 30 million each year (Rodenburg 2016), and over 60 million hectares of farmland worldwide are infested by *Striga* and *Orobanche* species, causing a loss quantified in billions of dollars every year (Parker 2009). Such discoveries led to a fascinating question on the reason why host plants produce compounds which stimulate their own parasitization. The answer to this question came in 2005 when the benefits of SL exudation for plants were clarified. In fact, an extensive hyphal branching in germinating spores of the AM fungus *Gigaspora margarita* was highlighted upon treatment with the natural strigolactones 5-deoxystrigol, sorgolactone, strigol and GR24, a synthetic analog (Akiyama et al. 2005). Only later, SL role as plant hormones was outlined, initially highlighting their function as shoot branching inhibitors (Gomez-Roldan et al. 2008; Umehara et al. 2008). Subsequently, a broader range of hormonal effects was discovered, including regulation of root architecture, secondary growth promotion, leaf senescence regulation and coordination of root responses during nutrient deficiency (Yoneyama et al. 2007; Umehara et al. 2010; Kohlen et al. 2011; Niu et al. 2013).

Strigolactones (SLs) are generally composed of a tricyclic lactone (ABC) linked by an enol-ether bond to a butenolide moiety (Figure 2). Many natural and synthetic SL

compounds present different variation in the ABC structures, such as avenaol, debranones, 5-deoxystrigol and carlactone. From such differences, two main classes of plant SLs were generated, based on stereochemical modifications in the B-C link: strigol and orobanchol type.

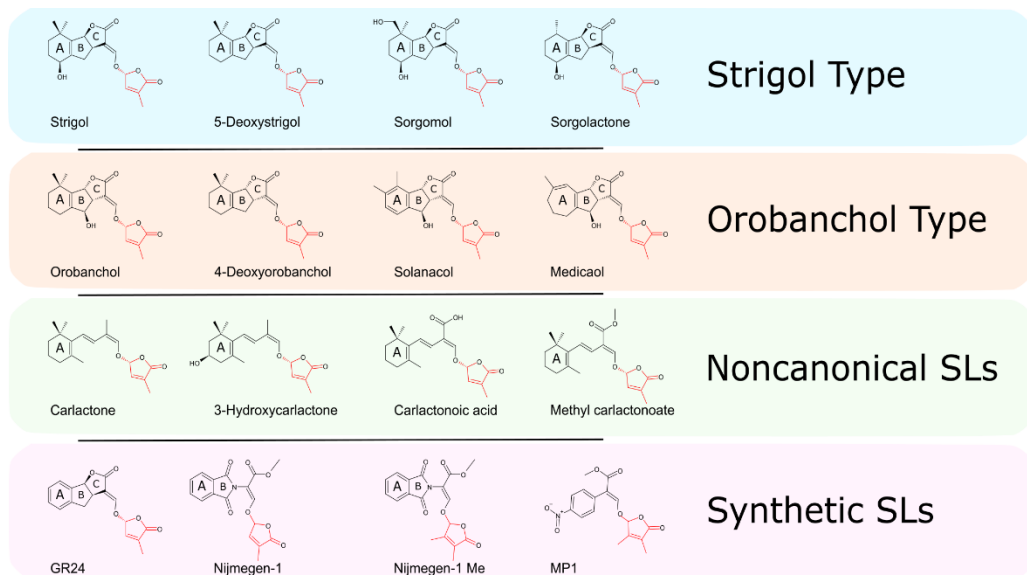


Figure 2. Classification and chemical structure of Strigolactones. These are generally composed of a tricyclic lactone (ABC) connected, by an enol-ether bond, to a butenolide moiety (red), which represents the most conserved trait of the molecule between plant taxa.

Strigol-like SLs are characterized by the β orientation (up; 8bS configuration) of the C ring, whereas orobanchol-like SLs contain an α -oriented (down; 8bR configuration) C ring. SLs that present the entire ABC-ring system are called canonical, in contrast to those lacking A, B, or C-rings, that are known as noncanonical. An example of such noncanonical SLs are avenaol, heliolactone and lotuslactone characterized from root exudates of wild oat, sunflower and *Lotus japonicus* respectively (Yoneyama et al. 2020). The only part of the molecule that appears to be conserved across all bioactive SLs is the D ring with 2'R configuration. In fact, several studies have demonstrated that SL activity is lost when the enol-ether-connected D ring section is modified (Kapulnik et al. 2011; Boyer et al. 2012, 2014; Fukui et al. 2013; Rasmussen et al. 2013; Abe et al. 2014; Prandi et al. 2014; Ueno et al. 2014; Fridlender et al. 2015; Tsuchiya et al. 2015; De Saint Germain et al. 2016). The majority of plant species contain a single type of molecule as the major SL component in root exudates. An exception is represented by

tobacco, which exudes significant quantities of both strigol and orobanchol (Xie et al. 2013), making the investigation of SL biosynthesis and transport particularly interesting for this species.

Even if a few steps in SL biosynthesis remain unclear, our current knowledge was built using information from different plants, which partially differ in their metabolic pathways. As depicted in Figure 3, SL biosynthesis starts from trans- β -carotene, which is converted to 9-cis- β -carotene by the isomerase DWARF27 (D27; Alder et al. 2012). Subsequently, CAROTENOID CLEAVAGE DIOXYGENASE7 (CCD7) and CCD8 complete the formation and orientation of the D ring, generating the inactive SL common precursor carlactone, which lacks the tricyclic structures and presents a β -ionone ring instead. In *Arabidopsis*, MORE AXILLARY GROWTH1 (MAX1), from the CYP711A family of cytochromes P450, converts carlactone to carlactonoic acid (CLA), which is subsequently methylated by an unknown enzyme to produce MeCLA (Abe et al. 2014). Rice has five homologs of MAX1 with different functions. One of them, Os01g0700900, oxidizes carlactone to 4-deoxyorobanchol (4DO), the precursor for orobanchol- type SLs. The subsequent conversion from 4DO to orobanchol is carried out by Os900 and the other rice MAX1 homologs (Zhang et al. 2014). In contrast to rice, CLA is directly converted into orobanchol in tomato, which only has one MAX1 homolog and is unable to produce orobanchol from 4DO (Yoneyama et al. 2018). A transcriptomic approach in cowpea recently identified the enzyme responsible for such direct conversion from CLA to orobanchol, as CYP722C, which belongs to a distant cytochrome P450 clade from MAX1 (Wakabayashi et al. 2019). However, in cotton, CYP722C converts CLA to 5-deoxystrigol (5DS) (Wakabayashi et al. 2020), while CYP728B35 (from an additional P450 clade), produces sorgomol from 5DS in sorghum (Wakabayashi et al. 2021). Besides the cytochromes P450 family, other enzymes have been related to the diversification of SL family members. Among them, LATERAL BRANCHING OXIDOREDUCTASE (LBO), a 2-oxoglutarate-dependent dioxygenase, is strongly co-expressed with canonical SL biosynthetic genes in transcriptomic and reverse genetic experiments in *A. thaliana* plants (Brewer et al. 2016). Furthermore, Brewer et al. (2016) highlighted a possible conversion from MeCLA to hydroxymethyl carlactonoate in in

vitro experiments with extracts from *Escherichia coli* expressing LBO. LBO-like proteins are present in the majority of land plants, and even if no *lbo* mutants have been characterized so far (Walker et al. 2019), the lack of lotuslactone production in *L. japonicus* mutant for a 2-oxoglutarate-dependent dioxygenase, related to LBO, validates the implication of this molecular family in noncanonical SL biosynthesis (Mori et al. 2020). In short, the canonical SL production from CLA is regulated by three different P450 clades, while MeCLA appears to be essential for the synthesis of noncanonical SLs, such as heliolactone (Wakabayashi et al. 2020). Redundancy in gene functions and parallel metabolic pathways - whereby mutants in individual biosynthetic genes display a phenotype, if any - limits the use of forward genetics to elucidate SL biosynthesis (Brewer et al. 2016). A major advance came from the introduction of transcriptomics and reverse genetics studies (Yoneyama and Brewer 2021), which provided a broader view of the biosynthesis of structurally unrelated SLs. The characterization of a great variety in SL composition within crop plant exudates, in combination with the knowledge derived from such new approaches, should increase the potential to manipulate SL diversity in crops, in order to boost agronomic performance in the near future (Chesterfield et al. 2020).

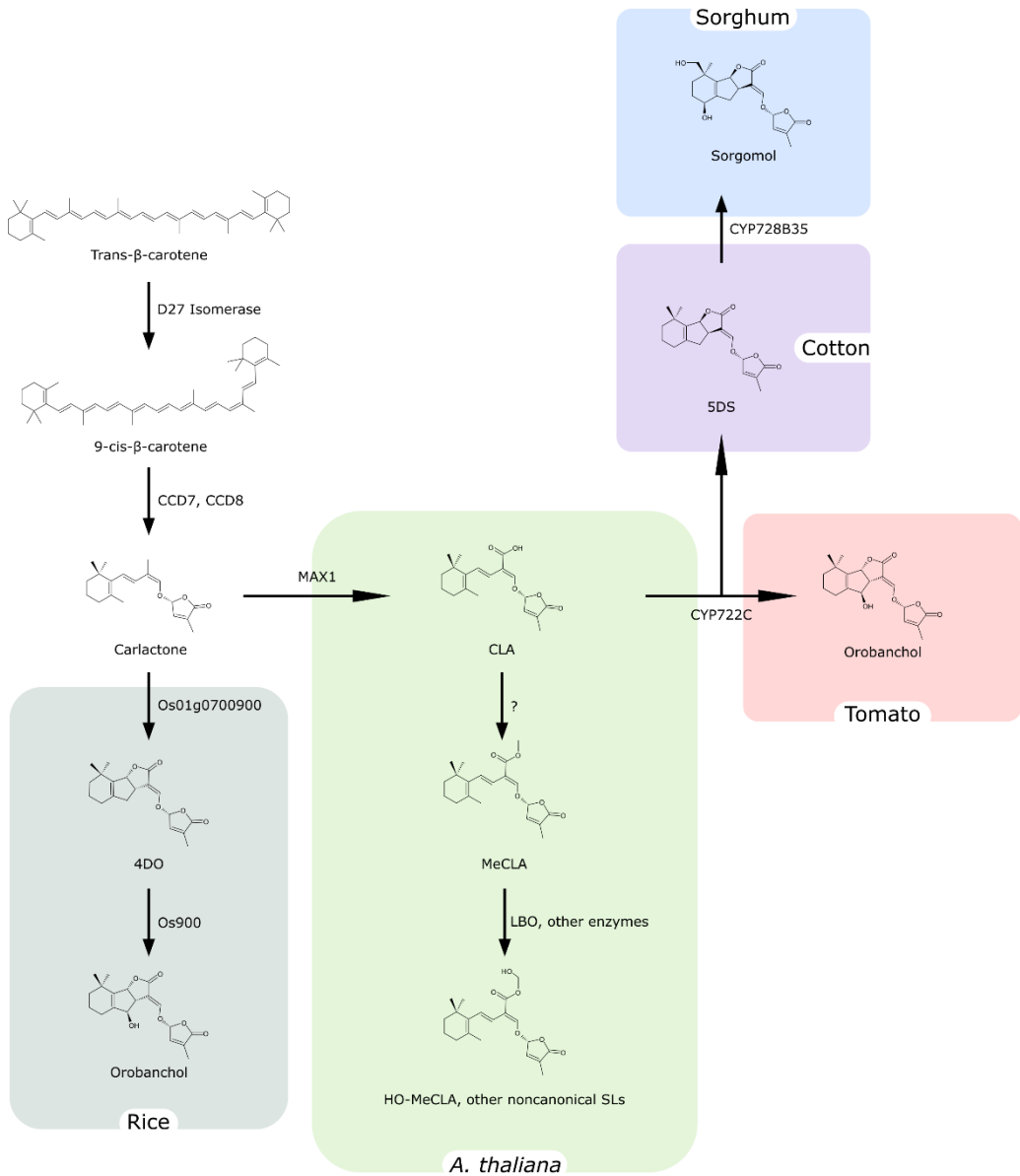


Figure 3. General scheme of Strigolactone biosynthesis. Strigolactones are synthesized from trans-β-carotene and the large diversity of SL structures is obtained thanks to the recruitment of different enzymes in different plant species.

Myc-factors

On the fungal side of the AM symbiotic dialogue, two structurally related classes of signaling molecules have been characterized in AM fungal exudates, stimulating symbiotic responses in their host plants: Myc-LCOs (Maillet et al. 2011) and Myc-COs (Genre et al. 2013). LCOs have been first characterized in rhizobium/legume symbiotic nitrogen fixation as bacterial signaling molecules (Nod-factors), whose recognition by the host plant is a prerequisite to symbiosis establishment (Denarie and Cullimore 1993). Studies on legumes have been fundamental to discover relevant similarities in molecular and cellular mechanisms between rhizobial and AM symbioses. The most striking example is represented by the common symbiotic signaling pathway (CSSP), a signaling pathway shared among such two mutualistic interactions, including the generation of repeated oscillations in nuclear Ca^{2+} concentration in plant cells. These similarities opened the way to the investigation of signal molecules produced by AM fungi, which led to the detection of sulphated and nonsulphated LCOs, structurally related to Nod-factors (Maillet et al. 2011), and short-chain chitin oligomers (COs; Genre et al. 2013). COs are chitin/chitosan derivatives (Figure 4), composed of N-acetylglucosamine (GlcNAc) and glucosamine (Glc) residues linked through a $\beta(1\rightarrow4)$ bond (Mourya et al. 2011; Lodhi et al. 2014). CO chemical properties and bioactivity are mostly influenced by their degree of polymerization (DP, number of GlcNAc/Glc residues), acetylation degree (AD, ratio between GlcNAc and total residues) and pattern of acetylation (PA, position of the acetylated residues within the molecule). Short-chain COs (with $\text{DP} \leq 8$) are easily soluble in aqueous media (Hao 2021), and include the best characterized and most active Myc-factors, CO4 and CO5 (Genre et al. 2013). LCOs (Figure 4) are short-chain chitin oligomers substituted with a fatty acid and different chemical groups at the nonreducing end (Khokhani et al. 2021). The most common fatty acids in fungal LCOs are C16:0, C18:0, C18:1, in contrast with C16:1 and C20:2 acyl groups commonly found in Nod-factors. Most of the remaining substitutions (acetyl, methyl, sulphate and fucosyl sulphate groups) are common to both microbial signals, while the presence of an arabinose residue is unique to Nod-factors (Dénarié et al. 1996; Rush et al. 2020).

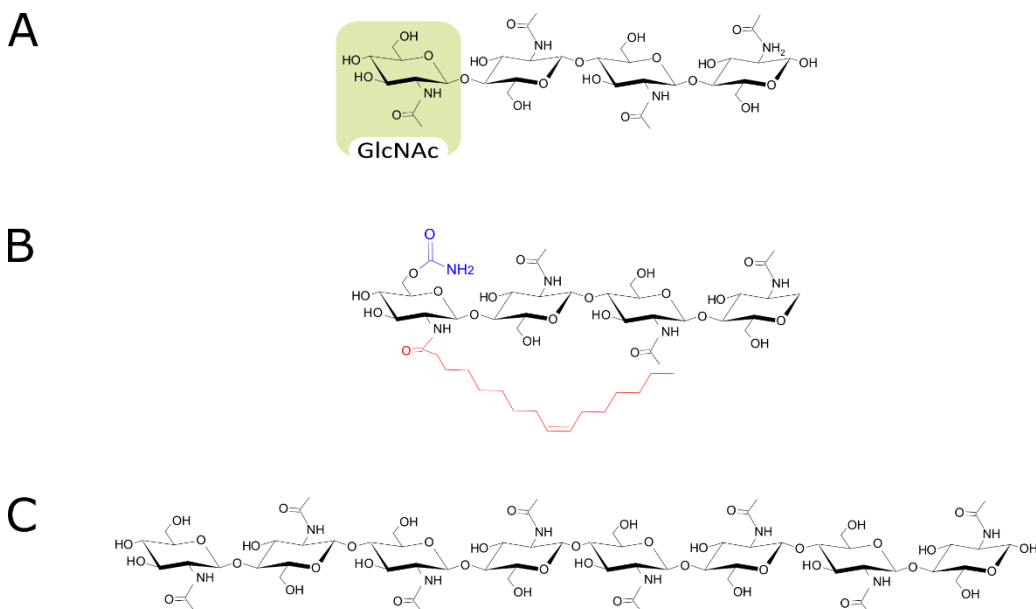


Figure 4. Chemical structure of chitin-derived fungal signals. Myc-factors characterized in arbuscular mycorrhizal fungi include (A) tetra-chito-oligosaccharide, composed of four monomers of N-acetylglucosamine (GlcNAc), and (B) tetra-lipo-chito-oligosaccharide bearing a 16:1 fatty acid chain (red) and a carbamoyl group (blue). (C) octa-chito-oligosaccharide (CO8) are common elicitors of defense responses.

Rush et al. (2020) found that 53 out of 59 fungal species tested, spread across most fungal phyla, were able to produce LCOs and the majority of fungal LCOs analyzed were similar to those exuded by AM fungi. Such work highlighted LCO production as a highly conserved trait in the fungal kingdom. However, very little is known about LCO biosynthesis in fungi. In fact, most of our knowledge of the metabolic reactions leading to LCO biogenesis comes from studies in N-fixing rhizobia, where the activation of the chitin synthase NodC leads to the assembly of the chitin backbone. Following a few substitutions (such as fucosylation), the chitin deacetylase NodB removes the acetyl group from the nonreducing end of the molecule. This is followed by the action of NodA, which adds the acyl chain to the CO deacetylated site, before additional substitutions (e.g. methylation, carbamoylation, arabinosylation) take place (Poinsot et al. 2016). On this basis, LCO biosynthesis in fungi has been suggested to involve the action of different endochitinases, cleaving short-chain COs from longer cell wall-associated chitin chains, and acyltransferases binding the acyl chain (Khokhani et al. 2021). By contrast, CO biosynthesis in fungi has been elucidated more clearly (Figure 5). Chitin is the main structural polymer of fungal cell wall. UDP-GlcNAc is used as substrate by cell

membrane-associated chitin synthase complexes and added to the nonreducing end of the lengthening chitin chain. The resulting chitin chains are extruded in the extracellular space via a cell membrane channel composed of chitin synthase transmembrane domains. Lastly, extruded chitin chains combine into parallel and antiparallel fibrils through hydrogen bonds (Merzendorfer 2011; Orlean and Funai 2019). The subsequent synergic activity of chitinases and monooxygenases generates reducing and nonreducing ends in each chitin chain. These grant exochitinases access, whose activity causes CO cleavage (Langner and Göhre 2016).

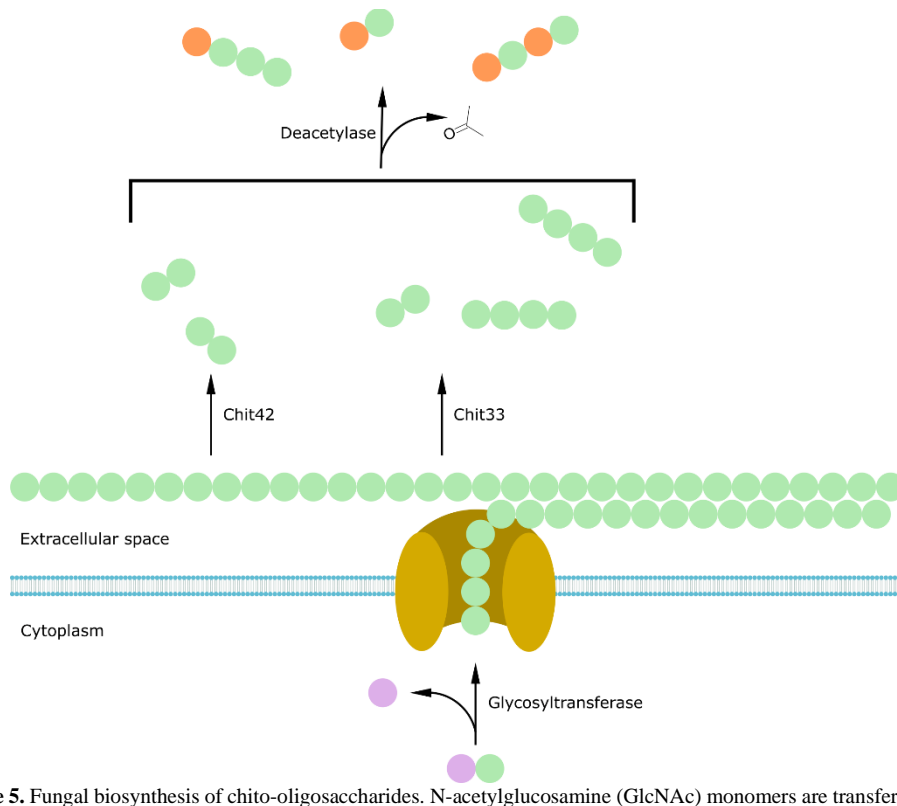


Figure 5. Fungal biosynthesis of chito-oligosaccharides. N-acetylglucosamine (GlcNAc) monomers are transferred from UDP-GlcNAc to the forming chitin chain by the action of the glycosyltransferase and the chitin synthase (yellow). Chitin chains extruded in the extracellular space through a channel composed of chitin synthase transmembrane domains can then be cleaved by several chitinases (Chit33, Chit42) to produce chito-oligosaccharides of different length. Finally, a deacetylase can further remove acetyl groups from the newly formed oligomers. Purple = UDP; green = GlcNAc monomers; orange = Glc monomers.

Different chitinases may generate COs of different DP. For example, in *Trichoderma harzianum*, both Chit33 and Chit42 produce CO₂ while Chit33 can also produce CO₄ (Berlemont 2017; Khokhani et al. 2021). Both chitin chains and COs can then be

deacetylated by fungal chitin deacetylases, generating chitosan and COs with different AD (Grifoll-Romero et al. 2018).

Perception of signal molecules in AM symbiosis

SLs

In plants, the hormonal function of SL is dependent on their perception by DWARF14 (D14), an α/β hydrolase that binds canonical SLs and splits them into hydroxymethylbutenolide (HMB) and an ABC ring formyltricyclic lactone (ABC-FTL, Figure 6; Hamiaux et al. 2012; Zhao et al. 2013; Nakamura et al. 2013). On this event, D14 undergoes a conformational change, ascribable to either the unbroken SL or to one of its hydrolysis products (De Saint Germain et al. 2016; Yao et al. 2016; Seto et al. 2019; Lee et al. 2020). This promotes the association of D14, D3 (AtMAX2; an F-box protein, part of the Skp1-Cullin-F-box complex) and D53 (homolog of SUPPRESSOR OF MAX2 1 in *A. thaliana*) in a complex. As a consequence, D53 undergoes ubiquitination and is degraded, ending its activity of downstream signaling inhibition (Hamiaux et al. 2012; Zhou et al. 2013) and allowing D14 proteasomal degradation (Chevalier et al. 2014). In addition, D3 was also reported to bind D14, inhibiting its hydrolytic activity (Shabek et al. 2018). An important cross-talk between SLs and karrikins has been recently identified. Karrikins are compounds derived from cellulose combustion, which are implicated in the germination of dormant seeds after a bush-fire (Flematti et al. 2015). Such molecules are detected by a group of receptors called KAI2/HTL-type, that are involved in seed germination and seedling growth.

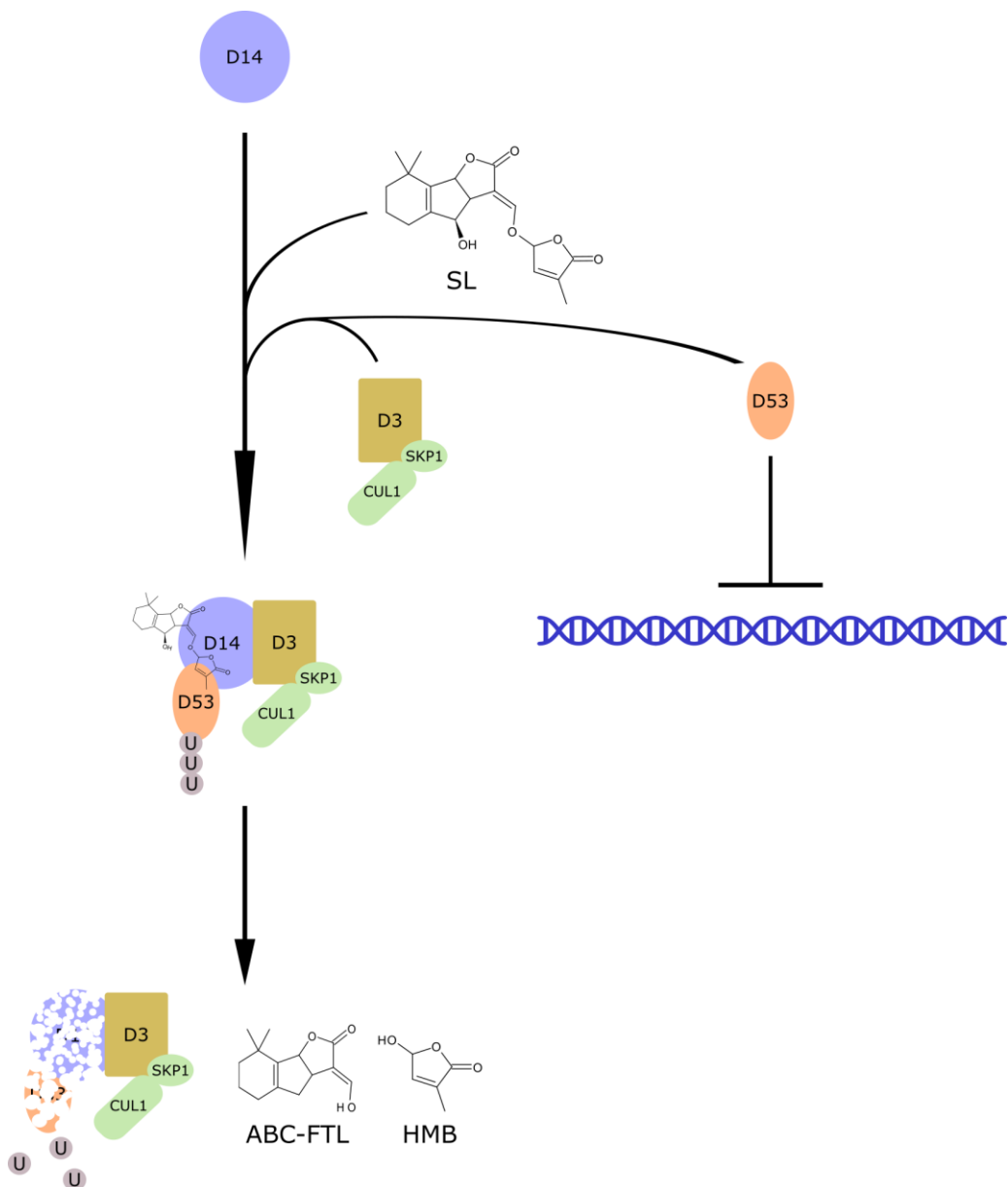


Figure 6. Perception of Strigolactones and signaling. Strigolactones are perceived by D14, which forms a complex with D3 and D53, a negative regulator of downstream signaling. The molecule is then hydrolyzed to hydroxymethylbutenolide (HMB) and an ABC ring formyltricyclic lactone (ABC-FTL), while D14 and D53 are degraded, allowing the activation of downstream signaling.

It has been proposed that karrikins mimic KAI2 ligand (KL), a putative endogenous ligand involved in early plant development, sharing part of the signaling pathway with SLs (Conn and Nelson 2016). In fact, in parasitic plants, SL perception takes place via

an HTL-type α/β hydrolase, a paralog of D14. HTL7 from *S. hermonthica* has the ability to hydrolyze SLs, generating an active intermediate essential for the transduction pathway that triggers seed germination (Shahul Hameed et al. 2018). However, due to their great variety in structure, only a fraction of SLs molecules activates the karrikin signaling pathway. Scaffidi et al. (2014) highlighted a preferential affinity between synthetic SL isomers and KAI2 receptor, underlying a relationship between the recognition of SLs by D14 or KAI2 and the structural variations in the chiral carbon orientations at the junction of the BC and D rings. Downstream of D3, karrikin signaling pathway differentiates from SLs signaling for the degradation of SUPPRESSOR OF MAX2 1 (SMAX1) and SMAX1-LIKE2 (SMXL2) (Stanga et al. 2016). SL perception in fungi remains largely unclear and has only been demonstrated in plant pathogenic fungi. In fact, mutant screening analyses highlighted the production of reactive oxygen species in response to SL treatment of *Botrytis cinerea* and *Cryphonectria parasitica* (Belmondo et al. 2017). Further investigations showed the up-regulation of genes involved in nuclear and cellular compartment reorganization, DNA-related functions and lipid metabolism after the application of GR24, a synthetic SL analog (Lanfranco et al. 2018). No evidence of D14-related genes has been found in the genomes of AM fungal symbionts and no alternative SL receptor has been characterized (Moscatiello et al. 2014; Chen et al. 2018). Nonetheless, regardless of their perception mechanism, SLs were shown to activate calcium-mediated signaling in the AM fungus *G. margarita* (Moscatiello et al. 2014). In conclusion, SL perception mechanisms appear to be mediated by different receptors in each group of organisms. Thorough elucidation of such mechanisms represents a major milestone on the way to their application in sustainable agriculture as modulators of specific plant interactions with beneficial as well as pathogenic or parasitic organisms (Chesterfield et al. 2020).

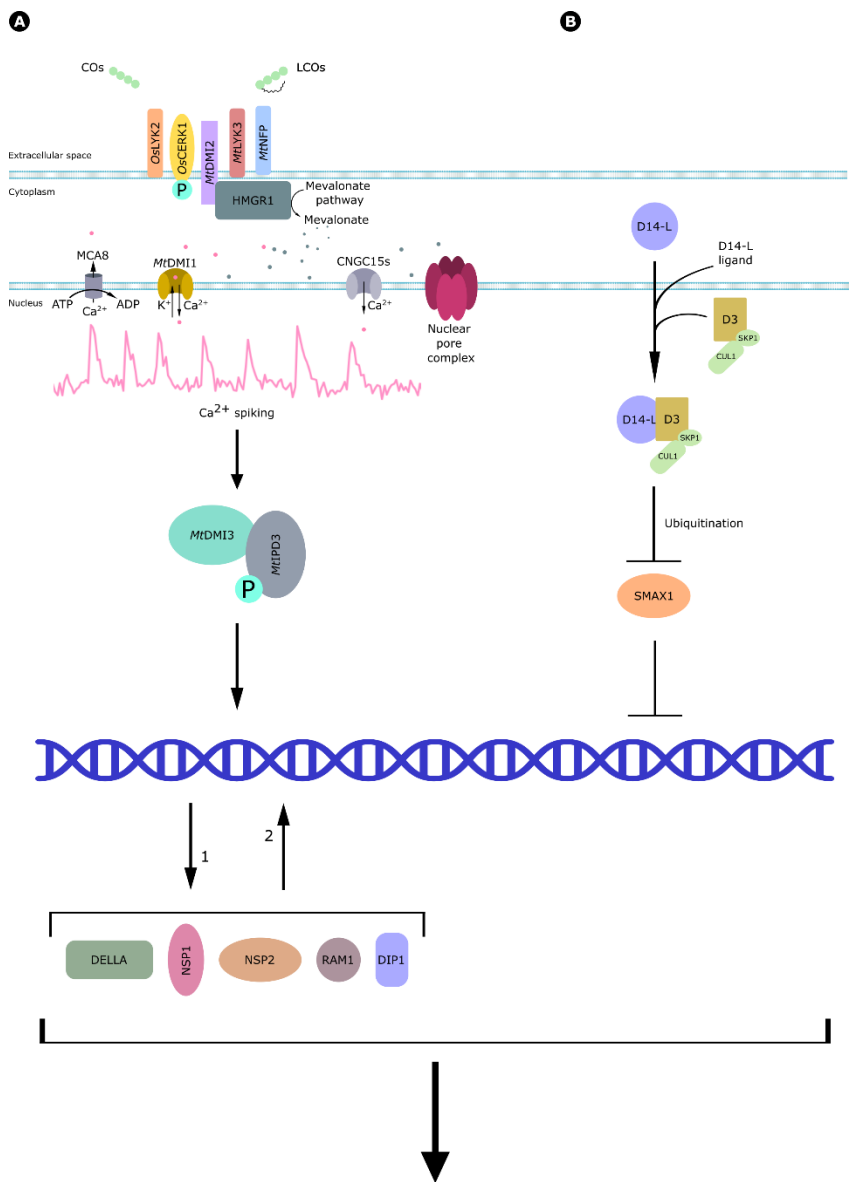
Growing evidence is indicating that differences in SL bioactivity in each organism are largely related to their molecular structure. In line with that, a conserved AB-ring structure was suggested to be essential to trigger AM hyphal branching, one of the most striking and studied SL-dependent responses (Akiyama et al. 2005; Besserer et al. 2006). Furthermore, Akiyama et al. (2010) demonstrated that an α -oriented hydroxyl group

insertion at the C4 position of the B-ring boosted the hyphal branching effect, suggesting the importance of this functional group as hydrogen bond donor during SL interaction with the putative fungal receptor. Additional SL-induced responses in AM fungi include the proliferation of nuclei in hyphal tips, the activation of lipid catabolism, a boost in mitochondrial activity and the release of chito-oligosaccharides (Besserer et al. 2006, 2008; Genre et al., 2013; Belmondo et al. 2017; Lanfranco et al. 2018). SLs were also reported to enhance hyphopodium formation on the host root surface (Kobae et al., 2018).

Myc-factors

In AM host plants, CO4/5 are perceived via plasma membrane-associated receptor-like kinase (RLK) complexes, which have been partially characterized in different species. In a recent study, He et al. (2019) demonstrated the ability of the rice LysM-RLK OsLYK2 to specifically recognize CO4/5 (but not longer chain COs or LCOs) forming a complex with a second LysM-RLK, CHITIN ELICITOR RECEPTOR KINASE 1 (OsCERK1) and activate it by phosphorylation. A third member of the RLK complex, SYMBIOSIS RECEPTOR-LIKE KINASE (SYMRK/DMI2), much more specific for Myc-LCOs, was characterized in legumes. In *M. truncatula*, its activation upon LCO binding triggers the so-called common symbiosis signaling pathway, or CSSP, together with LYK3 and NFP (Figure 7; Zipfel and Oldroyd 2017; Choi et al. 2018; Feng et al. 2019).

Little is known about the signal transduction from the plasma membrane to the nuclear envelope. One model suggests the association between SYMRK and the enzyme 3-hydroxy-3-methylglutaryl-CoA reductase 1 (HMGR1), essential for mevalonate synthesis (Kevei et al. 2007). Indeed, exogenous mevalonate application was shown to trigger downstream CSSP signaling such as nuclear Ca²⁺ spiking in the root epidermis (Venkateshwaran et al. 2015). In non-legumes, the complex formed between OsCERK1 and OsLYK2 seems to be essential to trigger Ca²⁺ spiking, since Oslyk2 mutants showed decreased levels of symbiotic responses (He et al. 2019).



AM symbiosis-related gene expression

Figure 7. Myc-factor perception. (A) Studies in rice demonstrated that COs are perceived by OsLYK2 and OsCERK1, which is activated by phosphorylation. Investigations in *M. truncatula* showed that CO and LCO perception requires the action of DMI2, LYK3 and NFP. DMI2 binds to HMGR1, which starts mevalonate production and downstream signaling. This includes nuclear Ca²⁺ spiking, which also requires the activity of a few nuclear envelope-localized proteins: the cationic channel DMI1, the cyclic nucleotide-gated Ca²⁺ channel CNGC15s, the MCA8 Ca²⁺ pump and several nucleoporins in the nuclear pore complex. Ca²⁺ spiking is further decoded by the calcium and calmodulin-dependent kinase DMI3, which phosphorylates the transcriptional regulator MtIPD3, activating in turn DELLA, DIP1, NSP2, NSP1 and RAM1 transcription factors and driving the expression of AM-related genes. (B) Perception of alternative AM fungal signals by D14-L. After the perception of an unidentified ligand, D14-L form a complex with D3, driving the ubiquitination of the negative regulator SMAX1 and thus allowing downstream signaling culminating in gene regulation and symbiotic plant responses.

This induction of repeated oscillations in nuclear Ca²⁺ concentration is mediated by the action of a few nuclear envelope-localized proteins, including cationic channels such as *MtDMI1*, *LjCASTOR*, *LjPOLLUX*, the cyclic nucleotide-gated Ca²⁺ channel CNGC15s, and the *MtMCA8* Ca²⁺ pump (Ané et al. 2002; Imaizumi-Anraku et al. 2005; Peiter et al. 2007; Venkateshwaran et al. 2012). The generation of Ca²⁺ spiking also requires NUCLEAR PORE COMPLEX PROTEIN 85 (NUP85), NUP133 and NENA, a WD40 repeat nucleoporin, most likely involved in the positioning of the above mentioned channels and pumps on the inner nuclear membrane (Kanamori et al. 2006; Saito et al. 2007; Groth et al., 2010). Nuclear Ca²⁺ spiking is believed to be sensed by the calcium – and calmodulin-dependent serine/threonine protein kinase (CCaMK/*MtDMI3*), whose activation causes dimerization with the transcriptional activator *MtIPD3/LjCYCLOPS*.

In turn, CYCLOPS phosphorylation boosts the activation of several transcription factors, including DELLA, DELLA Interacting Protein 1 (DIP1), Nodulation Signaling Pathway 2 (NSP2), NSP1 and Reduced Arbuscular Mycorrhiza 1 (RAM1), which drive the subsequent expression of AM symbiosis-related genes (Yu et al. 2014; Jin et al. 2016; Pimprikar et al. 2016; Zipfel and Oldroyd 2017).

Symbiosis or defense?

As highlighted in the previous sections, COs are perceived by plants through the CSSP, activating symbiotic outcomes. However, since COs are chitin derivatives and chitin is the main structural polymer of the majority of fungi, COs are produced by a great variety of fungi, including plant pathogens (Rush et al. 2020). Plant developed the ability to activate immune responses through the recognition of specific nonself-molecules, called PAMPs (pathogen-associated molecular pattern). Concerning fungal pathogens, part of such PAMPs are represented by fungal cell wall-derived COs, resulting from the action of plant or fungal chitinases during plant tissue infection (Kasprzewska 2003; Lee et al. 2008; Wan et al. 2008; Volk et al. 2019). The most supported hypothesis explaining how chitin-derived molecules may trigger either symbiotic or defense responses considers CO length: COs with DP_≥6 (typically CO8)

are more prone to activate the plant immune response, whereas shorter COs are associated to symbiotic signaling (Shimizu et al. 2010; Nasir et al. 2018; Feng et al. 2019). This ability of root cells to discriminate CO length is believed to depend on the composition of LysM-RLK complexes. In a recent model by Chiu and Paszkowski (2021) the ability of *Os*CERK1 to participate both in defense and in symbiotic responses is highlighted, and a mechanism of action, also involving *Os*MYR1 is proposed.

In this model, the *Os*CERK1-*Os*MYR1 complex forms in the presence of CO4/5 or LCOs, leading to the subsequent activation of symbiotic responses. By contrast, the presence of CO8 triggers *Os*CERK1-*Os*CEBiP (CHITIN ELICITOR- BINDING PROTEIN) complex formation, eliciting chitin-triggered immunity and driving the production of reactive oxygen species and the phosphorylation of mitogen- activated protein kinases (MAPKs). In a recent review, Yang et al. (2022) proposed an updated model, where two *Os*CEBiP monomers dimerize after binding to the same CO7-8 molecule, causing the recruitment and homodimerization of *Os*CERK1. Besides *Os*CEBiP, two additional effectors can bind long COs, *Os*LYP4 and *Os*LYP6, which are required to boost immunity outcomes (Yang et al. 2022). However, this model cannot be extended to all plants. In tomato, the *Os*CERK1 homolog SILYK12 is almost entirely associated to symbiotic signaling, while the activation of the defense responses is dependent on SILYK1 (Liao et al. 2018), indicating that the CERK1 homologs faced different duplication and subfunctionalization events in different families and species.

In spite of a broad set of experimental support, this model contrasts with a few recent observations. Feng et al. (2019) reported CSSP activation upon CO8 application. They also suggested that a CO/LCO mix can be required for a fully efficient symbiotic outcome. Furthermore, Khokhani et al. (2021) suggested three additional signaling mechanisms that may contribute to the successful stimulation of plant symbiotic responses. Firstly, high phosphate availability can activate plant immunity in the presence of any plant-fungus interaction and cause the degradation of DELLA transcription factors, thus inhibiting AM development. Secondly, the mechanical stimuli caused on the root epidermis by AM fungal hyphopodia or pathogenic fungal appressoria may also have a deep impact on downstream signaling. Lastly, the combination of chitin-

derived signals with yet-to-identify molecules exclusive of AM fungi could also contribute to symbiont recognition. This latter hypothesis appears to be in line with the increasing evidence in favor of CSSP-independent signaling in AM symbiosis.

CSSP independent signaling

Besides the discrimination between symbiotic and pathogenic signals, a further level of complexity is present in legumes, where the distinction between structurally-similar LCOs of different origins (Nod-LCOs vs. Myc-LCOs) has to activate specific responses. This raised the hypothesis that additional signaling pathways exist, acting in parallel with the CSSP, as proposed by Bonfante and Requena (2011). On this line, Gutjahr et al. (2015) demonstrated the involvement of D14-L/KAI2 in Myc-factor perception. In this study, rice *d14-l* mutants were completely unable to establish AM interaction; furthermore, a drastically impaired AM colonization was also observed in mutants in D3, the protein that acts immediately downstream of D14-L (Yoshida et al. 2012). A study conducted in rice by Choi et al. (2020) described the transcriptional repressor SUPPRESSOR OF MAX2 1 (OsSMAX1) as an additional component of this signaling pathway, downstream of D3. When inoculated with *R. irregularis*, *Ossmax1* mutants exhibited a higher level of colonization, overexpression of SL biosynthesis and AM-related genes, as well as increase in SL production, compared to WT plants. In addition, a restoration of WT mycorrhization level was achieved in *d14-l/smax1* double mutants. The resulting model suggests that, upon the perception of a yet-unknown fungal signal, D14-L forms a complex with D3 which suppresses SMAX1 and positively regulates AM-related genes. Such studies have only started to shed light on this novel D14-L pathway and additional studies are required to identify upstream signals (and their fungal or endogenous origin), downstream molecular actors and the possible cross-talk with the CSSP, for example by analyzing Ca²⁺ spiking activation in different mutants.

Extraction and application of signal molecules

Different attempts were performed in the last few years to achieve large-scale SL production for field application. Firstly, SL application was intended as a strategy to limit the onset of parasitic plants, the so-called suicidal seed germination. This technique consists in SL field treatment before crop cultivation, with the purpose of inducing the germination of parasitic weed seeds that, in absence of a host, face the death. In sorghum, T-010, a synthetic SL, decreased the emergence of *S. hermonthica* by 94–100% in pot trials and by around 30% in field, with concomitant increase in sorghum head yield of almost 200% (Samejima et al., 2016). In the same way, Zwanenburg et al. (2016), using the SL analogs Nijmegen-1 and Nijmegen-1 Me in tobacco crops, highlighted a reduction in *O. ramosa* emergence by at least 60% in six out of nine field trials. A further confirmation of the SL efficiency in suicidal seed germination comes from the work by Kountche et al. (2019), where the authors developed a protocol for *Striga* control in rain-fed African fields. The use of Nijmegen-1, MP1 and MP3 in sorghum and pearl millet, resulted in a drastic reduction of *Striga* emergence by 55% and 65%, respectively. Such studies point out suicidal seed germination as a valid method to control parasitic weed infestations and a potent and critical instrument that, in the future, could be embraced in the areas characterized by the most severe *Striga* and *Orobanchae* infestations, such as sub-Saharan Africa.

Following the discovery of SL role in AM establishment, SL application to promote AM development in agronomic contexts raised great interest. Nevertheless, even if SLs are of common use for research purposes and field trials, their introduction in agriculture and commercial release have not been achieved yet, largely due to difficulties in setting up their large scale production. Secondly, SL molecular instability, mainly due to the cleavage of the enol ether bond by nucleophilic agents such as water, makes commercial formulations, long-term storage and agronomic applications very difficult or ineffective (Aliche et al., 2020; Chesterfield et al., 2020). SL instability is a major issue under field conditions, such as soil pH and temperature (Zwanenburg & Pospíšil, 2013). The persistence of GR24 – which has better stability than natural compounds – is limited to 6–8 days in acidic soils and drops to an average of 1–3 days in alkaline soils (Miyakawa

et al., 2019). Formulations that improve SL stability have been developed for Nijmegen-1 and its 3'-Me congener: the use of polyoxyethylene sorbitol hexaoleate as a stabilizer allowed field trials in tobacco plants infested by *O. ramosa* (Zwanenburg & Pospisil, 2013). In short, additional studies will be necessary to develop specific formulations for each synthetic SL, extending its stability and uptake and reducing soil leaching, while also preventing environmental pollution with the selected stabilizers and their own effects on AM development (Aliche et al., 2020). A third problem comes from SL-dependent stimulation of parasitic weed germination. A possible solution to this comes from our understanding of SL diversity. Sorghum mutants for LOW GERMINATION STIMULANT 1 (LGS1) are resistant to *Striga hermonthica* and *Striga asiatica* infection. This was related to a change in SL profile, with a reduction in strigol and an increase in orobanchol content (Gobena, et al., 2017). Interestingly, *lgs1* mutants are not affected in their mycorrhization level compared to wild-type sorghum. Similarly, a *Striga*-resistant maize cultivar with a reduced level of 5-deoxystrigol and an increase in sorgomol exudation also had AM colonization levels comparable to wild-type plants (Yoneyama et al., 2015). Differently, a complete incapability to establish AM symbiosis was seen in the rice mutant d14-1 (AtKAI2 homolog) instead, showing a total absence of hyphopodia formation (Gutjahr et al., 2015). On the contrary, the rice d14 mutant presented normal or even slightly higher level of AM colonization compared to WT plants (Yoshida et al., 2012). A middle ground was represented by mutants defective in downstream signaling components; rice d3 and pea *rms4*, with low levels of arbuscule and vesicle formation (Yoshida et al., 2012; Foo et al., 2013). Being D3/RMS4 a common protein for both SL and karrikin signaling pathways, it is easy to assume that the karrikin signaling activation is essential for AM symbiosis establishment. Following the indication of Scaffidi et al. (2014), it could be interesting to evaluate if the preferential affinity of some SL compounds for KAI2 is reflected in higher AM colonization levels. All these observations, combined with the discoveries of Akiyama et al. (2010), have raised awareness that changes in SL chemical structure have a deep impact on their effectiveness towards either symbiotic fungi or parasitic weeds, paving the way to the

identification and design of specific SL treatments aimed at either promoting AM colonization or counteracting parasitic weed infection.

The very limited accumulation of SLs in plant tissues and exudates makes their extraction from plant materials not practical. For this reason, SLs are mainly produced by chemical synthesis. Unfortunately, the relative complexity of SL chemical structure requires over 20 steps, and also critically limits yield in the current production systems (Arshad & Frankenberger, 2002). A promising alternative is represented by the synthesis of just the bioactive part of the molecule. Such SL analogs can be synthesized in higher amounts and currently represent the most common source of SLs for research scopes (Chesterfield et al., 2020). An additional advantage of this method – whenever a clear structure-response relationship has been elucidated – is the possibility to exclusively produce the chemical structure that is responsible for the desired function (e.g. AM promotion, suicidal seed germination or drought stress tolerance, another effect of SLs). The most common SL analogs are currently Nijmegen- 1 (Nefkens et al., 1997), GR24 (Besserer et al. 2008), CISA-1 (Rasmussen et al. 2013), sphynolacten-7 (Uraguchi et al. 2018) and strigolactams (De Mesmaeker et al. 2019), which are mainly used for suicidal seed germination. Notwithstanding such promising advantages, production costs remain a limiting factor for process scale-up. Furthermore, SL and SL analog chemical synthesis generates 1:1 racemic mixtures, in which only one of the enantiomers is biologically active (weakening the overall effectiveness), or each isomer presents distinct biological activities, generating unwanted effects. A well characterized example is GR24, which is 100 times less efficient than natural SLs in enhancing *Orobanche* minor seed germination (Yoneyama et al. 2010). On the same line, Akiyama et al. (2010), found that (+)-5DS and (+)-GR24 were respectively 10 and 100-fold more effective in stimulating hyphal branching in AM fungi than their corresponding enantiomers.

Larger amounts of bioactive SLs might be obtained at smaller costs with the use of biosynthetic enzymes through microbial engineering. The central point of this approach is to reconstruct the SL biosynthetic pathway in a heterologous context, through the genetic transformation of bacterial or yeast strains. In addition, the use of enzymes catalyzing each biosynthetic reaction gives microbial engineering the potential to

produce enantiomerically pure molecules, an outstanding advantage compared to chemical synthesis (Chesterfield et al. 2020). A promising example of this approach was recently presented by Wu (2021), who successfully reconstituted CL, CLA, 4DO, 5DS and orobanchol biosynthesis in *Escherichia coli* – *Saccharomyces cerevisiae* consortia. Even if the yields of current attempts remain low, the optimization of microbial enzyme activity can be envisaged by gene editing. Lastly, this approach is also emerging as an accessible tool to functionally characterize SL biosynthetic enzymes, in analogy with the earlier development of enzyme-based industrial production of other valuable compounds, such as isoprenoids (Vickers et al. 2015). Since Myc-factor isolation from AM fungi is not suitable for their large-scale production, three alternative strategies have been pursued.

Chemical approaches

Chemical synthesis of Myc-factors appears as a very versatile approach, allowing the synthesis of COs of any length and AD, not to mention the possibility to add the lateral substitutions typical of LCOs. Nevertheless, an alternation of protection and deprotection steps is required to prevent the formation of unwanted glycosidic bonds between monomers (Naqvi and Moerschbacher 2015; Hao 2021). Furthermore, the use of GlcNAc donors may cause the formation of abundant side products, such as 1,2-O, N-oxazoline (Hao 2021). Overall, even if significant improvements have been introduced over the last few years, including new iterative glycosylation methods and automated synthesis, several remaining disadvantages, such as product contamination and low yield, still limit the interest in synthetic approaches to large scale and low-cost Myc-factor production (Yamago et al. 2004). As an alternative to chemical synthesis, chitin depolymerization by acid hydrolysis (Domard and Carter 1989; Kazami et al. 2015; Crosino et al. 2021), nitrous acid deamination (Tømmeraas et al. 2001), fluorolysis (Bosso et al. 1986; Defaye et al. 1994) or oxidative-reductive reactions with hydrogen peroxide (Tian et al. 2003) represent potentially easier and less expensive approaches to Myc-factor production. Large amounts of chitin can be obtained from waste products of fishing and food industry (crustacean exoskeletons and fungal biomass derived from the

production of edible mushrooms are rich in chitin). A general drawback of these techniques is the alteration of the chitin chain reducing ends, which has a negative impact on the bioactivity of short chain COs. Furthermore, acid hydrolysis can modify CO acetylation degree (Naqvi and Moerschbacher 2015), which also affects their activity as symbiotic signals (Crosino et al. 2021). Lastly, the use of strong acids and their disposal in wastes raises major environmental concerns. To overcome such problems and improve chitin fibril exposure in the starting materials, a few authors experimented with diverse physical pre – or co-treatments, including ultrasonication (Takahashi et al. 1995; Machová et al. 1999; Ajavakom et al. 2012; Zhang et al. 2021), microwave irradiation (Roy et al. 2003; Wu et al. 2011; Ajavakom et al. 2012), supercritical water and mechano-chemical grinding (Savage 1999; Osada et al. 2013), gamma irradiation (Kang et al. 2007) and steam explosion (Alvira et al. 2016). Other studies have tested relatively less toxic solvents, such as ionic liquids or molten salts (Wilkes 2004; Passos et al. 2014; Vekariya 2017). At present, CO production from chitin is an achievable strategy, but its economic and ecological costs remain a major limitation.

Enzymatic approaches

A more environment-friendly approach to CO production is by using isolated enzymes. Indeed, both CO synthesis and chitin depolymerization can be achieved via enzymatic methods. GlcNAc residues and short chain COs can be assembled through the transglycosylation (TG) activity of chitinolytic enzymes, such as chitinases and lysozymes (Ling et al. 2018). β -N-Acetylhexosaminidase from *Aspergillus oryzae* has been successfully employed to synthesize fully-acetylated COs (Singh et al. 1995). Hattori et al. (2012) polymerized COs with DP from 6 to 15, thanks to lysozyme TG activity using CO₃ as substrate. Similarly, Mallakuntla et al. (2017) isolated a transglycosylating chitinase (EcChi1) from *Enterobacter cloacae*, able to synthesize short chain COs (with DP ranging from 4 to 9), starting from CO₃ to CO₆. In summary, enzymatic synthesis by transglycosylation appears as a very promising approach in terms of production costs, time and environmental impact, however, a great amount of purified GlcNAc monomers or oligomers is required as starting substrate. As an alternative,

chitinase hydrolytic activity can be exploited for chitin depolymerization. By expressing a recombinant chitinase from *Chitinolyticabacter meiyuanensis* in *E. coli*, Zhang et al. (2018), were able to produce a considerable amount of CO₂ and traces of CO₃₋₄ from colloidal chitin. Similarly, a recombinant chitinase from *Trichoderma harzianum* expressed in *Pichia pastoris* led to the production of GlcNAc monomers and dimers from the digestion of colloidal chitin or chitosan (Kidibule et al. 2018). Lastly, Guan et al. (2020) identified novel chitin deacetylase (CDA20) and chitosanase (CHIS5) enzymes from marine metagenome and successfully combined their use to obtain deacetylated Glc dimers and trimers. Despite their major advantages, including mild reaction conditions, low pollution and time savings, enzymatic hydrolysis does not appear to be ideal for the large scale production of efficient Myc-factors, mainly because the reaction products are in most cases GlcNAc monomers, dimers or trimers, whereas the most active AM fungal signals are CO₄ and CO₅. Moreover, enzymatic techniques depend on the availability of high-quality enzymes, which have to be recovered after hydrolysis. This impacts on the production costs, limiting their application in industrial-scale production.

Biotechnological approaches

Genomic engineering of microbial cells (mainly bacteria) turned out to be a promising strategy to achieve higher CO yields for research and applicative uses. The design of optimized microbial strains by knockout, overexpression and transfer of target genes can be time and resource-consuming. Nevertheless it often grants high-yield and low-cost production of the desired molecules (Naqvi and Moerschbacher 2015). In 1995, Mergaert et al. expressed the nod gene cluster from *Azorhizobium caulinodans* in recombinant *E. coli* cells, obtaining different chitin oligomers and LCOs. Subsequently, Samain et al. (1997) pushed this approach further, by expressing nodB and nodC in *E. coli*, and purified consistent amounts of mono-deacetylated CO₅. More recently, Zhang et al. (2007) cultured recombinant *E. coli* expressing nodC gene from *Mesorhizobium loti*. By using a two-step fermentation process and GlcNAc as a precursor, these authors obtained up to 930 mg/L of CO₅ in a 10-L bioreactor. In 2019, Deng et al. blocked the

expression of nagA (GlcNAc- 6-phosphate deacetylase) and gamA (GlcN- 6-phosphate deaminase) in *Corynebacterium glutamicum* S9114, achieving a 54.8% increase in GlcNAc production and a final yield of 6.9 g/L GlcNAc in the culture broth. In conclusion, such cell factory-based approaches have a number of advantages, compared to the previous production methods. This technique can provide pure COs and LCOs with the desired chemical features. Moreover, it does not require polluting solvents nor expensive purified enzymes, it is easily scalable and relatively affordable. Nevertheless, the biotechnological production of Myc-factors is still far from being industrially adopted. Additional research is needed to identify novel, more efficient chitin synthases besides rhizobial nod genes, possibly taking advantage of metagenomic approaches, before an environmentally-friendly industrial production of COs and LCOs can be able to satisfy the increasing demand for agricultural applications. As a matter of fact, various formulations of chitin-derived products are being used in agriculture since decades, based on the empirical record of a general improvement in plant health, even if the precise mechanisms underpinning these positive effects had not been explained yet. As mentioned above, CO length has a major impact on the plant response they trigger. Mixed – often only partly characterized – formulations of COs have been shown to have antimicrobial and plant defense stimulation effects and are used for pest management. Xu et al. (2007) demonstrated the inhibitory effect of short-chain deacetylated COs against in vitro cultured *Phytophthora capsici*. The same effect was confirmed by Nguyen et al. (2018) using silver nanoparticles coated in short chitosan oligomers. COs antifungal activity was also investigated by Sun et al. (2018), who used COs in combination with ϵ -poly-L-lysine on tomato plants, obtaining a significant protection against tomato gray mold infection. On the same line, foliar spray application of COs was reported to be effective in combating powdery mildew (*Blumeria graminis*) on barley (Faoro et al. 2008) and several additional examples can be found in literature, supporting the efficiency of CO treatment against a wide range of plant pathogens (Sarathchandra et al. 2004; Iriti et al. 2006; El Hadrami et al. 2010). Most of these positive effects on plant health can be explained in the light of our current understanding of CO perception. The PAMP activity of longer COs is expected to trigger plant

immunity, inducing a pre-alert status (or priming) prior to actual pathogen infection (Basa et al. 2020). In parallel, short-chain COs can reach the roots by rain elution and act as promoters of AM development. AM symbiosis is well known to contribute to raise plant defense in a priming-like condition; furthermore, a more extensive development of symbiosis improves plant nutrition and overall health and fitness, most likely allowing faster and more efficient defense responses in the case of a subsequent pathogen attack. Besides their role in stimulating symbiosis and immunity, COs and LCOs have also been shown to promote plant growth, seed germination and photosynthesis in maize, rice, *A. thaliana*, cotton and wheat (Sun et al. 2015; Tanaka et al. 2015; Ané et al. 2016), while the induction of early flowering and an increased number of inflorescences was reported in orchids (Limpanavech et al. 2008). Such effects appear less directly related to either symbiosis – or defense-related signaling and stimulated further investigations. To this aim, Zhang et al. (2016) used fully deacetylated chitooligomers of different length (DP2 to 12) on wheat seedlings, identifying CO7 as the most effective molecule in promoting biomass production and changing organic acid, sugar and amino acid composition within foliar tissues; by contrast CO2 and CO3 were completely ineffective. Comparable results were also obtained by Jia et al. (2019) in soybean seedlings, where CO7 acted as a metabolic enhancer with the ability to modulate carbon and nitrogen metabolism. Recently, COs were also found to improve plant resistance to abiotic stresses, such as drought, salinity and heavy metal toxicity (Zong et al. 2017; Zhou et al. 2018; Al-Ghamdi 2019; Muley et al. 2019; Turk et al. 2019). Such effects may be explained with the convergence of several plant responses to both biotic and abiotic stresses (Zhang et al. 2019), including the activation of ROS production and detoxification, cell wall modifications, proline and secondary metabolite accumulation. In other words, the priming effect caused by CO perception could also protect the plant in a context of abiotic stress (Zhang et al. 2019). Indeed, by treating salt-stressed wheat seedlings with COs of different length, Zhang et al. (2017) showed that molecules with DP 6–8 (the best characterized chitin-derived PAMPs) were the most effective in stimulating antioxidant enzyme activity, photosynthesis and salt-related gene expression (SOS1 and NHX2).

Aim of the work

During the three years of my PhD, I focused my investigation on plant pre-symbiotic responses to AM fungi, in particular the perception and effects of fungal signals on AM host plants, evaluating the cellular and molecular aspects of exogenous Myc-factor application, using the model plants *M. truncatula*.

During my PhD activity I developed the following research lines:

1. The impact of exogenous CO application on SL biosynthesis and fungal accommodation on *M. truncatula* plants. This work was performed in collaboration with the Laboratory of Molecular Biology of Wageningen University & Research. The results have been published by New phytologist in 2023 and are presented in the next chapter of this work.
2. The second research line revolved around the establishment of a protocol for CO production from fungal biomass of different origin and their application on *M. truncatula* plants to stimulate AM interactions. The results have been published by Scientific Reports in 2021 and are shown in Chapter 3 of this thesis.
3. The role of clathrin-mediated endocytosis during myc-factor perception in arbuscular mycorrhizas. The results of this research line are presented in Chapter 4 of this thesis.
4. The subsequent research line concerned about the use of digital image analysis to quantify AM colonization. This project aimed to develop a new quantification method comparing image segmentation and machine learning softwares. This research was run in collaboration with Carl Zeiss Microscopy GmbH (Carl Zeiss Spa, Milan, Italy) and it will be the focus of chapter 5. Such results have been submitted to Scientific Reports and actually are under revision.
5. The last chapter is focused on the deciphering of the multiphasic nature of intracellular calcium signatures triggered by fungal signals in *Lotus japonicus* roots. This study was performed in collaboration with the Department of Biology of the University of Padova and the results have been submitted to the Journal of Experimental Botany and actually are under revision.

References

- Abe S, et al. 2014. Carlactone is converted to carlactonoic acid by MAX1 in Arabidopsis and its methyl ester can directly interact with AtD14 in vitro. *Proc Natl Acad Sci U S A* 111:18084–18089. doi:10.1073/pnas.1410801111.
- Ajavakom A, et al. 2012. Products from microwave and ultrasonic wave assisted acid hydrolysis of chitin. *Carbohydr Polym.* 90:73–77. doi:10.1016/j.carbpol.2012.04.064.
- Akiyama K, et al. 2005. Plant sesquiterpenes induce hyphal branching in arbuscular mycorrhizal fungi. *Nature.* 435:824–827.
- Akiyama K, et al. 2010. Structural requirements of strigolactones for hyphal branching in AM fungi. *Plant Cell Physiol.* 51:1104–1117. doi:10.1093/pcp/pcq058.
- Al-Babili S, Bouwmeester H. 2015. Strigolactones, a novel carotenoid-derived plant hormone. *Annu Rev Plant Biol* 66:161–186. doi:10.1146/annurev-arplant-043014-114759.
- Alder A, et al. 2012. The path from β -carotene to carlactone, a strigolactone-like plant hormone. *Science.* 335:1348–1351. doi:10.1126/science.1218094.
- Al-Ghamdi AA. 2019. Marjoram physiological and molecular performance under water stress and chitosan treatment. *Acta Physiol Plant* 41:44.
- Aliche EB, et al. 2020. Science and application of strigolactones. *New Phytol* 227:1001–1011. doi:10.1111/nph.16489.
- Alvira P, et al. 2016. Steam explosion for wheat straw pretreatment for sugars production. *Bioethanol.* 2:66–75. doi:10.1515/bioeth-2016-0003.
- Ané J-M, et al. 2002. Genetic and cytogenetic mapping of DMI1, DMI2, and DMI3 genes of *Medicago truncatula* involved in Nod factor transduction, nodulation, and mycorrhization. *Mol Plant-Microbe Interact* 15(11):1108–1118.
- Ané J-M, et al. 2016. Chitin oligomers for use in promoting non-leguminous plant growth and development. US Patent 2016/0366883 A1.
- Arshad M, Frankenberger WT. 2002. Ethylene in agriculture: synthetic and natural sources and applications. In: Arshad M, Frankenberger WT, editors. *Ethylene*. Boston: Springer; p. 290–294.
- Bago B, Pfeffer PE, Shachar-Hill Y. 2000. Carbon metabolism and transport in arbuscular mycorrhizas. *Plant Physiol.* 124, 949–957.
- Basa S, et al. 2020. The pattern of acetylation defines the priming activity of chitosan tetramers. *J Am Chem Soc* 142:1975–1986.
- Belmondo S, et al. 2017. Identification of genes involved in fungal responses to strigolactones using mutants from fungal pathogens. *Curr Genet.* 63:201–213. doi:10.1007/s00294-016-0626-y.
- Berlemont R. 2017. Distribution and diversity of enzymes for polysaccharide degradation in fungi. *Sci Rep* 7(1):222. doi:10.1038/s41598-017-00258-w.
- Besserer A, et al. 2006. Strigolactones stimulate arbuscular mycorrhizal fungi by activating mitochondria. *PLoS Biol* 4:e226. doi:10.1371/journal.pbio.0040226.
- Besserer A, et al. 2008. GR24, a synthetic analog of strigolactones, stimulates the mitosis and growth of the arbuscular mycorrhizal fungus *Gigaspora rosea* by boosting its energy metabolism. *Plant Physiol.* 148:402–413. doi:10.1104/pp.108.121400.
- Bonfante & Requena. 2011. Dating in the dark: how roots respond to fungal signals to establish arbuscular mycorrhizal symbiosis. *Curr Opin Plant Biol.* 14:451–457. doi:10.1016/j.pbi.2011.03.014.
- Bonfante P, Genre A. 2010. Mechanisms underlying beneficial plant-fungus interactions in mycorrhizal symbiosis. *Nature communications*, 1, p.48.
- Bonfante P, Genre A. 2008. Plants and arbuscular mycorrhizal fungi: an evolutionary-developmental perspective. *Trends in Plant Science.* 13: 492–498.
- Bonfante-Fasolo P, Grippolo R. 1984. Cytochemical and biochemical observations on the cell wall of the spore of *Glomus epigaeum*. *Protoplasma* 123, 140–151.

- Bosso C, et al. 1986. The behavior of chitin towards anhydrous hydrogen fluoride. Preparation of b-(1-4)-linked 2-acetamido-2-deoxy-d-glucopyranosyl oligosaccharides. *Carbohydr Res.* 156:57–68.
- Boyer FD, et al. 2012. Structure-activity relationship studies of strigolactone-related molecules for branching inhibition in garden pea: molecule design for shoot branching. *Plant Physiol* 159:1524–1544. doi:10.1104/pp.112.195826.
- Boyer FD, et al. 2014. New strigolactone analogs as plant hormones with low activities in the rhizosphere. *Mol. Plant.* 7:675–690. doi:10.1093/mp/sst163.
- Boyno G, Demir S. 2022. Plant-mycorrhiza communication and mycorrhizae in inter-plant communication. *Symbiosis.* 86:155–168. doi:10.1007/s13199-022-00837-0.
- Brewer PB, et al. 2016. Lateral branching oxidoreductase acts in the final stages of strigolactone biosynthesis in *Arabidopsis*. *Proc Natl Acad Sci U S A* 113:6301–6306. doi:10.1073/pnas.1601729113.
- Chen ECH, et al. 2018. High intraspecific genome diversity in the model arbuscular mycorrhizal symbiont *Rhizophagus irregularis*. *New Phytol.* 220:1161–1171. doi:10.1111/nph.14989.
- Chesterfield RJ, et al. 2020. Translation of strigolactones from plant hormone to agriculture: achievements, future perspectives, and challenges. *Trends Plant Sci.* 25(11):1087–1106. doi:10.1016/j.tplants.2020.06.005.
- Chevalier F, et al. 2014. Strigolactone promotes degradation of DWARF14, an α/β hydrolase essential for strigolactone signaling in *Arabidopsis*. *Plant Cell.* 26:1134–1150. doi:10.1105/tpc.114.122903.
- Chiu CH, Paszkowski U. 2021. How membrane receptors tread the fine balance between symbiosis and immunity signaling. *PNAS.* 118(24):e2106567118. doi:10.1073/pnas.2106567118.
- Choi J, et al. 2018. Mechanisms underlying establishment of arbuscular mycorrhizal symbioses. *Annu Rev Phytopathol.* 56:135–160. doi:10.1146/annurev-phyto-080516-035521.
- Choi J, et al. 2020. The negative regulator SMAX1 controls mycorrhizal symbiosis and strigolactone biosynthesis in rice. *Nat Commun.* 11:1114. doi:10.1038/s41467-020-16021-1.
- Conn CE, Nelson DC. 2016. Evidence that KARRIKIN-INSENSITIVE 2 (KAI2) receptors may perceive an unknown signal that is not Karrikin or strigolactone. *Front Plant Sci* 6:1219. doi:10.3389/fpls.2015.01219.
- Cook CE, et al. 1966. Germination of witchweed (*Striga lutea* Lour.): isolation and properties of a potent stimulant. *Science.* 154:1189–1190.
- Crosino A, et al. 2021. Extraction of short chain chitooligosaccharides from fungal biomass and their use as promoters of arbuscular mycorrhizal symbiosis. *Sci Rep.* 11:3798. doi:10.1038/s41598-021-83299-6.
- De Mesmaeker A, et al. 2019. Design, synthesis and biological evaluation of strigolactone and strigolactam derivatives for potential crop enhancement applications in modern agriculture. *Chimia (Aarau).* 73:549–560. doi:10.2533/chimia.2019.549.
- De Saint Germain A, et al. 2016. An histidine covalent receptor and butenolide complex mediates strigolactone perception. *Nat Chem Biol* 12:787–794. doi:10.1038/nchembio.2147.
- Defaye J, et al. 1994. A convenient access to beta-(1-4)-linked 2-amino-2-deoxy-D-glucopyranosyl fluoride oligosaccharides and beta-(1-4)-linked 2-amino-2-deoxy-D-glucopyranosyl oligosaccharides by fluorolysis and fluorohydrolysis of chitosan. *Carbohydr Res.* 261:267–277.
- Denarie J, Cullimore J. 1993. Lipo-oligosaccharide nodulation factors: a new class of signaling molecules mediating recognition and morphogenesis. *Cell.* 74:951–954. doi:10.1016/0092-8674(93)90717-5.
- Dénarié J, Debelle F, Promé JC. 1996. Rhizobium lipochitooligosaccharide nodulation factors: signaling molecules mediating recognition and morphogenesis. *Annu Rev Biochem* 65:503–535.
- Deng C, et al. 2019. Metabolic engineering of *Corynebacterium glutamicum* S9114 based on whole-genome sequencing for efficient N-acetylglucosamine synthesis. *Synthetic and Systems Biotechnology.* 4:120–129.
- Domard A, Carter C. 1989. Glucosamine oligomers: preparation and characterization. *Int J Biol Macromol.* 11:297–302.
- Duhamel M, Vandenkoornhuysse P. 2013. Sustainable agriculture: possible trajectories from mutualistic symbiosis and plant neodomestication. *Trends in Plant Science* 18:597–600.
- El Hadrami A, et al. 2010. Chitosan in plant protection. *Mar Drugs.* 8:968–987.
- Faoro F, et al. 2008. Chemical-induced resistance against powdery mildew in barley: the effects of chitosan and benzothiadiazole. *BioControl.* 53:387–401. doi:10.1007/s10526-007-9091-3.

- Feng F, et al. 2019. A combination of chitoooligosaccharide and lipochitoooligosaccharide recognition promotes arbuscular mycorrhizal associations in *Medicago truncatula*. *Nat Commun.* 10:5047. doi:10.1038/s41467-019-12999-5.
- Flematti GR, et al. 2015. What are karrikins and how were they 'discovered' by plants? *BMC Biol.* 13:108. doi:10.1186/s12915-015-0219-0.
- Foo E. 2013. Auxin influences strigolactones in pea mycorrhizal symbiosis. *J Plant Physiol.* 170:523–528. doi:10.1016/j.jplph.2012.11.002.
- Fridlender M, et al. 2015. Influx and efflux of strigolactones are actively regulated and involve the cell-trafficking system. *Mol. Plant.* 8:1809–812. doi:10.1016/j.molp.2015.08.013.
- Fukui K, et al. 2013. Selective mimics of strigolactone actions and their potential use for controlling damage caused by root parasitic weeds. *Mol. Plant.* 6:88–99. doi:10.1093/mp/sss138.
- Genre A, Chabaud M, Timmers T, Bonfante P, Barker DG. 2005. Arbuscular mycorrhizal fungi elicit a novel intracellular ap-paratus in *Medicago truncatula* root epidermal cells before infection. *Plant Cell* 17: 3489–3499.
- Genre A, et al. 2013. Short chain chitin oligomers from arbuscular mycorrhizal fungi trigger nuclear Ca²⁺ spiking in *Medicago truncatula* roots and their production is enhanced by strigolactone. *New Phytol* 198:190–202. doi:10.1111/nph.12146.
- Gobena D, et al. 2017. Mutation in sorghum LOW GERMINATION STIMULANT 1 alters strigolactones and causes striga resistance. *Proc Natl Acad Sci USA* 114:4471–4476. doi:10.1073/pnas.1618965114.
- Gomez-Roldan V, et al. 2008. Strigolactone inhibition of shoot branching. *Nature.* 455:189–194.
- Grifoll-Romero L, et al. 2018. Chitin deacetylases: structures, specificities, and biotech applications. *Polymers (Basel).* 10(4):352. doi:10.3390/polym10040352.
- Groth M, et al. 2010. NENA, a *Lotus japonicus* homolog of Sec13, is required for rhizodermal infection by arbuscular mycorrhiza fungi and rhizobia but dispensable for cortical endosymbiotic development.
- Guan F, et al. 2020. Highly efficient production of chitoooligosaccharides by enzymes mined directly from the marine metagenome. *Carbohydr Polym.* 234:115909. doi:10.1016/j.carbpol.2020.115909.
- Gutjahr C, et al. 2008. Arbuscular mycorrhiza-specific signaling in rice transcends the common symbiosis signaling pathway. *Plant Cell.* 20 (11):2989–3005. doi:10.1105/tpc.108.062414.
- Gutjahr C, et al. 2015. Rice perception of symbiotic arbuscular mycorrhizal fungi requires the karrikin receptor complex. *Science.* 350:1521–1524. doi:10.1126/science.aac9715.
- Gutjahr C, Parniske M. 2013. Cell and developmental biology of arbuscular mycorrhiza symbiosis. *Annu Rev Cell Dev Biol* 29:593–617. doi:10.1146/annurev-cellbio-101512-122413.
- Hamiaux C, et al. 2012. DAD2 is an α/β hydrolase likely to be involved in the perception of the plant branching hormone, strigolactone. *Curr Biol* 22:2032–2036. doi:10.1016/j.cub.2012.08.007.
- Hao W. 2021. Review: advances in preparation of chitoooligosaccharides with heterogeneous sequences and their bioactivity. *Carb. Pol.* 252:117206. doi:10.1016/j.carbpol.2020.117206.
- Harrison, M.J., 2012. Cellular programs for arbuscular mycorrhizal symbiosis. *Current Opinion in Plant Biology*, 15(6), pp.691–698.
- Hattori T, et al. 2012. Enzymatic synthesis of an α -chitin-like substance via lysozyme-mediated transglycosylation. *Carbohydr Res* 347:16–22. doi:10.1016/j.carres.2011.09.025.
- Hauck C, et al. 1992. A germination stimulant for parasitic flowering plants from *Sorghum bicolor*, a genuine host plant. *J Plant Physiol* 139:474–478.
- He J, et al. 2019. A LysM receptor heteromer mediates perception of arbuscular mycorrhizal symbiotic signal in rice. *Mol Plant.* 12:1561–1576. doi:10.1016/j.molp.2019.10.015.
- Humphreys Claire P., Franks Peter J., Rees Mark, Bidartondo Martin I., Leake Jonathan R. & Beetling David J. (2010). Mutualistic mycorrhiza-like symbiosis in the most ancient group of land plants. *Nature Communications* 1, Article number: 103.
- Imaizumi-Anraku H, et al. 2005. Plastid proteins crucial for symbiotic fungal and bacterial entry into plant roots. *Nature.* 433(7025):527–531. doi:10.1038/nature03237.
- Iriti M, et al. 2006. Cell death-mediated antiviral effect of chitosan in tobacco. *Plant Physiol Biochem.* 44:893–900.

- Jia Y, et al. 2019. Effects of different oligochitosans on isoflavone metabolites, antioxidant activity, and isoflavone biosynthetic genes in soybean (*Glycine max*) seeds during germination. *J Agric Food Chem* 67:4652–4661.
- Jin Y, et al. 2016. DELLA proteins are common components of symbiotic rhizobial and mycorrhizal signalling pathways. *Nat Commun.* 7:12433. doi:10.1038/ncomms12433.
- Kanamori N, et al. 2006. A nucleoporin is required for induction of Ca²⁺ spiking in legume nodule development and essential for rhizobial and fungal symbiosis. *Proceedings of the National Academy of*
- Kang B, et al. 2007. Synergetic degradation of chitosan with gamma radiation and hydrogen peroxide. *Polym Degrad Stab.* 92:359–362.
- Kapulnik, Y. et al. Strigolactones affect lateral root formation and root hair elongation in *Arabidopsis*. *Planta* 233, 209–216 (2011). doi:10.1007/s00425-010-1310-y
- Kasprzewska A. 2003. Plant chitinases—regulation and function. *Cell Mol Biol Lett* 8(3):809–824.
- Kazami N, et al. 2015. A simple procedure for preparing chitin oligomers through acetone precipitation after hydrolysis in concentrated hydrochloric acid. *Carbohydr. Polym.* 132:304–310. doi:10.1016/j.carbpol.2015.05.082.
- Kevei Z, et al. 2007. 3-Hydroxy-3-methylglutaryl coenzyme A reductase1 interacts with NORK and is crucial for nodulation in *Medicago truncatula*. *Plant Cell.* 19:3974–3989. doi:10.1105/tpc.107.053975.
- Khokhani D, et al. 2021. Deciphering the chitin code in plant symbiosis, defense, and microbial networks. *Annu Rev Microbiol.* 75:583–607. doi:10.1146/annurev-micro-051921-114809.
- Kidibule PE, et al. 2018. Use of chitin and chitosan to produce new chitooligosaccharides by chitinase Chit42: enzymatic activity and structural basis of protein specificity. *Microb. Cell. Fact.* 17:47. doi:10.1186/s12934-018-0895-x.
- Kiers ET, Duhamel M, Beesetty Y, Mensah JA, Franken O, Verbruggen E, Fellbaum CR, Kowalchuk GA, Hart MM, Bago A, Palmer TM, West SA, Vandenkoornhuys P, Jansa J, Bücking H. 2011. Reciprocal rewards stabilize cooperation in the mycorrhizal symbiosis. *Science* 333:880–882.
- Kobae Y. 2018. Strigolactone biosynthesis genes of rice are required for the punctual entry of arbuscular mycorrhizal fungi into the roots. *Plant Cell Physiol.* 59:544–553. doi:10.1093/pcp/pcy001.
- Kohlen W, et al. 2011. Strigolactones are transported through the xylem and play a key role in shoot architectural response to phosphate deficiency in nonarbuscular mycorrhizal host *Arabidopsis*. *Plant Physiol* 155:974–987. doi:10.1104/pp.110.164640.
- Kountche BA, et al. 2019. Suicidal germination as a control strategy for *Striga hermonthica* (Benth.) in smallholder farms of sub-saharan Africa. *Plants People Planet.* 1:107–118. doi:10.1002/ppp3.32.
- Lanfranco L, Bonfante P, Genre A. 2016. The mutualistic interaction between plants and arbuscular mycorrhizal fungi. *Microbiol. Spect.* 4:727–747. doi:10.1128/microbiolspec.funk-0012-2016.
- Lanfranco L, et al. 2018. Strigolactones cross the kingdoms: plants, fungi, and bacteria in the arbuscular mycorrhizal symbiosis. *J Exp Bot.* 69:2175–2188. doi:10.1093/jxb/erx432.
- Langner T, Göhre V. 2016. Fungal chitinases: function, regulation, and potential roles in plant/pathogen interactions. *Curr Genet* 62 (2):243–254. doi:10.1007/s00294-015-0530-x.
- Lee CG, et al. 2008. Chitin regulation of immune responses: an old molecule with new roles. *Curr Opin Immunol* 20(6):684–689. doi:10.1016/j.coi.2008.10.002.
- Lee HW, et al. 2020. Flexibility of the petunia strigolactone receptor DAD2 promotes its interaction with signaling partners. *J Biol Chem* 295:4181–4193. doi:10.1074/jbc.RA119.011509.
- Liao D, et al. 2018. Tomato LysM receptor-like kinase SILYK12 is involved in arbuscular mycorrhizal symbiosis. *Front Plant Sci.* 9:1004. doi:10.3389/fpls.2018.01004.
- Limpanavech P, et al. 2008. Chitosan effects on floral production, gene expression, and anatomical changes in the *Dendrobium* orchid. *Sci Hortic* 116:65–72.
- Ling M, et al. 2018. Metabolic engineering for the production of chitooligosaccharides: advances and perspectives. *Emerg. Top. Life Sci.* 2:377–388. doi:10.1042/ETLS20180009.
- Liu W, Zhang Y, Jiang S, Deng Y, Christie P, Murray PJ, Li X, Zhang J. 2016. Arbuscular mycorrhizal fungi in soil and roots respond differently to phosphorus inputs in an intensively managed calcareous agricultural soil. *Sci Rep* 6:24902.

- Lodhi, G., et al. 2014. Chitooligosaccharide and Its derivatives: preparation and biological applications. *BioMed Res Int*, ID 654913. doi:10.1155/2014/654913
- Machová E, et al. 1999. Effect of ultrasonic treatment on the molecular weight of carboxymethylated chitin–glucan complex from *Aspergillus niger*. *Ultrason Sonochem*. 5:169–172.
- Maillet F, et al. 2011. Fungal lipochitooligosaccharide symbiotic signals in arbuscular mycorrhiza. *Nature*. 469:58–63.
- Mallakuntla MK, et al. 2017. Transglycosylation by a chitinase from *Enterobacter cloacae* subsp. *cloacae* generates longer chitin oligosaccharides. *Sci Rep* 7:1–12. doi:10.1038/s41598-017-05140-3.
- Mergaert P, et al. 1995. Biosynthesis of *Azorhizobium caulinodans* nod factors. *J Biol Chem*. 270:29217–29223.
- Merzendorfer H. 2011. The cellular basis of chitin synthesis in fungi and insects: common principles and differences. *Eur J Cell Biol* 90 (9):759–769. doi:10.1016/j.ejcb.2011.04.014.
- Miller RM, Reinhardt DR, Jastrow JD. (1995). External hyphal production of vesicular-arbuscular mycorrhizal fungi in pasture and tallgrass prairie communities. *Oecologia* 103:17–23.
- Miyakawa T, et al. 2019. Molecular basis of strigolactone perception in root-parasitic plants: aiming to control its germination with strigolactone agonists/antagonists. *Cell Mol Life Sci*. 77:1103–1113. doi:10.1007/s00018-019-03318-8.
- Mori N, et al. 2020. Identification of two oxygenase genes involved in the respective biosynthetic pathways of canonical and non-canonical strigolactones in *Lotus japonicus*. *Planta*. 251:40. doi:10.1007/s00425-019-03332-x.
- Moscatiello R, et al. 2014. The intracellular delivery of TAT-aequorin reveals calcium mediated sensing of environmental and symbiotic signals by the arbuscular mycorrhizal fungus *Gigaspora margarita*. *New Phytol*. 203:1012–1020. doi:10.1111/nph.12849.
- Mourya VK, et al. 2011. Chitooligosaccharides: synthesis, characterization and applications. *Polym. Sci. Ser. A*. 53:583–612. doi:10.1134/S0965545X11070066.
- Mukherjee A, Ané J-M. 2011. Germinating spore exudates from arbuscular mycorrhizal fungi: molecular and developmental responses in plants and their regulation by ethylene. *Mol Plant-Microbe Interact* 24(2):260–270. doi:10.1094/MPMI-06-10-0146.
- Muley AB, et al. 2019. Gamma radiation degradation of chitosan for application in growth promotion and induction of stress tolerance in potato (*Solanum tuberosum* L. *Carbohydr Polym* 210:289–301.
- Müller S, et al. 1992. Germination stimulants produced by *Vigna unguiculata* Walp cv Saunders upright. *J Plant Growth Regul* 11:77–84.
- Nakamura H, et al. 2013. Molecular mechanism of strigolactone perception by DWARF14. *Nat Commun* 4:2613. doi:10.1038/ncomms3613.
- Naqvi S, Moerschbacher BM. 2015. The cell factory approach toward biotechnological production of high-value chitosan oligomers and their derivatives: an update. *Crit Rev Biotechnol*. doi:10.3109/07388551.2015.1104289.
- Nasir F, et al. 2018. Current understanding of pattern-triggered immunity and hormone-mediated defense in rice (*Oryza sativa*) in response to *Magnaporthe oryzae* infection. *Semin Cell Dev Biol*. 83:95–105. doi:10.1016/j.semcdb.2017.10.020.
- Nefkens GHL, et al. 1997. Synthesis of a phthaloylglycine-derived strigol analogue and its germination stimulatory activity toward seeds of the parasitic weeds *Striga hermonthica* and *Orobanche crenata*. *Journal of Agriculture and Food Chemistry*. 45:2273–2277.
- Nguyen VT, et al. 2018. Effect of oligochitosan-coated silver nanoparticles (OCAgNPs) on the growth and reproduction of three species *Phytophthora* in vitro. *Arch. Phytopathol. Plant Prot*. 51:227–240.
- Niu YF, et al. 2013. Responses of root architecture development to low phosphorus availability: a review. *Ann Bot* 112:391–408. doi:10.1093/aob/mcs285.
- Oldroyd GED. 2013. Speak, friend, and enter: signalling systems that promote beneficial symbiotic associations in plants. *Nat. Rev. Microbiol*. 11:252–263. doi:10.1038/nrmicro2990.
- Orlean P, Funai D. 2019. Priming and elongation of chitin chains: implications for chitin synthase mechanism. *The Cell Surface*. 5:100017. doi:10.1016/j.tcs.2018.100017.
- Osada M, et al. 2013. Effects of supercritical water and mechanochemical grinding treatments on physicochemical properties of chitin. *Carbohydr Polym*. 92:1573–1578. doi:10.1016/j.carbpol.2012.10.068.

- Parker C. 2009. Observations on the current status of Orobanche and Striga problems worldwide. *Pest Manag Sci* 65:453–459. doi:10.1002/ps.1713.
- Passos H, et al. 2014. Ionic liquid solutions as extractive solvents for value-added compounds from biomass. *Green Chem* 16:4786–4815. doi:10.1039/C4GC00236A.
- Peiter E, et al. 2007. The *Medicago truncatula* DMI1 protein modulates cytosolic calcium signaling. *Plant Physiol* 145(1):192–203. doi:10.1104/pp.107.097261.
- Physiol* 155:974–987. doi:10.1104/pp.110.164640.
- Pimprikar P, et al. 2016. A CCaMK-CYCLOPS-DELLA complex activates transcription of RAM1 to regulate arbuscule branching. *Curr Biol*. 26:987–998. doi:10.1016/j.cub.2016.01.069.
- Plant Cell*. 22:2509–2526. doi:10.1105/tpc.109.069807.
- Poinsot V, et al. 2016. New insights into Nod factor biosynthesis: analyses of chitooligomers and lipo-chitooligomers of *Rhizobium* sp. IRBG74 mutants. *Carbohydr Res* 434:83–93. doi:10.1016/j.carres.2016.08.001.
- Prandi C, et al. 2014. Tailoring fluorescent strigolactones for in vivo investigations: a computational and experimental study. *Org Biomol Chem* 12:2960–2968. doi:10.1039/C3OB42592D.
- Rapport DJ, Costanza R, McMichael A.J. 1998. Assessing ecosystem health. *TREE* vol. 13, no. 10.
- Rasmussen A, et al. 2013. A fluorescent alternative to the synthetic strigolactone GR24. *Mol. Plant*. 6:100–112. doi:10.1093/mp/sss110.
- Redecker D. (2000). Glomalean fungi from the Ordovician. *Science* 289: 1920–1921.
- Remy W, Taylor T, Hass H, Kerp H. 1994. Four hundred-million-year-old vesicular arbuscular mycorrhizae. *Proc Natl Acad Sci USA* 91: 11841– 11843.
- Rich MK, Nouri E, Courty PE, Reinhardt D. 2017. Diet of arbuscular mycorrhizal fungi: bread and butter? *Trends Plant Sc*. 22:652–660.
- Rodenburg J. 2016. Parasitic weed incidence and related economic losses in rice in Africa. *Agric Ecosyst Environ*. 235:306–317. doi:10.1016/j.agee.2016.10.020.
- Roy I, et al. 2003. Accelerating enzymatic hydrolysis of chitin by microwave pretreatment. *Biotechnol Prog*. 19:1648–1653.
- Rush TA, et al. 2020. Lipo-chitooligosaccharides as regulatory signals of fungal growth and development. *Nat Commun* 11(1):3897. doi:10.1038/s41467-020-17615-5.
- Saito K, et al. 2007. NUCLEOPORIN85 is required for calcium spiking, fungal and bacterial symbioses, and seed production in *Lotus japonicus*. *Plant Cell*. 19:610–624. doi:10.1105/tpc.106.046938.
- Samain E, et al. 1997. Gram-scale synthesis of recombinant chitooligosaccharides in *Escherichia coli*. *Carbohydr Res*. 302:35–42.
- Samejima H, et al. 2016. Practicality of the suicidal germination approach for controlling *Striga hermonthica*. *Pest Manag Sci* 72:2035–2042. doi:10.1002/ps.4215.
- Sarathchandra RG, et al. 2004. A chitosan formulation ElexaTM induces downy mildew disease resistance and growth promotion in pearl millet. *Crop Prot*. 23:881–888.
- Savage PE. 1999. Organic chemical reactions in supercritical water. *Chem Rev*. 99:603–622.
- Scaffidi A, et al. 2014. Strigolactone hormones and their stereoisomers signal through two related receptor proteins to induce different physiological responses in *Arabidopsis*. *Plant Physiol* 165:1221–1232. doi:10.1104/pp.114.240036.
- Sciences, USA*. 103:359–364. doi:10.1073/pnas.0508883103.
- Seto Y, et al. 2019. Strigolactone perception and deactivation by a hydrolase receptor DWARF14. *Nat Commun* 10:191. doi:10.1038/s41467-018-08124-7.
- Shabek N, et al. 2018. Structural plasticity of D3–D14 ubiquitin ligase in strigolactone signalling. *Nature*. 563:652–656. doi:10.1038/s41586-018-0743-5.
- Shahul Hameed U, et al. 2018. Structural basis for specific inhibition of the highly sensitive ShHTL7 receptor. *EMBO Rep* 19:e45619. doi:10.15252/embr.201745619.

- Shimizu T, et al. 2010. Two LysM receptor molecules, CEBiP and OsCERK1, cooperatively regulate chitin elicitor signaling in rice. *Plant J*. 64:204–214. doi:10.1111/j.1365-313X.2010.04324.x.
- Siame BA, et al. 1993. Isolation of strigol, a germination stimulant for *Striga asiatica*, from host plants. *J Agric Food Chem* 41:1486–1491.
- Singh S, et al. 1995. Glycosidase-catalysed oligosaccharide synthesis: preparation of N-acetylchitooligosaccharides using the b-N-acetylhexosaminidase of *Aspergillus oryzae*. *Carbohydr Res Res*. 279:293–305.
- Smith SE, Smith FA. (2011). Roles of arbuscular mycorrhizas in plant nutrition and growth: new paradigms from cellular to ecosystem scales. *Annu Rev Plant Biol* 62:227–250 h.
- Smith VSE, Read DJ. 2008. *Mycorrhizal Symbiosis*, 3rd ed. Academic Press, New York, NY.
- Smitha M, Knapp. 1999. Exotic plant species in a C4-dominated grassland: invasibility, disturbance, and community structure. *Oecologia* 120:605.
- Spatafora JW, Chang Y, Benny GL, Lazarus K, Smith ME, Berbee ML et al. 2016. A phylum-level phylogenetic classification of zygomycete fungi based on genome-scale data. *Mycologia* 108: 1028–1046.
- Stanga JP, et al. 2016. Functional redundancy in the control of seedling growth by the karrikin signaling pathway. *Planta*. 243:1397–1406. doi:10.1007/s00425-015-2458-2.
- Strullu-Derrien C, Selosse MA, Kenrick P, Martin F. 2018. The origin and evolution of mycorrhizal symbioses: from palaeomycology to phylogenomics. *New Phytologist*. doi: 10.1111/nph.15076.
- Sun G, et al. 2018. Synergistic effect of the combined bio-fungicides “-poly-L-lysine and chitooligosaccharide in controlling grey mould (*Botrytis cinerea*) in tomatoes. *Int. J. Food Microbiol*. 276:46–53.
- Sun J, et al. 2015. Activation of symbiosis signaling by arbuscular mycorrhizal fungi in legumes and rice. *Plant Cell*. 27:823–838. doi:10.1105/tpc.114.131326.
- Takahashi Y, et al. 1995. Effect of sonolysis on acid degradation of chitin to form oligosaccharides. *Bull Chem Soc Jpn*. 68:851–857.
- Tanaka K, et al. 2015. Effect of lipo-chitooligosaccharide on early growth of C4 grass seedlings. *J Exp Bot* 66(19):5727–5738.
- Tian F, et al. 2003. The depolymerization mechanism of chitosan by hydrogen peroxide. *J Mater Sci*. 38:4709–4712.
- Tømmeraaas K, et al. 2001. Preparation and characterisation of oligosaccharides produced by nitrous acid depolymerisation of chitosans. *Carbohydr Res*. 333:137–144.
- Tsuchiya Y, et al. 2015. Probing strigolactone receptors in *Striga hermonthica* with fluorescence. *Science*. 349:864–868. doi:10.1126/science.aab3831.
- Tsuzuki S, et al. 2016. Strigolactone-induced putative secreted protein 1 is required for the establishment of symbiosis by the arbuscular mycorrhizal fungus *Rhizophagus irregularis*. *Mol Plant-Microbe Interact* 29:277–286. doi:10.1094/MPMI-10-15-0234-R.
- Turk H, et al. 2019. Chitosan-induced enhanced expression and activation of alternative oxidase confer tolerance to salt stress in maize seedlings. *Plant Physiol Biochem* 141:415–422.
- Ueno K, et al. 2014. Heliolactone, a nonsesquiterpene lactone germination stimulant for root parasitic weeds from sunflower. *Phytochemistry*. 108:122–128. doi:10.1016/j.phytochem.2014.09.018.
- Umehara M, et al. 2008. Inhibition of shoot branching by new terpenoid plant hormones. *Nature*. 455:195–200.
- Umehara M, et al. 2010. Contribution of strigolactones to the inhibition of tiller bud outgrowth under phosphate deficiency in rice. *Plant Cell Physiol* 51:1118–1126. doi:10.1093/pcp/pcq084.
- Uraguchi D, et al. 2018. A femtomolar-range suicide germination stimulant for the parasitic plant *Striga hermonthica*. *Science*. 362:1301–1305. doi:10.1126/science.aau5445.
- Vassilev N, et al. 2015. Unexploited potential of some biotechnological techniques for biofertilizer production and formulation. *Appl Microbiol Biotechnol*. 99(12):4983–4996. doi:10.1007/s00253-015-6656-4.
- Vekariya RL. 2017. A review of ionic liquids: applications towards catalytic organic transformations. *J Mol Liq* 227:44–60. doi:10.1016/j.molliq.2016.11.123.

- Venkateshwaran M, et al. 2012. The recent evolution of a symbiotic ion channel in the legume family altered ion conductance and improved functionality in calcium signaling. *Plant Cell*. 24(6):2528–2545. doi:10.1105/tpc.112.098475.
- Venkateshwaran M, et al. 2015. A role for the mevalonate pathway in early plant symbiotic signaling. *Proceedings of the National Academy of Sciences, USA*. 112:9781–9786. doi:10.1073/pnas.1413762112.
- Vickers CE, et al. 2015. Production of industrially relevant isoprenoid compounds. In: Kamm B, editor. *Engineered microbes*. Springer; p. 303–334.
- Vitousek PM, Mooney HA, Lubchenco J, Melillo JM. 1997. Human Domination of Earth's Ecosystems. *Science*, 277, 494–499.
- Volk H, et al. 2019. Chitin-binding protein of *Verticillium nonalfalfae* disguises fungus from plant chitinases and suppresses chitin-triggered host immunity. *Mol Plant-Microbe Interact* 32(10):1378–1390. doi:10.1094/MPMI-03-19-0079-R.
- Volpe V, et al. 2020. Short chain chito-oligosaccharides promote arbuscular mycorrhizal colonization in *Medicago truncatula*. *Carbohydr Polym* 229:115505. doi:10.1016/j.carbpol.2019.115505.
- Wakabayashi T, et al. 2019. Direct conversion of carlactonic acid to orobanchol by cytochrome P450 CYP722C in strigolactone biosynthesis. *Sci Adv* 5:eaa9067. doi:10.1126/sciadv.aax9067.
- Wakabayashi T, et al. 2020. CYP722C from *Gossypium arboreum* catalyzes the conversion of carlactonic acid to 5-deoxystrigol. *Planta*. 251(5):97. doi:10.1007/s00425-020-03390-6.
- Wakabayashi T, et al. 2021. Identification and characterization of sorgomol synthase in sorghum strigolactone biosynthesis. *Plant. Phys.* 185 (3):902–913. doi:10.1093/plphys/kiaa113.
- Walker CH, et al. 2019. Strigolactone synthesis is ancestral in land plants, but canonical strigolactone signalling is a flowering plant innovation. *BMC Biol* 17:70. doi:10.1186/s12915-019-0689-6.
- Wan J, et al. 2008. A LysM receptor-like kinase plays a critical role in chitin signaling and fungal resistance in *Arabidopsis*. *Plant Cell*. 20 (2):471–481. doi:10.1105/tpc.107.056754.
- Wilkes JS. 2004. Properties of ionic liquid solvents for catalysis. *J.Mol. Catal. A*. 214:11–17. doi:10.1016/j.molcata.2003.11.029.
- Wu HS, et al. 2011. Process for producing glucosamine and acetyl glucosamine by microwave technique. US Patent 20110114472 A1.
- Wu S. 2021. Establishment of strigolactone-producing bacterium-yeast consortium. *Sci. Adv.* 7:eabh4048. doi:10.1126/sciadv.abh4048.
- Xie X, et al. 2013. Confirming stereochemical structures of strigolactones produced by rice and tobacco. *Mol. Plant*. 6:153–163.
- Xu J, et al. 2007. Antifungal activity of oligochitosan against *Phytophthora capsici* and other plant pathogenic fungi in vitro. *Pestic Biochem Physiol* 87:220–228.
- Yamago S, et al. 2004. Iterative glycosylation of 2-deoxy-2-aminothioglycosides and its application to the combinatorial synthesis of linear oligoglucosamines. *Angew Chem*. 116(16):2197–2200.
- Yang C, Wang E, Liu J. 2022. CERK1, more than a co-receptor in plant–microbe interactions. *New Phytol* 234:1606–1613. doi:10.1111/nph.18074.
- Yao R, et al. 2016. DWARF14 is a non-canonical hormone receptor for strigolactone. *Nature*. 536:469–473. doi:10.1038/nature19073.
- Yokota T, et al. 1998. Alectrol and orobanchol, germination stimulants for *Orobanche minor*, from its host red clover. *Phytochemistry*. 49:1967–1973.
- Yoneyama K, Brewer PB. 2021. Strigolactones, how are they synthesized to regulate plant growth and development? *Curr Opin Plant Biol*. 63:102072. doi:10.1016/j.pbi.2021.102072.
- Yoneyama K, et al. 2007. Nitrogen deficiency as well as phosphorus deficiency in sorghum promotes the production and exudation of 5-deoxystrigol, the host recognition signal for arbuscular mycorrhizal fungi and root parasites. *Planta*. 227:125–132.
- Yoneyama K, et al. 2010. Strigolactones as germination stimulants for root parasitic plants. *Plant Cell Physiol* 51:1095–1103. doi:10.1093/pcp/pcq055.

- Yoneyama K, et al. 2013. Nitrogen and phosphorus fertilization negatively affects strigolactone production and exudation in sorghum. *Planta*. 238:885–894. doi:10.1007/s00425-013-1943-8.
- Yoneyama K, et al. 2015. Difference in striga-susceptibility is reflected in strigolactone secretion profile, but not in compatibility and host preference in arbuscular mycorrhizal symbiosis in two maize cultivars. *New Phytol* 206:983–989. doi:10.1111/nph.13375.
- Yoneyama K, et al. 2018. Which are the major players, canonical or non-canonical strigolactones? *J Exp Bot* 69:2231–2239. doi:10.1093/jxb/ery090.
- Yoneyama K, et al. 2020. Hydroxyl carlactone derivatives are predominant strigolactones in *Arabidopsis*. *Plant Direct*. 4:5. doi:10.1002/pld3.219.
- Yoshida S, et al. 2012. The D3 F-box protein is a key component in host strigolactone responses essential for arbuscular mycorrhizal symbiosis. *New Phytol* 196:1208–1216. doi:10.1111/j.1469-8137.2012.04339.x.
- Yu N, et al. 2014. A DELLA protein complex controls the arbuscular mycorrhizal symbiosis in plants. *Cell Res*. 24:130–133. doi:10.1038/cr.2013.167.
- Zhang A, et al. 2018. Molecular characterization of a novel chitinase CmChi1 from *Chitinolyticbacter meiyuanensis* SYBC-H1 and its use in N-acetyl-d-glucosamine production. *Biotechnol Biofuels*. 11:179. doi:10.1186/s13068-018-1169-x.
- Zhang D, et al. 2007. A two-step fermentation process for efficient production of penta-N-acetyl-chitopentaose in recombinant *Escherichia coli*. *Biotechnol Lett*. 29:1729–1733. doi:10.1007/s10529-007-9462-y.
- Zhang X, et al. 2016. Size effects of chitoooligomers on the growth and photosynthetic characteristics of wheat seedlings. *Carbohydr Polym* 138:27–33.
- Zhang X, et al. 2017. Relationship between the degree of polymerization of chitoooligomers and their activity affecting the growth of wheat seedlings under salt stress. *J. Agric. Food Chem*. 65:501–509.
- Zhang X, et al. 2021. Efficient production of oligomeric chitin with narrow distributions of degree of polymerization using sonication-assisted phosphoric acid hydrolysis. *Carbohydr Polym*. 276:118736. doi:10.1016/j.carbpol.2021.118736.
- Zhang Y, et al. 2014. Rice cytochrome P450 MAX1 homologs catalyze distinct steps in strigolactone biosynthesis. *Nat Chem Biol* 10:1028–1033. doi:10.1016/j.jpowsour.2013.09.135.
- Zhang Y, et al. 2019. Chitoooligosaccharide plays essential roles in regulating proline metabolism and cold stress tolerance in rice seedlings. *Acta Physiol Plant* 41:77.
- Zhao LH, et al. 2013. Crystal structures of two phytohormone signal-transducing α/β hydrolases: karrikin-signaling KAI2 and strigolactone-signaling DWARF14. *Cell Res*. 23:436–439. doi:10.1038/cr.2013.19.
- Zhou F, et al. 2013. D14-SCFD3-dependent degradation of D53 regulates strigolactone signalling. *Nature*. 504:406–410. doi:10.1038/nature12878.
- Zhou J, et al. 2018. Chitoooligosaccharides enhance cold tolerance by repairing photodamaged PS II in rice. *J Agric Sci* 156:888–899.
- Zipfel C, Oldroyd GE. 2017. Plant signalling in symbiosis and immunity. *Nature*. 543:328–336. doi:10.1038/nature22009.
- Zong H, et al. 2017. Improvement in cadmium tolerance of edible rape (*Brassica rapa* L.) with exogenous application of chitoooligosaccharide. *Chemosphere*. 181:92–100.
- Zwanenburg B, et al. 2016. Suicidal germination for parasitic weed control. *Pest Manag Sci* 72:2016–2025. doi:10.1002/ps.4222.
- Zwanenburg B, Pospíšil T. 2013. Structure and activity of strigolactones: new plant hormones with a rich future. *Mol Plant*. 6:38–62. doi:10.1093/mp/sss141.

CHAPTER 2

The impact of long-term CO application on *Medicago truncatula* roots

Prologue

The bioactivity of COs as pre-symbiotic signals has been validated for many different plants, both monocots and dicots and their exudation is enhanced by SL perception (Nasir et al., 2021; Genre et al., 2013). As discussed in the previous section, COs can be produced in several ways, making them particularly interesting for agricultural large-scale applications. In this scenario, our research group had previously demonstrated the possibility to boost AM colonization by the application of exogenous COs prior to fungal colonization, increasing biomass accumulation and total photosynthetic surface, if compared to non-treated AM colonized plants (Volpe et al., 2020). By now, most of the published research has focused on short-term plant responses to CO (or LCO) treatment, demonstrating the activation of symbiotic signaling and gene regulation in the range of a few hours (Czaja et al., 2012; Camps et al., 2015; Giovannetti et al., 2015; Feng et al., 2019).

Here we focused on a longer time scale, in an attempt to track the molecular bases of the previously observed CO-dependent promotion of AM development over several weeks (Volpe et al., 2020). To this aim, we started with an RNA-seq analysis, in order to investigate genome-wide changes in root gene expression over four weeks after the initial CO treatment, followed by a few functional insights investigating particularly interesting aspects such as strigolactone production and cellular responses.

The AMforQuality project

The discovery of the key role played by COs in the early stages of AM establishment paved the way to possible applications in sustainable agriculture. Increasing the amount of AM symbiotic signals in agricultural soils is expected to reduce the recalcitrance to the symbiosis exhibited by some crops as the result of decades of cultivation under intensive soil fertilization. On this line, our research group developed a project called AMforQuality, where the experimental activity of this work buds from. The aim of the project was to improve plant receptiveness towards symbiotic fungi by adding COs to a mycorrhizal inoculum in pasture grounds, to enhance mycorrhization and eventually boost forage productivity and quality, as part of the production chain of Piedmont Fassona cow breed. Moreover, CO treatment may encourage plant colonization by the natural AM fungal community present in the agricultural soil, supporting the enrichment and conservation of fungal biodiversity irrespectively of the AM inoculum.

References

- Camps C, Jardinaud MF, Rengel D, Carrère S, Hervé C, Debellé F, Gamas P, Bensmihen S, Gough C. 2015. Combined genetic and transcriptomic analysis reveals three major signalling pathways activated by Myc-LCOs in *Medicago truncatula*. *New Phytologist* 208: 224–240.
- Czaja LF, Hogekamp C, Lamm P, Maillet F, Martinez EA, Samain E, Dénarié J, Küster H, Hohnjec N. 2012. Transcriptional responses toward diffusible signals from symbiotic microbes reveal MtNFP- and MtDMI3-dependent reprogramming of host gene expression by arbuscular mycorrhizal fungal lipochitoooligosaccharides. *Plant Physiology* 159: 1671–1685.
- Feng F, Sun J, Radhakrishnan GV, Lee T, Bozsoki Z, Fort S, Gavrin A, Gysel K, Thygesen MB, Andersen KR et al. 2019. A combination of chitoooligosaccharide and lipochitoooligosaccharide recognition promotes arbuscular mycorrhizal associations in *Medicago truncatula*. *Nature Communications* 10: 5047.
- Genre A, Chabaud M, Balzergue C, Puech-Pagés V, Novero M, Rey T, Fournier J, Rochange S, Bécard G, Bonfante P et al. 2013. Short-chain chitin oligomers from arbuscular mycorrhizal fungi trigger nuclear Ca²⁺ spiking in *Medicago truncatula* roots and their production is enhanced by strigolactone. *New Phytologist* 19: 190–202.
- Giovannetti M, Mari A, Novero M, Bonfante P. 2015. Early *Lotus japonicus* root transcriptomic responses to symbiotic and pathogenic fungal exudates. *Frontiers in Plant Science* 6: 480.
- Nasir F, Bahadur A, Lin X, Gao Y, Tian C. 2021. Novel insights into host receptors and receptor-mediated signaling that regulate arbuscular mycorrhizal symbiosis. *Journal of Experimental Botany* 72: 1546–1557.
- Volpe V, Carotenuto G, Berzero C, Cagnina L, Puech-Pagés V, Genre A. 2020. Short chain chitoooligosaccharides promote arbuscular mycorrhizal colonization in *Medicago truncatula*. *Carbohydrate Polymers* 229: 115505.

Long-lasting impact of chitooligosaccharide application on strigolactone biosynthesis and fungal accommodation promotes arbuscular mycorrhiza in *Medicago truncatula*

This paper was published as:

Veronica Volpe, Matteo Chialva, Teresa Mazzarella, Andrea Crosino, Serena Capitanio, Lorenzo Costamagna, Wouter Kohlen, Andrea Genre. “Long-lasting impact of chitooligosaccharide application on strigolactone biosynthesis and fungal accommodation promotes arbuscular mycorrhiza in *Medicago truncatula*”. *New Phytologists* 2023 doi: 10.1111/nph.18697

Long-lasting impact of chito oligosaccharide application on strigolactone biosynthesis and fungal accommodation promotes arbuscular mycorrhiza in *Medicago truncatula*

Veronica Volpe¹ , Matteo Chialva¹ , Teresa Mazzarella¹ , Andrea Crosino¹ , Serena Capitanio¹ , Lorenzo Costamagna¹ , Wouter Kohlen²  and Andrea Genre¹ 

¹Department of Life Sciences and Systems Biology, University of Turin, Viale Mattioli 25, 10125 Torino, Italy; ²Laboratory of Molecular Biology, Wageningen University & Research, Wageningen 6708, PB, the Netherlands

Author for correspondence:

Andrea Genre

Email: andrea.genre@unito.it

Received: 25 October 2022

Accepted: 13 December 2022

New Phytologist (2023)

doi: 10.1111/nph.18697

Key words: arbuscular mycorrhiza, chito oligosaccharides, *Medicago truncatula*, strigolactones, symbiosis.

Summary

- The establishment of arbuscular mycorrhiza (AM) between plants and Glomeromycotina fungi is preceded by the exchange of chemical signals: fungal released Myc-factors, including chito oligosaccharides (CO) and lipo-chito oligosaccharides (LCO), activate plant symbiotic responses, while root-exuded strigolactones stimulate hyphal branching and boost CO release. Furthermore, fungal signaling reinforcement through CO application was shown to promote AM development in *Medicago truncatula*, but the cellular and molecular bases of this effect remained unclear.
- Here, we focused on long-term *M. truncatula* responses to CO treatment, demonstrating its impact on the transcriptome of both mycorrhizal and nonmycorrhizal roots over several weeks and providing an insight into the mechanistic bases of the CO-dependent promotion of AM colonization.
- CO treatment caused the long-lasting regulation of strigolactone biosynthesis and fungal accommodation-related genes. This was mirrored by an increase in root dihydro-orobanchol content, and the promotion of accommodation responses to AM fungi in root epidermal cells. Lastly, an advanced downregulation of AM symbiosis marker genes was observed at the latest time point in CO-treated plants, in line with an increased number of senescent arbuscules.
- Overall, CO treatment triggered molecular, metabolic, and cellular responses underpinning a protracted acceleration of AM development.

Introduction

Mineral nutrition of most plants is supported by the mutualistic root symbiosis with Glomeromycotina, an ancient group of soil fungi (Spatafora *et al.*, 2016) that grant their host plants preferential access to soil inorganic nutrients, in change for plant-photosynthesized sugars and lipids (Smith & Read, 2008; Wewer *et al.*, 2014; Keymer *et al.*, 2017).

Plant–fungus recognition is essential for arbuscular mycorrhiza (AM) establishment and is based on an exchange of chemical signals (Bonfante & Reuena, 2011; Zipfel & Oldroyd, 2017). On the one hand, root-exuded strigolactones (SL), a class of terpenoid lactones, signal host proximity (Akiyama *et al.*, 2005) activating hyphal metabolism and branching, and eventually promoting physical encounter with the root surface (Besserer *et al.*, 2006; Waters *et al.*, 2017). On the other hand, AM fungi release diffusible molecules (Myc-factors) that activate a so-called Common Symbiotic Signalling Pathway, or CSSP (Zipfel & Oldroyd, 2017; Choi *et al.*, 2018). Downstream responses include local and systemic

changes in gene expression and metabolism, overall preparing the host plant to symbiosis establishment (MacLean *et al.*, 2017; Choi *et al.*, 2018; Pimprikar & Gutjahr, 2018).

Myc-factors include two classes of molecules: lipo-chito oligosaccharides, or LCO (Maillet *et al.*, 2011), structurally similar to rhizobial Nod-factors and composed of a short chitin chain with a few lateral substitutions, and short-chain chito oligosaccharides, or CO (Genre *et al.*, 2013), where only the chitin backbone is present. The activity of CO as AM fungal signals has been demonstrated in all tested host plants, including monocots and dicots (Sun *et al.*, 2015; Nasir *et al.*, 2021) and their release is boosted upon strigolactone perception (Genre *et al.*, 2013). Furthermore, CO can easily be produced through chitin hydrolysis (Crosino *et al.*, 2021) making them particularly interesting for large-scale agricultural applications (Volpe *et al.*, 2020). Indeed, our recent research project AM for Quality explored the effects of exogenous CO application on AM development in forage plants by running field treatments (V. Volpe & A. Genre, unpublished) alongside laboratory experiments, all based on a CO mix with the same

composition and concentration. CO treatment before fungal inoculation promoted a marked increase in arbuscule development, biomass accumulation, and total photosynthetic surface, than untreated mycorrhizal plants, in both field and laboratory conditions over several weeks (Volpe *et al.*, 2020). At present, most researches have investigated plant responses to CO or LCO treatment on a shorter time scale, demonstrating the activation of symbiotic signaling and gene regulation in the range of a few hours (Czaja *et al.*, 2012; Camps *et al.*, 2015; Giovannetti *et al.*, 2015; Feng *et al.*, 2019).

Here, we chose to focus on a longer time scale, in an attempt to track the molecular bases of the observed CO-dependent promotion of AM development over several weeks (Volpe *et al.*, 2020). To this aim, we used RNA-seq to investigate genome-wide changes in root gene expression over four weeks after the initial short-chain CO treatment, and further validated our results with functional insights. CO treatment changed the expression pattern of the whole strigolactone biosynthetic pathway and increased the dihydro-orobanchol content in root tissue. Moreover, RNA-seq data, targeted gene expression analyses, and live imaging of epidermal cell reorganization indicated a CO-dependent stimulation of intracellular accommodation processes. Lastly, the downregulation of AM symbiosis marker genes was consistent with the increased number of senescent arbuscules at the end of our experimental time frame. In conclusion, our results revealed that CO treatment impacted on molecular, cellular, and metabolic mechanisms that converged toward a global acceleration in AM development.

Materials and Methods

Plant and fungal materials

The model legume *Medicago truncatula* cv 'Jemalong' (line A17) was used for this study. Seeds were collected from the pods, kept for 2 d at room temperature to allow the oxygenation of internal tissues and scarified on sandpaper in order to break the seed coat. Seeds were then sterilized using 5% (v/v) sodium hypochlorite in sterile water and rinsed in sterile distilled water, each step for 5 min keeping the falcon tubes under constant stirring. To break dormancy and allow rapid and synchronized germination, seeds were placed on 0.6% Plant-Agar (Duchefa, Haarlem, the Netherlands) plates, maintained at 4°C in the dark for 2 d and then moved at 23°C until germination.

A commercial granular inoculum of the AM fungus *Funnelliformis mosseae* (strain BEG 12) from MycAgroLab (www.mycagrolab.com; France) was used for all experiments. The inoculum consisted of growth substrate of *Sorghum vulgare* plants, colonized root pieces, spores, and extraradical mycelium, with a minimum of 10 active propagules per g of inoculum.

Chitin oligomers

A mixture of short-chain chitoooligosaccharides, CO (Volpe *et al.*, 2020), was used for all plant treatments. The CO mixture was obtained from crustacean food manufacturing waste (Zhengzhou Sigma Chemical Co. Ltd, Zhengzhou, Henan, China) and

contained fully acetylated, mono-deacetylated, and di-deacetylated molecules composed of 2–5 *N*-acetyl-glucosamine residues (Volpe *et al.*, 2020). Chitoooligosaccharides were applied as a 1 g l⁻¹ solution in sterile distilled water supplemented with Tween 20 (0.005%) as a surfactant. Sterile water with Tween 20 (0.005%) was used in control treatments.

Pot culture

Young *M. truncatula* seedlings were transferred into 9 cm × 9 cm × 12 cm pots (one seedling per pot) filled with sterile coarse sand (0.4–0.8 mm; Valle Po, Revello, CN, Italy). A plastic bag was placed on the pots during the first week, to protect the young plants from desiccation. Plants were grown in phytochambers under controlled conditions (23°C : 21°C, day : night temperature, 16 h : 8 h, light : dark photoperiod) and fertilized once per week using a modified Long Ashton (LA) nutrient solution (Hewitt, 1966) containing 3.2 μM phosphate and 1 mM nitrate. During the rest of the week, pots were watered when necessary with tap water.

Four experimental conditions were set up: control (CTR) plants, lacking both CO treatment and AM inoculation; CO-treated control (CTR + CO); mycorrhizal (MYC), where AM inoculum was added in the absence of CO treatments; and CO-treated mycorrhizal (MYC + CO), where plants were both inoculated and exposed to the CO solution. Chitoooligosaccharides treatment and fungal inoculum were applied as previously described by Volpe *et al.* (2020). In short, 5 ml of CO solution were sprayed over the pot substrate surface 4 and 2 d before inoculation with 22.5 ml of fungal inoculum.

Plants were harvested at 10, 14, 21, 28 d postinoculation (dpi) and carefully washed under tap water to remove sand. Arbuscular mycorrhiza colonization was assessed based on the presence of root-bound extraradical mycelium before rapid sampling, dip-freezing in liquid nitrogen, and storage at –80°C until RNA extraction. We used five plants for each experimental condition at each time point, except at 10 dpi, when the limited extension of root systems required the sampling of a larger number of plants (12). We collected at least three biological replicates (plants) for each condition, selecting the best developed plants, with no visible sign of pathogenesis or stress and an extensive extraradical fungal development.

RNA isolation and sequencing

Total RNA was extracted from all samples using the RNeasy™ Plant Mini kit (Qiagen). Samples were mechanically homogenized using a TissueLyser system for 2 min at 18 Hz. An aliquot of each sample was mixed with RLT buffer (Qiagen), and further treated following the manufacturer's protocol. RNA quantity and quality were spectrophotometrically checked using a NanoDrop ND-1000 instrument (ThermoFisher Scientific, Rodano, Italy). RNA samples were further quantified and tested for integrity by capillary electrophoresis using Agilent 2100 Bioanalyzer instrument with the Agilent RNA 6000 Nano Kit (Agilent Technologies Italia Spa, Cernusco sul Naviglio, Italy) following the manufacturer's instructions. As requested by the sequencing company (IGATech, Udine, Italy), samples dedicated to RNA-seq were not treated with DNase.

RNA-seq analysis on root RNA samples was performed at IGA Technology services. TruSeq stranded mRNA kit (Illumina, San Diego, CA, USA) was used for library preparation and sequencing performed using Illumina NextSeq 500 platform (Illumina) in single-end mode at 75 bp read-length and with a sequencing depth ranging from 20 to 30 M of reads per sample (Supporting Information Table S1).

Bioinformatics

Adapter sequences were masked with CUTADAPT v.1.11 (Martin, 2011) from raw reads using the following parameters: – anywhere (on both adapter sequences) – overlap 5-times 2 – minimum-length 35-mask-adapter. Raw reads were then trimmed removing lower quality bases and adapters using the ERNE software (Del Fabro *et al.*, 2013). The expression level of each gene in each library was calculated by mapping filtered reads on Mt4.1 reference genome (Young *et al.*, 2011; Tang *et al.*, 2014) using STAR splice-aware aligner (Dobin *et al.*, 2013) with default parameters. Reads overlapping with annotated exons were counted using HTSEQ (Anders *et al.*, 2015) and differential expression analysis performed for each comparison (CTR + CO vs CTR, MYC vs CTR, MYC + CO vs CTR and MYC + CO vs MYC) at each time points (10, 14, 21, 28 dpi) using the DESEQ2 R package (Love *et al.*, 2014) at a False discovery rate (FDR or adjusted *P*-value) (Benjamini & Hochberg, 1995) threshold of 0.05 (Datasets S1–S4). The RNA-seq dataset obtained in this study was included in the Medicago Expression Atlas (MtExpress V3; Carrere *et al.*, 2021).

Differentially expressed genes were plotted into KEGG (Kyoto Encyclopedia of Genes and Genomes) pathway maps using the PATHVIEW R package (Luo & Brouwer, 2013) and the *M. truncatula* annotation available at the KEGG website. Metabolic pathways visualization was achieved using MAPMAN software (Usadel *et al.*, 2005). MAPMAN functional annotation for *M. truncatula* (Table S2) was obtained from the proteome using MERCATOR4 annotation tool (Schwacke *et al.*, 2019).

Gene ontology (GO) enrichment analyses were carried out on each of the previously generated contrasts using the GOSEQ R package (Young *et al.*, 2010) at a FDR cutoff of 0.1. The $-\log_{10}$ of the corrected *P*-value was plotted.

Variance partitioning analysis (VPA) was performed using the ‘varpart’ function in the R package VEGAN (Oksanen *et al.*, 2019) using gene counts normalized with DESEQ2 through the Variance Stabilizing Transformation (vst). Fractions of variance explained by single factors were tested for significance on the RDA model using permutational ANOVA (999 permutation, $P < 0.05$). Principal component analysis (PCA) was calculated with the ‘prcomp’ function in the BASE R package, using same normalization used for VPA. Statistical and graphical elaborations were performed in R programming environment (R Core Team, 2020) using the GGLOT2 package (Wickham, 2016).

Gene expression analysis by real-time qPCR

RNA-seq data were validated by quantitative real-time PCR (qRT-PCR) analysis of the expression profile of 10 differentially

expressed genes (DEGs) across all treatments and time points (Fig. S1).

Specific primers (listed in Table S3) were designed using PERL-PRIMER software (<http://perlprimer.sourceforge.net>) on *M. truncatula* CDS sequences from NCBI (<http://www.ncbi.nlm.nih.gov/>) and *M. truncatula* genome database (<http://www.medicagogenome.org>). All primers were first tested by PCR on genomic *M. truncatula* and *F. mosseae* DNA, to confirm their plant-specificity.

To remove any trace of genomic DNA before cDNA synthesis, RNA samples were treated with Turbo™ DNase (Qiagen) according to the manufacturer’s instructions, followed by second NanoDrop quantification. The RNA samples were routinely checked for DNA contamination by PCR analysis, using primers *MtTEF-F*: 5'-AAGCTAGGAGGTATTGAAAG-3' and *MtTEF-R*: 5'-ACTGTGCAGTAGTACTTGGTG-3' for *MtTEF* (Elongation Factor, NCBI Ref. Seq.: XM_013595882).

For single-strand cDNA synthesis, *c.* 700 ng of total RNA was denatured at 65°C for 5 min and then reverse-transcribed using the Super-Script II kit (Invitrogen) at 25°C for 10 min, 42°C for 50 min, and 70°C for 15 min. The final volume was 20 µl volume and contained 10 µM of random primers, 0.5 mM deoxynucleoside triphosphates, 4 µl 5 × buffer, 2 µl 0.1 M dithiothreitol (DTT), and 1 µl Superscript II enzyme. Control PCR was set with TEF primers to test the presence of cDNA.

To confirm the results of our transcriptomic analysis of SL biosynthesis and transport-related genes, root systems from CTR and CTR + CO plants were sampled at 21 dpi in an independent experiment. Hundred milligrams of root powder was used for RNA extraction and analyzed by qRT-PCR.

Lastly, in order to monitor local, short-time occurrence of early gene regulation in response to CO perception, 1 g l⁻¹, 1 mg l⁻¹ or 1 µg l⁻¹ CO solutions were applied to WT and *dmi3-1 Agrobacterium rhizogenes*-transformed root organ cultures (ROCs) expressing the nuclear targeted NUPYC2.1 protein (Sieberer *et al.*, 2009), which was used as a visual reporter of cell viability. Root organ culture lines were propagated on M medium (Bécard & Fortin, 1988) at 25°C in the dark, in vertically oriented petri dishes to favor the regular fishbone-shaped root system (Chaubaud *et al.*, 2002) and grown for 3 wk. For local CO treatment, small disks of filter paper (Ø 4 mm) soaked in 20 µl of CO solution were applied on several lateral roots, 10–15 mm from the root tip, following Chaubaud *et al.* (2011). Six hours later, 1-cm-long root segments underlying each disk were excised, immediately frozen, and stored at –80°C until RNA extraction and analysis for the expression of AM fungal perception and accommodation marker genes.

qRT-PCR analyses were performed according to the Rotor-Gene SYBR Green PCR Kit instructions (Qiagen) and were run in a final volume of 15 µl for each tube containing 7.5 µl of Rotor-Gene SYBR Green PCR Master Mix, 5.5 µl of 3 µM specific primers mix (Table S4), and 10 ng of cDNA. A Rotor Gene machine (Qiagen) was used with the following program: 3-min preincubation at 95°C, followed by 40 cycles of 15 s at 95°C, and 30 s at 60°C. Each amplification was followed by melting curve analysis (60–94°C) with a heating rate of 0.5°C every 15 s. All reactions were performed with two technical replicates, and only *C_t* values with a standard deviation that did not

exceed 0.5 were considered. Relative RNA levels were calibrated using the elongation factor (TEF) mRNA as endogenous reference and normalized to the control line. Results were validated statistically using the unpaired Student's *t*-test to compare two means: differences were considered significant at $P < 0.05$.

Strigolactone analysis in root systems and exudates

CTR and CTR + CO plants were twice, respectively, treated with water or CO solution, and then grown for 21 d. Twenty-one-day-old *M. truncatula* plants were carefully sampled and washed free of sand. They were put inside a tube (two plants for tube) with 40 ml of LA solution covering the whole root system and closed with Parafilm; the tubes were placed into a closed Magenta box and the root system was covered with a black shield. Plants (four biological replicates for each treatment) were placed in a growth chamber for 36 h for exudate collection. After 36 h, the root exudate was recovered and stored at -20°C for the next step.

Whole plant fresh weight (FW), as well as shoot and root biomass separately, was measured for each biological replicate, before each root system was ground to a fine powder in a mortar using liquid nitrogen and stored at -80°C .

For the analysis of SL content, 500 mg of each ground sample was transferred to 2-ml Eppendorf tubes, and SL were extracted with 2 ml of ethyl acetate with 10^{-8} M GR24 as internal standard (end concentration 10^{-7} M). Tubes were vortexed, sonicated for 20 s (Branson Ultrasonics sonication bath; Emerson Automation Solutions, Busseno, Italy), and centrifuged for 10 min at 2500 *g* at RT. Subsequently, the organic phases were transferred to 4-ml glass vials, and the solvent was evaporated in a speed vacuum system (SPD121P; ThermoSavant, Hastings, UK). Root exudates were purified and concentrated as previously described for tomato (Kohlen *et al.*, 2012); SL from root tissues and exudates were quantified according to Liu *et al.* (2011).

Live imaging of prepenetration responses

To further investigate whether CO treatment altered cell responses to fungal contact, we modified the targeted AM inoculation technique used by Genre *et al.* (2005, 2008) for visualizing the prepenetration apparatus (PPA) in WT roots. In short, *Agrobacterium rhizogenes*-transformed ROCs expressing the endoplasmic reticulum-targeted GFP-HDEL (Haseloff *et al.*, 1997) were grown on M medium (Boisson-Dernier *et al.*, 2001) in vertically oriented Petri dishes and inoculated with pregerminated spores of *Gigaspora margarita*. One milliliter of filtered CO solution (1 mg l^{-1}) or sterilized water (as control) was then added over the root culture before covering it with a gas-permeable plastic film (bioFOLIE 25; Sartorius, Goettingen, Germany). Fungus–root interaction was monitored daily using a stereomicroscope and contact sites were imaged at 7, 10, and 14 dpi using a Leica TCS SP2 confocal microscope fitted with a long distance $\times 40$ water-immersion objective (HCX Apo 0.80). GFP fluorescence was excited with the argon laser band at 488 nm and recorded with an emission window set at 500–525 nm.

Morphological and functional analysis of AM colonization

Total and root fresh biomass were measured in mycorrhizal WT plants in the presence or absence of CO treatment. Biomass data were compared, and the results were validated statistically using the unpaired Student's *t*-test (differences were considered significant at $P < 0.05$). Furthermore, inoculated WT and *dm3-1* mutant plants, treated or not with CO, were sampled at 28 dpi to quantify fungal colonization according to Trouvelot *et al.* (1986). At least four plants were used for the root mycorrhization intensity assessment and 100 1-cm-long root pieces were analyzed per plant. The same method was adapted for the *dm3-1* mutant (where intraradical colonization is blocked) to determine frequency (*F*) and intensity (*M*) parameters with reference to hyphopodium presence on the root surface instead of intraradical fungal structures.

For detailed microscope analysis of arbuscule morphology, root segments of WT plants were excised and individually embedded in agarose (5%). Hundred micrometers vibratome sections was then moved to microscope slides and treated for 5 min in phosphate buffer containing 0.5% commercial bleach, rinsed three times, and then incubated overnight in $10\text{ }\mu\text{g ml}^{-1}$ wheat germ agglutinin–fluorescein isothiocyanate (WGA–FITC; Sigma-Aldrich) to label the fungal wall. A Leica TCS SP2 confocal microscope (Leica Microsystems GmbH, Wetzlar, Germany) equipped with a $\times 40$ water immersion objective was used for imaging with fluorescence excitation at 488 nm and acquisition at 500–550 nm.

Results

CO treatment impacted on the root transcriptome for several weeks

In a first global analysis of the RNA-seq dataset, PCA (Fig. 1a) and variance partitioning analysis (VPA; Fig. 1b) revealed a high level of variation in the transcriptome between conditions and time points. As shown in Fig. 1(a), CTR, CTR + CO, MYC, and MYC + CO transcriptomes clustered in different areas of the PCA plot, indicating that both AM inoculation and CO treatment had a strong influence on the root gene expression profiles. In order to grant a homogeneous code for sample timing, we refer to dpi for both inoculated and noninoculated (but same age) plants. At 10 dpi, CTR + CO, MYC, and MYC + CO samples were clearly separated from CTR along the PC1 axis (explaining 33.38% of variance), highlighting the distance in the transcriptional profile of CTR samples compared with the remaining treatments. A major distinction along the PC1 axis became evident since 14 dpi between inoculated (MYC and MYC + CO) and noninoculated samples (CTR and CTR + CO), as expected in relation with AM establishment. A specific effect of the CO treatment was evident at 10 dpi (with a clear separation between CTR and CTR + CO, and a milder but evident separation between MYC and MYC + CO), and partially rebounded at 28 dpi between MYC and MYC + CO samples.

Variance partitioning analysis (Fig. 1b) highlighted time as the most influential variable in our time-course study, in line with

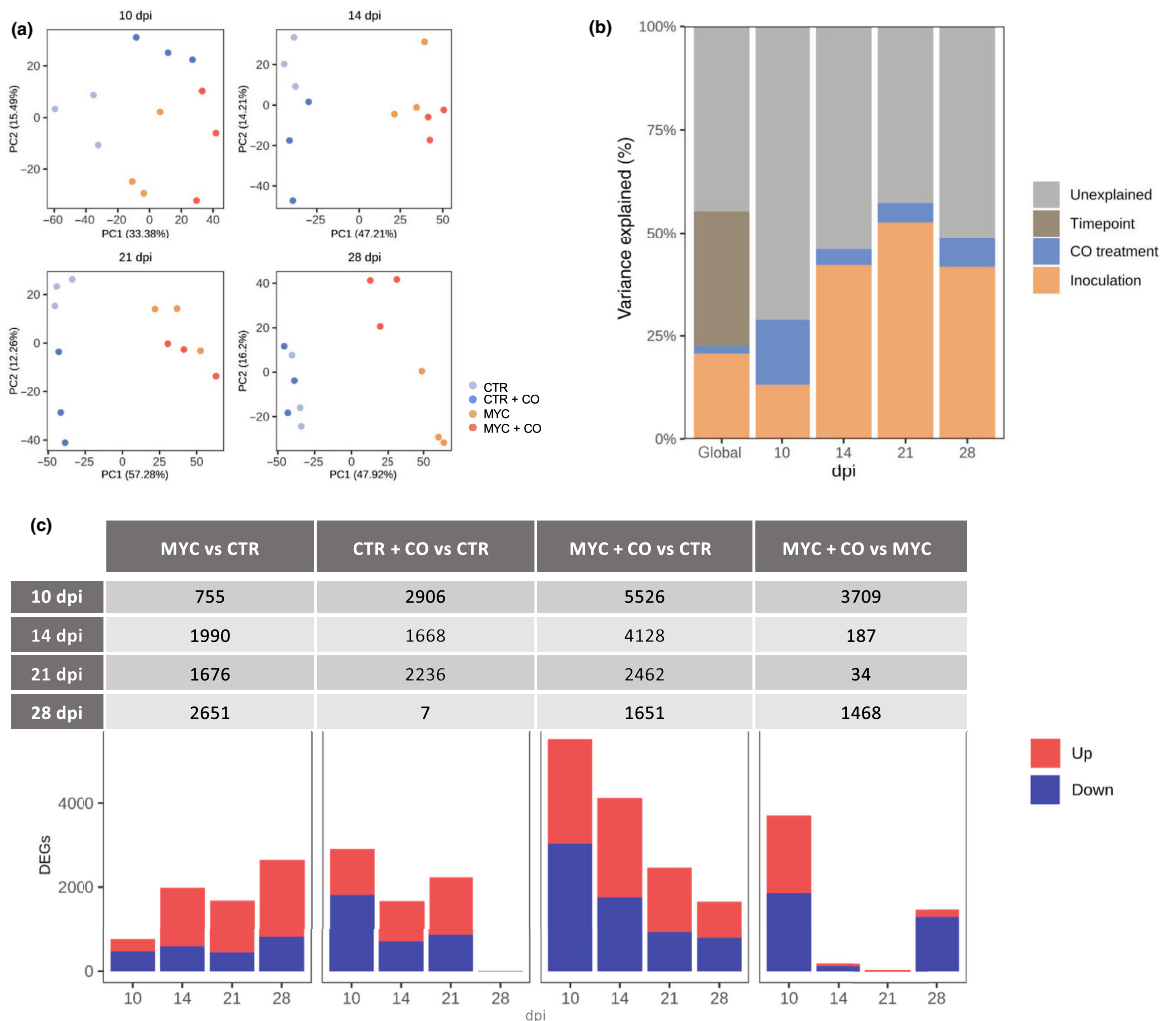


Fig. 1 Global overview of transcriptomic data. (a) Principal component analysis (PCA) plots highlighted a clear separation of the expression profiles between arbuscular mycorrhiza (AM) inoculated (dark and light orange) and noninoculated (dark and light blue) samples, as well as between treated (dark orange and dark blue) and nontreated (light orange and light blue) ones. Three biological replicates (individual dots) are plotted per condition and time point. (b) Variance partitioning analysis (VPA) considered three factors: AM fungus presence (inoculation), chitoooligosaccharides (CO) treatment and time (10, 14, 21, 28 d postinoculation (dpi)). The strongest influence on gene regulation resulted to depend on time, while CO treatment had a major effect at the earliest time point (10 dpi). All the fractions explained by the factors were significant (ANOVA on RDA model, $P < 0.05$), except for the fraction explained by CO treatment at 14 dpi. (c) Differentially expressed genes (DEGs) in the four comparisons and at different time points. Number and expression trend of DEGs. Upregulation is shown in red, downregulation in blue (FDR < 0.05).

the expected major changes in gene expression throughout AM development (Handa *et al.*, 2015). Variance partitioning analysis was subsequently used to address individual time points: this correlated CO treatment to the highest amount of variance in gene regulation at 10 dpi, an early time point in root colonization in our experimental conditions, while AM inoculation became the most influential variable in the later time points. Also in this case, the CO effect extended across all four time points, with a partial reinforcement at 28 dpi.

In conclusion, both PCA and VPA indicated an impact of CO treatment across our whole time-course analysis, with the strongest effect at the earliest time point in both inoculated and non-inoculated plants.

The number and proportion of differentially expressed genes (DEGs) among the four conditions at each of the four time points is summarized in Fig. 1(c). The MYC vs CTR comparison highlighted a progressive increase in gene regulation, in line with the ongoing colonization of the root system by the AM fungus.

In the CTR+CO vs CTR comparison, the CO effect was strongest at 10 dpi (with 2906 DEGs), intermediate at 14 and 21 dpi, and minimal at 28 dpi (with only 7 DEGs). This pattern can be explained with the progressive degradation/leaching of CO from the pot over the weeks that follow the initial treatments (4 and 2 d before inoculation). The strongest differences in gene regulation were observed when comparing MYC+CO vs CTR samples (which represent the most dissimilar conditions in our experiment). Here, the strongest impact of the CO treatment was recorded at 10 dpi (5526 DEGs), with a progressive decrease thereafter. This is suggestive of a synergistic effect of exogenous CO and fungal-secreted Myc-factors during early root colonization, and is in line with the progressive decrease of CO effect over time (as highlighted in CTR+CO vs CTR). Lastly, the effect of MYC+CO vs MYC comparison aimed to dissect the effect of exogenous CO on the AM interaction. Also in this case, a major impact was evident at 10 dpi (3709 DEGs), in line with the reinforcement of fungal signaling by the applied CO. Nevertheless, differential gene regulation peaked again at 28 d (1468 DEGs) with a large majority of downregulated sequences, whereas intermediate time points displayed a very similar gene regulation scenario in the two conditions.

In summary, differential gene expression analysis convincingly supported the evidence emerging from multivariate analysis, indicating an impact of CO on plant gene regulation throughout our experimental time frame, with a major effect during early root colonization.

Functional enrichment analysis suggests that CO treatment mimics fungal presence

To gain insights into the molecular processes impacted by CO treatment, we performed a GO enrichment analysis of DEGs (Datasets S5–S8; <http://geneontology.org/docs/ontology-documentation/>). We will focus here on the two most strongly regulated time points: 10 and 28 dpi, and the most over-represented GO terms for each comparison, as presented in Figs S2–S5. Interestingly, in the MYC vs CTR comparison (Fig. S2), *Defense responses* were over-represented both at 10 and 28 dpi, in agreement with the well-documented regulation of defense-related genes during AM interaction (Salzer *et al.*, 2000; Jung *et al.*, 2012; Cameron *et al.*, 2013). *Protein serine/threonine kinase activity* emerged at 10 and 28 dpi and *DNA-binding transcription factor activity* at 28 dpi, reflecting the extensive impact of symbiosis on regulatory pathways (Liu *et al.*, 2003; Küster *et al.*, 2004; Sanchez *et al.*, 2004; Hohnjec *et al.*, 2005; Hoge Kamp & Küster, 2013). The whole ubiquitination system (*ubiquitin ligase complex*, *protein ubiquitination*, *ubiquitin protein transferase activity*) was regulated at 28 dpi, possibly indicating the onset of senescence-related mechanisms. Lastly, *fatty acid biosynthesis* appeared at 28 dpi, likely related to both the extensive synthesis of perifungal membranes and the intense production of lipids feeding the fungus (Wewer *et al.*, 2014; Luginbuehl *et al.*, 2017; MacLean *et al.*, 2017).

Since no enriched GO category emerged at 28 dpi for the CTR+CO vs CTR comparison (Fig. S3), we only comment here on the 10 dpi time point. In this case, a remarkable analogy

emerged with the same time point of the MYC vs CTR comparison (Fig. S6): in fact, the global pattern of gene regulation was very similar for *kinase activity*, *signal transduction*, *defense response*, and *acyl transferase activity*. This supports the role of CO as mimics of fungal presence and elicitors of symbiotic signaling and gene regulation in the host root.

In the MYC+CO vs CTR comparison at 10 dpi (Fig. S4), a massive activation was observed in protein biosynthesis (*translation*, *ribosome*, and *ribosome constituents*), cytoskeleton-associated processes (*microtubule-associated complex*, *microtubule-based movement*, and *microtubule motor activity*), and chromatin reorganization (*nucleosome*, and *nucleosome assembly*). This is suggestive of intense cell reorganization and is supported by our knowledge of the fungal accommodation process that takes place inside each colonized cell (Gutjahr & Parniske, 2013; Carotenuto *et al.*, 2019). At 28 dpi (Fig. S4), GO terms related to transport (*transporter activity*, *transport*, *heme binding*, *sulfate transport*, *transmembrane transport*, *secondary active sulfate transmembrane transport activity*, and *membrane*) were highly represented, likely related to the extensive AM colonization promoted by CO treatment (Benedito *et al.*, 2010; Gaude *et al.*, 2012; Handa *et al.*, 2015).

Finally, the MYC+CO vs MYC comparison (Fig. S5) suggested that exogenous CO enhanced *cell cycle regulation*, *chromatin rearrangement*, and *cytoskeleton-associated processes* at 10 dpi, hinting at an intensification of the fungal accommodation responses in CO-treated plants. By contrast, a major impact on regulatory and proteolytic processes appeared at 28 dpi in CO-treated plants, suggesting the appearance of senescence-related processes.

In conclusion, our analysis of GO enrichment indicated a global consistency between the regulatory responses induced by AM fungi and CO treatment, with a reinforcement and an advancement of symbiotic processes in plants that were exposed to both stimuli.

CO treatment stimulated strigolactone signaling and fungal accommodation

Among the various gene pathways related to AM establishment that were highlighted by GO enrichment analysis (Table 1), we chose to validate the observed regulation of signaling- and cell reorganization-related genes with functional analyses.

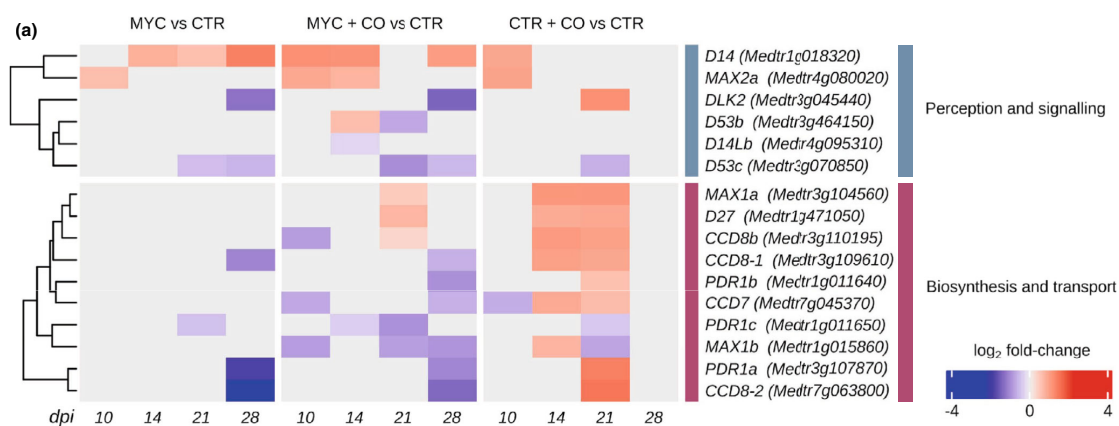
First, we focused on the regulation of Strigolactone (SL) signaling. Strigolactone are carotenoid-derived plant hormones (Gomez-Roldan *et al.*, 2008; Umehara *et al.*, 2008) that also function as extraradical signals to activate AM fungi (Waters *et al.*, 2017). Strigolactone biosynthesis (*CCD8-1* and *CCD8-2*) and transport (*PDR1a*) marker genes were downregulated at 28 dpi in MYC compared with CTR plants (Fig. 2a), which is in line with the inhibition of rhizospheric SL signaling upon maximum root colonization (López-Ráez *et al.*, 2011). Remarkably, this downregulation of SL biosynthesis and transport genes occurred as early as 10–14 dpi in CO-treated plants (MYC+CO vs CTR). A rather different scenario was recorded in CO-treated plants that were not inoculated with AMF (CTR+CO vs CTR, Dataset S1). Under these conditions, SL biosynthesis and

Table 1 Main arbuscular mycorrhiza (AM) symbiosis-related gene categories impacted at 10 d postinoculation (dpi) by chitoooligosaccharides (CO) treatment.

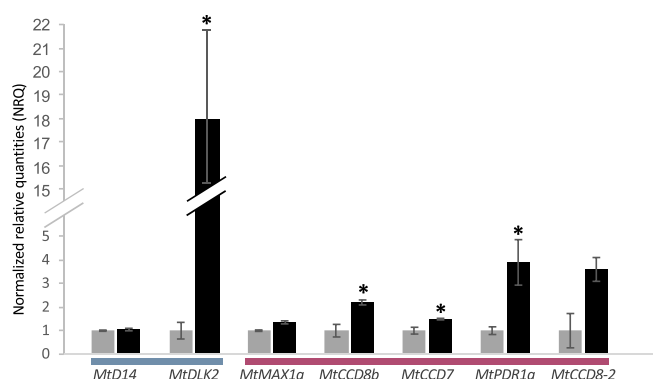
Gene ID	MYC vs CTR	MYC + CO vs CTR	CTR + CO vs CTR	MYC + CO vs MYC	Annotation
<i>Log₂ fold-change value</i>					
<i>Strigolactone signaling</i>					
Medtr3g045440	nr	nr	1.21	nr	Sigma factor sigb regulation rsbq-like protein DLK2
Medtr3g110195	nr	0.35	1.00	nr	Retinal pigment epithelial membrane protein CCD8b
Medtr3g104560	nr	0.47	1.13	nr	Cytochrome P450 family protein MAX1a
Medtr7g045370	nr	nr	0.66	nr	Carotenoid cleavage dioxygenase CCD7
Medtr1g471050	nr	0.75	0.63	nr	Beta-carotene isomerase D27
Medtr3g109610	nr	nr	0.94	nr	Carotenoid cleavage dioxygenase CCD8-1
Medtr3g107870	nr	nr	1.41	nr	Drug resistance transporter-like ABC domain protein PDR1a
Medtr7g063800	nr	nr	1.52	nr	Carotenoid cleavage dioxygenase CCD8-2
<i>External stimuli response</i>					
Medtr5g076900	nr	5.82	nr	nr	Glutathione S-transferase amino-terminal domain protein
Medtr5g035640	nr	4.73	nr	nr	Polygalacturonase 1 beta-like protein 3
Medtr7g068600	nr	3.91	nr	nr	myb-like transcription factor family protein MYB1
Medtr1g040500	1.04	3.73	nr	nr	Glycerol-3-phosphate acyltransferase RAM2
Medtr1g109110	0.82	3.02	nr	nr	Palmitoyl-acyl carrier thioesterase FatM
Medtr6g011490	nr	2.56	nr	nr	AP2 domain transcription factor RAM1
Medtr4g104020	0.77	2.26	nr	nr	GRAS family transcription factor RAD1
Medtr5g030910	1.13	1.19	nr	-0.94	Lipid transporter STR
<i>Cytoskeleton organization</i>					
Medtr6g082470	nr	0.93	nr	1.20	ATP-binding microtubule motor family protein
Medtr1g082920	nr	0.79	nr	1.20	Kinesin motor domain protein
Medtr5g094310	nr	0.79	nr	1.15	Kinesin motor domain protein
Medtr7g091290	nr	0.71	nr	1.07	Kinesin motor catalytic domain protein
Medtr1g075680	nr	0.74	nr	1.06	Kinesin motor domain protein
Medtr6g053680	nr	0.75	nr	1.03	ATP-binding microtubule motor family protein
Medtr7g061020	nr	0.80	nr	0.96	ATP-binding microtubule motor family protein
Medtr2g010760	nr	0.73	nr	0.96	Kinesin motor catalytic domain protein
Medtr4g092140	nr	0.68	nr	0.95	Kinesin motor catalytic domain protein
Medtr1g017540	nr	0.62	nr	0.93	Kinesin motor catalytic domain protein
Medtr5g031470	nr	0.68	nr	0.93	Kinesin motor domain Di-glucose-binding protein
Medtr3g107650	0.74	1.65	nr	-0.91	Kinesin-associated protein
<i>Cell cycle organization</i>					
Medtr3g102530	-0.62	0.59	nr	1.21	Carboxy-terminal domain cyclin, Cyclin A
Medtr7g113510	nr	0.94	nr	1.19	Cyclin family protein, putative; mitosis division plane proteinTAN1
Medtr3g110405	nr	0.88	nr	1.16	Serine/Threonine-kinase aurora-like protein, homolog to AtAUR1
Medtr5g088980	nr	0.80	nr	1.15	Carboxy-terminal domain cyclin, Cyclin B
Medtr3g088415	nr	0.85	nr	1.11	Carboxy-terminal domain cyclin, Cyclin A
Medtr5g012010	nr	0.73	nr	1.10	Syntaxin of plants 122 protein, KNOLLE protein
Medtr8g074000	nr	0.84	nr	1.06	Carboxy-terminal domain cyclin, Cyclin B
Medtr7g089080	nr	0.71	nr	1.05	Cyclin B
Medtr5g023790	nr	0.73	nr	1.02	Carboxy-terminal domain cyclin, Cyclin B
Medtr5g011390	nr	0.71	nr	0.86	Cell cycle regulated microtubule-associated protein, AURORA
<i>Cell wall organization</i>					
Medtr8g009560	nr	1.73	1.45	nr	Fatty acid hydroxylase superfamily protein
Medtr7g062250	nr	1.52	nr	1.15	Laccase/diphenol oxidase family protein
Medtr5g075320	nr	1.30	nr	0.93	Expansin A10
Medtr2g097030	nr	1.20	0.88	0.68	Expansin A10
Medtr4g053380	nr	1.12	nr	1.41	Fasciclin-like arabinogalactan protein
Medtr4g081950	nr	1.04	nr	nr	Expansin-A1-like protein
Medtr5g079950	nr	1.03	0.90	0.62	Expansin A10
Medtr2g086070	nr	-1.00	-0.72	nr	Gland-specific fatty acyl-CoA reductase
Medtr4g019225	nr	-1.07	nr	nr	Laccase/diphenol oxidase family protein
Medtr3g098980	nr	-1.10	-0.70	-0.83	Omega-hydroxypalmitate O-feruloyl transferase
Medtr6g086365	-1.16	nr	-2.20	nr	Arabinogalactan protein
Medtr6g086390	nr	nr	-1.59	nr	Arabinogalactan peptide-like protein
Medtr4g059720	nr	nr	nr	0.83	Fasciclin-like arabinogalactan protein
Medtr5g081810	nr	nr	nr	1.18	Laccase/diphenol oxidase family protein

CTR, control; MYC, mycorrhizal; nr, not significantly regulated.

14698710 downloaded from https://onlinelibrary.wiley.com/doi/10.1111/nph.18697 by Universita Degli Studi Di Tori, Wiley Online Library on [27/01/2023]. See the Terms and Conditions (https://onlinelibrary.wiley.com/terms-and-conditions) on Wiley Online Library for rules of use. OA articles are governed by the applicable Creative Commons License



(b) Gene expression at 21 dpi in CTR and CTR+CO



(c) Didehydro-orobanchol content

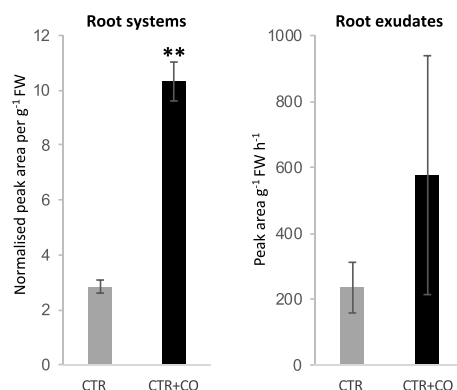


Fig. 2 Chitoooligosaccharides (CO) effect on strigolactone (SL)-related gene expression and SL accumulation. (a) Heatmap plot of SL-related genes in each comparison and time points. A progressive decrease in SL biosynthesis (blue) is in line with the progress of arbuscular mycorrhiza (AM) development in mycorrhizal (MYC) vs control (CTR). This downregulation was earlier and more extensive in MYC + CO vs CTR comparison, in line with the acceleration of colonization observed in the presence of CO treatment. Remarkably, a strong upregulation (red) was evident in both SL biosynthesis and transport until 21 d postinoculation (dpi) in the CTR + CO vs CO comparison. Genes are clustered within each category according to Spearman's distance (Müller *et al.*, 2019). (b) Independent experiment confirming SL gene expression analysis in CO treated and untreated roots at 21 dpi. Mean values \pm SEs of three biological replicates for each treatment are shown. Asterisks indicate statistically significant differences (Student's *t*-test): *, $P < 0.05$. (c) Didehydro-orobanchol (DDO) content in root tissues and exudates of CTR and CTR + CO plants sampled at 21 dpi. A significant increase in DDO root content correlated with CO treatment. A similar trend was observed in the exudates, even if the difference between CTR and CTR + CO plants was statistically not significant. Mean values \pm SDs of four biological replications for each treatment are shown. Each biological replication was composed by two plants. Asterisks indicate statistically significant differences (Student's *t*-test: **, $P < 0.01$).

transport-related genes were found to be upregulated between 14 and 21 dpi. Such an upregulation of SL-related genes suggests a CO-dependent boosting of fungus-directed signaling in the absence of an effective interaction with the symbiont.

An independent experiment confirmed a comparable pattern of gene regulation at 21 dpi in CTR + CO compared with CTR plants, with an unchanged expression of *MtD14*, a significant upregulation of *MtDLK2*, *MtCCD8b*, *MtCCD7*, and *MtPDR1a* and a comparable (albeit not significant) trend for *MtMAX1a* and *MtCCD8-2* (Fig. 2b).

To correlate the observed regulation of SL-related gene expression to SL metabolomics, we analyzed SL content in root tissues and

exudates from 21-d-old CTR and CTR + CO plants. In our samples, only one SL, didehydro-orobanchol (DDO), was above the detection level. This SL has been identified in roots of several AM host plants (López-Ráez *et al.*, 2008; Yoneyama *et al.*, 2008; Kohlen *et al.*, 2012), and characterized as the major strigolactone in *M. truncatula*, with a role in stimulating hyphal branching in the AM fungus *Gigaspora margarita* (Liu *et al.*, 2011; Tokunaga *et al.*, 2015). Interestingly, CTR + CO roots contained a significantly higher level of DDO than CTR roots. A comparable trend (albeit statistically not significant) was also observed in root exudates (Fig. 2c).

Second, MYC + CO vs CTR and MYC + CO vs MYC comparisons (Table 1; Datasets S4, S5) highlighted the upregulation

of a consistent group of functional categories related to cell remodeling, such as *Cytoskeleton Organization* and *Cell Wall Organization*. This is in line with the activation of intracellular fungal accommodation by the host tissues (Luginbuehl & Oldroyd, 2017; Pimprikar & Gutjahr, 2018), requiring the reorganization of cytoskeletal elements (Genre *et al.*, 2005), the onset of massive exocytic processes (Genre *et al.*, 2012), cell wall material deposition and remodeling (Balestrini & Bonfante, 2014) to generate the symbiotic interface (Balestrini *et al.*, 2005). Furthermore, a significant upregulation was also observed in *Cell Cycle Organization* for numerous cell cycle regulators (*CYCA*, *CYCB*, *alpha-AURORA kinase activator*) and cell plate-associated proteins (*KNOLLE*), in strong agreement with the described activation of cell division (Russo *et al.*, 2018) and endoreduplication (Carotenuto *et al.*, 2019) as part of the fungal accommodation response.

In the light of this data, and because fungal accommodation responses such as prepenetration apparatus (PPA) development are known to occur in the range of a few hours (Genre *et al.*, 2005), we decided to further investigate earlier responses to CO, by applying local, 6-h-long treatments to *M. truncatula* ROCs (Fig. 3) and analyzing the regulation of *MtKNOLLE* (Richter *et al.*, 2014; Russo *et al.*, 2019) and two additional cell cycle-related markers known to be expressed in early AM development, *MtAPC2*, the *alpha subunit of the Adaptor Protein complex2* (Van Damme *et al.*, 2011; Russo *et al.*, 2018) and *MtCYCL3*, a cyclin-like F-box protein (Russo *et al.*, 2019). Two additional early symbiotic markers were also analyzed: *MtPUB1* (*Plant U-box protein1*), an E3 ubiquitin ligase (Vernié *et al.*, 2016) and *MtCBF3*, a CAAT box-binding transcription factor (Hogekamp *et al.*, 2011).

As shown in Fig. 3, each gene was upregulated upon either 1 g l^{-1} , 1 mg l^{-1} , or $1\text{ }\mu\text{g l}^{-1}$ CO treatment, with 1 mg l^{-1} CO solution resulting to significantly upregulate *MtPUB1*, *MtCBF3*, *MtVapyrin*, *MtKNOLLE*, and *MtAPC2*, whereas *MtCYCL3* was significantly induced only in response to 1 g l^{-1} treatment. By comparing these results with the available data on the Noble *MtGEA V3* database (Benedito *et al.*, 2008; <https://lipm-browsers.toulouse.inra.fr/pub/expressionAtlas/app/mtgeav3>), we observed a general overlap with the regulation of the same genes during early root-fungus contact (Ortu *et al.*, 2012) and 6 h LCO treatment (Czaja *et al.*, 2012).

In conclusion, our targeted investigation of gene expression confirmed the CO-dependent activation of several early AM markers and revealed that a 6-h CO application is sufficient to activate a set of genes related to prepenetration responses. Together, this gene expression pattern corroborated our RNA-seq data and was fully compatible with the observed acceleration of AM development in CO-treated plants, providing molecular evidence in favor of a CO-dependent advance of prepenetration responses in root cells.

CO treatment stimulated prepenetration responses upon AM inoculation

We then decided to investigate the effect of CO treatment on prepenetration responses in the presence of an AM fungal

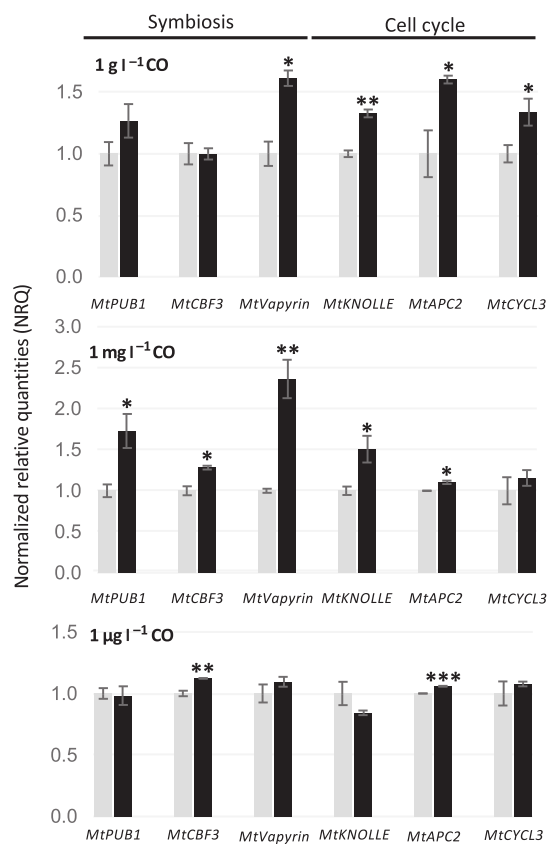


Fig. 3 Local regulation of early arbuscular mycorrhiza (AM) marker genes. Local chitoooligosaccharides (CO) treatment stimulated concentration-independent expression of several genes involved in fungal accommodation. The highest number of significantly upregulated genes was recorded upon 1 mg l^{-1} CO application. Grey bars, control, water treated roots; black bars, CO treated roots. Mean values \pm SEs of five biological replicates for each treatment are shown. Asterisks indicate statistically significant differences (Student's *t*-test): *, $P < 0.05$; **, $P < 0.01$; ***, $P < 0.001$.

inoculum. To this aim, we grew *M. truncatula* ROCs expressing GFP-HDEL in the presence of 1 mg l^{-1} CO solution (the most active concentration in our gene expression analyses) or sterile water as a control. GFP-HDEL is a fluorescent marker for the endoplasmic reticulum (ER) that has previously been used to track cytoplasmic aggregations and PPA development during AM colonization (Genre *et al.*, 2005, 2008, 2012). The asynchronous progression of hyphal development and root colonization limits our ability to fully control the timing of fungus–plant contact even using the so-called targeted inoculation method that we here adapted (Chabaud *et al.*, 2002). For this reason, observations were done at 7, 10, or 14 dpi with pregerminated *G. margarita* spores, a time frame that corresponds to hyphopodium formation and initial epidermis colonization. Using hyphopodia as a hallmark to locate plant–fungus contact sites, we focused our observations on the surrounding epidermal cells. As expected,

broad ER aggregations were observed at all time points, extending between the hyphopodium contact site and the epidermal cell nucleus, as previously described during PPA formation (Genre *et al.*, 2005). Such aggregations were observed both in the presence or in the absence of the CO treatment. Nevertheless, such PPA-related ER aggregations appeared to be more frequent in CO-treated roots, as confirmed by quantitative analysis (Fig. 4). Indeed, the percent of cells showing ER aggregations in hyphopodium-contacted areas was significantly higher in treated than untreated roots both at 7 and at 10 dpi, while the two data were comparable at 14 dpi. The major impact of CO treatment on earlier time points can be explained with the progressive decrease in residual CO concentration and/or the inhibition of new hyphopodium formation as arbuscules start developing in the inner root tissues. In this scenario, the observed significant stimulation of prepenetration responses in early time points provides a functional validation of our transcriptomic data (Table 1) and the first cellular basis for the observed CO-dependent promotion of AM colonization (Volpe *et al.*, 2020).

Long-term effects of the CO treatment

The 28 dpi time point was associated with a significant increase in plant development for MYC+CO than MYC plants (Fig. S7a). According to our previous studies (Volpe *et al.*, 2020), this is also the time of maximum AM development in our pot cultured *M. truncatula*. This was confirmed by our quantitative analysis, which also highlighted a significant promotion of AM colonization in MYC+CO compared with MYC plants (Fig. S7b). Nevertheless, when comparing MYC+CO to MYC root transcriptome and to MtExpress V3 gene expression data (Carrere *et al.*, 2021), we observed a surprising decline in the

expression of several AM markers, including transcription factors (*MtMYB* and *MtRAM2*) and arbuscule-specific phosphate (*MtPT4*) and ammonium (*MtAMT1*) transporters (Fig. 5a; Dataset S4). We suspected that this could indicate the inception of symbiosis senescence, possibly related to space limitations to root development in our pot cultures: in fact, the root system of MYC+CO plants had extended to the whole substrate volume at 28 dpi, which was not the case for MYC plants.

We therefore used confocal microscopy to image and compare arbuscule morphology in MYC and MYC+CO root samples. To obtain a more dynamic view of the colonization process, we extended our analysis to both 21 and 28 dpi. Selected roots were stained with WGA-FITC for detailed imaging of the fungal cell wall and individual arbuscules were classified into four developmental stages based on their morphological features to generate a quantitative comparison (Fig. 5b): Stage I (developing arbuscules with a limited number of large branches); Stage II (intermediate maturity, with several fine branching occupying part of the host cell lumen); Stage III (mature arbuscules, with fine branches in most of the host cell volume); Stage IV (senescent arbuscules displaying clusters of collapsed branches). As shown in the histogram of Fig. 5(b), arbuscule morphology in MYC and MYC+CO plants was comparable at 21 dpi, even if a nonsignificant decrease in Stage II and an increase in Stage IV arbuscules was observed. Interestingly, this trend became more evident – and statistically significant – at 28 dpi, where the arbuscule population in MYC+CO plants also displayed a significant increase in Stage III. At 28 dpi, this resulted in a shift in the distribution of arbuscule classes, with a maximum frequency in Stage II for MYC plants and in Stage III for MYC+CO plants. Altogether, we interpret this developmental shift as the consequence of the CO-induced advancement in fungal accommodation responses –

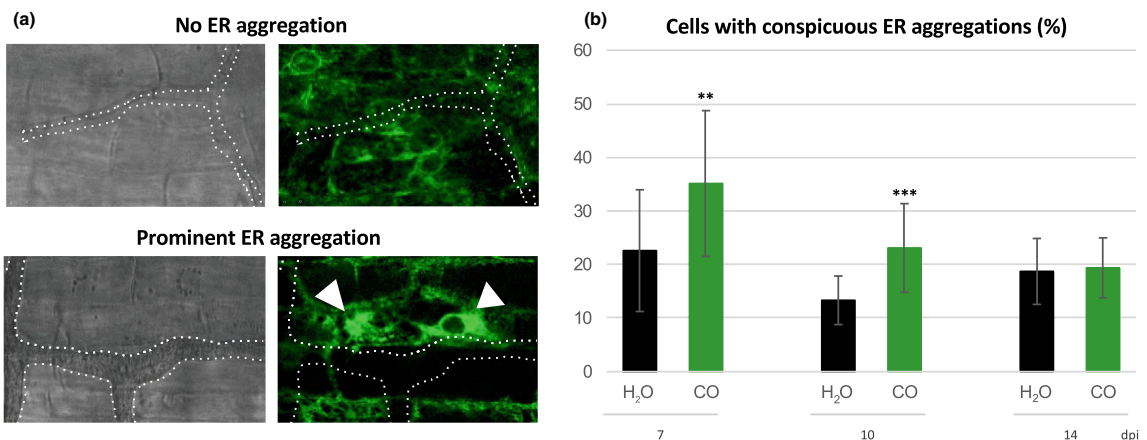


Fig. 4 Prepenetration apparatus (PPA) formation in epidermal cells of *Medicago truncatula*. Root organ cultures expressing GFP-HDEL in the endoplasmic reticulum (ER) were treated with 1 mg l^{-1} chitoooligosaccharides (CO) or water (H₂O) as control at the time of inoculation with pregerminated *Gigaspora margarita* spores. Epidermal cells in the vicinity of fungal hyphopodia (dashed white outline) were then imaged at 7, 10, 14 d postinoculation (dpi) and categorized based on the absence or presence of ER aggregations (arrowhead) (a). A statistically significant increase in the percentage of epidermal cells with prominent ER aggregation was recorded in CO-treated roots at 7 and 10 dpi (b). At least 100 independent infection events were visualized for each treatment, error bars indicate SD. Asterisks indicate statistically significant differences (Student's *t*-test): **, $P < 0.01$; ***, $P < 0.001$.

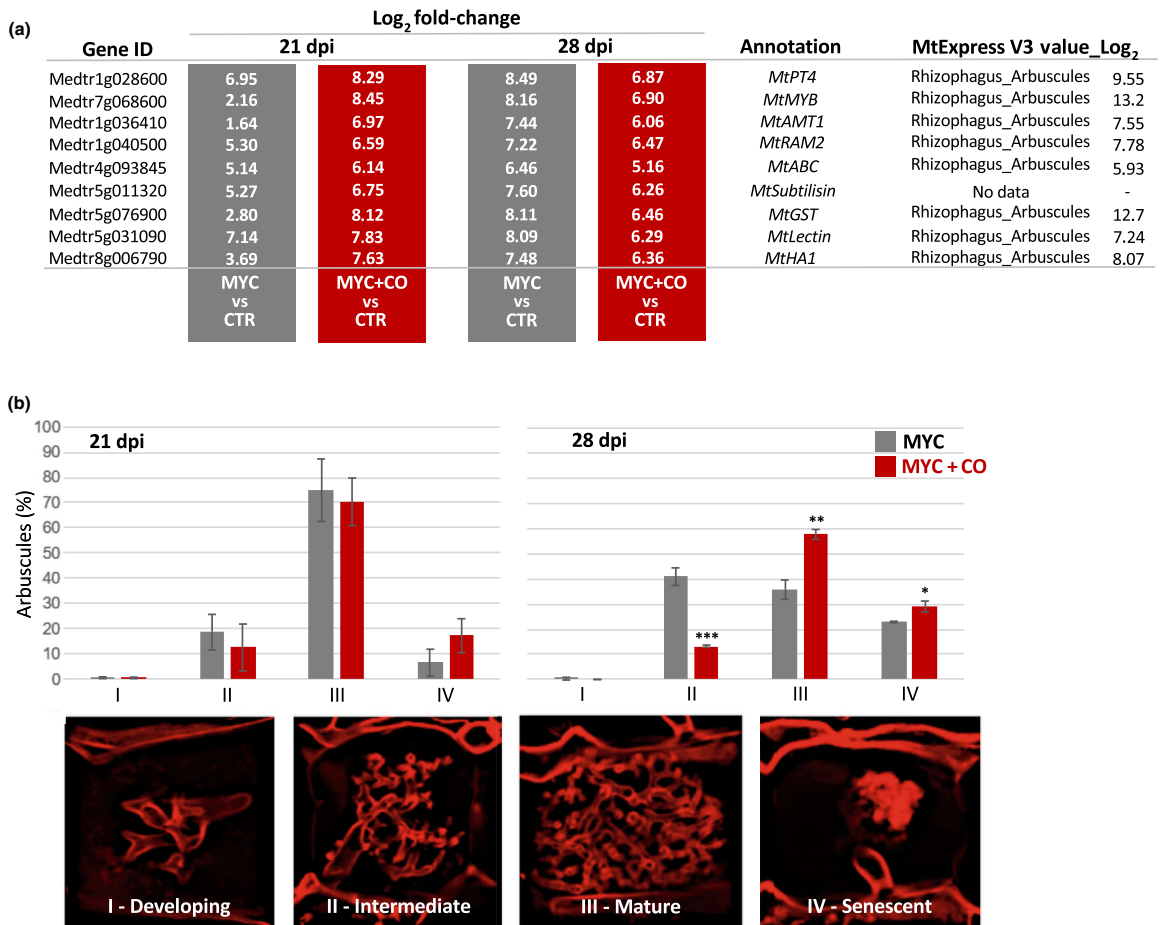


Fig. 5 Quantitative analyses of mycorrhizal phenotypes between mycorrhizal (MYC) and MYC + chitoooligosaccharides (CO) plants. (a) Expression of arbuscular mycorrhiza (AM)-induced genes increased at 21 but declined at 28 d postinoculation (dpi) in the comparison MYC + CO vs control (CTR) compared with MYC vs CTR, suggesting the onset of arbuscule senescence at the latest time point. Normalized log₂ expression values from Expression Atlas of Medicago (MtExpress V3; Reference dataset 20220901; <https://lipm-browsers.toulouse.inra.fr/pub/expressionAtlas/app/v3/>) are reported in the right column. (b) Arbuscules were imaged at 21 and 28 dpi in MYC and MYC + CO plants and classified based on their developmental stage: developing arbuscules with a trunk and very few branches (Stage I), intermediate arbuscules with thick branches (Stage II), fully mature arbuscules with abundant fine branches (Stage III), and senescent arbuscules with clusters of collapsed branches (Stage IV). A comparable distribution between MYC and MYC + CO plants was observed at 21 dpi, even if a nonsignificant reduction and increase were, respectively, observed in Stage II and Stage IV arbuscules. Such trends became statistically significant at 28 dpi, associated with an increase in the abundance of Stage III arbuscules in MYC + CO plants. Data are based on the measurements of 30 infection units for each of four biological replicates. Mean values \pm SDs of four biological replicates for each treatment are shown. Asterisks indicate statistically significant differences (Student's *t*-test): *, $P < 0.05$; **, $P < 0.01$; ***, $P < 0.001$.

as indicated by our molecular analyses and further demonstrated in epidermal cells by live cell imaging – culminating in a significant advance in arbuscule development and senescence in CO-treated plants.

CO promotion of AM development depends on DMI3

In a previous study, we demonstrated the promotion of AM colonization by CO treatment (Volpe *et al.*, 2020), confirmed also in

this study (Fig. S7b). In order to verify whether the observed effect was dependent on CSSP-mediated CO perception, we now applied the same CO treatment to *dmi3-1* mutant plants (Lévy *et al.*, 2004; Mitra *et al.*, 2004) and compared the AM phenotype at 28 dpi between treated and untreated roots. The *M. truncatula* *Dmi3* gene encodes a nuclear localized Ca²⁺ and calmodulin-dependent kinase that is a central hub of the CSSP (Choi *et al.*, 2018). Its mutation blocks AM colonization at the root epidermis. As described in the literature, the only recognizable

fungal structures associated with *dmi3-1* roots were hyphopodia, while no intraradical fungal development was observed in any of our samples, independent of the CO treatment. Furthermore, our quantitative analysis revealed a comparable abundance of hyphopodia developed in the presence or absence of the CO treatment (Fig. S8a). Such a lack of any evident effect associated with the CO treatment in the *dmi3-1* mutant, strongly suggested that the effects observed in WT plants depend on the CSSP activity.

In an additional set of experiments, we investigated the transcriptional response to COs in *dmi3-1* ROCs, by testing the expression of early AM markers (*MtPUB1*, *MtCBF3*, and *MtVapyrin*) and prepenetration-related genes (*MtKNOLLE*, *MtAPC2*, and *MtCYCL3*; Fig. S8b). The regulation of five out of those six genes (*MtCBF3*, *MtVapyrin*, *MtKNOLLE*, *MtAPC2*, and *MtCYCL3*) was comparable with that reported in the central panel of Fig. 3 for the WT. This upregulation of AM responsive genes in *dmi3* mutants exposed to AM fungal signals has indeed been reported in *M. truncatula* (Kosuta *et al.*, 2003) and rice (Gutjahr *et al.*, 2009), and interpreted as clue to the existence of alternative signaling, acting in parallel to at least one part of the CSSP. A remarkable exception is represented by *MtPUB1*, which was significantly induced in WT samples but downregulated in *dmi3-1* mutants, in line with the canonical CSSP-based model of AM signaling. This pattern of gene regulation, including *Dmi3*-dependence of *MtPUB1*, is comparable with the results of previous studies on early root-fungus contact (Ortu *et al.*, 2012) and 6 h LCO application (Czaja *et al.*, 2012).

Discussion

The main aim of this investigation was to test the hypothesis that CO stimulate symbiotic responses in the host root throughout AM development. In fact, we recently demonstrated that early CO treatment promotes root infection by AM fungi over 28–48 d (Volpe *et al.*, 2020), but a major gap was left in our understanding of the impact of CO treatment on root transcriptome, metabolism, and cellular responses throughout AM colonization.

Indeed, several studies have investigated early plant responses to exogenous treatment with AM fungal raw exudates or purified LCO and CO, revealing the rapid (< 1 h) activation of plant symbiotic signaling processes (Maillet *et al.*, 2011; Genre *et al.*, 2013) and short-term (1–48 h) transcriptional reprogramming (Czaja *et al.*, 2012; Giovannetti *et al.*, 2015; Feng *et al.*, 2019). All of these investigations were anyway analyzing plant responses occurring in the absence of any fungal inoculation.

By analyzing the root transcriptome alongside symbiosis development in a period of over four weeks following initial CO treatment, the present study breaks through this limitation. The consolidation of our gene expression analysis with functional insights generated a first, consistent outlook on CO-dependent plant responses. At any rate, our large transcriptomic dataset, combining four different conditions and four time points, remains available (link in [Data availability](#)) to drive further investigations.

Exogenous CO stimulate plant symbiotic responses throughout AM development

Our present results demonstrate that, besides the well-characterized activation of early symbiotic signaling and gene regulation, CO also influenced key symbiotic features of the host tissues from as soon as 6 h after treatment to 28 dpi. Altogether, CO impacted on the expression of root genes related to SL metabolism and transport, altered root SL content; repressed pathogenesis-related genes, and actors of effector-triggered immunity and gene pathways involved in secondary metabolism (isoflavonoid and terpenoid synthesis); increased the expression of lipid and mineral nutrient transporters, globally suggesting the reinforcement of the host response to the AM fungus and the promotion of a symbiosis-oriented metabolic and physiological context. Furthermore, CO also promoted the expression of genes involved in cell-cycle reactivation and fungus accommodation, in association with an observed induction of prepenetration responses, and caused an advance in the root colonization process that extended to 28 dpi.

In short, our experimental results indicate a general and long-lasting stimulation of symbiotic responses in both inoculated and

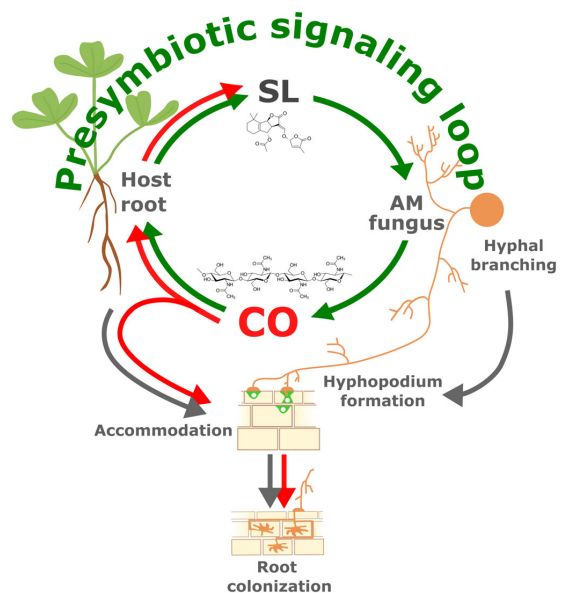


Fig. 6 Schematic representation of exogenous chitoooligosaccharides (CO) effects on arbuscular mycorrhizal (AM) symbiosis development. The perception of root-released strigolactones (SL) by AM fungi is known to induce hyphal branching and boost CO release. In turn, CO perception activates root symbiotic responses leading to intracellular fungal accommodation and symbiosis establishment (grey arrows). Our current results (red arrows) indicate that exogenous CO application further stimulates SL biosynthetic gene expression and SL accumulation in the host root, suggesting the presence of a positive feedback mechanism that we propose here as a presymbiotic signaling loop (green arrows). As an additional consequence of CO application, we also observed a stimulation of intracellular fungal accommodation, supporting the observed advance in root colonization and symbiosis development.

uninoculated CO-treated plants, demonstrating that CO have all the predicted features of Myc-factors, intended as fungal-secreted molecules that prepare the host plant to symbiosis establishment (Gutjahr & Parniske, 2013) and actively promote it.

The strange case of an unattainable love

Root exposure to fungal signaling molecules in the absence of the fungus (our CTR + CO condition) represents a markedly artificial situation. In nature, as AM fungal hyphae approach a host root, Myc-factor perception takes place alongside (or shortly before) additional, largely uncharacterized signals (Bonfante & Requena, 2011), including the physical contact between hyphae and root epidermal cells, and the subsequent development of intraradical colonization (Choi *et al.*, 2018). The progression of AM development has an impact on root responses, by transiently triggering defense reactions (García-Garrido & Ocampo, 2002; Jung *et al.*, 2012; Cameron *et al.*, 2013), progressively reducing SL synthesis and secretion (López-Ráez *et al.*, 2011; this paper) and overall outlining the context of a successful symbiotic interaction. By contrast, our CTR + CO plants lack this second set of fungal stimuli, which are crucial modulators of the host response. When interpreting the gene regulation pattern in these root samples, the presence of a certain degree of overreaction should therefore be taken into account. With this caveat, the CTR + CO condition provided the experimental tool to dissect otherwise unseen CO effects. A remarkable example of this artificial amplification of plant responses is the boosting of SL-related gene expression, which extended for a few weeks after CO treatment in CTR + CO plants. We interpret this as a climax in plant presymbiotic signaling, in a condition where physical plant–fungus interaction is not going to occur. While the biological significance of this observation can be limited, with reference to a natural context, it convincingly indicates that CO effects extend over several weeks and impact on SL content, a root feature that is directly linked to AM symbiosis establishment.

A symbiotic signaling loop?

Plants exude diverse mixtures of SL, depending on plant species, growth conditions, and developmental stages (Wang & Bouwmeester, 2018). With reference to AM signaling, DDO has been characterized as the most active molecule in *M. truncatula* (López-Ráez *et al.*, 2008; Yoneyama *et al.*, 2008; Kohlen *et al.*, 2012). In this frame, our novel observation of SL metabolism-related gene upregulation upon CO treatment is further reinforced by DDO accumulation in the root, suggesting a redirection of SL metabolism toward AM fungus-directed signals in CO-treated roots.

Furthermore, previous investigations have recorded an increase in CO release by SL-treated AM fungi (Genre *et al.*, 2013). Altogether, this suggests the existence of a positive feedback mechanism that reinforces reciprocal plant–fungus signaling in support of symbiosis establishment.

To summarize our conclusions, we propose a model – schematized in Fig. 6 – where the exogenous application of CO does not

only boost signal exchange in this symbiotic signaling loop, but also stimulates intracellular accommodation responses in the host root, facilitating fungal colonization and eventually accelerating symbiosis development.

Acknowledgements

We are grateful to David Barker and Paola Bonfante for constructive discussion and their critical revision of the manuscript draft. We also thank David Barker to kindly providing *Medicago dmi3-1* mutant seeds. This research was funded by Fondazione Cassa di Risparmio di Cuneo (Bando Ricerca Scientifica 2015 – Project AM for Quality 2015/17271). We are grateful to Erik Limpens for hosting LC in his laboratory in Wageningen for an Erasmus+ traineeship.









Competing interests

None declared.

Author contributions

VV and TM performed experiments and data analysis. MC performed data analysis and contributed figure editing and manuscript writing. AC, SC, LC and WK performed experiments. VV and AG conceived experiments and wrote the manuscript.

ORCID

Serena Capitanio  <https://orcid.org/0000-0002-1609-0499>
 Matteo Chialva  <https://orcid.org/0000-0002-6996-6642>
 Lorenzo Costamagna  <https://orcid.org/0000-0003-1129-6495>
 Andrea Crosino  <https://orcid.org/0000-0001-6219-1920>
 Andrea Genre  <https://orcid.org/0000-0001-5029-6194>
 Wouter Kohlen  <https://orcid.org/0000-0001-9057-2392>
 Teresa Mazzarella  <https://orcid.org/0000-0003-3435-3771>
 Veronica Volpe  <https://orcid.org/0000-0002-3559-7615>

Data availability

Raw RNA-seq data are openly available in the NCBI Sequence Read Archive (SRA) under BioProject accession no. PRJNA813377.

References

- Akiyama K, Matsuzaki K, Hayashi H. 2005. Plant sesquiterpenes induce hyphal branching in arbuscular mycorrhizal fungi. *Nature* 43: 824–827.
- Anders S, Pyl PT, Huber W. 2015. HTSEQ – a Python framework to work with high-throughput sequencing data. *Bioinformatics* 31: 166–169.
- Balestrini R, Bonfante P. 2014. Cell wall remodeling in mycorrhizal symbiosis: a way towards biotrophism. *Frontiers in Plant Science* 5: 237.
- Balestrini R, Cosgrove DJ, Bonfante P. 2005. Differential location of α -expansin proteins during the accommodation of root cells to an arbuscular mycorrhizal fungus. *Planta* 220: 889–899.
- Bécard G, Fortin JA. 1988. Early events of vesicular–arbuscular mycorrhiza formation on Ri T-DNA transformed roots. *New Phytologist* 108: 211–218.

- Benedito VA, Li H, Dai X, Wandrey M, He J, Kaundal R, Torres-Jerez I, Gomez SK, Harrison MJ, Tang Y *et al.* 2010. Genomic inventory and transcriptional analysis of *Medicago truncatula* transporters. *Plant Physiology* 152: 1716–1730.
- Benedito VA, Torres-Jerez I, Murray JD, Andriankaja A, Allen S, Kakar K, Wandrey M, Verdier J, Zuber H, Ott T *et al.* 2008. A gene expression atlas of the model legume *Medicago truncatula*. *The Plant Journal* 55: 504–513.
- Benjamini Y, Hochberg Y. 1995. Controlling the false discovery rate: a practical and powerful approach to multiple testing. *Journal of the Royal Statistical Society: Series B (Statistical Methodology)* 57: 289–300.
- Besserer A, Puech-Pagès V, Kiefer P, Gomez-Roldan V, Jauneau A, Roy S, Portais JC, Roux C, Bécard G, Séjalon-Delmas N. 2006. Strigolactones stimulate arbuscular mycorrhizal fungi by activating mitochondria. *PLoS Biology* 4: e226.
- Boisson-Dernier A, Chabaud M, Garcia F, Bécard G, Rosenberg C, Barker DG. 2001. *Agrobacterium rhizogenes*-transformed roots of *Medicago truncatula* for the study of nitrogen-fixing and endomycorrhizal symbiotic associations. *Molecular Plant–Microbe Interactions* 14: 695–700.
- Bonfante P, Requena N. 2011. Dating in the dark: how roots respond to fungal signals to establish arbuscular mycorrhizal symbiosis. *Current Opinion in Plant Biology* 14: 451–457.
- Cameron DD, Neal AL, van Wees SC, Ton J. 2013. Mycorrhiza-induced resistance: more than the sum of its parts. *Trends in Plant Science* 18: 539–545.
- Camps C, Jardinaud MF, Rengel D, Carrière S, Hervé C, Debelle F, Gamas P, Bensmihen S, Gough C. 2015. Combined genetic and transcriptomic analysis reveals three major signalling pathways activated by Myc-LCOs in *Medicago truncatula*. *New Phytologist* 208: 224–240.
- Carotenuto G, Volpe V, Russo G, Politi M, Sciascia I, de Almeida-Engler J, Genre A. 2019. Local endoreduplication as a feature of intracellular fungal accommodation in arbuscular mycorrhizas. *New Phytologist* 223: 430–446.
- Carrere S, Verdier J, Gamas P. 2021. MtExpress, a comprehensive and curated RNAseq-based gene expression atlas for the model legume *Medicago truncatula*. *Plant and Cell Physiology* 62: 1494–1500.
- Chabaud M, Genre A, Sieberer BJ, Faccio A, Fournier J, Novero M, Barker DG, Bonfante P. 2011. Arbuscular mycorrhizal hyphopodia and germinated spore exudates trigger Ca^{2+} spiking in the legume and nonlegume root epidermis. *New Phytologist* 189: 347–355.
- Chabaud M, Venard C, Defaux-Petras A, Bécard G, Barker DG. 2002. Targeted inoculation of *Medicago truncatula* *in vitro* root cultures reveals *MeENOD11* expression during early stages of infection by arbuscular mycorrhizal fungi. *New Phytologist* 156: 265–273.
- Choi J, Summers W, Paszkowski U. 2018. Mechanisms underlying establishment of arbuscular mycorrhizal symbioses. *Annual Review of Phytopathology* 56: 135–160.
- Crosino A, Moscato E, Blangetti M, Carotenuto G, Spina F, Bordignon S, Puech-Pagès V, Anfossi L, Volpe V, Prandi C *et al.* 2021. Extraction of short chain chitoooligosaccharides from fungal biomass and their use as promoters of arbuscular mycorrhizal symbiosis. *Scientific Reports* 11: 3798.
- Czaja LF, Hogekamp C, Lamm P, Mailet F, Martinez EA, Samain E, Dénarié J, Küster H, Hohnjec N. 2012. Transcriptional responses toward diffusible signals from symbiotic microbes reveal *MtNFP*- and *MtDMI3*-dependent reprogramming of host gene expression by arbuscular mycorrhizal fungal lipochitoooligosaccharides. *Plant Physiology* 159: 1671–1685.
- Del Fabbro C, Scalabrini S, Morgante M, Giorgi FM. 2013. An extensive evaluation of read trimming effects on Illumina NGS data analysis. *PLoS ONE* 8: e85024.
- Dobin A, Davis CA, Schlesinger F, Drenkow J, Zaleski C, Jha S, Batut P, Chaisson M, Gingeras TR. 2013. STAR: ultrafast universal RNA-seq aligner. *Bioinformatics* 29: 15–21.
- Feng F, Sun J, Radhakrishnan GV, Lee T, Bozsóki Z, Fort S, Gavrin A, Gysel K, Thygesen MB, Andersen KR *et al.* 2019. A combination of chitoooligosaccharide and lipochitoooligosaccharide recognition promotes arbuscular mycorrhizal associations in *Medicago truncatula*. *Nature Communications* 10: 5047.
- García-Garrido JM, Ocampo JA. 2002. Regulation of the plant defence response in arbuscular mycorrhizal symbiosis. *Journal of Experimental Botany* 53: 1377–1386.
- Gaude N, Bortfeld S, Duensing N, Lohse M, Krajinski F. 2012. Arbuscule-containing and non-colonized cortical cells of mycorrhizal roots undergo a massive and specific reprogramming during arbuscular mycorrhizal development. *The Plant Journal* 69: 510–528.
- Genre A, Chabaud M, Balergue C, Puech-Pagès V, Novero M, Rey T, Fournier J, Rochange S, Bécard G, Bonfante P *et al.* 2013. Short-chain chitin oligomers from arbuscular mycorrhizal fungi trigger nuclear Ca^{2+} spiking in *Medicago truncatula* roots and their production is enhanced by strigolactone. *New Phytologist* 19: 190–202.
- Genre A, Chabaud M, Faccio A, Barker DG, Bonfante P. 2008. Prepenetration apparatus assembly precedes and predicts the colonization patterns of arbuscular mycorrhizal fungi within the root cortex of both *Medicago truncatula* and *Daucus carota*. *Plant Cell* 20: 1407–1420.
- Genre A, Chabaud M, Timmers T, Bonfante P, Barker DG. 2005. Arbuscular mycorrhizal fungi elicit a novel intracellular apparatus in *Medicago truncatula* root epidermal cells before infection. *Plant Cell* 17: 3489–3499.
- Genre A, Ivanov S, Fendrych M, Faccio A, Zársky V, Bisseling T, Bonfante P. 2012. Multiple exocytotic markers accumulate at the sites of perifungal membrane biogenesis in arbuscular mycorrhizas. *Plant and Cell Physiology* 53: 244–255.
- Giovannetti M, Mari A, Novero M, Bonfante P. 2015. Early *Lotus japonicus* root transcriptomic responses to symbiotic and pathogenic fungal exudates. *Frontiers in Plant Science* 6: 480.
- Gomez-Roldan V, Ferasas B, Brewer PB, Puech-Pagès V, Dun EA, Pillot JP, Letisse F, Matusova R, Danoun S, Portais JC *et al.* 2008. Strigolactone inhibition of shoot branching. *Nature* 455: 189–194.
- Gutjahr C, Novero M, Guether M, Montanari O, Udvardi M, Bonfante P. 2009. Presymbiotic factors released by the arbuscular mycorrhizal fungus *Gigaspora margarita* induce starch accumulation in *Lotus japonicus* roots. *New Phytologist* 183: 53–61.
- Gutjahr C, Parniske M. 2013. Cell and developmental biology of arbuscular mycorrhizal symbiosis. *Annual Review of Cellular and Developmental Biology* 29: 593–617.
- Handa Y, Nishide H, Takeda N, Suzuki Y, Kawaguchi M, Saito K. 2015. RNA-seq transcriptional profiling of an arbuscular mycorrhiza provides insights into regulated and coordinated gene expression in *Lotus japonicus* and *Rhizophagus irregularis*. *Plant and Cell Physiology* 56: 1490–1511.
- Haseloff J, Siemering KR, Prasher DC, Hodge S. 1997. Removal of a cryptic intron and subcellular localization of green fluorescent protein are required to mark transgenic Arabidopsis plants brightly. *Proceedings of the National Academy of Sciences, USA* 94: 2122–2127.
- Hewitt EJ. 1966. Sand and water culture methods used in the study of plant nutrition. *Experimental Agriculture* 3: 104.
- Hogekamp C, Arndt D, Pereira PA, Becker JD, Hohnjec N, Küster H. 2011. Laser microdissection unravels cell-type-specific transcription in arbuscular mycorrhizal roots, including CAAT-box transcription factor gene expression correlating with fungal contact and spread. *Plant Physiology* 157: 2023–2043.
- Hogekamp C, Küster H. 2013. A roadmap of cell-type specific gene expression during sequential stages of the arbuscular mycorrhiza symbiosis. *BMC Genomics* 14: 306.
- Hohnjec N, Vieweg MF, Pühler A, Becker A, Küster H. 2005. Overlaps in the transcriptional profiles of *Medicago truncatula* roots inoculated with two different *Glomus* fungi provide insights into the genetic program activated during arbuscular mycorrhiza. *Plant Physiology* 137: 1283–1301.
- Jung SC, Martínez-Medina A, Lopez-Raez JA, Pozo MJ. 2012. Mycorrhiza-induced resistance and priming of plant defenses. *Journal of Chemical Ecology* 38: 651–664.
- Keymer A, Pimpririk P, Wewer V, Huber C, Brands M, Bucierius SL, Delaux PM, Klingl V, Röpenack-Lahaye EV, Wang TL *et al.* 2017. Lipid transfer from plants to arbuscular mycorrhiza fungi. *eLife* 6: e29107.
- Kohlen W, Charnikhova T, Lammers M, Pollina T, Tóth P, Haider I, Pozo MJ, de Maagd RA, Ruyter-Spira C, Bouwmeester HJ *et al.* 2012. The tomato CAROTENOID CLEAVAGE DIOXYGENASE8 (SICCD8) regulates rhizosphere signaling, plant architecture and affects reproductive development through strigolactone biosynthesis. *New Phytologist* 196: 535–547.
- Kosuta S, Chabaud M, Lounson G, Gough C, Dénarié J, Barker DG, Bécard G. 2003. A diffusible factor from arbuscular mycorrhizal fungi induces symbiosis-

- specific MtENOD11 expression in roots of *Medicago truncatula*. *Plant Physiology* 131: 952–962.
- Küster H, Hohnjec N, Krajinski F, El Yahyaoui F, Manthey K, Gouzy J, Dondrup M, Meyer F, Kalinowski J, Brechenmacher L *et al.* 2004. Construction and validation of cDNA-based Mt6k-RIT macro- and microarrays to explore root endosymbioses in the model legume *Medicago truncatula*. *Journal of Biotechnology* 108: 95–113.
- Lévy J, Bres C, Geurts R, Chalhoub B, Kulikova O, Duc G, Journet EP, Ané JM, Lauber E, Bisseling T *et al.* 2004. A putative Ca^{2+} and calmodulin-dependent protein kinase required for bacterial and fungal symbioses. *Science* 303: 1361–1364.
- Liu J, Blaylock LA, Endre G, Cho J, Town CD, VandenBosch KA, Harrison MJ. 2003. Transcript profiling coupled with spatial expression analyses reveals genes involved in distinct developmental stages of an arbuscular mycorrhizal symbiosis. *Plant Cell* 15: 2106–2123.
- Liu W, Kohlen W, Lillo A, Op den Camp R, Ivanov S, Hartog M, Limpens E, Jamil M, Smaczniak C, Kaufmann K. 2011. Strigolactone biosynthesis in *Medicago truncatula* and rice requires the symbiotic GRAS-type transcription factors NSP1 and NSP2. *Plant Cell* 23: 3853–3865.
- López-Ráez JA, Charnikhova T, Fernández I, Bouwmeester H, Pozo MJ. 2011. Arbuscular mycorrhizal symbiosis decreases strigolactone production in tomato. *Journal of Plant Physiology* 168: 294–297.
- López-Ráez JA, Charnikhova T, Mulder P, Kohlen W, Bino R, Levin I, Bouwmeester H. 2008. Susceptibility of the tomato mutant *high pigment-2^{hc}* (*hp-2^{hc}*) to *Orobanche* spp. infection. *Journal of Agricultural and Food Chemistry* 56: 6326–6332.
- Love MI, Huber W, Anders S. 2014. Moderated estimation of fold change and dispersion for RNA-seq data with DESeq2. *Genome Biology* 15: 550.
- Luginbuehl LH, Menard GN, Kurup S, Van Erp H, Radhakrishnan GV, Breakspear A, Oldroyd GED, Eastmond PJ. 2017. Fatty acids in arbuscular mycorrhizal fungi are synthesized by the host plant. *Science* 356: 1175–1178.
- Luginbuehl LH, Oldroyd G. 2017. Understanding the arbuscule at the heart of endomycorrhizal symbioses in plants. *Current Biology* 27: R952–R963.
- Luo W, Brouwer C. 2013. PATHVIEW: an R/bioconductor package for pathway-based data integration and visualization. *Bioinformatics* 29: 1830–1831.
- MacLean AM, Bravo A, Harrison MJ. 2017. Plant signaling and metabolic pathways enabling arbuscular mycorrhizal symbiosis. *Plant Cell* 29: 2319–2335.
- Maillet F, Poinot V, André O, Puech-Pagès V, Haouy A, Gueunier M, Cromer L, Giraudet D, Formey D, Niebel A *et al.* 2011. Fungal lipochitoooligosaccharide symbiotic signals in arbuscular mycorrhiza. *Nature* 469: 58–63.
- Martin M. 2011. Cutadapt removes adapter sequences from high-throughput sequencing reads. *EMBnet Journal* 17: 10–12.
- Mitra RM, Gleason CA, Edwards A, Hadfield J, Downie JA, Oldroyd GE, Long SR. 2004. A Ca^{2+} /calmodulin-dependent protein kinase required for symbiotic nodule development: gene identification by transcript-based cloning. *Proceedings of the National Academy of Sciences, USA* 30: 4701–4705.
- Müller LM, Flokova K, Schnabel E, Sun X, Fei Z, Frugoli J, Bouwmeester HJ, Harrison MJ. 2019. A CLE-SUNN module regulates strigolactone content and fungal colonization in arbuscular mycorrhiza. *Nature Plants* 5: 933–939.
- Nasir F, Bahadur A, Lin X, Gao Y, Tian C. 2021. Novel insights into host receptors and receptor-mediated signaling that regulate arbuscular mycorrhizal symbiosis. *Journal of Experimental Botany* 72: 1546–1557.
- Oksanen J, Blanchet FG, Friendly M, Kindt R, Legendre P, McGlenn D, Minchin PR, O'Hara RB, Simpson GL, Solyom P *et al.* 2019. *VEGAN: community ecology package*. R package v.2.5-5. [WWW document] URL <https://CRAN.R-project.org/package=vegan> [accessed 27 April 2022].
- Ortu G, Balestrini R, Pereira PA, Becker JD, Küster H, Bonfante P. 2012. Plant genes related to gibberellin biosynthesis and signaling are differentially regulated during the early stages of AM fungal interactions. *Molecular Plant* 5: 951–954.
- Pimprikar P, Gutjahr C. 2018. Transcriptional regulation of arbuscular mycorrhiza development. *Plant and Cell Physiology* 59: 673–690.
- R Core Team. 2020. *R: a language and environment for statistical computing*. Vienna, Austria: R Foundation for Statistical Computing. [WWW document] URL <https://www.R-project.org/> [accessed 31 May 2021].
- Richter S, Kientz M, Brumm S, Nielsen ME, Park M, Gavidia R, Krause C, Voss U, Beckmann H, Mayer U *et al.* 2014. Delivery of endocytosed proteins to the cell-division plane requires change of pathway from recycling to secretion. *eLife* 3: e02131.
- Russo G, Carotenuto G, Fiorilli V, Volpe V, Chiapello M, Van Damme D, Genre A. 2018. Ectopic activation of cortical cell division during the accommodation of arbuscular mycorrhizal fungi. *New Phytologist* 221: 1036–1048.
- Russo G, Carotenuto G, Fiorilli V, Volpe V, Faccio A, Bonfante P, Chabaud M, Chiapello M, Van Damme D, Genre A. 2019. TPLATE recruitment reveals endocytic dynamics at sites of symbiotic interface assembly in arbuscular mycorrhizal interactions. *Frontiers in Plant Science* 10: 1628.
- Salzer P, Bonanomi A, Beyer K, Vögeli-Lange R, Aeschbacher RA, Lange JAW, Kim D, Cook DR, Bolter T. 2000. Differential expression of eight chitinase genes in *Medicago truncatula* roots during mycorrhiza formation, nodulation, and pathogen infection. *Molecular Plant–Microbe Interactions* 13: 763–777.
- Sanchez L, Weidmann S, Brechenmacher L, Batoux M, van Tuinen D, Lemanceau P, Gianinazzi S, Gianinazzi-Pearson V. 2004. Common gene expression in *Medicago truncatula* roots in response to *Pseudomonas fluorescens* colonization, mycorrhiza development and nodulation. *New Phytologist* 161: 855–863.
- Schwacke R, Ponce-Soto GY, Krause K, Bolger AM, Arsova B, Hallab A, Gruden K, Stitt M, Bolger ME, Usadel B. 2019. MAPMAN4: a refined protein classification and annotation framework applicable to multi-omics data analysis. *Molecular Plant* 12: 879–892.
- Sieberer BJ, Chabaud M, Timmers AC, Monin A, Fournier J, Barker DG. 2009. A nuclear-targetedameleon demonstrates intranuclear Ca^{2+} spiking in *Medicago truncatula* root hairs in response to rhizobial nodulation factors. *Plant Physiology* 151: 1197–1206.
- Smith SE, Read DJ. 2008. *Mycorrhizal symbiosis*. San Diego, CA, USA: Academic Press.
- Spatafora JW, Chang Y, Benny GL, Lazarus K, Smith ME, Berbee ML, Bonito G, Corradi N, Grigoriev I, Gryganskyi A *et al.* 2016. A phylum-level phylogenetic classification of zygomycete fungi based on genome-scale data. *Mycologia* 108: 1028–1046.
- Sun J, Miller JB, Granqvist E, Wiley-Kalil A, Gobatto E, Maillet F, Cottaz S, Samain E, Venkateshwaran M, Fort S *et al.* 2015. Activation of symbiosis signaling by arbuscular mycorrhizal fungi in legumes and rice. *Plant Cell* 27: 823–838.
- Tang H, Krishnakumar V, Bidwell S, Rosen B, Chan A, Zhou S, Gentzblatt L, Childs KL, Yandell M, Gundlach H *et al.* 2014. An improved genome release (v.Mt4.0) for the model legume *Medicago truncatula*. *BMC Genomics* 15: 312.
- Tokunaga T, Hayashi H, Akiyama K. 2015. Medicoal, a strigolactone identified as a putative dihydro-orobanchol isomer, from *Medicago truncatula*. *Phytochemistry* 111: 91–97.
- Trouvelot A, Kough JL, Gianinazzi-Pearson V. 1986. Mesure du taux de mycorhization VA d'un système racinaire. Recherche de méthodes d'estimation ayant une signification fonctionnelle. In: Gianinazzi-Pearson V, Gianinazzi S, eds. *Physiological and genetical aspects of mycorrhizae*. Paris, France: INRA, 217–221.
- Umehara M, Hanada A, Yoshida S, Akiyama K, Arite T, Takeda-Kamiya N, Magome H, Kamiya Y, Shirasu K, Yoneyama K *et al.* 2008. Inhibition of shoot branching by new terpenoid plant hormones. *Nature* 455: 195–200.
- Usadel B, Nagel A, Thimm O, Redestig H, Blaesing OE, Palacios-Rojas N, Selbig J, Hannemann J, Piques MC, Steinhauser D *et al.* 2005. Extension of the visualization tool MAPMAN to allow statistical analysis of arrays, display of corresponding genes, and comparison with known responses. *Plant Physiology* 138: 1195–1204.
- Van Damme D, Gadeyne A, Vanstraelen M, Inze D, Van Montagu MC, De Jaeger G, Russinova E, Geelen D. 2011. Adaptin-like protein TPLATE and clathrin recruitment during plant somatic cytokinesis occurs via two distinct pathways. *Proceedings of the National Academy of Sciences, USA* 108: 615–620.
- Vernié T, Camut S, Camps C, Remblière C, de Carvalho-Niebel F, Mbengue M, Timmers T, Gascioli V, Thompson R, le Signor C *et al.* 2016. PUB1 interacts with the receptor kinase DMI2 and negatively regulates rhizobial and arbuscular mycorrhizal symbioses through its ubiquitination activity in *Medicago truncatula*. *Plant Physiology* 170: 2312–2324.

- Volpe V, Carotenuto G, Berzero C, Cagnina L, Puech-Pagès V, Genre A. 2020. Short chain chitooligosaccharides promote arbuscular mycorrhizal colonization in *Medicago truncatula*. *Carbohydrate Polymers* 229: 115505.
- Wang Y, Bouwmeester HJ. 2018. Structural diversity in the strigolactones. *Journal of Experimental Botany* 69: 2219–2230.
- Waters MT, Gutjahr C, Bennett T, Nelson DC. 2017. Strigolactone signaling and evolution. *Annual Review of Plant Biology* 68: 291–322.
- Wewer V, Brands M, Dörmann P. 2014. Fatty acid synthesis and lipid metabolism in the obligate biotrophic fungus *Rhizopogon irregularis* during mycorrhization of *Lotus japonicus*. *The Plant Journal* 79: 398–412.
- Wickham H. 2016. *GGPLOT2: elegant graphics for data analysis, 2nd edn*. Cham, Switzerland: Springer International.
- Yoneyama K, Xie X, Sekimoto H, Takeuchi Y, Ogasawara S, Akiyama K, Hayashi H, Yoneyama K. 2008. Strigolactones, host recognition signals for root parasitic plants and arbuscular mycorrhizal fungi, from Fabaceae plants. *New Phytologist* 179: 484–494.
- Young MD, Wakefield MJ, Smyth GK, Oshlack A. 2010. Gene ontology analysis for RNA-seq: accounting for selection bias. *Genome Biology* 11: R14.
- Young ND, Debellé F, Oldroyd GE, Geurts R, Cannon SB, Udvardi MK, Benedito VA, Mayer KF, Gouzy J, Schoof H *et al.* 2011. The *Medicago* genome provides insight into the evolution of rhizobial symbioses. *Nature* 480: 520–524.
- Zipfel C, Oldroyd GE. 2017. Plant signaling in symbiosis and immunity. *Nature* 543: 328–336.

Supporting Information

Additional Supporting Information may be found online in the Supporting Information section at the end of the article.

- Dataset S1** RNA-seq-based expression data for all genes expressed in CCO vs C during time-course experiment.
- Dataset S2** RNA-seq-based expression data for all genes expressed in M vs C during time-course experiment.
- Dataset S3** RNA-seq-based expression data for all genes expressed in MCO vs C during time-course experiment.
- Dataset S4** RNA-seq-based expression data for all genes expressed in MCO vs M during time-course experiment.
- Dataset S5** Gene Ontology functional enrichments ($P_{\text{adj}} < 0.1$) of DEGs list in CTR+CO vs CTR.
- Dataset S6** Gene Ontology functional enrichments ($P_{\text{adj}} < 0.1$) of DEGs list in MYC vs CTR.

Dataset S7 Gene Ontology functional enrichments ($P_{\text{adj}} < 0.1$) of DEGs list in MYC + CO vs CTR.

Dataset S8 Gene Ontology functional enrichments ($P_{\text{adj}} < 0.1$) of DEGs list in MYC+CO vs MYC.

Fig. S1 RNA-seq and qRT-PCR data correlation.

Fig. S2 Gene Ontology enrichment analysis in the comparison MYC vs CTR at 10 and 28 dpi.

Fig. S3 Gene Ontology enrichment analysis in the comparison CTR + CO vs CTR at 10 dpi.

Fig. S4 Gene Ontology enrichment analysis in the comparison MYC + CO vs CTR at 10 and 28 dpi.

Fig. S5 Gene Ontology enrichment analysis in the comparison MYC + CO vs MYC at 10 and 28 dpi.

Fig. S6 Gene regulation pattern in CTR + CO and MYC plants compared with CTR.

Fig. S7 Morphological analysis in mycorrhized plants.

Fig. S8 CO responses in *dmi3-1* mutants.

Table S1 Summary statistics for the Illumina sequencing and mapping against *M. truncatula* genome assembly, v.4.1.

Table S2 List of overrepresented MapMan functional categories.

Table S3 List of primers used for RNA-seq validation experiments.

Table S4 List of primers used for qRT-PCR experiments.

Please note: Wiley is not responsible for the content or functionality of any Supporting Information supplied by the authors. Any queries (other than missing material) should be directed to the *New Phytologist* Central Office.

CHAPTER 3

Production and application of exogenous COs

Prologue

As mentioned in the previous chapters, COs are among the elicitors of AM-specific activation of the CSSP. The first evidence in favor of their function as AM symbiosis signals emerged from the results of a treatment with chitinase on *Gigaspora margarita* exudate that completely abolished the typical Ca^{2+} spiking response in the host epidermis (Genre et al., 2013). The authors went on to test the ability of COs of various length to elicit Ca^{2+} spiking and it was found that CO4 and CO5 are the best elicitors of spiking patterns that resembled the irregular spiking triggered by AM spore exudates. (Genre et al. 2013).

The great availability of chitin in nature, opens the way to the potential large-scale CO production and their use in agronomic context. Currently, commercial COs are obtained from fishing waste processing industries, hydrolyzing chitin and chitosan derived from shrimp shells. However, their production costs make the use of purified shrimp shell COs not practical for large-scale applications, because of several issues such as seasonality, environmental sustainability and the presence of additional chemical steps due to the exoskeleton nature (e.g. decalcification, demineralization). In order to overcome these essential problems, other chitin sources might be used, for example fungal walls. In fact, the cell wall of filamentous fungi contains up to 10–30% of chitin in dry weight (Lodhi et al. 2014.). Furthermore, fungal chitin can be extracted from mycelial waste, which is almost costless and easy to obtain in large quantities from fungal fermentation industries.

The fungal cell wall

Fungal cell wall is substantially made up of glucans, chitin and chitosan. The percentage of each element may vary depending on the different fungal phylum considered.

Glucans

Glucans are part of a heterogeneous group of polymers composed by glucose units forming a linear chain. In fungal cell wall, glucans are found in two different forms: α -glucans and β -glucans. The majority of α -glucans are linked through a α -1,3-bond, this linkage confers water insolubility to the glucan chain.

β -1,3-glucan represents the most abundant β -glucan found in fungal walls, which links to β -1,6-glucan to form ramified polysaccharides, conferring a gelatinous texture to the cell wall (Fesel & Zuccaro, 2016).

Chitin and chitosan

Chitin is the main component of the fungal cell wall. It is also present in arthropods exoskeleton (crustaceans and insects), in the radula of mollusks and in the gladius of cephalopods (Lodhi et al. 2014.). In fungal cell wall, chitin is often associated to β -glucans and proteins forming a stratified polysaccharidic matrix (Fesel & Zuccaro, 2016). After cellulose, chitin is the most abundant biopolymer in nature. Chemically, chitin is synthesized from units of N-acetyl-D-glucosamine (NAG). These units form covalent β -(1 \rightarrow 4)-linkages (Lodhi et al. 2014). Chitin is insoluble both in water and organic solvents due to its high crystallinity degree.

Chitosan, the deacetylated form of chitin, is also present in fungal cell wall. This compound is more common in mucoromycetes than in ascomycetes and basidiomycetes: many fungi, in fact, catalyze chitin conversion to chitosan deacetylating NAG units thanks to chitin deacetylase enzymes (Grifoll-Romero et al., 2018).

The experimental activities of this research line aimed at purifying COs from fungal mycelia by chitin purification and chemical hydrolysis, with the subsequent evaluation of the bioactivity of extracted COs as Myc factors. For my experiments I used mycelial biomass from the basidiomycete *Pleurotus ostreatus* (chosen for its high chitin content

in the cell wall), the mucoromycete *Cunninghamella bertholletiae* (for its growth speed) and the ascomycete *Trichoderma viride* (considered a safe fungus for field application). The bioactivity of purified putative COs was evaluated through their ability to trigger nuclear Ca^{2+} spiking in the root atrichoblasts of *Medicago truncatula*. A potted-system experiment, using *M. truncatula* plants and extracted COs coupled with the AM fungus *Funelliformis mosseae*, was also performed.

References

- Fesel PH & Zuccaro A. 2016. β -glucan: Crucial component of the fungal cell wall and elusive MAMP in plants. *Fungal Genetics and Biology* 90: 53–60. Doi: <http://dx.doi.org/10.1016/j.fgb.2015.12.004>.
- Genre A, Chabaud M, Balzergue C, Puech-Pagés V, Novero M, Rey T, Fournier J, Rochange S, Bécard G, Bonfante P et al. 2013. Short-chain chitin oligomers from arbuscular mycorrhizal fungi trigger nuclear Ca^{2+} spiking in *Medicago truncatula* roots and their production is enhanced by strigolactone. *New Phytologist* 19: 190–202.
- Grifoll-Romero L, et al. 2018. Chitin deacetylases: structures, specificities, and biotech applications. *Polymers (Basel)*. 10(4):352. doi:10.3390/polym10040352.
- Lodhi, G., et al. 2014. Chitooligosaccharide and Its derivatives: preparation and biological applications. *BioMed Res Int*, ID 654913. doi:10.1155/2014/654913.

Extraction of short chain chitooligosaccharides from fungal biomass and their use as promoters of arbuscular mycorrhizal symbiosis

This paper was published as:

Crosino, A., Moscato, E., Blangetti, M. et al. Extraction of short chain chitooligosaccharides from fungal biomass and their use as promoters of arbuscular mycorrhizal symbiosis. *Sci Rep* 11, 3798 (2021). <https://doi.org/10.1038/s41598-021-83299-6>



OPEN

Extraction of short chain chitooligosaccharides from fungal biomass and their use as promoters of arbuscular mycorrhizal symbiosis

Andrea Crosino¹, Elisa Moscato¹, Marco Blangetti², Gennaro Carotenuto¹, Federica Spina¹, Simone Bordignon², Virginie Puech-Pagès³, Laura Anfossi², Veronica Volpe¹, Cristina Prandi², Roberto Gobetto², Giovanna Cristina Varese¹ & Andrea Genre¹✉

Short chain chitooligosaccharides (COs) are chitin derivative molecules involved in plant-fungus signaling during arbuscular mycorrhizal (AM) interactions. In host plants, COs activate a symbiotic signalling pathway that regulates AM-related gene expression. Furthermore, exogenous CO application was shown to promote AM establishment, with a major interest for agricultural applications of AM fungi as biofertilizers. Currently, the main source of commercial COs is from the shrimp processing industry, but purification costs and environmental concerns limit the convenience of this approach. In an attempt to find a low cost and low impact alternative, this work aimed to isolate, characterize and test the bioactivity of COs from selected strains of phylogenetically distant filamentous fungi: *Pleurotus ostreatus*, *Cunninghamella bertholletiae* and *Trichoderma viride*. Our optimized protocol successfully isolated short chain COs from lyophilized fungal biomass. Fungal COs were more acetylated and displayed a higher biological activity compared to shrimp-derived COs, a feature that—alongside low production costs—opens promising perspectives for the large scale use of COs in agriculture.

Agriculture is experiencing an urgent need to shift toward low-input practices that can be integrated with the environment and aim at food safety for the growing human population. Arbuscular mycorrhizal (AM) fungi can play a key role in this scenario⁴. AM is the most widespread plant symbiosis, in terms of geographical distribution and phylogenetic coverage in the plant kingdom¹. In this mutualistic symbiosis, part of the plant sugars and lipids are fed to the fungus², while soil mineral nutrients and water are scavenged by the extraradical mycelium and transferred to the plant, improving its fitness¹.

AM symbiosis plays a central ecological role in the functioning of natural ecosystems, but most crop plants establish this beneficial interaction too⁴. In this context, the potential use of AM fungi in sustainable production under low chemical input conditions is currently raising a broad interest in agronomic context³. Promoting and maintaining functional and persistent mycorrhizal symbioses in crop fields to improve soil quality and productivity requires proper management of agroecosystems with strategies that include shallow tillage, low fertilizer input, perennial crop development, as well as AM promotion with fungal inoculation and treatments that stimulate symbiosis establishment^{4,5}.

Plants interact with a multitude of microbes and their ability to recognize them and deploy appropriate responses is largely based on the recognition of microbe-specific molecules known as microbe-associated molecular patterns⁶. Among them, long-chain oligomers of chitin—which is the main fibrillar component of fungal cell wall—are strong elicitors of plant defense responses^{7–9}. The perception of long-chain chito-oligomers such as chitooctaose (composed of 8 N-acetyl-glucosamine residues) activates powerful defense strategies of the plant, such as the release of chitinases, phytoalexins, reactive oxygen species and callose deposition in the cell wall¹⁰.

Other chitin-related molecules are known to play a signalling role in symbiosis as so-called mycorrhizal factors, or Myc-factors. Among them, tetra/penta-chito-oligosaccharides (CO4-5) activate symbiotic signalling in all tested dicot and monocot AM hosts^{11,12}. The plant signal transduction pathway mediating Myc-factor

¹Department of Life Science and Systems Biology, University of Turin, 10125 Turin, Italy. ²Department of Chemistry, University of Turin, 10125 Turin, Italy. ³Laboratoire de Recherche en Sciences Végétales, Université de Toulouse, CNRS, UPS, 31320 Castanet-Tolosan, France. ✉email: andrea.genre@unito.it

	Chitin		Chitosan		COs	
	g	%	g	%	g	%
<i>Pleurotus ostreatus</i>	3.7	24.7	0.006	0.04	0.202	6.70
<i>Cunninghamella bertholletiae</i>	1.2	8.30	0.027	0.18	0.362	29.20
<i>Trichoderma viride</i>	2.6	17.30	0.039	0.26	0.042	1.70

Table 1. Chitin, chitosan and CO yield from each of the three fungi. Yields are expressed as both dry mass (g) and percentage values (%) of the starting fungal dry biomass (for chitin and chitosan) or the starting chitin amount (for COs).

recognition includes the activation of intense oscillations in Ca^{2+} concentration in the nuclei of root epidermal cells¹³, which is now commonly used as a hallmark of Myc-factor perception^{13,14}.

Myc-factors activate plant symbiotic responses ranging from gene regulation to metabolic and developmental changes^{15,16} that have been defined as part of an anticipation program preparing the host to a successful association¹⁷. Furthermore, the application of exogenous COs was recently demonstrated to stimulate lateral root development and branching in *Oryza sativa*¹³ and AM establishment in the model legume *Medicago truncatula*⁴, paving the way to possible use of CO treatments to promote AM in agricultural applications.

Currently, commercial COs of different length are obtained from fishing waste processing industries, mainly through hydrolysis of shrimp shell-derived chitin and chitosan^{18,19}. Seasonal availability, environmental concerns and purification costs are the main drawbacks of the use of shrimp-derived COs in large-scale applications. An alternative, more sustainable and cheaper source of COs are fungal biomass wastes from fermentation industries. In fact, in spite of having lower chitin content than crustaceans (10–26% as a chitin-glucan complex), fungal biomass does not need aggressive acid treatments—normally required for the removal of calcium carbonate and other minerals from crustacean shells—prior to CO extraction. Furthermore fungal biomass production is not subject to seasonal and regional limitations¹⁹.

Here we present a protocol (see Supplementary Fig. S1 online) to efficiently extract COs from fungal biomass of different origin (*Pleurotus ostreatus*, *Cunninghamella bertholletiae* and *Trichoderma viride*); we confirm the chemical properties of the extracted COs and demonstrate their stronger biological activity as promoters of AM symbiosis when compared with commercial COs.

Results

Extraction yields. When grown on a standard medium (liquid malt extract), *P. ostreatus* provided the highest amount of mycelium with a yield of 10 g/L. The quantity of products obtained after the extraction of chitosan and chitin and after chitin acid hydrolysis are shown in Table 1. The amount of chitin extracted varied among species, with *P. ostreatus* biomass displaying the highest yield in chitin (24.7%). All tested fungi presented a low yield in chitosan, ranging between 0.26 and 0.04% of the starting biomass.

Due to the very limited amount of extracted chitosan, only chitin was treated by acid hydrolysis for CO production. The yield in putative COs was 6.70% of the starting chitin amount for *P. ostreatus*, 29.20% for *C. bertholletiae* and 1.70% for *T. viride*.

Altogether, putative CO yield resulted to be 1.65% of the original mycelium dry weight for *P. ostreatus*, 3.69% for *C. bertholletiae* and 0.30% for *T. viride* (Table 1). By combining growth speed, biomass, chitin and CO yield and lower CO polymerization (max CO6), we decided to use COs from *P. ostreatus*, which is also considered as a GRAS (Generally Recognized As Safe) organism, for all subsequent pot culture analyses.

Extracted samples contain COs of the expected size and acetylation degree. Direct infusion mass spectrometry (DIMS) indicated that the extracted samples contained acetylated and de-acetylated COs with length comprised between 2 and 7 residues (see Supplementary Fig. S2 online). Pseudo-molecular ions $[\text{M} + \text{H}^+]$ of COs composed of 2 to 7 N-acetyl-glucosamine residues were detected, while double-charged ions and longer chains, if existing, were below the limit of detection of the system.

High-performance liquid chromatography-Mass spectrometry (HPLC-MS/MS) analysis of the CO mixture (see Supplementary Fig. S3 online) confirmed that our extracted samples contained fully acetylated, mono-deacetylated and di-deacetylated CO molecules composed of 2 to 5 N-acetyl-glucosamine residues.

Solid-State Nuclear Magnetic Resonance (¹³C CPMAS SSNMR) was used to characterize the materials under study, while solution ¹H NMR was applied for the determination of percent acetylation for each CO sample^{20,21}. Figure 1 shows the ¹³C CPMAS SSNMR spectra of COs from *C. bertholletiae*, *P. ostreatus*, *T. viride* and shrimps. Both *C. bertholletiae* and shrimp CO spectra exhibited wider and less sharp spikes than those present in *P. ostreatus* and *T. viride* spectra. These differences indicated that *C. bertholletiae* and shrimp COs were composed of a heterogeneous mix of COs containing a different number of N-acetyl-D-glucosamine units, whereas *P. ostreatus* and *T. viride* COs appeared to have a more uniform composition in terms of molecule length. *C. bertholletiae* COs and shrimp shell COs only differed in the acetylation degree, which resulted to be higher in *C. bertholletiae* COs. Overall, SSNMR spectra, albeit intrinsically not quantitative, suggested rather diverse degrees of acetylation for the four samples, with the lowest acetyl peaks for shrimp-derived and the tallest for *T. viride*-derived COs.

This prompted us to investigate CO acetylation in more detail through solution ¹H NMR analyses. To this aim we also prepared a batch of peracetylated shrimp COs by increasing their acetylation degree with a treatment in

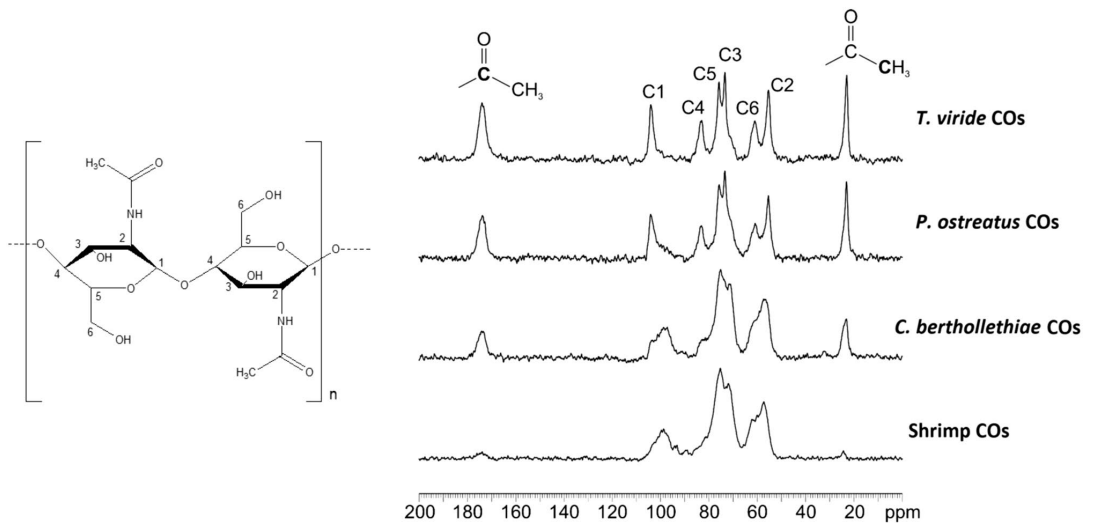


Figure 1. ^{13}C CPMAS SSNMR spectra of chitoooligosaccharides from *T. viride*, *P. ostreatus*, *C. bertholletiae* and shrimps, acquired at room temperature at a spinning speed of 20 kHz. The labels of carbon atoms (C1–C6) refer to the scheme on the left. The spectra indicate that the four samples are characterized by different degrees of acetylation; in particular, this is lowest in shrimp-derived COs and highest in *T. viride*-derived COs.

acetic acid (see “Methods” section). Figure 2 and Supplementary Fig. S4 display the ^1H spectra of the analyzed samples. In order to quantify the acetylation degree (AD) and compare it among samples, the signals ascribable to protons in the polymeric chain were normalized at 100.0, so that the integrals for acetyl groups could directly represent percent values of acetylation, as reported in Table 2. Solution NMR results confirmed the assumption from the solid-state analysis: *T. viride* resulted to provide the most acetylated COs (AD = 45%), followed by *P. ostreatus* (AD = 31.7%) and *C. bertholletiae* (AD = 19.4%). The analysis also confirmed the efficiency of N-acetylation on shrimp COs, indicating a significant increase in their AD from 3.8 to 19.7%. In conclusion, a combination of chemical analyses confirmed the presence of short chain COs in the extracted samples and the efficiency of our N-acetylation protocol on the otherwise poorly acetylated shrimp-derived commercial COs.

Extracted COs are active as symbiotic signals. Each CO sample was tested for its ability to elicit symbiotic signalling in an AM host plant. To this aim, 1 mg/L CO solutions were applied to *M. truncatula* root organ cultures (ROCs) expressing the NUP-YC2.1 probe (see “Methods” section), and nuclear Ca^{2+} signals were recorded in epidermal cells by live confocal imaging. As expected, control treatments with sterile distilled water did not activate any variation in nuclear Ca^{2+} concentration. On the contrary, repeated nuclear Ca^{2+} oscillations (spiking) were observed in atrichoblasts upon treatment with all CO solutions (Fig. 3).

In order to compare the spiking response elicited by each CO solution, we used the method developed by Russo et al.²² for quantifying a few characteristic features of the Ca^{2+} spiking response: the percentage of responding epidermal cells (atrichoblasts) and the average number of peaks per responding cell. This quantitative analysis did not reveal any statistically significant difference in the percent of responding cells between shrimp- and fungal-derived COs. However, fungal COs induced a significantly higher number of peaks, on average, compared to shrimp-derived COs. No significant difference could be observed between fungal samples. Lastly, both the percent of responding atrichoblasts and the average peak number in response to shrimp CO treatment were significantly increased following CO peracetylation.

In short, all tested COs were able to activate symbiotic signalling in *M. truncatula* ROCs, but fungal COs and peracetylated shrimp COs elicited a stronger response than commercial shrimp-derived COs.

Plant treatment with fungal COs enhances arbuscular mycorrhizal colonization. A precise quantification of root colonization by the AM fungus was done according to Trouvelot et al.²³ As summarized in Fig. 4, the main effect of CO treatment was a general increase in all parameters describing root colonization, in agreement with Volpe et al.⁴ In more detail, a 1 g/L solution of *P. ostreatus* COs produced a significant increase in colonization frequency (F%) and arbuscule abundance in the whole root system (A%). A more diluted treatment (1 mg/L) with *P. ostreatus* COs generated an analogous (albeit not statistically confirmed) trend on F%, and had a major impact on arbuscule abundance within the colonized areas (a%). Concentrated shrimp COs (1 g/L) significantly increased M% (average extension of fungal colonization in the root system) and A%—but not F%—and never significantly outperformed concentrated (nor diluted) fungal COs. Importantly, diluted shrimp COs (1 mg/L) achieved the overall lowest efficiency in AM promotion, with poor increases in F%, M%, m% (intensity of mycorrhization in colonized parts of the root) and A% and a significant increase compared to

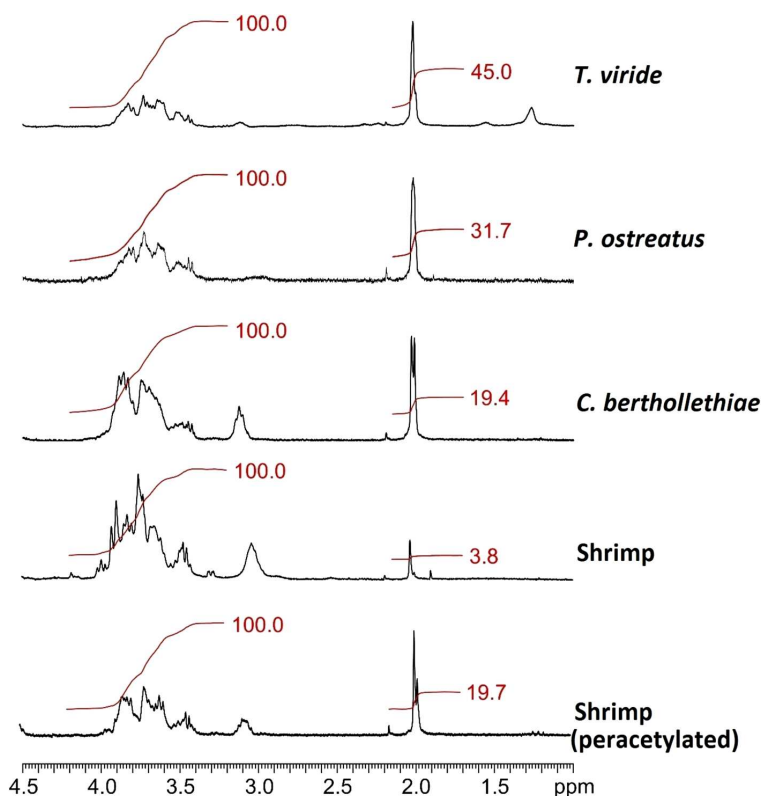


Figure 2. Detail of solution ^1H NMR spectra shown in Supplementary Fig. S4. Red lines and numbers represent integrals for both chain protons (between 3.2 and 4.2 ppm, normalized at 100.0) and methyl protons of the acetyl groups (at ~ 2.0 ppm).

	<i>T. viride</i>	<i>P. ostreatus</i>	<i>C. bertholletiae</i>	Shrimp	Peracetyl. shrimp
Acetylation (%)	45.0	31.7	19.4	3.8	19.7

Table 2. Percent degree of acetylation of the extracted COs, as resulting from ^1H NMR spectra.

controls only for a%. Altogether, fungal COs promoted AM development more efficiently than shrimp COs, with a dose-dependent response.

Discussion

The modifications we have introduced to the method by Di Mario et al.²⁴, in order to reduce reagent use and processing time, provided a 61% increase in chitin recovery from *P. ostreatus* dry biomass, compared to the original article where the chitin recovery was $15.3\% \pm 2.2\%$. However, this value remains within the range described by Jones et al.¹⁹. Also chitin recovery from *C. bertholletiae* did not differ significantly from literature results²⁵. Since literature data report a high chitosan/chitin ratio in mucoromycetes^{26,27}, we were not surprised to extract a large amount of chitosan from *C. bertholletiae*, but—unexpectedly—this fungus also provided a relevant major amount of chitin, which was indeed about 46 times more abundant than chitosan in terms of percent yield. Lastly, a very high chitosan yield was also surprisingly obtained from *T. viride*, even if ascomycota cell walls are reported to be richer in chitin^{26,27}. Such differences between expected and actual yields may be ascribed to several causes: growth conditions and strain-specific features may have a major role, but we cannot exclude that the changes we introduced to the extraction protocol differently affect chitin and chitosan extraction efficiency.

In addition to a considerable improvement in chitin extraction efficiency, our protocol also provided a very high yield in COs: a +65% increase was achieved from acid hydrolysis of *C. bertholletiae* chitin, compared to the chitin acid hydrolysis from crab shell and squid pen performed by Kazami et al.²⁸, while short chain CO recovery

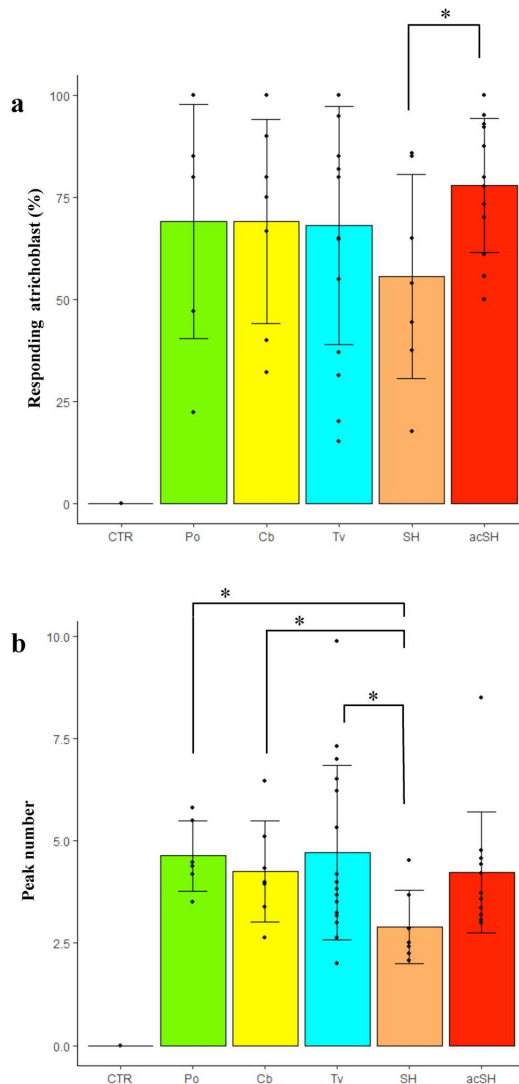


Figure 3. Calcium spiking response to 1 mg/L CO treatment in *M. truncatula* atrichoblasts. All CO solutions activated nuclear calcium spiking, in a comparable number of cells (expressed as percentage in **a**). Nevertheless, the average number of peaks recorded over 30 min (**b**) indicated a significantly stronger response to fungal compared to shrimp COs. Remarkably, this difference was canceled when shrimp COs acetylation degree was increased by peracetylation. CTR = water-treated control; Po = *P. ostreatus* COs; Cb = *C. bertholletiae* COs; Tv = *T. viride* COs; SH = shrimp-derived COs; acSH = peracetylated shrimp-derived COs. A minimum of six biological replicates were evaluated for each treatment. Significant differences are marked by an asterisk (Student's t test: $P < 0.05$); the difference between CTR and each CO treatment was highly significant in both analyses (Student's t test: $P < 0.005$).

from *P. ostreatus* did not differ significantly from the expected yield²⁸. The presence of different amounts of lipid, glucan or protein traces in the chitin powder may have affected CO hydrolysis and solubilisation efficiency, and account for such differences.

NMR analysis of extracted COs generated spectra with relatively broad and low peaks. Such features are often associated with polymers, whereas NMR spectra of oligomers generally have narrower and more defined spikes²⁹. However, this consideration applies to purified solutions of homogeneous oligomers (e.g. tetramers); in our case, fungal chitin was randomly hydrolysed, producing a mix of COs of different length. This range of variability can

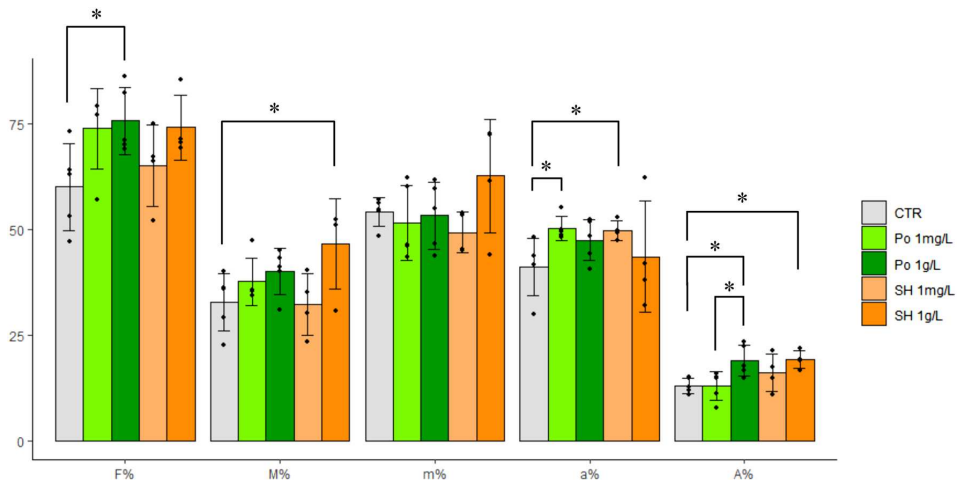


Figure 4. Quantitative analysis of fungal colonization in mycorrhizal *M. truncatula* roots treated with different CO solutions. A general promotion of fungal colonization was induced by all treatments. In more detail, the application of 1 g/L COs from *P. ostreatus* (Po 1 g/L) induced a significant increase in colonization frequency (F%) and arbuscule abundance in the whole root system (A%) compared to water-treated controls. A comparable increase in F% was also obtained using a 1 mg/L solution (Po 1 mg/L), which also produced a significant increase in arbuscule abundance in the colonized areas (a%). By contrast, shrimp-derived COs produced a significant increase in A% and M% (representing the average extension of fungal colonization in the root system), as well as a relevant but statistically non significant elevation of F%, when applied at high concentration (SH 1 g/L), but SH 1 mg/L produced the lowest increase in F% and only a significant increase in arbuscule abundance in the colonized areas (a%). No significant differences were observed in the intensity of the mycorrhization in colonized parts of the root system (m%). In short, *P. ostreatus* COs resulted to be more efficient promoters of AM colonization than shrimp COs, especially when used at low dosage. A minimum of four biological replicates were evaluated for each treatment. Asterisks indicate significant differences (Student's t test: $P < 0.05$).

explain the observed spectral features, as suggested by the analogous results of Kazami et al.²⁸, who identified six peaks in GPC chromatography of water-extracted COs as *N*-acetyl-glucosamine monomers, di-chitooligosaccharides (CO₂), tri-chitooligosaccharides (CO₃), tetra-chitooligosaccharides (CO₄), penta-chitooligosaccharides (CO₅) and hexa-chitooligosaccharides (CO₆) based on their retention times: the amounts of CO₄, CO₅ and CO₆ recovered exceeded those of *N*-acetyl-glucosamine and CO₂. The presence of CO₄–CO₅ oligomers in all our CO samples was also confirmed by HPLC–MS/MS analyses as described. However, considering that the samples were not subjected to further purification, we cannot completely exclude the presence of longer chain oligomers.

Beside glomeromycetes, other fungi have been reported to produce small amounts of LCOs⁴¹. Their presence in our extracts appears unlikely for several reasons: the relatively harsh treatments included in the extraction process are not supposed to preserve this type of molecules; furthermore, LCOs are poorly soluble in water and have only been detected using specific butanol extraction⁴¹. In this context, the small traces of acyl chains detected only in *T. viride* extracts by NMR analysis (peaks at 1.2 and 0.9 ppm in Supplementary Fig. S4 online) appears surprising and could be related to sample contamination (e.g. by paraffins used to grease the glassware junctions). Confirming the presence and origin of this anomalous signal goes beyond the scope of this work, also considering the low yield of *T. viride* (Table 1), which makes the use of this strain unpractical for low-cost production of chitinic molecules to be used for field-scale applications.

Among hydrolysed products, the highest acetylation degree (45%) was observed in *T. viride* COs. In addition, *T. viride* and *P. ostreatus* CO spectra showed narrower and clearer spikes than those of *C. bertholletiae* and shrimp COs, a possible clue of higher homogeneity in oligomer length in the former two samples. By contrast, shrimp-derived COs displayed the lowest acetylation degree (3.8%), which raised to 19.7% following our peracetylation treatment.

NMR analysis showed acetylation degree as the only major difference between fungal and shrimp COs. This is not surprising because chitin in arthropods and fungi presents the same α polymorphic form (the most abundant in nature), despite their very distant phylogenetic positions¹⁸; β -chitin occurring only in squid pen, sea tube worms, and some algae^{30,31}. Significantly, the higher acetylation degree of fungal COs was associated with their higher activity as elicitors symbiotic signalling in the AM host plant. In line with this observation, our tests demonstrated that shrimp CO bioactivity was boosted upon peracetylation, with a significant enhancement of the nuclear Ca²⁺ spiking response (average number of peaks and percent of activated atrichoblasts). These converging results hint at acetylation as a fundamental feature for CO bioactivity in symbiotic signalling, shedding new light on the molecular basis of plant-fungus recognition in AM.

Plants have evolved refined receptorial mechanisms to perceive and discriminate between COs, with important differences between plant lineages. In *Arabidopsis*, long chain molecules (CO8) elicit defence responses when recognized by a homodimer of the plasma membrane-associated receptors-like kinase Chitin Elicitor Receptor Kinase 1 (*AtCERK1*³²); in rice, *OsCERK1* has lost the ability to directly bind COs, but this function in defence elicitation is played by Chitin Elicitor Binding Protein (*OsCEBiP*⁷), which interacts with *OsCERK1* in a hetero-tetrameric receptor complex^{33,34}. Recently, Feng et al.¹⁶ showed the activation of defence and symbiotic signalling as a result of short chain COs perception by the *MtCERK1* and the *AtLYK5* (*A. thaliana* chitin receptor) homolog *LYR4* in *M. truncatula*. They also observed that diverse combinations of stimuli and receptors, including the receptor-kinase *MtDMI2*, might contribute to inhibit plant defence responses and to promote symbiosis signalling after CO perception³⁴. A role in both symbiosis and immunity regulation has also been shown for the LysM receptor-like kinase *MtLYK9* by Gibelin-Viala et al.³⁵. On the same line, a putative CO receptor with a strong affinity for short chain but not for longer chain COs has recently been characterized in rice as *OsMYR1*³⁶. The *OsMYR1/OsCERK1* heterodimer assembles and activates upon CO4 binding to *OsMYR1*, triggering symbiotic signalling through nuclear Ca^{2+} spiking³⁶.

All such CO-binding proteins have extracellular domains containing three tandem LysM motifs (LysM1-3) that bind *N*-acetyl-glucosamine residues³⁷. Detailed structural analyses revealed a crucial role for the second motif, LysM2, which discriminates chitin from other polysaccharides by interacting with *N*-acetyl groups³⁸. Furthermore, the structure of chitin-bound *AtCERK1*-ECD shows that saccharide units exhibit an alternation of 180° flipping along the chitin chain, with the acetyl groups from one side of the chitin chain being solvent-exposed, suggesting that full acetylation may not be necessary for maximal chitin interaction with *AtCERK1*³⁹, and possibly for all LysM domain receptors.

This scenario is fully consistent with our observation that all short chain COs tested were able to elicit symbiotic Ca^{2+} signals, but stronger bioactivity was recorded for COs with higher degrees of acetylation, in line with the key role of the *N*-acetyl group in receptor-ligand interaction. The relevance of acetylation degree of chitin, chitosan and their derivatives is also highlighted in other biological processes, such as the ability of wound recovery in animals, as described by Jones et al.¹⁹.

Chitin-derived molecules have previously been used in laboratory conditions, with beneficial effects on plant growth and stress tolerance⁴. As shown in the Results section, our CO treatments generally increase fungal colonization, in agreement with Volpe et al.⁴.

Our results provide a more detailed set of data on dose–response correlation regarding AM colonization on *M. truncatula*. Evidence shows that COs dose–response correlation is also demonstrated in the pre-symbiotic stage, as described by Oldroyd¹³, who compared Ca^{2+} spiking triggered by different molecules, including rhizobial Nod factors, LCOs (lipo-chitoooligosaccharides) and short COs.

Rush et al.⁴¹ observed that COs slightly enhance spore germination in *Aspergillus fumigatus* and pseudohyphae formation in *Candida glabrata*, albeit to a significantly more limited extent, compared to LCOs⁴⁰. Further analyses will be necessary to investigate if analogous effects are also present in AM fungi.

According to our results, the progressive enhancement of AM colonization in *M. truncatula* correlates with increasing concentrations of *P. ostreatus*-derived COs from 1 mg/L to 1 g/L. Further investigations will be needed to define the optimal concentrations for biologically relevant improvements in AM development for agricultural applications.

Perspectives. Despite the positive results in protocol optimization, both extraction and hydrolysis protocols still appear to be considerably time-consuming and complex: further simplifications will have to be tested in the next experiments to shorten the total processing time, improve extraction yields and reduce costs. To this aim, the protocol could significantly be improved by reusing media and reagents, skipping a few redundant steps in the purification phase, combined with the possibility to use organic waste from industrial food processing activities as growth media.

Water-soluble chitin oligomers, in addition to their acknowledged role in stimulating the development of AM symbiosis⁴, have many additional applications, including lowering of blood cholesterol and blood pressure^{41,42}, inducing protective effects against infections⁴³ and enhancing antitumor properties and anti-adhesion activity^{44–46}. They are also used in food and biomedical industries^{47–49}. Furthermore, they are considered to be functional foods because of their non-digestibility by intestinal enzymes, which allows their use as prebiotics. They stimulate beneficial bacteria in the gastrointestinal tract (*Bifidobacterium* and *Lactobacillus* sp.)^{50,51}. They can also act as thickeners and stabilizing agents³⁰.

Consequently, large-scale and low-cost CO production is of great interest for industrial and agricultural application.

Methods

Fungi. The mucoromycete *Cunninghamella bertholletiae* MUT 2861, the basidiomycete *Pleurotus ostreatus* MUT 2976 and the ascomycete *Trichoderma viride* MUT 3170 were grown on malt extract broth (ME), containing 20 g/L glucose, 20 g/L malt extract, and 2 g/L peptone, as described by Spina et al.⁵². In more detail, fungi were inoculated as conidial suspension in 500 mL flasks containing 350 mL of medium and incubated at 24 ± 2 °C in the dark on an orbital shaker set at 130 rpm. After 12 days, the biomass was filtered, washed and lyophilized.

Chitin purification. Chitin was purified from lyophilized biomass of *P. ostreatus*, *C. bertholletiae* and *T. viride*, using a modified version of the method described by Di Mario et al.²⁴. Briefly, fungal biomass was deproteinated by treatment of 15 g of lyophilized mycelium with 500 mL of 1 N NaOH under vigorous stirring over-

night at 40 °C. The suspension was centrifuged at 4500×g for 45 min and the supernatant, containing proteins and other impurities, was discarded. This treatment was repeated three times. The pellet, containing fungal wall polysaccharides, was suspended in 500 mL of boiling distilled water in a round-bottom flask equipped with a reflux condenser and stirred overnight at reflux in order to remove glucans. The suspension was then centrifuged at 4500×g for 45 min. The supernatant containing wall glucans was discarded. The pellet was washed three times with distilled water at 100 °C. In a round-bottom flask equipped with a reflux condenser, the pellet was treated with 500 mL of aqueous acetic acid (5%) and stirred for 3 h at 90 °C. After centrifugation at 4500×g for 45 min, the chitin pellet was separated from the supernatant (containing chitosan), washed three times with distilled water and lyophilized. Chitosan was precipitated by adding 1 N NaOH until pH reached 12 and centrifuged at 4500×g for 45 min. The resulting pellet was washed twice with distilled water and lyophilized. Fresh and dry weight of both extracted chitin and chitosan were measured before and after lyophilization.

Chitoooligosaccharide production. Chitin hydrolysis under acidic conditions was performed following a modified version of the method described by Kazami et al.²⁸. Briefly, 1 g of lyophilized chitin for each fungus was hydrolysed in 30 mL of 37% HCl at 40 °C for 1 h. After cooling back to room temperature, the reaction mixture was then poured into 160 mL of acetone and stirred overnight at 4 °C. The solution was then centrifuged at 10,000×g for 10 min (4 °C) and the precipitate was washed with acetone until pH reached 5. Finally, the pellet was re-suspended in cold diethyl ether, centrifuged at 10,000×g for 10 min at 4 °C and dried under vacuum over P₂O₅.

The dried precipitate was soaked in 25 mL of distilled water and stirred overnight at 20 °C. Subsequently, the pellet was centrifuged at 15,000 g for 10 min (20 °C). Centrifugation produced a precipitate (which was soaked in 10 mL of distilled water and stirred overnight at 20 °C) and a supernatant (which was stored). The suspended precipitate was further centrifuged at 15,000 g for 10 min at 20 °C. The combined supernatant obtained for each fungus—expected to contain water-soluble chitin oligomers—was completely lyophilized to obtain a powder of purified chitoooligomers.

Shrimp CO peracetylation. In order to check for differences in the biological activity of COs with different acetylation degree, shrimp shell-derived COs (Zhengzhou Sigma Chemical Co., Ltd.—Zhengzhou, Henan, China) were N-acetylated following the protocol described by Trombotto et al.³³.

100 mg of shrimp CO mixture were dissolved in 25 mL of methanol/water (50/50, v/v) solution and adding 50.3 mL of acetic anhydride. After stirring at room temperature for 5 min the solution was concentrated to dryness, the solid residue was re-dissolved in distilled water and evaporated under vacuum. This treatment was repeated twice, then the CO sample was dissolved in 50 mL of 0.01 M HCl and, after freeze-drying, isolated as a white powder.

Chemical analyses. Extracted COs were initially analysed by DIMS on an LCQFleet Ion trap mass spectrometer (Thermo Fisher, USA) equipped with an electrospray source. Extracts were dissolved in MilliQ water (10 mg L⁻¹) added with 20% of acetic acid:methanol (1:100, v/v) and filtered by 0.2 µm cellulose acetate syringe filter. The syringe pump was used at a flow rate of 10 mL min⁻¹ to infuse samples directly into the mass spectrometer. The electrospray source was operated in positive ion mode, and the following source conditions were set: spray voltage at 3.5 kV, sheat gas flow at 20 arbitrary units, auxiliary and sweep gas flow at 0 arbitrary units, ion transfer temperature at 280 °C. The mass spectrometer was operated in full scan mode; exploring the scan range m/z 200–2000 and splitting the scan range in six scans (m/z 200–600, 500–900, 800–1200, 1100–1500, 1400–1800, 1700–2000).

COs were subsequently characterized by HPLC using an Ultimate 3000 (Dionex). Separation was performed using a hypercarb column (5 µm, 2 × 100 mm; Hypercarb, Thermo). Solutions of acetic acid:water (1/1000, v/v) and acetonitrile were pumped at 0.4 mL min⁻¹. The gradient used was 100% acetic acid:water for 1 min, then 100% to 50% acetic acid:water in 30 min then 50% to 0% acetic acid:water in 3 min.

COs were identified in the multiple reaction monitoring (MRM) mode using a 4500 Q Trap mass spectrometer (Applied Biosystems, Foster City, CA, USA) with an electrospray ionization in the positive ion mode by monitoring the transitions from parent ion > common daughter ions (m/z: 204, 407, 610), and for quantification using the MRM 425 > 204 m/z (CO₂), 628 > 204 m/z (CO₃), 831 > 204 m/z (CO₄), 1034 > 204 m/z (CO₅). Mono-deacetylated (deAc) COs were identified in MRM mode by monitoring the transitions from parent ion > common daughter ions (m/z: 162, 365, 568), and for quantification using the MRM 383 > 162 m/z (deAc-CO₂), 586 > 162 m/z (deAc-CO₃), 789 > 162 m/z (deAc-CO₄), 992 > 162 m/z (deAc-CO₅). The capillary voltage was fixed at 5500 V, source temperature at 400 °C. Fragmentation was performed by collision-induced dissociation (CID) with nitrogen, collision energy 20 to 54 V, declustering potential 90 to 130 V depending on molecules¹¹.

Furthermore, ¹³C CPMAS SSNMR^{54–57} and solution ¹H NMR⁵⁸, were used to obtain detailed structural information of both chitin and COs.

SSNMR spectra were acquired with a Bruker Avance II 400 Ultra Shield instrument, operating at 400.23 and 100.63 MHz, respectively for ¹H and ¹³C nuclei. Samples were packed into cylindrical zirconia rotors with a 4 mm o.d. and an 80 µL volume. A small amount of sample (40 to 150 mg, depending on the sample) was collected from each batch and shredded into pieces, small enough to fill the rotor. ¹³C CPMAS spectra were acquired at a spinning rate of 12 kHz, using a ramp cross-polarization pulse sequence with a contact time of 3 ms, a 90° ¹H pulse of 3.60 µs, optimized recycle delays between 1 and 2.1 s, for a number of scans between 400 and 3170, depending on the sample. For every spectrum, a two-pulse phase modulation (TPPM) decoupling scheme was used, with a radiofrequency field of 69.4 kHz. The ¹³C chemical shift scale was calibrated through the methylenic signal of external standard glycine (at 43.7 ppm).

Solution (D₂O) ¹H NMR spectra were acquired on a Jeol Eclipse 400 instrument, operating at 400.23 MHz for ¹H nuclei. About 5 mg of each sample was dissolved in 600 µL of D₂O and the solution was transferred in an NMR tube. The spectra were collected at room temperature. In order to ensure a complete relaxation of the magnetization, a relaxation delay of 60 s for 256 scans was employed for each spectrum.

Bioactivity assay. The bioactivity of purified COs was analysed using an established test for the activation of the common symbiotic signalling pathway, based on live imaging of root epidermal cells in confocal microscopy⁵⁹. Biological analyses were done using *Agrobacterium rhizogenes*-transformed ROCs of wild-type *Medicago truncatula* (genotype Jemalong A17) expressing the 35S:NupYC2.1 construct⁶⁰. The ROC line, available in the lab¹¹, was propagated in vertically-oriented Petri dishes containing M medium⁶¹ and incubated at 25 °C in the dark for 10–14 days. Explants with consistent morphology and an identical number of lateral roots were chosen for all technical replicates.

Excised 1–2 cm-long lateral *M. truncatula* roots were treated with 1 mg/L solution of COs, extracted from each fungus (*P. ostreatus*, *C. bertholletiae* and *T. viride*); sterile distilled water was used as negative control and 1 mg/L solutions of short chain COs purified from shrimp shells (acetylated and non-acetylated) were used as positive control, based on previous studies^{11,62}. A Leica TCS SP2 AOBS confocal laser-scanning microscope, equipped with a 40× water-immersion objective, was used for live cell imaging of NupYC2.1 fluorescence in root atrichoblasts. Ratiometric analysis of NupYC2.1 FRET intensity over time was used to visualize variations in calcium concentration for each imaged nucleus during 30 min following the treatments. A minimum of 20 atrichoblasts from at least 6 independent root segments were analysed for each treatment.

Pot cultures. The efficiency of *P. ostreatus* COs as stimulants of AM colonization was tested on pot-grown *M. truncatula* plants. Seeds were first scarified on sand paper in order to break the seed coat. They were sterilized using 5% sodium hypochlorite in water and washed several times in sterile distilled water. Seeds were then imbibed on 0.6% agar plates at 4 °C in the dark for 48 h to break dormancy, then moved at 23 °C for 5 days to allow germination. 10 days-old seedlings were transferred to 10 × 10 × 12 cm flowerpots with sterile quartz sand and grown for two weeks before further treatment.

1 g/L and 1 mg/L solutions were prepared in sterile distilled water using *P. ostreatus* COs (Po 1 g/L and Po 1 mg/L, respectively) or shrimp-derived COs (SH 1 g/L and SH 1 mg/L). Sterile distilled water was used for control treatments (CTR). All test solutions were added with 0.005% Tween 20 as a surfactant. Each plant was sprayed with 5 mL of test solution and the treatment was repeated 2 days later, prior to inoculation with the AM fungus *Funnelliformis mosseae*, (strain BEG 12) using a commercial inoculum (MycAgroLab, Bretenière, France) mixed at 5% with sand.

Ten replicates were done for each of the following lines: CTR, Po 1 mg/L, Po 1 g/L, SH 1 mg/L and SH 1 g/L. During the first week, a plastic bag was placed on the flowerpots to prevent excessive desiccation and allow progressive plant acclimatisation. Plants were grown for 28 days in phytochamber under photoperiod of 16 h/day (23 °C) and 8 h/night (21 °C) and each plant was fertilized once a week with 20 mL of a modified Long Ashton nutrient solution containing 3.2 µM KH₂PO₄ as P source⁶³.

Plants were harvested 28 days post inoculation and washed from sand before fresh weight of roots and shoots was determined. The shoots of 5 plants for each line were then dried at 60 °C until their weight was stabilised, to determine their dry weight (see Supplementary Fig. S5 online).

To determine the extension of fungal colonization, the remaining 5 plants for each test line were stained following the 'lactic blue' protocol developed by Trouvelot et al. (1986): root systems were excised, placed in 50 mL-tubes and submerged in the staining solution (0.1% cotton blue in lactic acid) for 12 h, then rinsed 2 times in water and 2 times in lactic acid (2 h for each rinsing) until all the excessive dye was removed. For microscope observation, each stained root system was cut randomly in 1 cm length pieces and distributed on 5 microscope slides (20 pieces for slide), until 1 m of root was collected for each plant.

The staining of intraradical fungal structures with lactic blue allowed both a morphological characterisation and a statistical quantification of root colonization according to the method by Trouvelot et al. (1986). Four quantitative parameters were calculated and used to compare the intensity of root colonization between samples. F%, colonization frequency in the root system, represents the percentage of segments containing intraradical fungal structures and is considered as a general indicator of the plant mycorrhizal status; M%, intensity of mycorrhizal colonization in the root system, reports on the average volume occupied by the fungus in each fragment, providing more detailed information on the extension of single infection units; m%, intensity of the mycorrhization in colonized parts of the root; a%, arbuscule abundance in colonized areas, indicates the average percentage of arbusculated cells within colonized segments and represents a reporter of symbiosis efficiency; A%, arbuscule abundance in the root system, estimates the average abundance of arbuscules in the whole root system, including non-colonized parts.

Data availability

The datasets generated during and/or analysed during the current study are available from the corresponding author on reasonable request.

Received: 3 November 2020; Accepted: 29 January 2021

Published online: 15 February 2021

References

- Smith, S. & Read, D. *Mycorrhizal Symbiosis* (Elsevier Ltd, Amsterdam, 2008).
- Rich, M. K., Nouri, E., Courty, P. E. & Reinhardt, D. Diet of arbuscular mycorrhizal fungi: Bread and butter?. *Trends Plant Sci.* **22**, 652–660 (2017).
- Lanfranco, L., Bonfante, P. & Genre, A. The mutualistic interaction between plants and arbuscular mycorrhizal fungi. *Microbiol. Spect.* **4**, 727–747 (2016).
- Volpe, V. *et al.* Short chain chito-oligosaccharides promote arbuscular mycorrhizal colonization in *Medicago truncatula*. *Carbohydr. Polym.* **229**, 115505 (2020).
- Lanfranco, L., Fiorilli, V., Venice, F. & Bonfante, P. Strigolactones cross the kingdoms: Plants, fungi, and bacteria in the arbuscular mycorrhizal symbiosis. *J. Exp. Bot.* **69**, 2175–2188 (2018).
- Schmitz, A. M. & Harrison, M. J. Signaling events during initiation of arbuscular mycorrhizal symbiosis. *J. Integr. Plant Biol.* **56**, 250–261 (2014).
- Kaku, H. *et al.* Plant cells recognize chitin fragments for defense signaling through a plasma membrane receptor. *Proc. Natl. Acad. Sci. USA* **103**, 11086–11091 (2006).
- Wan, J. *et al.* LYK4, a lysin motif receptor-like kinase, is important for chitin signaling and plant innate immunity in Arabidopsis. *Plant Physiol.* **160**, 396–406 (2012).
- Cao, Y. *et al.* The kinase LYK5 is a major chitin receptor in Arabidopsis and forms a chitin-induced complex with related kinase CERK1. *eLife* **3**, 3766 (2014).
- Hamel, L. P. & Beaudoin, N. Chitoooligosaccharide sensing and downstream signaling: Contrasted outcomes in pathogenic and beneficial plant-microbe interactions. *Planta* **232**, 787–806 (2010).
- Genre, A. *et al.* Short chain chitin oligomers from arbuscular mycorrhizal fungi trigger nuclear Ca²⁺ spiking in *Medicago truncatula* roots and their production is enhanced by strigolactone. *New Phytol.* **198**, 190–202 (2013).
- Sun, J. *et al.* Activation of symbiosis signaling by arbuscular mycorrhizal fungi in legumes and rice. *Plant Cell* **27**, 823–838 (2015).
- Oldroyd, G. E. D. Speak, friend, and enter: Signalling systems that promote beneficial symbiotic associations in plants. *Nat. Rev. Microbiol.* **11**, 252–263 (2013).
- Barker, D. G., Chabaud, M., Russo, G. & Genre, A. Nuclear Ca²⁺ signalling in arbuscular mycorrhizal and actinorhizal endosymbioses: On the trail of novel underground signals. *New Phytol.* **214**, 533–538 (2017).
- Bonfante, P. & Genre, A. Arbuscular mycorrhizal dialogues: Do you speak “plantish” or “fungish”? *Trends Plant Sci.* **20**, 150–154 (2015).
- Feng, F. *et al.* A combination of chitoooligosaccharide and lipochitoooligosaccharide recognition promotes arbuscular mycorrhizal associations in *Medicago truncatula*. *Nat. Commun.* <https://doi.org/10.1038/s41467-019-12999-52> (2019).
- Gutjahr, C. & Parniske, M. Cell and developmental biology of arbuscular mycorrhiza symbiosis. *Annu. Rev. Cell Dev. Biol.* **29**, 593–617 (2013).
- Hamed, I., Özogul, F. & Regenstein, J. M. Industrial applications of crustacean by-products (chitin, chitosan, and chitoooligosaccharides): A review. *Trends Food Sci. Technol.* **48**, 40–50 (2016).
- Jones, M., Kujundzic, M., John, S. & Bismarck, A. Crab vs. Mushroom: A review of crustacean and fungal chitin in wound treatment. *Mar. Drugs* <https://doi.org/10.3390/md18010064> (2020).
- Heux, L., Brugnerotto, J., Desbrières, J., Versali, M. F. & Rinaudo, M. Solid state NMR for determination of degree of acetylation of chitin and chitosan. *Biomacromol* **1**, 746–751 (2000).
- Mourya, V. K., Inamdar, N. N. & Choudhari, Y. M. Chitoooligosaccharides: Synthesis, characterization and applications. *Polym. Sci. A* **53**, 583–612 (2011).
- Russo, G., Spinella, S., Sciacca, E., Bonfante, P. & Genre, A. Automated analysis of calcium spiking profiles with CaSA software: Two case studies from root-microbe symbioses. *BMC Plant Biol.* **13**, 224 (2013).
- Trouvelot, A., Kough, J. L. & Gianinazzi-Pearson, V. Mesure du taux de mycorhization VA d'un système racinaire. Recherche de méthodes d'estimation ayant une signification fonctionnelle. in *Physiological and Genetical Aspects of Mycorrhizae* (eds Gianinazzi-Pearson, V. & Gianinazzi, S.), INRA edition, Paris (1986).
- Di Mario, F., Rapanà, P., Tomati, U. & Galli, E. Chitin and chitosan from basidiomycetes. *Int. J. Biol. Macromol.* **43**, 8–12 (2008).
- Berger, L. R. R. *et al.* Green conversion of agroindustrial wastes into chitin and chitosan by rhizopus arrizus and cunninghamella elegans strains. *Int. J. Mol. Sci.* **15**, 9082–9102 (2014).
- Raghukumar, S. & Raghukumar, S. *Fungi: Characteristics and Classification. Fungi in Coastal and Oceanic Marine Ecosystems* 1–15 (Springer International Publishing, New York, 2017).
- Lecoite, K., Cornu, M., Leroy, J., Coulon, P. & Sendid, B. Polysaccharides cell wall architecture of mucorales. *Front. Microbiol.* <https://doi.org/10.3389/fmicb.2019.00469> (2019).
- Kazami, N. *et al.* A simple procedure for preparing chitin oligomers through acetone precipitation after hydrolysis in concentrated hydrochloric acid. *Carbohydr. Polym.* **132**, 304–310 (2015).
- Saito, H., Mamizuka, T. & Tabet, R. High resolution ¹³C NMR spectra of chitin oligomers in aqueous solution. *Chem. Lett.* **10**, 1483–1484 (1981).
- Rinaudo, M. Chitin and chitosan: Properties and applications. *Progress Polym. Sci.* **31**, 603–632 (2006).
- Abo Elsoud, M. M. & el Kady, E. M. Current trends in fungal biosynthesis of chitin and chitosan. *Bull. Natl. Res. Centre* <https://doi.org/10.1186/s42269-019-0105-y> (2019).
- Wan, J. *et al.* A LysM receptor-like kinase plays a critical role in chitin signaling and fungal resistance in Arabidopsis. *Plant Cell* **20**, 471–481 (2008).
- Antolin-Llovera, M. *et al.* Knowing your friends and foes: Plant receptor-like kinases as initiators of symbiosis or defence. *New Phytol.* **204**, 791–802 (2014).
- Zipfel, C. & Oldroyd, G. E. D. Plant signalling in symbiosis and immunity. *Nature* **543**, 328–336 (2017).
- Gibelin-Viala, C. *et al.* The *Medicago truncatula* LysM receptor-like kinase LYK9 plays a dual role in immunity and the arbuscular mycorrhizal symbiosis. *New Phytol.* **223**, 1516–1529 (2019).
- He, J. *et al.* A LysM receptor heteromer mediates perception of arbuscular mycorrhizal symbiotic signal in rice. *Mol. Plant* **12**, 1561–1576 (2019).
- Petutschnig, E. K., Jones, A. M. E., Serazetdinova, L., Lipka, U. & Lipka, V. The lysin motif receptor-like kinase (LysM-RLK) CERK1 is a major chitin-binding protein in Arabidopsis thaliana and subject to chitin-induced phosphorylation. *J. Biol. Chem.* **285**, 28902–28911 (2010).
- Hayafune, M. *et al.* Chitin-induced activation of immune signaling by the rice receptor CEBiP relies on a unique sandwich-type dimerization. *Proc. Natl. Acad. Sci. USA* **111**, E404–E413 (2014).
- Liu, T. *et al.* Chitin-induced dimerization activates a plant immune receptor. *Science* **336**, 1160–1164 (2012).
- Rush, T. *et al.* Lipo-chitoooligosaccharides as regulatory signals of fungal growth and development. *Nat. Commun.* <https://doi.org/10.1038/s41467-020-17615-5> (2020).
- Choi, C. R. *et al.* Chitoooligosaccharides decreases plasma lipid levels in healthy men. *Int. J. Food Sci. Nutr.* **63**, 103–106 (2012).
- Giustina, A. & Ventura, P. Weight-reducing regimens in obese subjects: Effects of a new dietary fibre integrator. *Acta Toxicol. Ther.* **16**, 199–214 (1995).

43. Tokoro, A. *et al.* Protective effect of N-acetyl chitohexaose on *Listeria monocytogenes* infection in mice. *Microbiol. Immunol.* **33**, 357–367 (1989).
44. Xu, W. *et al.* Chitooligosaccharides and N-acetyl-D-glucosamine stimulate peripheral blood mononuclear cell-mediated antitumor immune responses. *Mol. Med. Rep.* **6**, 385–390 (2012).
45. Xu, C., Lei, C., Meng, L., Wang, C. & Song, Y. Chitosan as a barrier membrane material in periodontal tissue regeneration. *J. Biomed. Mater. Res. B* **100**, 1435–1443 (2012).
46. Nishimura, K. *et al.* Macrophage activation with multi-porous beads prepared from partially deacetylated chitin. *J. Biomed. Mater. Res.* **20**, 1359–1372 (1986).
47. Kim, S. K. & Rajapakse, N. Enzymatic production and biological activities of chitosan oligosaccharides (COS): A review. *Carbohydr. Polym.* **62**, 357–368 (2005).
48. Seyfarth, F., Schliemann, S., Elsner, P. & Hipler, U. C. Antifungal effect of high- and low-molecular-weight chitosan hydrochloride, carboxymethyl chitosan, chitosan oligosaccharide and N-acetyl-d-glucosamine against *Candida albicans*, *Candida krusei* and *Candida glabrata*. *Int. J. Pharm.* **353**, 139–148 (2008).
49. Xia, W., Liu, P., Zhang, J. & Chen, J. Biological activities of chitosan and chitooligosaccharides. *Food Hydrocoll.* **25**, 170–179 (2011).
50. Morganti, P., Morganti, G. & Morganti, A. Transforming nanostructured chitin from crustacean waste into beneficial health products: A must for our society. *Nanotechnol. Sci. Appl.* **4**, 123–129 (2011).
51. Harish Prashanth, K. V. & Tharanathan, R. N. Chitin/chitosan: modifications and their unlimited application potential—an overview. *Trends Food Sci. Technol.* **18**, 117–131 (2007).
52. Spina, F., Tigrini, V., Romagnolo, A. & Varese, G. C. Bioremediation of landfill leachate with fungi: Autochthonous vs. allochthonous strains. *Life* **8**, 27 (2018).
53. Trombotto, S., Ladavière, C., Delolme, F. & Domard, A. Chemical preparation and structural characterization of a homogeneous series of chitin/chitosan oligomers. *Biomacromol* **9**, 1731–1738 (2008).
54. Fernandez-Diaz-Rullo, F. *et al.* Synthesis and hyperpolarisation of eNOS substrates for quantification of NO production by ¹H NMR spectroscopy. *Bioorg. Med. Chem.* **25**, 2730–2742 (2017).
55. Pauli, G. F., Gödecke, T., Jaki, B. U. & Lankin, D. C. Quantitative ¹H NMR Development and potential of an analytical method: An update. *J. Nat/ Prod.* **75**, 834–851 (2012).
56. Bharti, S. K. & Roy, R. Quantitative ¹H NMR spectroscopy. *Trends Anal. Chem.* **35**, 5–26 (2012).
57. Zuriarrain, A., Zuriarrain, J., Villar, M. & Berregi, I. Quantitative determination of ethanol in cider by ¹H NMR spectrometry. *Food Control* **50**, 758–762 (2015).
58. Schanda, P. & Ernst, M. Studying dynamics by magic-angle spinning solid-state NMR spectroscopy: Principles and applications to biomolecules. *Prog. Nucl. Magn. Reson. Spectrosc.* **96**, 1–46 (2016).
59. Chabaud, M. *et al.* Arbuscular mycorrhizal hyphopodia and germinated spore exudates trigger Ca²⁺ spiking in the legume and nonlegume root epidermis. *New Phytol.* **189**, 347–355 (2011).
60. Sieberer, B. J. *et al.* A nuclear-targetedameleon demonstrates intranuclear Ca²⁺ spiking in *Medicago truncatula* root hairs in response to rhizobial nodulation factors. *Plant Physiol.* **151**, 1197–1206 (2009).
61. Becard, G. & Fortin, J. A. Early events of vesicular-arbuscular mycorrhiza formation on Ri T-DNA transformed roots. *New Phytol.* **108**, 211–218 (1988).
62. Carotenuto, G. *et al.* The rice LysM receptor-like kinase OsCERK1 is required for the perception of short-chain chitin oligomers in arbuscular mycorrhizal signaling. *New Phytol.* **214**, 1440–1446 (2017).
63. Hewitt, E. J. *Sand and Water Culture Methods Used in the Study of Plant Nutrition* (Springer, New York, 1952).

Author contributions

A.C. performed the fungal cultures, mycelia production, chitin, chitosan and CO extraction, bioactivity analyses, contributed to the pot cultures experiments and wrote the manuscript's original draft. E.M. contributed to the mycelia production, chitin and chitosan extraction, CO purification, bioactivity analyses and performed the pot cultures experiments. M.B. supervised chitin and CO extraction, reviewed and edited the manuscript. G.C. contributed to chitin and CO extraction and bioactivity analyses. F.S. supervised the fungal culture, reviewed and edited the manuscript. S.B. performed the NMR analyses and contributed to the original draft. V.P.P. performed the HPLC analyses and contributed editing the manuscript. L.A. performed the DIMS analyses and contributed editing the text. V.V. supervised the pot culture experiments and reviewed and edited the text. C.P. contributed to the experimental set up and revised the text. R.G. contributed to the experimental set up and revised the text. G.C.V. contributed to experimental design and text writing. A.G. designed the research and experiments and wrote the text.

Funding

This work was supported by MIUR, through a PhD fellowship to AC and FFABR 2017 grant to AG; University of Torino grants to AG (Ricerca Locale 2018–2019). Support for mass spectrometry analyses was provided by the MetaboHUB (Grant ANRINBS-0010)-Metatoul- AgromIX Facilities.

Competing interests

The authors declare no competing interests.

Additional information

Supplementary Information The online version contains supplementary material available at <https://doi.org/10.1038/s41598-021-83299-6>.

Correspondence and requests for materials should be addressed to A.G.

Reprints and permissions information is available at www.nature.com/reprints.

Publisher's note Springer Nature remains neutral with regard to jurisdictional claims in published maps and institutional affiliations.



Open Access This article is licensed under a Creative Commons Attribution 4.0 International License, which permits use, sharing, adaptation, distribution and reproduction in any medium or format, as long as you give appropriate credit to the original author(s) and the source, provide a link to the Creative Commons licence, and indicate if changes were made. The images or other third party material in this article are included in the article's Creative Commons licence, unless indicated otherwise in a credit line to the material. If material is not included in the article's Creative Commons licence and your intended use is not permitted by statutory regulation or exceeds the permitted use, you will need to obtain permission directly from the copyright holder. To view a copy of this licence, visit <http://creativecommons.org/licenses/by/4.0/>.

© The Author(s) 2021

CHAPTER 4

Role of clathrin-mediated endocytosis during CO perception in arbuscular mycorrhizas

Introduction

Clathrin-mediated endocytosis (CME) is a critical eukaryotic cellular process that regulates a wide range of physiological processes, such as the internalization of receptors and transporters (Johnson et al., 2021). Endocytosis occurs through the invagination of the plasma membrane with the resulting formation of an endocytic vesicle (or early endosome) that carries its cargo (lipids, proteins and/or extracellular materials) into the cytoplasm. All components of early endosomes can be recycled back to the plasma membrane or delivered into late endosomes, pre-vacuoles and vacuoles for degradation (Paez Valencia, et al., 2016). The main molecule involved in CME is clathrin, a protein combining three heavy chains (CHCs) and three light chains (CLCs) that can assemble in a three-dimensional structure called triskelion (Figure 8; Wang et al., 2016).

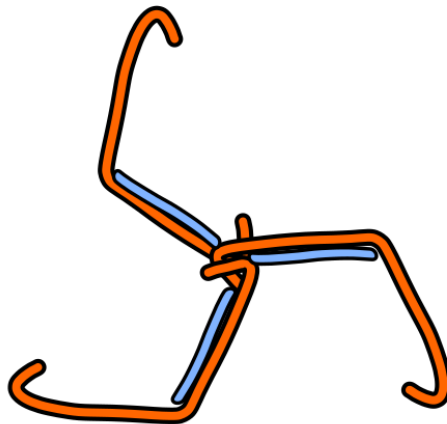


Figure 8 Clathrin triskelion. CHCs are represented in orange while CLCs in light blue.

In addition, different adaptor proteins are important structural components of the CME machinery, involved in cargo recognition, curvature formation and stabilization, and the recruitment of several other proteins (Zhang et al., 2015). The heterotetrameric Adaptor Protein2 (AP-2) complex is the best-studied CME adaptor active at the plasma membrane and it comprises two large (α and β), one medium (μ), and one small subunit (σ) (Zhang et al., 2015). Thanks to AP-2 clathrin-binding motifs, triskelia are recruited and coat the emerging vesicles (Figure 9). After sufficient membrane deformation, dynamin GTPases form a spiral that encloses the neck of the new vesicle causing its

separation from the donor membrane (Zhang et al., 2015). In several intracellular membrane trafficking events, adaptor proteins can recognize specific types of cargoes through the so-called ‘cargo recognition motifs’, that generally contain a residue of tyrosine (Banbury et al., 2003; Zhang et al., 2015). The medium chain (μ) subunit of AP-2 can interact with the motif YXX ϕ (where ϕ represents a bulky hydrophobic residue), linking the cytosolic domains of integral membrane proteins to the clathrin coat (Banbury et al., 2003).

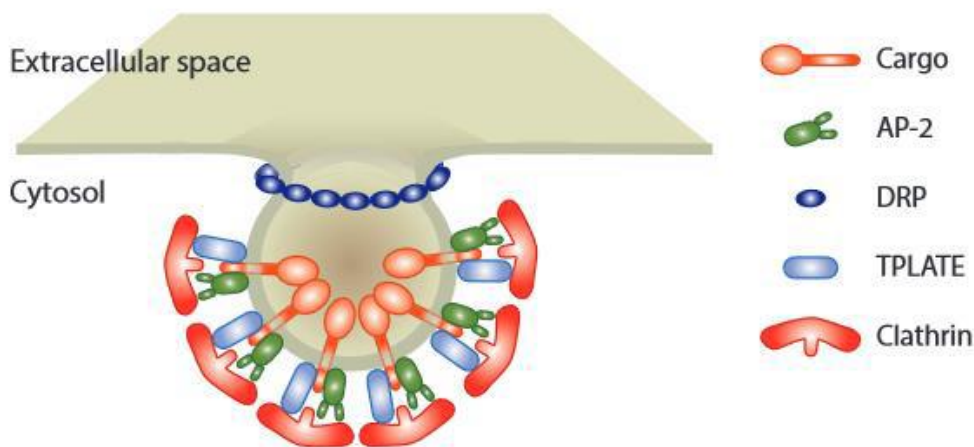


Figure 9 Clathrin-mediated endocytosis in plant (Paez Valencia et al., 2016). CME begins with the association of adaptor proteins such as adaptor protein 2 complexes (AP-2) and TPLATE complex at the plasma membrane. These initial adaptors recruit clathrin triskelions, which polymerize and lead to coat assembly. After vesicle maturation, dynamin-related proteins (DRP) are recruited to the neck site of the forming bud, where they polymerize and induce the scission of vesicle.

CME inhibitors

Tyrphostins

In recent years, tyrphostins have been developed and used as a pharmacological tool to interfere with CME in animal and plant cells. Among them, tyrphostin A23, blocking the interaction between YXX ϕ motifs and the μ 2 subunit of the AP-2 adaptor complex, inhibits cargo recruitment into clathrin-coated vesicles from the plasma membrane (Wang et al., 2016; Banbury et al., 2003). On the other hand, tyrphostin A51 is a biologically inactive structural analogue of A23 and it is often used as a negative control (Wang et al., 2016).

Dynasore

Dynasore is a non-competitive inhibitor of dynamin GTPase activity and blocks dynamin-dependent endocytosis in cells. It is reported to act in a few seconds and its inhibitory effect in cells can be reversed by washout (Kirchhausen et al., 2008).

Aim of this work

Wang et al. (2016) described a role for CME in Nod-factor perception and downstream responses in the model legume *Lotus japonicus*. In that study, the expression of a dominant-negative variant of Clathrin Heavy Chain 1 (CHC1) or treatment with tyrphostin A23 affected Nod-factor-dependent gene regulation, *Rhizobium* infection and nodulation.

Extensive research in the model legumes *L. japonicus* and *Medicago truncatula* has supported the hypothesis that symbiotic nitrogen fixation (SNF) has evolved in legumes by co-opting elements of the signaling and accommodation processes from the evolutionarily more ancient AM symbiosis (Chen et al., 2009). In this scenario, the work by Wang et al (2016) raised a major interest in the investigation of analogous roles for CME in AM, in order to clarify whether this is a legume innovation or rather one of the signaling traits that are conserved between the two symbioses.

The aim of our research is therefore to better clarify the role of CME in Myc-factor perception by using CME inhibitors and studying symbiotic responses in *M. truncatula* root organ culture. In particular we focused on the activation of nuclear calcium spiking and the regulation of early AM marker genes.

Materials and methods

Plant material

Agrobacterium rhizogenes-transformed root organ cultures (ROCs) of wild-type *M. truncatula* (genotype Jemalong A17), expressing the 35S:NupYC2.1 (Sieberer et al., 2009) construct, available in the lab, were used for all the experiments. ROCs were propagated in vertically-oriented Petri dishes containing M medium (Bécard & Fortin, 1988) and incubated at 25°C in the dark for 10-14 days.

FM4-64 staining

The red fluorescent lipophilic dye FM4-64 is commonly used to track endocytosis, due to its quick integration in the plasma membrane and the subsequent translocation across the endomembranes system and eventually the tonoplast. We used FM4-64 to verify the efficiency of our inhibitors in blocking the endocytic pathway.

Immediately before confocal microscopy observation, treated samples on microchamber were incubated with 200 µl of one the following solutions:

- FM4-64 20µg/ml and A23 30µM in liquid M medium
- FM4-64 20µg/ml and A51 30µM in liquid M medium
- FM4-64 20µg/ml in liquid M medium (control)

Using a 40x water-immersion objective, images were scanned at a resolution of 2048x2048 pixels and collected every 10 min over a period of 40-50 min.

CME inhibitors treatments

Excised 3-4 cm-long lateral roots, comprising a segment of the main root, were immersed in one of the following solutions:

- 30 µM tyrphostin A23 dissolved in dimethyl sulfoxide (DMSO) within liquid M medium
- 30 µM tyrphostin A51 dissolved in DMSO within liquid M medium.
- 80 µM dynasore dissolved in DMSO within liquid M medium.
- DMSO in liquid M medium (control)

Following one hour incubation in the dark, samples were moved to a microscope chamber, immersed in 200 μ L of the same solution used for the treatment to avoid wash out, plus 10 μ g/L COs and covered with a coverslip.

Live confocal microscopy imaging

Microscopic analyses were performed using Leica TCS SP2 AOBS confocal laser-scanning microscope equipped with a long-distance HCX Apo L NA40X 0.80 water-immersion objective (Leica Microsystems GmbH, Wetzlar, Germany). Fluorescence intensity for both the CFP and YFP moieties of NupYC2.1 were collected, setting the pinhole diameter at 6 Airy units, exciting the probe at 458 nm (80% Ar. laser) and recording the emitted fluorescence at 470–500 and 530–570 nm, respectively. Root samples were first observed in bright field to frame atrichoblasts located between 0,5 and 1 cm from the root tip (the main target of AM fungal signaling and colonization). Images were then scanned at a resolution of 512x512 pixels and collected every 5 s for a period of 30 mins after treatment.

Gene expression analysis

For RNA extraction and gene expression analysis, ROCs were grown for 21 days at 25°C in the dark in vertically oriented petri dishes to favor the development of a regular fishbone-shaped root system. 0.5x2 cm sterilized filter papers soaked in different treatment solutions were then placed on 2 cm-long ROC segments. Petri dishes were incubated at 25 °C for 6 h in the dark.

Treatment solutions:

- 30 μ M tyrphostin A23 dissolved in dimethyl sulfoxide (DMSO) and 10 μ g/L COs within liquid M medium;
- 80 μ M dynasore dissolved in DMSO and 10 μ g/L COs within liquid M medium;
- 10 μ g/L COs and DMSO in liquid M medium (positive control);
- DMSO in liquid M medium (negative control).

Root segments under each filter were then excised, immediately frozen in liquid nitrogen, and stored for RNA extraction.

qRT-PCR analyses were done according to Rotor-Gene SYBR Green PCR Kit instructions (QIAGEN, Hilden, Germany). All reactions were performed with two technical replicates and only Ct values with a standard deviation that did not exceed 0.5 were considered. Relative RNA levels were calibrated using the elongation factor (TEF) mRNA as endogenous reference. Results were validated statistically using the unpaired Student's t-test to compare two means: differences were considered significant at $P < 0.05$.

We analyzed the expression of the following *M. truncatula* AM marker genes, known to be expressed during early AM development:

- **Plant U-box protein 1 (PUB1)**, which codes for an E3 ubiquitin ligase. PUB1 is expressed specifically in symbiotic conditions, being both induced by Nod factors and highly regulated at different steps of AM colonization (Mbengue et al., 2010);
- **Vapyrin (VPY)**, essential for the establishment of both AM symbiosis and nodulation. Vapyrin is induced transiently in the root epidermis, coincident with hyphal penetration, and later on in the cortex, during arbuscule formation (Murray et al., 2011). Vapyrin mutants have been found to have an intact calcium spiking response, indicating that Vapyrin acts downstream of the CSSP (Murray et al., 2011);
- **Glutathione S transferase -early (GST-early)**, which was found to be expressed during the pre-symbiotic phase in *M. truncatula* interacting with *Glomus intraradices* (Wulf et al., 2007);
- **CAAT-box transcription factor 3 (CBF3)**, known to be strongly upregulated in the pre-symbiotic stage by both sulphated and non-sulphated Myc-LCOs, and in mycorrhizal roots (Hogekamp & Küster 2013).

Results

Clathrin-mediated endocytosis inhibition

The efficiency of tyrphostin A23 as an inhibitor of clathrin-mediated endocytosis was validated using FM4-64 staining. As described in Wang et al. (2016), we used tyrphostin A51, a biologically inactive structural analog of tyrphostin A23, as a negative control. We focused our observations on differentiated atrichoblasts 0.5 - 1 cm off the root tip, where Myc factors are known to be perceived (Chabaud et al., 2011; Genre et al., 2013). Samples were treated as described above and imaged every 10 min after 1h incubation in each treatment.

FM4-64 internalization was strongly inhibited by A23 treatment, as shown in Figure 10.

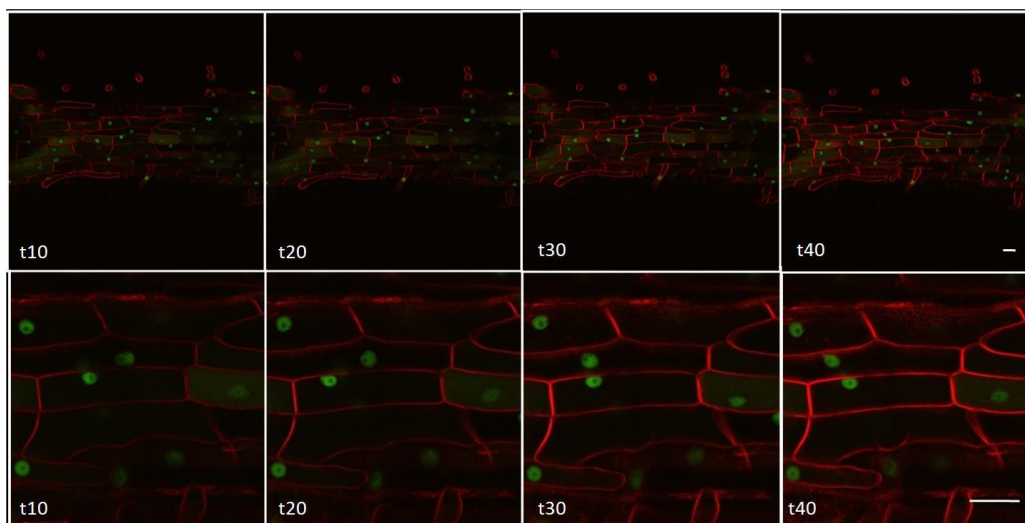


Figure 10 Representative images of CME inhibition by tyrphostin A23 in root epidermal cells. FM4-64 stained cells were imaged at different magnification (top 1X, bottom 4X zoom), every 10 min following 1h incubation in tyrphostin A23. Red FM4-64 fluorescence increasingly accumulated in the plasma membrane but no internalization in endosome-like bodies was observed. Green: nuclear NUPYC2.1 signal. Scale bar: 18,75 μm .

In more detail, FM4-64 fluorescence accumulated over time in the plasma membrane, but no internalization was observed in the form of labelled endosome-like bodies. Furthermore, the observed increment in fluorescence intensity at the plasma membrane can be related to dye accumulation in the absence of its translocation towards the endomembranes via CME.

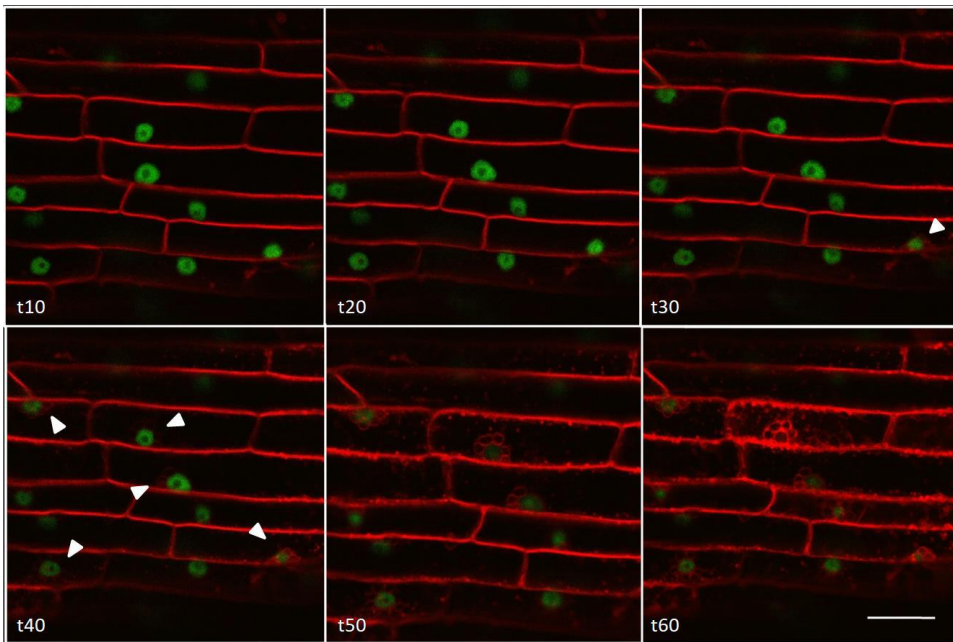


Figure 11 Representative images of FM4-64 internalization in the presence of tyrphostin A51. High magnification images of epidermal cells were recorded every 10 min from A51-treated, FM4-64-stained roots. FM4-64 red fluorescence progressively extended from the plasma membrane to endosomes and endomembranes (arrow heads), indicative that A51 was unable to inhibit CME. Green: nuclear NUPYC2.1 signal. Scale bar: 18,75 μ m.

Tyrphostin A51 was unable to block CME also in differentiated cells. As shown in Figure 11, an increasing number of red structures started to appear within the cytoplasm of observed cells since 30 min after dye incubation. Comparable FM4-64 internalization dynamics were observed in untreated roots (Figure 12).

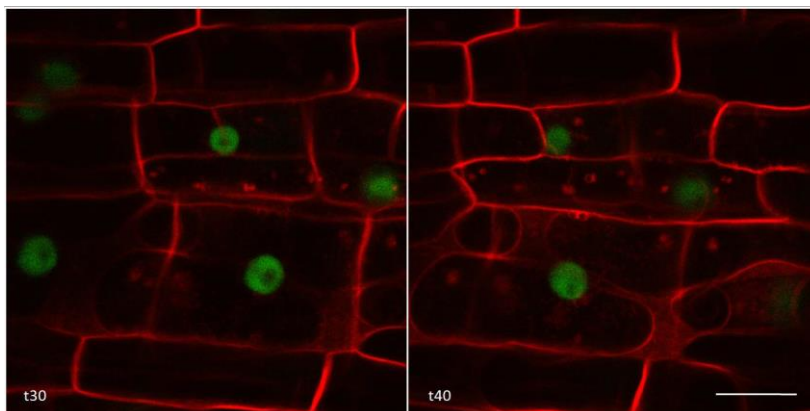


Figure 12 FM4-64 staining of root epidermal cells in untreated *M. truncatula* ROCs. Epidermal cells located between 0,5 and 1 cm from the root tip were imaged 30 and 40 min after FM4-64 staining. Red endosome-like bodies accumulated in the cytoplasm and are considered a hallmark of active CME. Green: nuclear NUPYC2.1 signal. Scale bar: 18,75 μ m.

The expression level of genes involved in the early stage of mycorrhization was analyzed with and without treatment with tyrphostin A23 and dynasore. Relative RNA levels were calibrated using the elongation factor (TEF) mRNA as endogenous reference.

We focused on four AM marker genes: CBF3, GSTearly, Vapyrin, PUB1, which, according to the most recent literature, are up-regulated in response to the perception of Myc-factors, during the first stages of the AM symbiosis.

All values were compared to the CO+ DMSO positive control, to which the arbitrary value of 1 was attributed.

At any rate, dynasore treatment (DYN+CO) significantly downregulated all AM marker genes. A similar trend was observed upon tyrphostin A23 incubation (A23+CO), even if only the downregulation of GSTearly and Vapyrin resulted to be statistically significant (Figure 13). In conclusion, our gene expression analyses of AM marker regulators by CO treatment in the presence or absence of CME inhibitors convincingly indicated that CME is required for Myc-factor signaling, in line with the results obtained with Nod-factors by Wang et al. (2016).

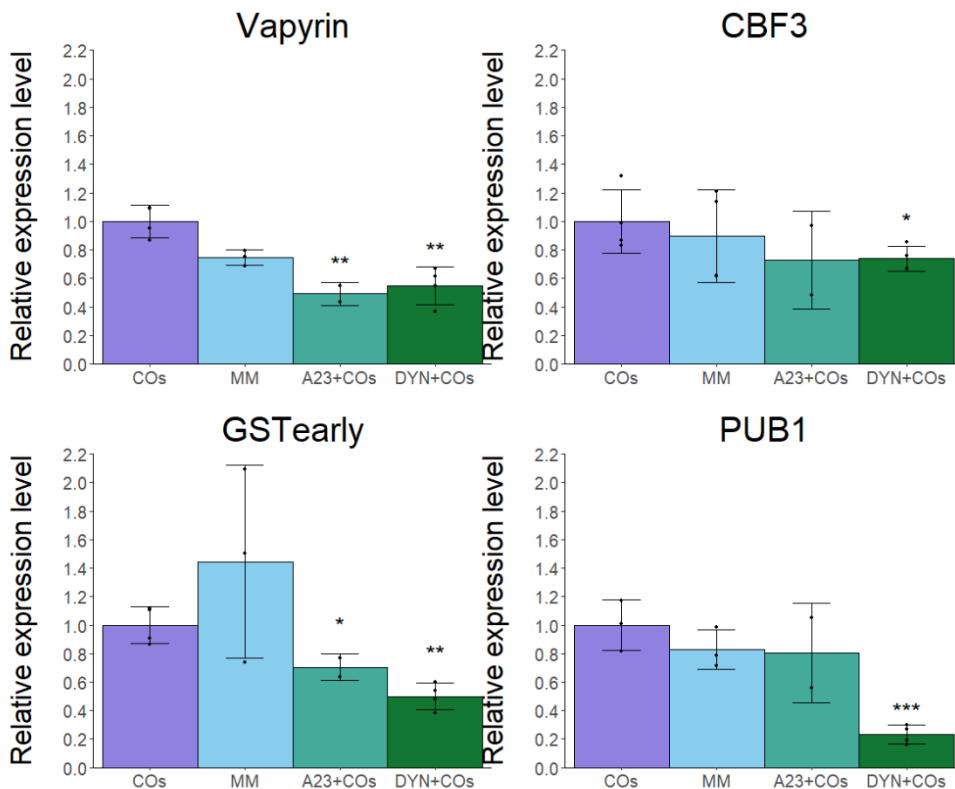


Figure 13 Effects of CME inhibitors tyrphostin A23 (A23) and DYNASORE (DYN) on the expression of early AM marker genes. Dynasore treatment significantly suppressed the upregulation of all four AM markers in response to Myc-factor (COs) treatment. A comparable trend was observed upon A23 incubation, even if only Vapyrin and GSTearly displayed statistically significant changes. DMSO (used as a solvent for all CME inhibitors) was also included in positive (COs) and negative (MM) controls. Points represent single replicates. Bars indicate SDs for at least three technical replicates. Statistically significant differences (* $p < 0.05$, ** $p < 0.01$, *** $p < 0.001$) were determined by Student’s t test.

Calcium spiking

Average YFP and CFP fluorescence intensities were calculated for each nucleus using Leica LCS software. The YFP/CFP ratio for each time frame was calculated. Ratio values were then plotted over time to obtain a graphical representation of FRET intensity (Figure 14), corresponding to relative variations in Ca^{2+} concentration within the nucleoplasm. Ca^{2+} peaks were then counted manually and epidermal cells were considered to be active when at least 3 peaks were recorded in 30 min.

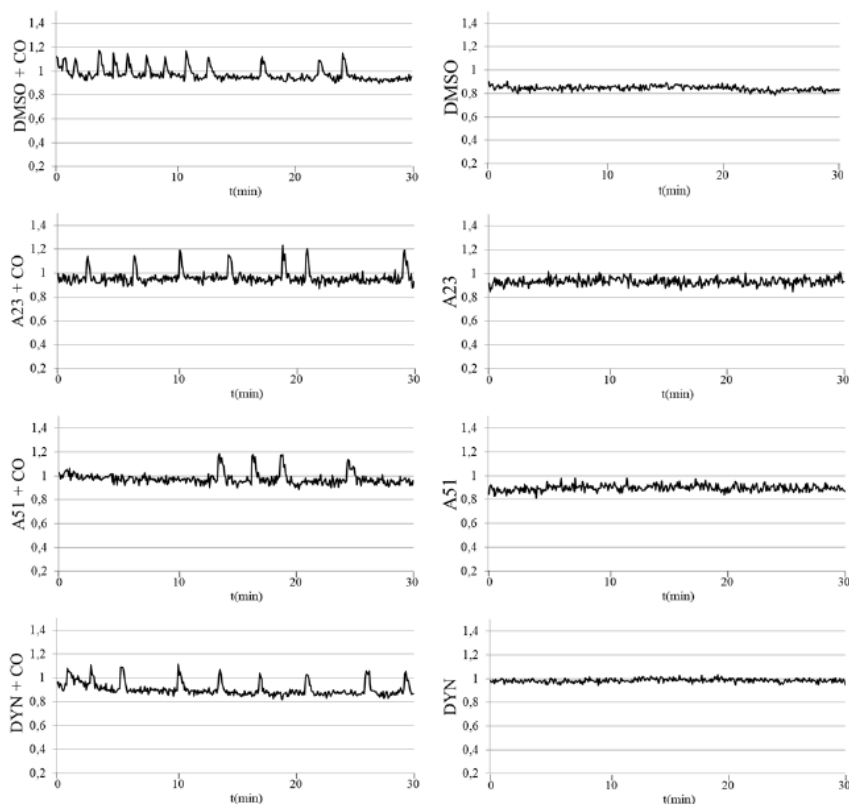


Figure 14 Representative nuclear calcium spiking profiles in treated root atrichoblasts. Calcium concentration was monitored for 30 min following CO treatment (left) in all experimental conditions. No spiking was induced by control treatments without COs (right). Y axis corresponds to YC2.1 FRET ratio. X axis corresponds to time.

A quantitative analysis of the calcium spiking records (Figure 15) revealed that comparable Ca^{2+} spiking responses were observed in all CO-treated samples, irrespectively of the presence or absence of any inhibitor. This convincingly suggested that CSSP activation and calcium-mediated signaling are independent of CME in our experimental conditions.

These results appear particularly interesting because they are in contrast with those obtained from molecular analyses, where we recorded a significant downregulation of AM marker genes upon CME inhibition.

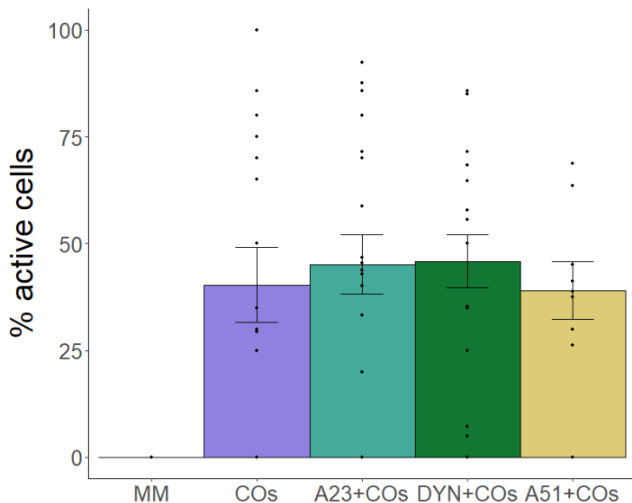


Figure 15 Percent of active cells in response to CO treatment remained unchanged in the absence or presence of the CME inhibitor A23 and its inactive analog A51 or DYNOSORE (DYN). (Student t test, **p<0.01, ***p<0.001). Points represent single replicates. Bars on each histogram indicate \pm standard error.

Discussion

CME is often associated with the internalization of receptor-ligand complexes, leading to the generation of signaling endosomes. Wang et al. (2015) reported that A23 treatment blocks the expression of several root nodule symbiosis-related genes in response to Nod-factors. Considering the cellular and molecular similarities and the evolutionary connection between AM and root nodule symbiosis (with particular reference to CSSP-mediated signaling), our initial hypothesis was that tyrphostin A23 and dynasore should also affect the root response to Myc-COs.

To test this hypothesis we carried out a gene expression analysis on genes known to be activated during pre-symbiotic signaling.

In contrast with the study by Wang et al (2015), where selected genes are modulated upon Nod-factor perception, it was difficult to choose equivalent Myc-factor-regulated genes for the present study. Firstly, most of the proteins and transcripts involved in the CSSP signaling cascade are expressed constitutively. Secondly, literature data on early plant gene regulation in response to AM colonization and Myc-factor perception is limited and mostly reports the initial activation of genes that are also expressed during later steps of the interaction. In short, the selection of very specific early markers was not obvious, and this has to be taken into consideration for result evaluation.

The limited and statistically non-significant upregulation of all selected markers may be related to a weak response of these genes to the treatment with purified COs, compared to raw fungal exudates, as reported by of Pimprikar & Gutjahr (2018).

Nevertheless, our results clearly outlined a general repression of gene regulation for all our markers in the presence of CME inhibitors. This consistent result is in line with the conclusions by Wang et al (2015) and supports the hypothesis that analogous mechanisms regulate AM and SNF signaling.

On the base of these results, we therefore hypothesized a role for CME in CSSP signaling upstream of gene regulation. In fact, receptor internalization by CME has been shown to be a critical factor in several signaling pathways. The best characterized example is BRI1/BAK1 (BRASSINOSTEROID INSENSITIVE1/BRI1 ASSOCIATED KINASE1) a receptor complex involved in the reception of brassinosteroids which

requires internalization via CME for its activation (Russeinova et al. 2004; Geldner et al. 2007). Another example is the CLV1 (clavata1) complex that perceives the CLV3 (clavata3) peptide, this interaction is an important regulator of stem cell maintenance in floral and shoot meristems. Nimchuk et al. (2011) demonstrated that the endocytosis of the CLV1 receptor depends on the CLV3 peptide, because CLV1 accumulates in the plasma membrane in the *clv3-2* mutant and application of the CLV3 peptide induces CLV1 internalization and its targeting to the vacuole.

In our first hypothetical model, active Myc-factor receptors could be internalized by CME inside an endosome, where DMI2 interaction with HMGR would lead to the activation of the CSSP, induce calcium spiking in the nucleus and consequently activate the genes involved in the AM response (Figure 16).

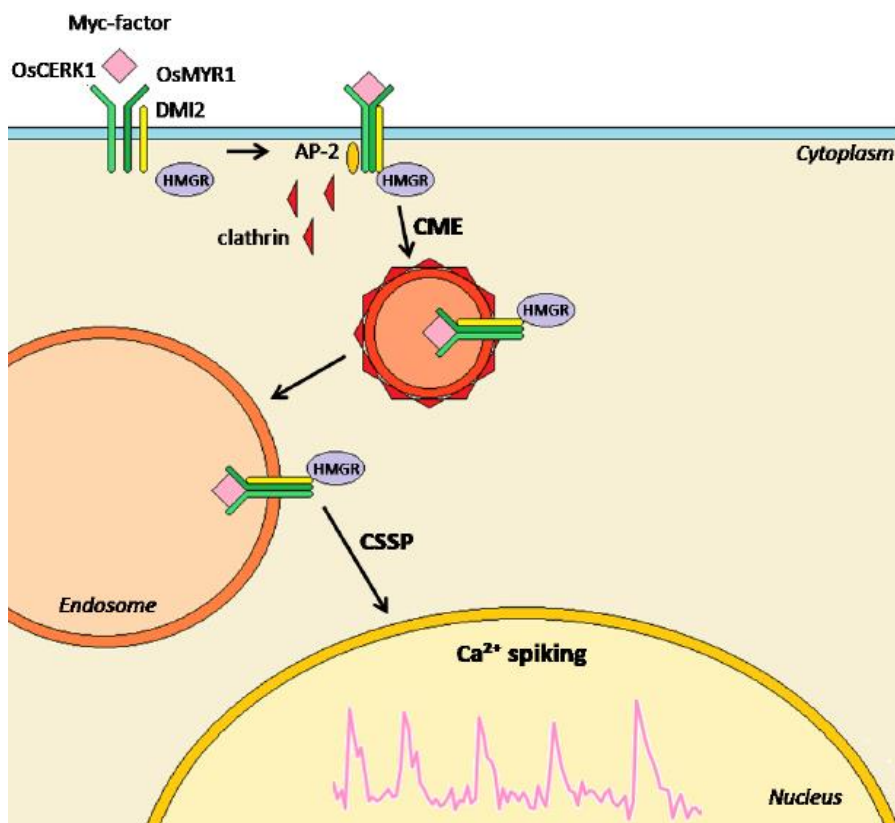


Figure 16 Our first hypothetical model. Myc-factor receptor complex is composed by Chitin Elicitor Receptor Kinase 1 (CERK1), Myc Factor Receptor 1 (MYR1) and DMI2. CME, mediated by AP-2 association and clathrin recruitment, carries the receptor complex in the endosome, where DMI2, interacting with HMGR, activates the CSSP, leading to the generation of calcium spiking in the nucleus.

To test this hypothesis we investigated calcium signaling in root atrichoblasts, as a proxy of CSSP activation upon Myc-factor perception. Surprisingly, experimental evidence was in sharp contrast with our hypothesis: nuclear calcium spiking was induced with comparable characteristics both in the absence and presence of CME inhibitors.

This unexpected observation raises a number of questions and will have to be addressed with new experiments that could not be developed during the course of my PhD.

A first major question concerns our current model of the CSSP and its regulation of symbiotic responses: if CME is required for AM gene regulation, how can its inhibition leave nuclear calcium signaling unaffected, when CSSP activation (and the induction of calcium spiking) is expected to act upstream gene regulation? Answering this question will not be obvious: a first element to be checked is the localization of symbiotic RLKs on the plasma membrane and/or endosomes during Myc-factor perception. This could be achieved by immunolabelling or the expression of GFP-fusions targeting one or more members of the Myc-factor receptor complex.

Receptor internalization by CME might in fact be a requisite for effective symbiotic signaling, but our inhibitor treatments might have a limited efficiency: the resulting partial inhibition would therefore be sufficient to induce visible changes in gene expression, even if the CSSP and its calcium spiking remain detectable. In fact, it is still unclear what feature(s) of the calcium spiking signal (e.g. peak frequency, regularity, amplitude, number) is required for the activation of downstream members of the CSSP and gene regulation, and our current analysis, based on the presence/absence of spiking and average number of peaks per cell, may simply not be addressing the key feature.

It will also be important to test the induction of nuclear calcium spiking in root hairs upon Nod-factor treatment, in the presence of CME inhibitors. This test was in fact not run by Wang et al. (2015), leaving a gap in our comparison of the two sets of results. Assuming this investigation confirms CSSP activation, this would reinforce the scenario of functional overlap between the two types of symbiotic signals (for AM and SNF) in legumes. If, by contrast, Nod-factor-dependent CSSP activation results to be absent in root hairs treated with CME inhibitors, a more complex picture would be outlined, where receptor internalization is required for SNF signaling but at least partially dispensable

for AM-associated CSSP activation. This sort of differences in CSSP signaling are currently being searched for with increasing attention, because they might give us novel clues about the mechanisms allowing legumes to discriminate between AM and SNF activation of CSSP-mediated signaling (Genre & Russo, 2016).

Furthermore, it will be critical to test if nuclear Ca^{2+} spiking and gene regulation are inhibited or not by tyrphostin A23 and dynasore upon root treatment with raw AM fungal or rhizobial exudates and in the presence of the living microbes, where CSSP signaling and gene regulation have been characterized (Chabaud et al., 2011; Granqvist et al., 2015).

In our experiment we were only capable to test nuclear Ca^{2+} spiking in root epidermal cells, while the result of gene expression analyses is represented by the expression levels of all the cell layers composing roots. We hypothesize that each cell layer can differently respond to myc-factors in presence of the CME inhibition treatment and activate different molecular mechanisms (Figure 17). Such a behavior could explain the basal level of gene expression seen in our analysis upon CME inhibitor treatment. A strategy to clarify whether CME is involved in myc-factor signaling in deeper root layers, is represented by testing gene expression analyses on diverse root layers, separated by laser microdissection.

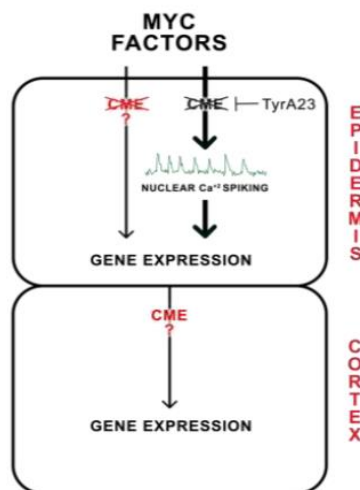


Figure 17 Different root cell layers could have different behavior in response to myc-factors upon CME inhibitor treatment.

References

- Akiyama, K., Matsuzaki, K., & Hayashi, H. (2005). Plant sesquiterpenes induce hyphal branching in arbuscular mycorrhizal fungi. *Nature*, 435(7043), 824–827. <https://doi.org/10.1038/nature03608>
- Bahadur, A., Batool, A., Nasir, F., Jiang, S., Mingsen, Q., Zhang, Q., Pan, J., Liu, Y., & Feng, H. (2019). Mechanistic Insights into Arbuscular Mycorrhizal Fungi-Mediated Drought Stress Tolerance in Plants. *International journal of molecular sciences*, 20(17), 4199. <https://doi.org/10.3390/ijms20174199>
- Banbury, D. N., Oakley, J. D., Sessions, R. B., & Banting, G. (2003). Tyrphostin A23 inhibits internalization of the transferrin receptor by perturbing the interaction between tyrosine motifs and the medium chain subunit of the AP-2 adaptor complex. *The Journal of biological chemistry*, 278(14), 12022–12028. <https://doi.org/10.1074/jbc.M211966200>
- Bauman, J. M., Keiffer, C. H.; Hiremath, S.; McCarthy, B. C. , Kardol P. (2013). Soil preparation methods promoting ectomycorrhizal colonization and American chestnut *Castanea dentata* establishment in coal mine restoration. *Journal of Applied Ecology*. 50. 10.1111/1365-2664.12070.
- Bécard, G., & Fortin, J. A. (1988). Early events of vesicular-arbuscular mycorrhiza formation on Ri T-DNA transformed roots. *The New phytologist*, 108(2), 211–218. <https://doi.org/10.1111/j.1469-8137.1988.tb03698.x>
- Besserer, A., Puech-Pagès, V., Kiefer, P., Gomez-Roldan, V., Jauneau, A., Roy, S., Portais, J. C., Roux, C., Bécard, G., & Séjalon-Delmas, N. (2006). Strigolactones stimulate arbuscular mycorrhizal fungi by activating mitochondria. *PLoS biology*, 4(7), e226. <https://doi.org/10.1371/journal.pbio.0040226>
- Bonfante P. (2018). The future has roots in the past: the ideas and scientists that shaped mycorrhizal research. *The New phytologist*, 220(4), 982–995. <https://doi.org/10.1111/nph.15397>
- Bonfante, P., & Genre, A. (2015). Arbuscular mycorrhizal dialogues: do you speak 'plantish' or 'fungish'?. *Trends in plant science*, 20(3), 150–154. <https://doi.org/10.1016/j.tplants.2014.12.002>
- Brewer, P. B., Koltai, H., & Beveridge, C. A. (2013). Diverse roles of strigolactones in plant development. *Molecular plant*, 6(1), 18–28. <https://doi.org/10.1093/mp/sss130>
- Brundrett, M. C., & Tedersoo, L. (2018). Evolutionary history of mycorrhizal symbioses and global host plant diversity. *The New phytologist*, 220(4), 1108–1115. <https://doi.org/10.1111/nph.14976>
- Bürger, M., & Chory, J. (2020). The Many Models of Strigolactone Signaling. *Trends in plant science*, 25(4), 395–405. <https://doi.org/10.1016/j.tplants.2019.12.009>
- Capoen, W., Sun, J., Wysham, D., Otegui, M. S., Venkateshwaran, M., Hirsch, S., Miwa, H., Downie, J. A., Morris, R. J., Ané, J. M., & Oldroyd, G. E. (2011). Nuclear membranes control symbiotic calcium signaling of legumes. *Proceedings of the National Academy of Sciences of the United States of America*, 108(34), 14348–14353. <https://doi.org/10.1073/pnas.1107912108>
- Carotenuto, G., Chabaud, M., Miyata, K., Capozzi, M., Takeda, N., Kaku, H., Shibuya, N., Nakagawa, T., Barker, D. G., & Genre, A. (2017). The rice LysM receptor-like kinase OsCERK1 is required for the perception of short-chain chitin oligomers in arbuscular mycorrhizal signaling. *The New phytologist*, 214(4), 1440–1446. <https://doi.org/10.1111/nph.14539>
- Ceballos, I., Ruiz, M., Fernández, C., Peña, R., Rodríguez, A., & Sanders, I. R. (2013). The in vitro mass-produced model mycorrhizal fungus, *Rhizophagus irregularis*, significantly increases yields of the globally important food security crop cassava. *PloS one*, 8(8), e70633. <https://doi.org/10.1371/journal.pone.0070633>
- Chabaud, M., Genre, A., Sieberer, B. J., Faccio, A., Fournier, J., Novero, M., Barker, D. G., & Bonfante, P. (2011). Arbuscular mycorrhizal hyphopodia and germinated spore exudates trigger Ca²⁺ spiking in the legume and nonlegume root epidermis. *The New phytologist*, 189(1), 347–355. <https://doi.org/10.1111/j.1469-8137.2010.03464.x>
- Charpentier, M., Bredemeier, R., Wanner, G., Takeda, N., Schleiff, E., & Parniske, M. (2008). Lotus japonicus CASTOR and POLLUX are ion channels essential for perinuclear calcium spiking in legume root endosymbiosis. *The Plant cell*, 20(12), 3467–3479. <https://doi.org/10.1105/tpc.108.063255>
- Charpentier, M., Sun, J., Vaz Martins, T., Radhakrishnan, G. V., Findlay, K., Soumpourou, E., Thouin, J., Véry, A. A., Sanders, D., Morris, R. J., & Oldroyd, G. E. (2016). Nuclear-localized cyclic nucleotide-gated channels mediate symbiotic calcium oscillations. *Science (New York, N.Y.)*, 352(6289), 1102–1105. <https://doi.org/10.1126/science.aae0109>
- Chen, C., Fan, C., Gao, M., & Zhu, H. (2009). Antiquity and function of CASTOR and POLLUX, the twin ion channel-encoding genes key to the evolution of root symbioses in plants. *Plant physiology*, 149(1), 306–317. <https://doi.org/10.1104/pp.108.131540>

- Chen, C., Gao, M., Liu, J., & Zhu, H. (2007). Fungal symbiosis in rice requires an ortholog of a legume common symbiosis gene encoding a Ca²⁺/calmodulin-dependent protein kinase. *Plant physiology*, 145(4), 1619–1628. <https://doi.org/10.1104/pp.107.109876>
- Chen, M., Arato, M., Borghi, L., Nouri, E., & Reinhardt, D. (2018). Beneficial Services of Arbuscular Mycorrhizal Fungi - From Ecology to Application. *Frontiers in plant science*, 9, 1270. <https://doi.org/10.3389/fpls.2018.01270>
- Choi, J., Summers, W., & Paszkowski, U. (2018). Mechanisms Underlying Establishment of Arbuscular Mycorrhizal Symbioses. *Annual review of phytopathology*, 56, 135–160. <https://doi.org/10.1146/annurev-phyto-080516-035521>
- Danell, E., & Camacho, F. Successful cultivation of the golden antlerelle. *Nature* 385, 303 (1997). <https://doi.org/10.1038/385303a0>
- D'Haese, W., & Holsters, M. (2002). Nod factor structures, responses, and perception during initiation of nodule development. *Glycobiology*, 12(6), 79R–105R. <https://doi.org/10.1093/glycob/12.6.79R>
- Elliott A. D. (2020). Confocal Microscopy: Principles and Modern Practices. *Current protocols in cytometry*, 92(1), e68. <https://doi.org/10.1002/cpcy.68>
- Fernie, A. R., & Yan, J. (2019). De Novo Domestication: An Alternative Route toward New Crops for the Future. *Molecular plant*, 12(5), 615–631. <https://doi.org/10.1016/j.molp.2019.03.016>
- Finlay R. D. (2008). Ecological aspects of mycorrhizal symbiosis: with special emphasis on the functional diversity of interactions involving the extraradical mycelium. *Journal of experimental botany*, 59(5), 1115–1126. <https://doi.org/10.1093/jxb/ern059>
- Fiorilli, V., Vannini, C., Ortolani, F., Garcia-Seco, D., Chiapello, M., Novero, M., Domingo, G., Terzi, V., Morcia, C., Bagnaresi, P., Moulin, L., Bracale, M., & Bonfante, P. (2018). Omics approaches revealed how arbuscular mycorrhizal symbiosis enhances yield and resistance to leaf pathogen in wheat. *Scientific reports*, 8(1), 9625. <https://doi.org/10.1038/s41598-018-27622-8>
- Fotin, A., Cheng, Y., Sliz, P., Grigorieff, N., Harrison, S. C., Kirchhausen, T., & Walz, T. (2004). Molecular model for a complete clathrin lattice from electron cryomicroscopy. *Nature*, 432(7017), 573–579. <https://doi.org/10.1038/nature03079>
- Geldner, N., Hyman, D. L., Wang, X., Schumacher, K., & Chory, J. (2007). Endosomal signaling of plant steroid receptor kinase BRI1. *Genes & development*, 21(13), 1598–1602. <https://doi.org/10.1101/gad.1561307>
- Genre, A., & Russo, G. (2016). Does a Common Pathway Transduce Symbiotic Signals in Plant-Microbe Interactions?. *Frontiers in plant science*, 7, 96. <https://doi.org/10.3389/fpls.2016.00096>
- Genre, A., Chabaud, M., Balzergue, C., Puech-Pagès, V., Novero, M., Rey, T., Fournier, J., Rochange, S., Bécard, G., Bonfante, P., & Barker, D. G. (2013). Short-chain chitin oligomers from arbuscular mycorrhizal fungi trigger nuclear Ca²⁺ spiking in *Medicago truncatula* roots and their production is enhanced by strigolactone. *The New phytologist*, 198(1), 190–202. <https://doi.org/10.1111/nph.12146>
- Genre, A., Lanfranco, L., Perotto, S., & Bonfante, P. (2020). Unique and common traits in mycorrhizal symbioses. *Nature reviews. Microbiology*, 18(11), 649–660. <https://doi.org/10.1038/s41579-020-0402-3>
- Gibelin-Viala, C., Amblard, E., Puech-Pages, V., Bonhomme, M., Garcia, M., Bascaules-Bedin, A., Fliegmann, J., Wen, J., Mysore, K. S., le Signor, C., Jacquet, C., & Gough, C. (2019). The *Medicago truncatula* LysM receptor-like kinase LYK9 plays a dual role in immunity and the arbuscular mycorrhizal symbiosis. *The New phytologist*, 223(3), 1516–1529. <https://doi.org/10.1111/nph.15891>
- Gough, C., & Cullimore, J. (2011). Lipo-chitooligosaccharide signaling in endosymbiotic plant-microbe interactions. *Molecular plant-microbe interactions: MPMI*, 24(8), 867–878. <https://doi.org/10.1094/MPMI-01-11-0019>
- Gradmann, D., & Robinson, D. G. (1989) Does turgor prevent endocytosis in plant cells? *Plant Cell Environ* 12(2), 151–154. <https://doi.org/10.1111/j.1365-3040.1989.tb01927.x>
- Granqvist, E., Sun, J., Op den Camp, R., Pujic, P., Hill, L., Normand, P., Morris, R. J., Downie, J. A., Geurts, R., & Oldroyd, G. E. (2015). Bacterial-induced calcium oscillations are common to nitrogen-fixing associations of nodulating legumes and nonlegumes. *The New phytologist*, 207(3), 551–558. <https://doi.org/10.1111/nph.13464>
- Groth, M., Takeda, N., Pery, J., Uchida, H., Dräxl, S., Brachmann, A., Sato, S., Tabata, S., Kawaguchi, M., Wang, T. L., & Parniske, M. (2010). NENA, a *Lotus japonicus* homolog of Sec13, is required for rhizodermal infection by arbuscular mycorrhiza fungi and rhizobia but dispensable for cortical endosymbiotic development. *The Plant cell*, 22(7), 2509–2526. <https://doi.org/10.1105/tpc.109.069807>

- Gutjahr, C., Banba, M., Croset, V., An, K., Miyao, A., An, G., Hirochika, H., Imaizumi-Anraku, H., & Paszkowski, U. (2008). Arbuscular mycorrhiza-specific signaling in rice transcends the common symbiosis signaling pathway. *The Plant cell*, 20(11), 2989–3005. <https://doi.org/10.1105/tpc.108.062414>
- He, J., Zhang, C., Dai, H., Liu, H., Zhang, X., Yang, J., Chen, X., Zhu, Y., Wang, D., Qi, X., Li, W., Wang, Z., An, G., Yu, N., He, Z., Wang, Y. F., Xiao, Y., Zhang, P., & Wang, E. (2019). A LysM Receptor Heteromer Mediates Perception of Arbuscular Mycorrhizal Symbiotic Signal in Rice. *Molecular plant*, 12(12), 1561–1576. <https://doi.org/10.1016/j.molp.2019.10.015>
- Hogekamp, C., & Küster, H. (2013). A roadmap of cell-type specific gene expression during sequential stages of the arbuscular mycorrhiza symbiosis. *BMC genomics*, 14, 306. <https://doi.org/10.1186/1471-2164-14-306>
- Horváth, B., Yeun, L. H., Domonkos, A., Halász, G., Gobbato, E., Ayaydin, F., Miró, K., Hirsch, S., Sun, J., Tadege, M., Ratet, P., Mysore, K. S., Ané, J. M., Oldroyd, G. E., & Kaló, P. (2011). Medicago truncatula IPD3 is a member of the common symbiotic signaling pathway required for rhizobial and mycorrhizal symbioses. *Molecular plant-microbe interactions : MPMI*, 24(11), 1345–1358. <https://doi.org/10.1094/MPMI-01-11-0015>
- Ivanov, S., Austin, J., 2nd, Berg, R. H., & Harrison, M. J. (2019). Extensive membrane systems at the host-arbuscular mycorrhizal fungus interface. *Nature plants*, 5(2), 194–203. <https://doi.org/10.1038/s41477-019-0364-5>
- Janos D. P. (2007). Plant responsiveness to mycorrhizas differs from dependence upon mycorrhizas. *Mycorrhiza*, 17(2), 75–91. <https://doi.org/10.1007/s00572-006-0094-1>
- Jin, Y., Liu, H., Luo, D., Yu, N., Dong, W., Wang, C., Zhang, X., Dai, H., Yang, J., & Wang, E. (2016). DELLA proteins are common components of symbiotic rhizobial and mycorrhizal signalling pathways. *Nature communications*, 7, 12433. <https://doi.org/10.1038/ncomms12433>
- Jin, Y., Liu, H., Luo, D., Yu, N., Dong, W., Wang, C., Zhang, X., Dai, H., Yang, J., & Wang, E. (2016). DELLA proteins are common components of symbiotic rhizobial and mycorrhizal signalling pathways. *Nature communications*, 7, 12433. <https://doi.org/10.1038/ncomms12433>
- Johnson, A., Dahhan, D. A., Gnyliukh, N., Kaufmann, W. A., Zheden, V., Costanzo, T., Mahou, P., Hrtyan, M., Wang, J., Aguilera-Servin, J., van Damme, D., Beaurepaire, E., Loose, M., Bednarek, S. Y., & Friml, J. (2021). The TPLATE complex mediates membrane bending during plant clathrin-mediated endocytosis. *Proceedings of the National Academy of Sciences of the United States of America*, 118(51), e2113046118. <https://doi.org/10.1073/pnas.2113046118>
- Kanamori, N., Madsen, L. H., Radutoiu, S., Frantescu, M., Quistgaard, E. M., Miwa, H., Downie, J. A., James, E. K., Felle, H. H., Haaning, L. L., Jensen, T. H., Sato, S., Nakamura, Y., Tabata, S., Sandal, N., & Stougaard, J. (2006). A nucleoporin is required for induction of Ca²⁺ spiking in legume nodule development and essential for rhizobial and fungal symbiosis. *Proceedings of the National Academy of Sciences of the United States of America*, 103(2), 359–364. <https://doi.org/10.1073/pnas.0508883103>
- Kevei, Z., Lougnon, G., Mergaert, P., Horváth, G. V., Kereszt, A., Jayaraman, D., Zaman, N., Marcel, F., Regulski, K., Kiss, G. B., Kondorosi, A., Endre, G., Kondorosi, E., & Ané, J. M. (2007). 3-hydroxy-3-methylglutaryl coenzyme A reductase 1 interacts with NORK and is crucial for nodulation in Medicago truncatula. *The Plant cell*, 19(12), 3974–3989. <https://doi.org/10.1105/tpc.107.053975>
- Kim, S., Zeng, W., Bernard, S., Liao, J., Venkateshwaran, M., Ane, J. M., & Jiang, Y. (2019). Publisher Correction: Ca²⁺-regulated Ca²⁺ channels with an RCK gating ring control plant symbiotic associations. *Nature communications*, 10(1), 4607. <https://doi.org/10.1038/s41467-019-12590-y>
- Kirchhausen, T., Macia, E., & Pelish, H. E. (2008). Use of dynasore, the small molecule inhibitor of dynamin, in the regulation of endocytosis. *Methods in enzymology*, 438, 77–93. [https://doi.org/10.1016/S0076-6879\(07\)38006-3](https://doi.org/10.1016/S0076-6879(07)38006-3)
- Kobae, Y., Kameoka, H., Sugimura, Y., Saito, K., Ohtomo, R., Fujiwara, T., & Kyojuka, J. (2018). Strigolactone Biosynthesis Genes of Rice are Required for the Punctual Entry of Arbuscular Mycorrhizal Fungi into the Roots. *Plant & cell physiology*, 59(3), 544–553. <https://doi.org/10.1093/pcp/pcy001>
- Kwaaitaal, M. A., de Vries, S. C., & Russinova, E. (2005). Arabidopsis thaliana Somatic Embryogenesis Receptor Kinase 1 protein is present in sporophytic and gametophytic cells and undergoes endocytosis. *Protoplasma*, 226(1-2), 55–65. <https://doi.org/10.1007/s00709-005-0111-9>
- Lehmann, A., Veresoglou, S. D., Leifheit, E. F. & Rillig, M. C. (2014). Arbuscular mycorrhizal influence on zinc nutrition in crop plants – a meta-analysis. *Soil Biology and Biochemistry*, 69, 123–131. <https://doi.org/10.1016/j.soilbio.2013.11.001>.

- Leppyanen, I. V., Shakhnazarova, V. Y., Shtark, O. Y., Vishnevskaya, N. A., Tikhonovich, I. A., & Dolgikh, E. A. (2017). Receptor-Like Kinase LYK9 in *Pisum sativum* L. Is the CERK1-Like Receptor that Controls Both Plant Immunity and AM Symbiosis Development. *International journal of molecular sciences*, 19(1), 8. <https://doi.org/10.3390/ijms19010008>
- Luginbuehl, L. H., & Oldroyd, G. (2017). Understanding the Arbuscule at the Heart of Endomycorrhizal Symbioses in Plants. *Current biology : CB*, 27(17), R952–R963. <https://doi.org/10.1016/j.cub.2017.06.042>
- Matusova, R., Rani, K., Verstappen, F. W., Franssen, M. C., Beale, M. H., & Bouwmeester, H. J. (2005). The strigolactone germination stimulants of the plant-parasitic *Striga* and *Orobanch* spp. are derived from the carotenoid pathway. *Plant physiology*, 139(2), 920–934. <https://doi.org/10.1104/pp.105.061382>
- Mbengue, M., Camut, S., de Carvalho-Niebel, F., Deslandes, L., Froidure, S., Klaus-Heisen, D., Moreau, S., Rivas, S., Timmers, T., Hervé, C., Cullimore, J., & Lefebvre, B. (2010). The *Medicago truncatula* E3 ubiquitin ligase PUB1 interacts with the LYK3 symbiotic receptor and negatively regulates infection and nodulation. *The Plant cell*, 22(10), 3474–3488. <https://doi.org/10.1105/tpc.110.075861>
- Meharg, A. A., & Cairney, J. W. G. (2000). Ectomycorrhizas - extending the capabilities of rhizosphere remediation? *Soil Biology and Biochemistry*, 32, 1475-1484.
- Miyawaki, A., Llopis, J., Heim, R., McCaffery, J. M., Adams, J. A., Ikura, M., & Tsien, R. Y. (1997). Fluorescent indicators for Ca²⁺ based on green fluorescent proteins and calmodulin. *Nature*, 388(6645), 882–887. <https://doi.org/10.1038/42264>
- Moscatiello, R., Sello, S., Novero, M., Negro, A., Bonfante, P., & Navazio, L. (2014). The intracellular delivery of TAT-aequorin reveals calcium-mediated sensing of environmental and symbiotic signals by the arbuscular mycorrhizal fungus *Gigaspora margarita*. *The New phytologist*, 203(3), 1012–1020. <https://doi.org/10.1111/nph.12849>
- Murat C. (2015). Forty years of inoculating seedlings with truffle fungi: past and future perspectives. *Mycorrhiza*, 25(1), 77–81. <https://doi.org/10.1007/s00572-014-0593-4>
- Murray, J. D., Muni, R. R., Torres-Jerez, I., Tang, Y., Allen, S., Andriankaja, M., Li, G., Laxmi, A., Cheng, X., Wen, J., Vaughan, D., Schultze, M., Sun, J., Charpentier, M., Oldroyd, G., Tadege, M., Ratet, P., Mysore, K. S., Chen, R., & Udvardi, M. K. (2011). Vapyrin, a gene essential for intracellular progression of arbuscular mycorrhizal symbiosis, is also essential for infection by rhizobia in the nodule symbiosis of *Medicago truncatula*. *The Plant journal : for cell and molecular biology*, 65(2), 244–252. <https://doi.org/10.1111/j.1365-313X.2010.04415.x>
- Nadal, M., & Paszkowski, U. (2013). Polyphony in the rhizosphere: presymbiotic communication in arbuscular mycorrhizal symbiosis. *Current opinion in plant biology*, 16(4), 473–479. <https://doi.org/10.1016/j.pbi.2013.06.005>
- Nasir, F., Bahadur, A., Lin, X., Gao, Y., & Tian, C. (2021). Novel insights into host receptors and receptor-mediated signaling that regulate arbuscular mycorrhizal symbiosis. *Journal of experimental botany*, 72(5), 1546–1557. <https://doi.org/10.1093/jxb/eraa538>
- Nimchuk, Z. L., Tarr, P. T., Ohno, C., Qu, X., & Meyerowitz, E. M. (2011). Plant stem cell signaling involves ligand-dependent trafficking of the CLAVATA1 receptor kinase. *Current biology: CB*, 21(5), 345–352. <https://doi.org/10.1016/j.cub.2011.01.039>
- Oldroyd G. E. (2013). Speak, friend, and enter: signalling systems that promote beneficial symbiotic associations in plants. *Nature reviews. Microbiology*, 11(4), 252–263. <https://doi.org/10.1038/nrmicro2990>
- Oliveira, R. S., Franco, A. R., Vosátka, M. & Castro, P. M. (2010). Management of nursery practices for efficient ectomycorrhizal fungi application in the production of *Quercus ilex*. *Symbiosis*. 52. 125-131. [10.1007/s13199-010-0092-0](https://doi.org/10.1007/s13199-010-0092-0).
- Paez Valencia, J., Goodman, K., & Otegui, M. S. (2016). Endocytosis and Endosomal Trafficking in Plants. *Annual review of plant biology*, 67, 309–335. <https://doi.org/10.1146/annurev-arplant-043015-112242>
- Peterson, R. L., Massicotte, H. B., & Melville, L. H. (2004) *Mycorrhizas: anatomy and cell biology*. CABI Publishing, pp. 169 plus index, ISBN 0-85199-901-9.
- Pimprakar, P., & Gutjahr, C. (2018). Transcriptional Regulation of Arbuscular Mycorrhiza Development. *Plant & cell physiology*, 59(4), 673–690. <https://doi.org/10.1093/pcp/pcy024>
- Pimprakar, P., Carbonnel, S., Paries, M., Katzer, K., Klingl, V., Bohmer, M. J., Karl, L., Floss, D. S., Harrison, M. J., Parniske, M., & Gutjahr, C. (2016). A CCaMK-CYCLOPS-DELLA Complex Activates Transcription of RAM1 to Regulate Arbuscule Branching. *Current biology : CB*, 26(8), 987–998. <https://doi.org/10.1016/j.cub.2016.01.069>

- Remy, W., Taylor, T. N., Hass, H., & Kerp, H. (1994). Four hundred-million-year-old vesicular arbuscular mycorrhizae. *Proceedings of the National Academy of Sciences of the United States of America*, 91(25), 11841–11843. <https://doi.org/10.1073/pnas.91.25.11841>
- Roth, R., Hillmer, S., Funaya, C., Chiapello, M., Schumacher, K., Lo Presti, L., Kahmann, R., & Paszkowski, U. (2019). Arbuscular cell invasion coincides with extracellular vesicles and membrane tubules. *Nature plants*, 5(2), 204–211. <https://doi.org/10.1038/s41477-019-0365-4>
- Russinova, E., Borst, J. W., Kwaaitaal, M., Caño-Delgado, A., Yin, Y., Chory, J., & de Vries, S. C. (2004). Heterodimerization and endocytosis of Arabidopsis brassinosteroid receptors BRI1 and AtSERK3 (BAK1). *The Plant cell*, 16(12), 3216–3229. <https://doi.org/10.1105/tpc.104.025387>
- Saito, K., Yoshikawa, M., Yano, K., Miwa, H., Uchida, H., Asamizu, E., Sato, S., Tabata, S., Imaizumi-Anraku, H., Umehara, Y., Kouchi, H., Murooka, Y., Szczyglowski, K., Downie, J. A., Parniske, M., Hayashi, M., & Kawaguchi, M. (2007). NUCLEOPORIN85 is required for calcium spiking, fungal and bacterial symbioses, and seed production in *Lotus japonicus*. *The Plant cell*, 19(2), 610–624. <https://doi.org/10.1105/tpc.106.046938>
- Sieberer, B. J., Chabaud, M., Timmers, A. C., Monin, A., Fournier, J., & Barker, D. G. (2009). A nuclear-targetedameleon demonstrates intranuclear Ca²⁺ spiking in *Medicago truncatula* root hairs in response to rhizobial nodulation factors. *Plant physiology*, 151(3), 1197–1206. <https://doi.org/10.1104/pp.109.142851>
- Smith, S. E., & Read, D. J. (2008). *Mycorrhizal Symbiosis*. Academic Press, ISBN 9780123705266.
- Sosa-Hernández, M. A., Leifheit, E. F., Ingraffia, R., & Rillig, M. C. (2019). Subsoil Arbuscular Mycorrhizal Fungi for Sustainability and Climate-Smart Agriculture: A Solution Right Under Our Feet?. *Frontiers in microbiology*, 10, 744. <https://doi.org/10.3389/fmicb.2019.00744>
- Sousa, N. R., Franco, A. R., Oliveira, R. S., & Castro, P. M. (2012). Ectomycorrhizal fungi as an alternative to the use of chemical fertilisers in nursery production of *Pinus pinaster*. *Journal of environmental management*, 95 Suppl, S269–S274. <https://doi.org/10.1016/j.jenvman.2010.07.016>
- Spatafora, J. W., Chang, Y., Benny, G. L., Lazarus, K., Smith, M. E., Berbee, M. L., Bonito, G., Corradi, N., Grigoriev, I., Gryganskyi, A., James, T. Y., O'Donnell, K., Roberson, R. W., Taylor, T. N., Uehling, J., Vilgalys, R., White, M. M., & Stajich, J. E. (2016). A phylum-level phylogenetic classification of zygomycete fungi based on genome-scale data. *Mycologia*, 108(5), 1028–1046. <https://doi.org/10.3852/16-042>
- Stracke, S., Kistner, C., Yoshida, S., Mulder, L., Sato, S., Kaneko, T., Tabata, S., Sandal, N., Stougaard, J., Szczyglowski, K., & Parniske, M. (2002). A plant receptor-like kinase required for both bacterial and fungal symbiosis. *Nature*, 417(6892), 959–962. <https://doi.org/10.1038/nature00841>
- Strullu-Derrien, C., Selosse, M. A., Kenrick, P., & Martin, F. M. (2018). The origin and evolution of mycorrhizal symbioses: from palaeomycology to phylogenomics. *The New phytologist*, 220(4), 1012–1030. <https://doi.org/10.1111/nph.15076>
- Sun, J., Miller, J. B., Granqvist, E., Wiley-Kalil, A., Gobbato, E., Maillet, F., Cottaz, S., Samain, E., Venkateshwaran, M., Fort, S., Morris, R. J., Ané, J. M., Dénarié, J., & Oldroyd, G. E. (2015). Activation of symbiosis signaling by arbuscular mycorrhizal fungi in legumes and rice. *The Plant cell*, 27(3), 823–838. <https://doi.org/10.1105/tpc.114.131326>
- Tedersoo, L., Bahram, M., & Zobel, M. (2020). How mycorrhizal associations drive plant population and community biology. *Science (New York, N.Y.)*, 367(6480), eaba1223. <https://doi.org/10.1126/science.aba1223>
- Torres, N., Antolín, M. C., & Goicoechea, N. (2018). Arbuscular Mycorrhizal Symbiosis as a Promising Resource for Improving Berry Quality in Grapevines Under Changing Environments. *Frontiers in plant science*, 9, 897. <https://doi.org/10.3389/fpls.2018.00897>
- van der Heijden, M., Martin, F. M., Selosse, M. A., & Sanders, I. R. (2015). Mycorrhizal ecology and evolution: the past, the present, and the future. *The New phytologist*, 205(4), 1406–1423. <https://doi.org/10.1111/nph.13288>
- Venkateshwaran, M., Cosme, A., Han, L., Banba, M., Satyshur, K. A., Schleiff, E., Parniske, M., Imaizumi-Anraku, H., & Ané, J. M. (2012). The recent evolution of a symbiotic ion channel in the legume family altered ion conductance and improved functionality in calcium signaling. *The Plant cell*, 24(6), 2528–2545. <https://doi.org/10.1105/tpc.112.098475>
- Venkateshwaran, M., Jayaraman, D., Chabaud, M., Genre, A., Balloon, A. J., Maeda, J., Forshey, K., den Os, D., Kwiecien, N. W., Coon, J. J., Barker, D. G., & Ané, J. M. (2015). A role for the mevalonate pathway in early plant symbiotic signaling. *Proceedings of the National Academy of Sciences of the United States of America*, 112(31), 9781–9786. <https://doi.org/10.1073/pnas.1413762112>
- Vernié, T., Camut, S., Camps, C., Rembliere, C., de Carvalho-Niebel, F., Mbengue, M., Timmers, T., Gascioli, V., Thompson, R., le Signor, C., Lefebvre, B., Cullimore, J., & Hervé, C. (2016). PUB1 Interacts with the Receptor Kinase

- DMI2 and Negatively Regulates Rhizobial and Arbuscular Mycorrhizal Symbioses through Its Ubiquitination Activity in *Medicago truncatula*. *Plant physiology*, 170(4), 2312–2324. <https://doi.org/10.1104/pp.15.01694>
- Wang, C., Hu, T., Yan, X., Meng, T., Wang, Y., Wang, Q., Zhang, X., Gu, Y., Sánchez-Rodríguez, C., Gadeyne, A., Lin, J., Persson, S., Van Damme, D., Li, C., Bednarek, S. Y., & Pan, J. (2016). Differential Regulation of Clathrin and Its Adaptor Proteins during Membrane Recruitment for Endocytosis. *Plant physiology*, 171(1), 215–229. <https://doi.org/10.1104/pp.15.01716>
- Wang, C., Xu, X., Hong, Z., Feng, Y., & Zhang, Z. (2015). Involvement of ROP6 and clathrin in nodulation factor signaling. *Plant signaling & behavior*, 10(7), e1033127. <https://doi.org/10.1080/15592324.2015.1033127>
- Wulf, A., Manthey, K., Doll, J., Perlick, A. M., Linke, B., Bekel, T., Meyer, F., Franken, P., Küster, H., & Krajinski, F. (2003). Transcriptional changes in response to arbuscular mycorrhiza development in the model plant *Medicago truncatula*. *Molecular plant-microbe interactions : MPMI*, 16(4), 306–314. <https://doi.org/10.1094/MPMI.2003.16.4.306>
- Yano, K., Yoshida, S., Müller, J., Singh, S., Banba, M., Vickers, K., Markmann, K., White, C., Schuller, B., Sato, S., Asamizu, E., Tabata, S., Murooka, Y., Perry, J., Wang, T. L., Kawaguchi, M., Imaizumi-Anraku, H., Hayashi, M., & Parniske, M. (2008). CYCLOPS, a mediator of symbiotic intracellular accommodation. *Proceedings of the National Academy of Sciences of the United States of America*, 105(51), 20540–20545. <https://doi.org/10.1073/pnas.0806858105>
- Yu, N., Luo, D., Zhang, X., Liu, J., Wang, W., Jin, Y., Dong, W., Liu, J., Liu, H., Yang, W., Zeng, L., Li, Q., He, Z., Oldroyd, G. E., & Wang, E. (2014). A DELLA protein complex controls the arbuscular mycorrhizal symbiosis in plants. *Cell research*, 24(1), 130–133. <https://doi.org/10.1038/cr.2013.167>
- Zhang, H.-H., Tang, M., Chen, H., & Zheng, C.-L. (2010). Effects of inoculation with ectomycorrhizal fungi on microbial biomass and bacterial functional diversity in the rhizosphere of *Pinus tabulaeformis* seedlings. *European Journal of Soil Biology*, 46(1), 55–61. <https://doi.org/10.1016/j.ejsobi.2009.10.005>
- Zhang, Y., Persson, S., Hirst, J., Robinson, M. S., van Damme, D., & Sánchez-Rodríguez, C. (2015). Change your TPLATE, change your fate: plant CME and beyond. *Trends in plant science*, 20(1), 41–48. <https://doi.org/10.1016/j.tplants.2014.09.002>
- Zipfel, C., & Oldroyd, G. E. (2017). Plant signalling in symbiosis and immunity. *Nature*, 543(7645), 328–336. <https://doi.org/10.1038/nature22009>

CHAPTER 5

Quantifying AM root colonization using automated image segmentation and machine learning approaches

Prologue

Arbuscular mycorrhizas (AM) are one of the most widespread symbiosis on earth. This plant-fungus interaction involves around 72% of plant species, including most crops. AM symbiosis improves plant nutrition and tolerance to biotic and abiotic stresses. The fungus, in turn, receives carbon compounds derived from the plant photosynthetic process, such as sugars and lipids.

Most studies investigating AM and their applications in agriculture requires a precise quantification of the intensity of plant colonization. At present, the majority of researchers in the field base AM quantification analyses on manual visual methods, prone to operator errors and limited reproducibility.

Here we propose a novel semi-automated approach to quantify AM fungal root colonization based on digital image analysis comparing three methods: manual quantification, image thresholding and machine learning. We recognize machine learning as a very promising tool for accelerating, simplifying and standardizing critical steps in analysing AM quantification, answering to an urgent need by the scientific community studying this symbiosis.

Key words: agriculture, image segmentation, microscopy, arbuscular mycorrhiza, digital thresholding, machine learning

This work was submitted to Scientific Reports and is currently under revision:

Ivan Sciascia, Andrea Crosino and Andrea Genre. Quantifying root colonization by a symbiotic fungus using automated image segmentation and machine learning approaches.

Introduction

Arbuscular mycorrhizas (AM) are widespread plant endosymbioses that develop between Glomeromycotina fungi and the roots of the majority of plant species, including most crops. The symbiosis benefits extend to both partners by improving plant mineral absorption, tolerance to biotic and abiotic stresses and fitness, while rewarding the fungal symbionts with carbohydrates compounds derived from photosynthesis process, such as sugars and lipids [1]. The nutrient exchange represents the functional core of the symbiosis and occurs at the contact surfaces of highly branched fungal structures - called arbuscules - that are hosted within the living cortical cells of the plant roots [2]. The central ecological role of AM in the functioning of low-input ecosystems and the ability of most crop plants to develop this symbiosis has focused a growing number of investigations on the use of AM in sustainable agricultural practices. A critical step in all studies on AM is represented by the precise quantification of root colonization by AM fungi, with particular attention to arbuscule abundance [3]. Nevertheless, molecular analyses, based on the quantification of fungal sequences in total root DNA or arbuscule-specific markers in total root RNA extracts, are still outnumbered by direct microscopic quantification of the intraradical fungal structures, after histochemical staining [4], [5]. In one of the most commonly used methods, root samples are stained with lactic blue or alternative dyes to label intraradical fungal structures; roots are then cut into 1cm-long segments, mounted on microscope slides and carefully observed under an optical microscope to classify each segment, based on visual criteria such as the extension of intraradical hyphae and the abundance of arbuscules in the colonized areas [6]. Such methods are extremely time consuming, based on the ability of trained operators and subject to errors.

An emerging alternative, improving speed, repeatability, and reliability of root colonization measurements, is offered by automated pixel-based classification of digital images from optical microscopy. This can be achieved either with a traditional method, known as thresholding, which classifies pixels according to their grayscale intensity, or using a more complex analysis, based on machine learning, where each pixel is described by a set of parameters extracted from the environment of neighbouring pixels.

Here we compared the commonly used visual method developed by Trouvelot et al (1986) with a semi-automated algorithm to generate quantitative indexes of root colonization, deriving from image thresholding using ImageJ and an innovative approach based on machine learning [7], taking advantage of the commercial software Zeiss Intellesis [8]. Our analyses identify machine learning as the most promising alternative to visual quantification of AM root colonization.

Materials and methods

To quantify the extent of AM fungal root colonization, we acquired a dataset of 180 root images of *Solanum pennellii* colonized with the AM fungus *Funelliformis mosseae* and not colonized, stained with 0.1% methylene blue in lactic acid. Quantitative AM fungal colonization first was measured based on the frequency and abundance of fungal structures following Trouvelot et al. (1986) as described in Volpe et al. (2020) [9] considering it as the i) visual method. A schematic representation of colonization process and structures is described in Figure 18. The images were acquired with CI-L fitted with a 4x / 0.10 WD30 objective or Leica DMA500 fitted with a PLAN4x/0.10 objective. The fungal structures were stained blue while the plant tissues and cells remained transparent or light blue.

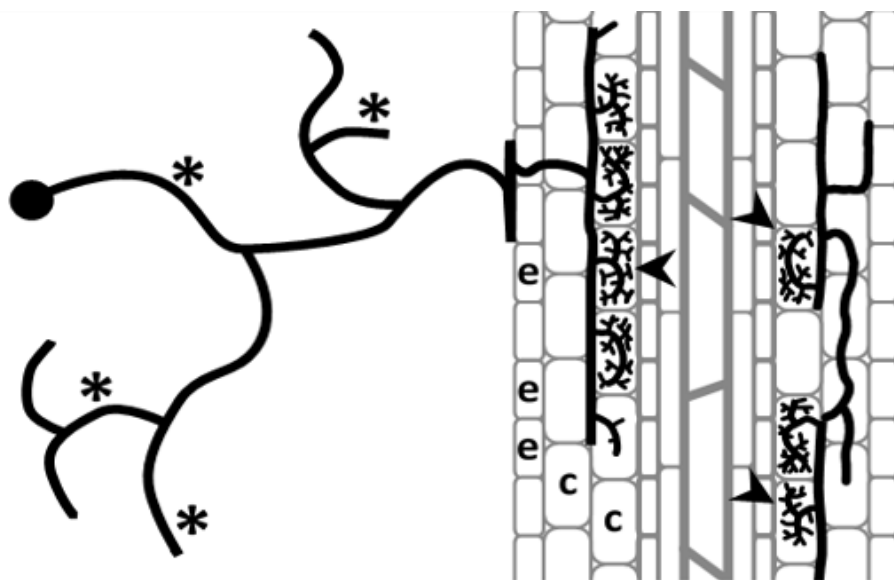


Figure 18. Schematic representation of a host root (grey) colonized by an arbuscular mycorrhizal fungus (black). The extraradical mycelium (*) explores the soil surrounding the root, while intraradical structures produced from the hyphopodium (h) penetrate root epidermal cells (e), colonizing single cortical cells (c), where they eventually develop into branched arbuscules (arrowhead), the sites of nutrient exchanges between symbionts.

Visual method

Fungal presence could thus be detected based on contrast in staining intensity. The dataset of 180 images was visually scored for six root colonisation intensity classes, ranging from not mycorrhizal to >90% mycorrhizal roots, using the procedure of

Trouvelot et al (1986). Each fragment is then assigned to a mycorrhization class, according to the following criteria:

Class 1 without infection

Class 2 few traces

Class 3 less than 10%

Class 4 from 11% to 50%

Class 5 from 51% to 90%

Class 6 more than 90%

In particular, the method of Trouvelot et al. (1986) [6] and Brundrett et al.(1996) [10] are based on non-vital staining of fungal cell wall in mycorrhizal roots, followed by the visual ranking of a representative sample of root segments and a statistical analysis of the results, to extrapolate whole root system estimates.

Digital Image thresholding

A multicolour digital image can be represented by three components [11]: red, green and blue (RGB) and the shades of each colour can be represented by $2^8 \rightarrow [0,255]$ bits (1byte). A digital image is therefore a function of the type:

$$f: D \rightarrow [0,255]$$

Where D is a spatial domain composed of coordinates (x, y) in a sampling grid, each element of which is called a pixel.

For this approach we used the Fiji/ImageJ software [12]. After converting each RGB channel into a grayscale image, a threshold can be set to select all pixels whose brightness is below the given value. The software will then measure the area of the selected pixels (Figure 19).

After applying the segmentation macro to all our images, a set of quantitative values was obtained, corresponding to the supposed colonised area (darkest pixels) and the total root section area (as isolated from the image background). For statistical analysis, the thresholding (t) index was considered, which referred to root colonisation intensity based on contrast thresholding and expressed as the ratio between the mycorrhized area and

the total area. Statistical analyses were carried out with the SPSS software (IBM Statistics for Windows version 26.0).

$$t = \frac{\text{mycorrhzied area}}{\text{total area}} * 100$$

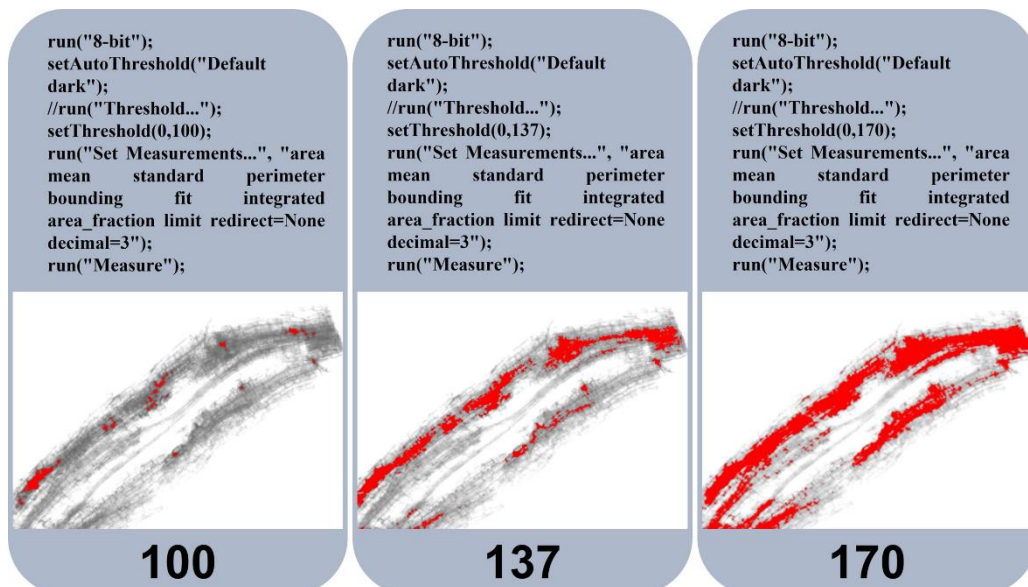


Figure 19. Pixel brightness-based thresholding of the same image from a mycorrhizal root segment. Pixels are selected (in red) based on arbitrary thresholds set at 100, 137, 170 in a range from 0 (black) to 255 (white) using Fiji/ImageJ. Above images, the corresponding Fiji/ImageJ macros are shown.

Machine learning

As our last approach, we tested an image analysis procedure, based on machine learning, using Zeiss Zen Intellesis application (Carl Zeiss Microscopy GmbH Jena, Germany) [13]. Machine learning is a branch of artificial intelligence that solves tasks using algorithms that are capable of learning from experience (training), without being explicitly programmed for a specific task.

As specified in the introduction section, the method we used in this analysis was based on the characteristics of neighbouring pixels that were subsequently classified based on description vectors. The Zeiss Intellesis software proposes up to 7 different machine learning techniques. For this analysis, the software developers suggested to apply the simplest algorithm proposed, the basic feature 25. Such an algorithm applies different feature descriptors (Gaussian Filter using 5 parameters, Sobel of Gaussians for 5 parameters, Gabor Filter for 12 parameters and Hessian Filter for 3 parameters) to create

a final description vector composed of 25 parameters. The algorithm training phase was performed from the same operator who manually classified the image dataset. During this phase, individual fungal structures such as intracellular hyphae and arbuscules were manually selected to generate a model that the software then applied to the whole image dataset.

Also in this case, we developed a root colonization intensity index (machine learning index, ml-index) as the ratio between the colonized area and the sum between the colonized area and the not colonized area:

$$ml = \frac{\textit{colonized area}}{\textit{colonized area} + \textit{non colonized area}} * 100$$

Results

Digital image thresholding

As described in the Materials and Methods section, the dataset composed of 180 colonized and uncolonized root images was processed, setting the intensity threshold to 100 in our Fiji/ImageJ macro previously mentioned. Once the t index was extrapolated, different statistical analyses were performed, using the SPSS software.

Table 1 shows the descriptive parameters of the t index (mean, standard deviation and range) for the comparison between the categories identified by the thresholding method and those obtained after visual classification.

Table 1. Variability of the t-index comparing thresholding analysis and visual classification

Visual classification	Number of images	Colonization (%)	Mean (t)	St. dev (t)	Range (t)
1	30	0	1.01	1.19	5.58
2	30	< 5	5.87	4.40	16.44
3	30	5-10	14.39	10.19	38.98
4	30	11-50	15.17	8.36	28.64
5	30	51-90	29.75	13.22	51.33
6	30	> 90	29.97	11.68	45.35
Total	180		16.03	14.20	60.32

The subsequent ANOVA variance analysis revealed a highly significant statistical difference in the distribution of the t index between the six classes (Table 2).

Table 2. ANOVA variance for the six groups of digital images for the t index

Variance	Sum of Squares	df	Mean Square	F	Probability
Between Groups	21439.36	(5)	4287.87	(50.82)	(<0.01)
Within Groups	14680.18	(174)	84.36		
Total	36119.54	(179)			

Furthermore, the ANOVA pairwise correlation analysis (Table 3) confirmed that the thresholding method allowed a significant level of discrimination for 12 out of 15 pairwise comparisons.

Table 3. ANOVA pairwise correlation analyses of the root colonisation intensities as inferred by the t-index in the visual categories. Statistics with pairwise post hoc multiple comparisons (Bonferroni method). *Mean difference is significant at 0.05 level.

Visual categories	1	2	3	4	5	6
1		4.86	13.38*	14.16*	28.74*	28.95*
2			8.51*	9.29*	23.87*	24.09*
3				0.77	15.35*	15.57*
4					14.57*	14.79*
5						0.21
6						

We then performed a regression analysis to study the fitness of theoretical functions to our experimental data (Figure 20). This analysis showed that the cubic model:

$$y_{t\ index} = a + b_1x + b_2x^2 + b_3x^3$$

better fits with the experimental distribution ($R^2=0.687$).

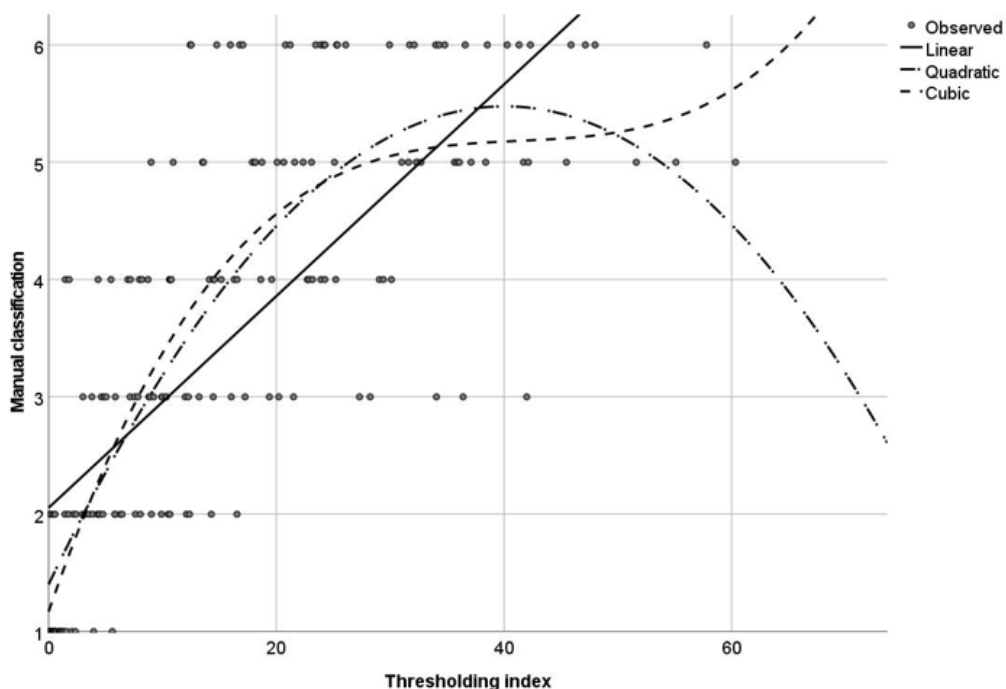


Figure 20. Root colonisation intensities based on t index distribution (x axis) and manual image scoring (y axis). Cubic fit $R^2=0.687$.

Machine learning

In analogy with the thresholding method, we calculated the descriptive parameters (Table 4), ANOVA variance analysis (Table 5) and ANOVA pairwise comparisons (Table 6) for the ml-index.

Table 4. Variability of the *ml*-index based on manually processed images

Visual classification	Number of images	Colonization (%)	Mean (ml)	St. dev (ml)	Range (ml)
1	30	0	6.42	6.20	18.60
2	30	< 5	7.88	8.64	41.81
3	30	5-10	17.30	11.75	40.66
4	30	11-50	26.79	10.59	49.60
5	30	51-90	44.15	11.37	37.43
6	30	> 90	48.43	8.84	33.87
Total	180		25.16	19.06	65.74

Also in this case, the ANOVA variance analysis showed a statistically significant difference in the distribution of the ml index between the six classes (Table 5), which was confirmed by the ANOVA pairwise analysis, highlighting 13 significant comparisons out of 15 (Table 6).

Table 5. ANOVA variance for the six groups of digital images for the *ml*-index

Variance	Sum of Squares	df	Mean Square	F	Probability
Between Groups	48474.66	(5)	9694.93	(101.84)	(<0.01)
Within Groups	16563.85	(174)	95.19		
Total	65038.52	(179)			

Table 6. ANOVA pairwise correlation analyses of the root colonisation intensities as inferred by the ml-index in the visual categories. Statistics with pairwise post hoc multiple comparisons (Bonferroni method). *Mean difference is significant at 0.05 level.

Visual categories	1	2	3	4	5	6
1		1.46	10.87*	20.36*	37.72*	42.00*
2			9.41*	18.90*	36.26*	40.54*
3				9.49*	26.84*	31.12*
4					17.35*	21.63*
5						4.27
6						

Furthermore, a prediction model for the level of mycorrhization was also built for the machine learning method, revealing that the cubic model:

$$y_{ml\ index} = a + b_1x + b_2x^2 + b_3x^3$$

best fits the experimental data (Figure 21) with $R^2 = 0.728$.

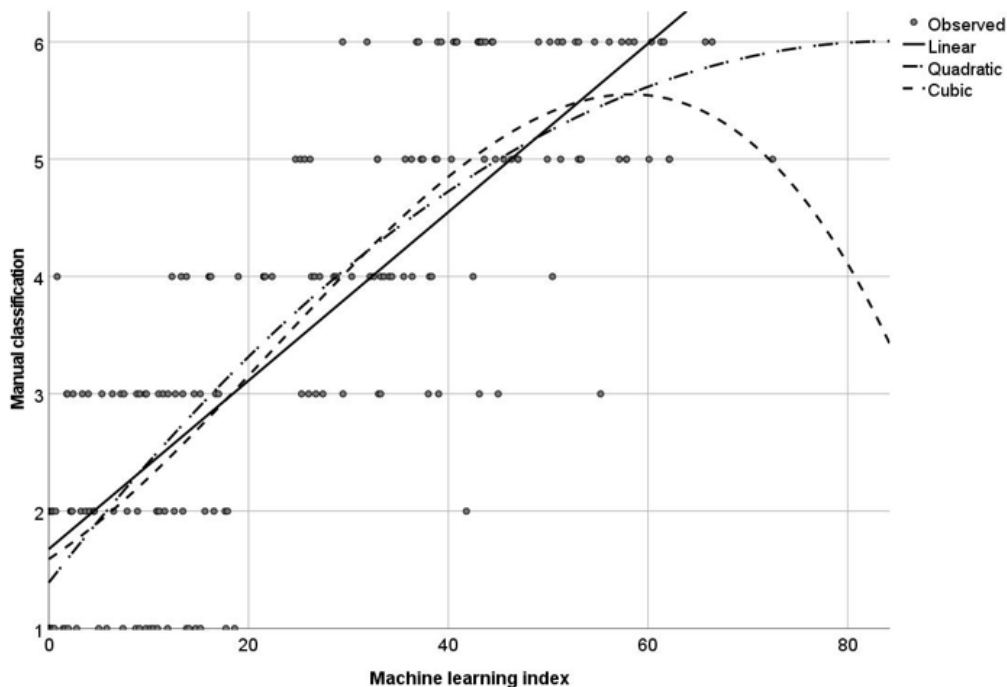


Figure 21. Root colonisation intensities as determined by simple image machine learning and as classified by manual image scoring. Cubic fit $R^2=0.728$.

In conclusion, a comparison between the two semi-automated methods (Table 7) indicated the machine learning method based on the Zeiss Zen Intellesis application as the most efficient in discriminating between image classes, with a very high correlation (Pearson correlation coefficient 0.824) with manual analysis.

Table 7. Model performances comparisons. *Significant pairwise post hoc multiple comparisons on total comparisons, Bonferroni method. Mean difference is significant at 0.05 level.

Performance index	Thresholding	Machine learning
R ² Linear	0.56	0.71
R ² Quadratic	0.673	0.72
R ² Cubic	0.687	0.728
Significant*	12/15	13/15

Discussion

The degree of root colonization is a fundamental parameter in most studies on AM. Assessing an extent of AM fungal root system provides a direct indication of symbiosis development and functioning. Indeed, quantitative estimates of AM colonization are a pre-requisite for studies reporting promotion of plant nutrition and growth by the AM symbiosis [14]. Two main approaches are currently used to quantify root colonization: molecular- and microscopy-based quantification [15]. Overall, the molecular approach is relatively fast and sensitive to quantify the fungal abundance, but cannot discriminate among fungal structures (e.g arbuscules and hyphae), which limits its suitability when studying symbiosis functioning, unless used in combination with functional markers, such as plant P or Zn transporters that are only expressed in arbusculated cells [3].

By contrast, microscopic methods, albeit time consuming, provide more direct information on AM development and thus are very often used.

Even if it is based on objective traits, microscopic quantification is subject to observer bias and performs best when the same person analyses all samples [16]. The present study thus evaluated the reliability of two semi-automated image analysis methods in comparison to manual scoring [6], [17] demonstrating that image analysis is suitable for ranking samples according to root colonization intensity, in analogy with recent studies [18], [19].

The thresholding method uses the gradient of pixel brightness (inversely related to cotton blue staining) as an indicator of fungal presence. Quantification of root colonization by thresholding resolved the six root colonization intensity classes, as for the visual scoring, and could therefore be considered reliable for rapidly screening root samples. A few critical aspects should anyway be considered. One major limitation of the thresholding method was the variability of brightness range between images: different dyes, optical setups, root translucence and the presence of additional microorganisms (such as bacteria, algae, endophytic fungi, invertebrates) especially from field samples, often cannot be discriminated from fungal structures simply based on pixel brightness. In addition, the method is strongly affected by image background noise and magnification.

Lastly, the segmentation process can only be set *ex ante*, by changing the macro settings without subsequent adjustments by the user.

The machine learning-based procedure of the Zeiss Zen Intellesis resulted to be the most efficient. It allowed the discrimination among the different fungal structures, such as hyphae, arbuscules and vesicles, based on the manual training phase, and generated a model that the software then applied to all analysed samples. This approach also resolved the six classes of intensity and achieved the best correlation with manual colonization scoring. Importantly, training phase was relatively short (it required 50 minutes overall) and resulted to be effective, even when using a limited number of images (10 images). Lastly, the machine-learning performed a reliable discrimination between intra- and extraradical hyphae, as well as intraradical hyphae and arbuscules, a major advantage compared to the pixel brightness thresholding method.

Perspectives and conclusions

A critical factor for accurate machine learning-based root colonization level assessment is that the software should be trained by an expert operator. Nevertheless, the Zeiss Intellesis software allows the storage of all images used for the training phase in a reference folder. This set of images can therefore be shared with other researchers and integrated with additional reference images. This opens a new perspective for data reproducibility: research groups can share their expertise with the scientific community by simply sharing the images in a public online repository. Furthermore, the training file can also become a shared resource for reference and make the quantification of AM colonization more uniform and repeatable between different laboratories. The current model of machine learning could be implemented to reach beyond the simple assessment of mycorrhization intensity classes, but also reliably quantify the presence of arbuscules, vesicles, hyphal coils and so forth. Furthermore, the versatility of this approach opens new perspectives and possibilities regarding its application to other plant interactions such as those with endophytic fungi [20]. At present, the commercial nature of the software hampers the modification of the image analysis algorithm, unlike open-source software such as the one used by Evangelisti et al. (2021) [18]. Nevertheless, a commercial software has the advantage of regular and coordinated upgrades by the. Recently, two other AM quantifying machine learning based methods were developed, based on (and aimed to replace) a different manual quantification method, the so-called grid line intersection technique [18]; [19]; Indeed, such methods were described to reliably discriminate among fungal structures (arbuscules, hyphae and vesicles). It would be extremely interesting to investigate the possibility to merge the three algorithms in an attempt to develop a more powerful tool for image analysis that could make quantification of root colonization by AM fungi more reproducible and with more efficient structure discrimination.

Ethics approval and consent to participate

Not applicable

Consent for publication

Not applicable

Availability of data and material

The analysed datasets are available from Figshare:

Segmentation using thresholding and machine learning of mycorrhizal roots DOI

<https://doi.org/10.6084/m9.figshare.14679729>

Segmentation using thresholding and machine learning of non mycorrhizal roots DOI

<https://doi.org/10.6084/m9.figshare.14679684>

Competing interests

The authors declare that they have no conflicting interests.

Funding

Ministero dell'Istruzione, dell'Università e della Ricerca: PhD fellowship to AC Università degli Studi di Torino

Author contributions

IS designed the images analysis approach, performed images analyses and statistical analyses, and wrote the text; AC contributed to design the images analysis approach, performed images analyses and wrote the text; AG contributed to the experimental design, and wrote the text. All authors have read and approved the final manuscript.

Acknowledgements

We are grateful to Carl Zeiss Microscopy GmbH for the licensing agreement of the Zeiss Zen Intellesis software and to Alessandro Cometta and Francesco Biancardi (Carl Zeiss Spa, Milan, Italy) for fruitful discussions. This work was supported by MIUR (PhD fellowship to AC and FFABR 2017 to AG) and the University of Torino (Ricerca Locale 2020 to AG).

References

1. Rich MK, Nouri E, Courty PE, Reinhardt D (2017) Diet of arbuscular mycorrhizal fungi: bread and butter? *Trends Plant Sci* 22:652–660 <https://doi.org/10.1016/j.tplants.2017.05.008>
2. Gutjahr C, Parniske M (2013) Cell and Developmental Biology of Arbuscular Mycorrhiza Symbiosis. *Annu RevCell Dev Bi* 29:593–617. <https://doi.org/10.1146/annurev-cellbio-101512-122413>
3. Ferrol N, Lanfranco, L. (2020) Arbuscular mycorrhizal fungi: methods and protocols. New York, Springer US. <https://doi.org/10.1007/978-1-0716-0603-2?nosfx=y>
4. McGonigle TP, Miller MH, Evans DG, et al (1990) A new method which gives an objective measure of colonization of roots by vesicular-arbuscular mycorrhizal fungi. *New Phytol* 115:495–501. <https://doi.org/10.1111/j.1469-8137.1990.tb00476.x>
5. Novero M, Faccio A, Genre A, et al (2002) Dual requirement of the LjSym4 gene for mycorrhizal development in epidermal and cortical cells of *Lotus japonicus* roots. *New Phytol* 154:741–749. <https://doi.org/10.1046/j.1469-8137.2002.00424.x>
6. Trouvelot, A, Kough JL, Gianinazzi-Pearson V (1986) Mesure du taux de mycorhization VA d'un système racinaire. Recherche de méthodes d'estimation ayant une signification fonctionnelle. In: Gianinazzi-Pearson V, Gianinazzi S (Eds) *Physiological and Genetical Aspects of Mycorrhizae* INRA Press, Paris, 217–221.
7. Arganda-Carreras I, Kaynig V, Rueden C, et al (2017) Trainable Weka Segmentation: A machine learning tool for microscopy pixel classification. *Bioinformatics* 33:2424–2426. <https://doi.org/10.1093/bioinformatics/btx180>
8. Volkenandt T, Freitag S, Rauscher M (2018) Machine learning powered image segmentation. *Microsc and Microanal* 24:520–521. <https://doi.org/10.1017/s1431927618003094>
9. Volpe V., Carotenuto G., Berzero C., Cagnina L., Puech-Pagès V., Genre A. (2020) Short chain chitooligosaccharides promote arbuscular mycorrhizal colonisation in *Medicago truncatula*. *Carbohydr. Polym.* 229, 115505. <https://doi.org/10.1016/j.carbpol.2019.115505>
10. Brundrett MC, Bougher N, Dell B, Grove T (1996) Roots and VAM fungi. In *Working with mycorrhizas in forestry and agriculture*, 184–187. Aust. Centre Int. Agricult. Res., Canberra, Australia.
11. Tekli, J. (2022). An overview of cluster-based image search result organization: background, techniques, and ongoing challenges. *Knowl Inf Syst* 64, 589–642. <https://doi.org/10.1007/s10115-021-01650-9>
12. Rueden CT, Schindelin J, Hiner MC, DeZonia BE, Waler AE, Arena ET, Eliceiri KW (2017) ImageJ2: ImageJ for the next generation of scientific image data. *BMC Bioinformatics* 18:529. <https://doi.org/10.1186/s12859-017-1934-z>
13. Nesbit M, Mamo, JC, Majimbi M, Lam, V, Takechi R. (2021). Automated quantitative analysis of *ex vivo* blood-brain barrier permeability using intellesis machine-learning. *Front Neurosci*, 15, 617221. <https://doi.org/10.3389/fnins.2021.617221>
14. Lekberg Y, Koide RT (2005) Is plant performance limited by abundance of arbuscular mycorrhizal fungi? A meta-analysis of studies published between 1988 and 2003. *New Phytologist* 168:189–204. <https://doi.org/10.1111/j.1469-8137.2005.01490.x>
15. Vierheilig H, Schweiger P, Brundrett M (2005) An overview of methods for the detection and observation of arbuscular mycorrhizal fungi in roots. *Physiol Plantarum* <https://doi.org/10.1111/j.1399-3054.2005.00564.x>
16. Sun XG, Tang M (2012) Comparison of four routinely used methods for assessing root colonization by arbuscular mycorrhizal fungi. *Botany* 90:1073–1083. <https://doi.org/10.1139/b2012-084>

17. Vierheilig H, Piché Y (1998) A modified procedure for staining arbuscular mycorrhizal fungi in roots. *Zeitschrift für Pflanzenernährung und Bodenkunde* 161:601–602. <https://doi.org/10.1002/jpln.1998.3581610515>
18. Evangelisti, E., Turner, C., McDowell, A., Shenhav, L., Yunusov, T., Gavrín, A., Servante, E.K., Quan, C. and Schornack, S. (2021), Deep learning-based quantification of arbuscular mycorrhizal fungi in plant roots. *New Phytol.* <https://doi.org/10.1111/nph.17697>
19. Muta K, Takata S, Utsumi Y, Matsumura A, Iwamura M, Kise K. (2022). TAIM: Tool for Analyzing Root Image to Calculate the Infection Rate of Arbuscular Mycorrhizal Fungi. *Front. Plant Sci.* 13:881382. doi: 10.3389/fpls.2022.881382
20. Al Khoury C. (2021). Can colonization by an endophytic fungus transform a plant into a challenging host for insect herbivores? *Fungal Biology*. Vol 125, Issue 12, 1009-1016, ISSN 1878-6146. <https://doi.org/10.1016/j.funbio.2021.08.001>.

CHAPTER 6

Unlocking the multiphasic nature of CO- triggered intracellular calcium signatures in *Lotus japonicus* roots

Prologue

The recognition of different microbe-associated molecular patterns in the rhizosphere triggers in the plant root the activation of either an immune response or an accommodation program. In both types of responses, Ca^{2+} is a crucial intracellular messenger, mediating the early stages of the respective signalling pathways. In this work, we analysed the cytosolic and nuclear Ca^{2+} changes activated by a set of chitin-related oligomers in different genetic backgrounds of *Lotus japonicus* roots by using specifically targeted aequorin-based Ca^{2+} reporters. By means of pharmacological and genetic approaches, we dissected the Ca^{2+} signal into two temporally distinct components: a rapid initial transient, followed by a longer and milder elevation in Ca^{2+} concentration. Taking advantage of a complementary analysis using a cameleon-based bioassay in *Medicago truncatula* root organ cultures, we showed that the second phase can be interpreted as the Ca^{2+} spiking that is widely described in response to the perception of symbiotic signals. By contrast, the rapid first phase, critically dependent on elicitor concentration, was found to correlate with the activation of plant immunity marker genes. Overall, our study provides novel clues to a better understanding of the subtle boundaries between symbiotic and immunity responses in root-fungus interactions.

This work has been submitted to the Journal of Experimental Botany and currently is under revision:

Filippo Binci, Elisabetta Offer, Andrea Crosino, Ivan Sciascia, Jürgen Kleine-Vehn, Andrea Genre, Marco Giovannetti, Lorella Navazio. Unlocking the multiphasic nature of intracellular calcium signatures triggered by fungal signals in *Lotus japonicus* roots.

Introduction

In the rhizosphere, plant roots encounter myriads of microorganisms that can activate distinct transcriptional and developmental programs upon the recognition of microbe-associated molecular patterns (Verbon and Liberman, 2016; Bonhomme *et al.*, 2021; Delaux and Schornack, 2021; Chiu *et al.*, 2022). These include highly conserved microbial components such as chitin or flagellin, normally driving the plant response towards an immunity-like program (Wan *et al.* 2012; Platre *et al.*, 2022), as well as specific microbe-released signals such as Myc-factors and Nod-factors, two classes of diffusible chitin-based molecules that trigger root endosymbiotic programs, in arbuscular mycorrhizas and legume nodulation, respectively (Choi *et al.*, 2018; Ghahremani and MacLean, 2021). In both cases - immunity and symbiosis -, although microbial signals are perceived by the plant host through a set of plasma membrane-associated receptors (Zipfel and Oldroyd, 2017), a pivotal common mediator of most downstream signalling pathways is calcium. Indeed, transient increases in intracellular calcium concentration ($[Ca^{2+}]$) have been shown to be generated during plant responses to both pathogens (Ranf *et al.*, 2011; Wan *et al.*, 2012; Nars *et al.*, 2013; Keinath *et al.*, 2015; Feng *et al.*, 2019; Zhang *et al.*, 2021, Köster *et al.*, 2022) and symbionts (Navazio *et al.*, 2007; Capoen *et al.*, 2011; Genre *et al.*, 2013; Feng *et al.*, 2019; Zhang *et al.*, 2021). Such Ca^{2+} -mediated signals display subtle and not fully elucidated differences (the so-called Ca^{2+} signature) that are believed to control the activation of tailored downstream molecular, cellular and metabolic responses (Zipfel and Oldroyd, 2017). In this frame, crosstalks and overlaps have been highlighted in plant symbiotic and pathogenic interactions between microbe-released molecules, receptor roles and Ca^{2+} -mediated signal transduction pathways (Ried *et al.*, 2019; Zhang *et al.*, 2021).

In this research, we focused on arbuscular mycorrhizal (AM) symbiosis, the most ancient and widespread root endosymbiosis established between the vast majority of land plants and Glomeromycotina fungi (Choi *et al.*, 2018; Genre *et al.*, 2020). AM fungi-released Myc-factors include short-chain chitin oligomers, such as tetrameric chitooligosaccharides (CO4), and lipochitooligosaccharides (mycLCOs) with structural similarities to rhizobial Nod-factors (Maillet *et al.*, 2011; Genre *et al.*, 2013; Feng *et al.*,

2019). The recognition of Nod- and Myc-factors and the activation of the respective symbiotic programs rely on the Common Symbiotic Signalling Pathway (CSSP), encompassing a diverse set of co-receptors (LjSYMRK/MtDMI2), cation channels (LjCASTOR/MtDMI1, LjPOLLUX, MtCNGC15), Ca²⁺ transporters (MtMCA8) and Ca²⁺ sensor proteins (LjCCaMK/MtDMI3) (Charpentier, 2018; Choi *et al.*, 2018; Radhakrishnan *et al.*, 2020). Nevertheless, the cell wall of AM fungi - like all fungi - contains a large amount of long-chain chitin, a well-known pathogen-associated molecular pattern (PAMP) eliciting immunity-related responses in plants. For this reason, a number of recent studies has investigated the role of different chitin-based molecules in AM signalling, with sometimes contrasting results, likely depending on the experimental setup. While, for example, short-chain (but not long-chain) chitooligosaccharides were shown to trigger AM-specific Ca²⁺-based symbiotic signals (Genre *et al.*, 2013), a different study suggested that long-chain oligomers such as CO8 trigger both pathogenic and symbiotic signalling (Feng *et al.*, 2019). This ambiguity is also due to our limited understanding of the complexity of signal exchange during early plant-microbe interactions and the role of plant receptors and co-receptors in different interactions and different plant species (Yu *et al.*, 2017; Zhang *et al.*, 2021). In fact, the rice chitin receptor *OsCERK1* is crucial for both AM symbiosis and immunity (Zhang *et al.*, 2014, Miyata *et al.*, 2014, Carotenuto *et al.*, 2017) and the discrimination between the two responses has recently been shown to depend on the competition between two alternative co-receptors for associating with *OsCERK1* in the presence of different ligands (Zhang *et al.*, 2021). The scenario is even more complex in legumes, where the family of LysM receptor-like kinases (which include the receptors for chitin-based signals) is much more expanded than in other plants. In *Lotus japonicus*, *LjCERK6* is responsible for chitin-triggered immunity in response to fungal pathogens (Bozsoki *et al.*, 2017) but the corresponding receptors involved in AM symbiosis remain elusive (Chiu *et al.*, 2020). Altogether, a picture is emerging where the composition of fungal signals and the overlapping roles of plant plasma membrane receptors generate an intricate continuum between immunity and symbiosis (Zhang *et al.*, 2021).

A second level of confounding factors derives from the use of distinct methodological

approaches to the analysis of Ca²⁺-mediated plant responses (Costa *et al.*, 2018; Grenzi *et al.*, 2021). On the one hand, intracellular Ca²⁺ elevations in response to the perception of different PAMPs mainly have been investigated in entire plants by using the cytosolic-expressed bioluminescent probe aequorin (Ranf *et al.*, 2011; Monaghan *et al.*, 2015). On the other hand, CO- and LCO-triggered oscillations in perinuclear and nuclear Ca²⁺ concentrations (the so-called Ca²⁺ spiking) have been characterised at the single-cell level with the use of fluorescent genetically encoded calcium indicators (GECIs), such as cameleon or GECO (Genre *et al.*, 2013; Kelner *et al.*, 2018; Feng *et al.*, 2019; Zhang *et al.*, 2021). This has largely hampered the possibility of a direct comparison between the two sets of results, with few exceptions. Flagellin- and chitin-induced cytosolic Ca²⁺ elevations revealed an oscillatory nature when analysed with Yellow Cameleon 3.6 and GECO (Thor and Peiter *et al.*, 2014, Keinath *et al.*, 2015). Furthermore, symbiotic signals were found to induce a characteristic cytosolic Ca²⁺ elevation (Miwa *et al.*, 2006; Navazio *et al.*, 2007) that was described as a Ca²⁺ influx and - in the case of legume nodulation - was required for symbiosis development (Moriere *et al.*, 2013). In short, the need is emerging to investigate and integrate Ca²⁺-mediated plant responses to biotic signals by using multiple approaches and combining qualitative (Ca²⁺ imaging) and quantitative (Ca²⁺ measurement) approaches.

In this work, we analysed the effects induced by a set of chitin-related oligomers on cytosolic and nuclear Ca²⁺ levels in different genetic backgrounds of *L. japonicus* roots by using specifically targeted aequorin-based Ca²⁺ reporters. We accurately quantified the root Ca²⁺ signatures upon treatment with specific fungal molecules and showed that CO4-, CO8- and mycLCO-induced Ca²⁺ elevations are distinct for their intracellular localization, temporal dynamics and plant genetic requirements. An alternative approach based on Ca²⁺ imaging with a nuclear-localized cameleon probe in *Medicago truncatula* root organ cultures further supported our description of two distinct temporal phases in the observed Ca²⁺ responses, depending on the concentration of the stimulus and the genetic background. Our analyses of the overall plant root response in terms of intracellular Ca²⁺ changes help disentangling the complex communication circuits in the rhizosphere and enhance our quantitative understanding of how plant roots can perceive

and transduce different fungal molecules.

Materials and Methods

Molecular cloning and bacterial transformation

The nucleotide sequence encoding the bioluminescent Ca²⁺ indicator aequorin fused to Yellow Fluorescent Protein (YFP) and targeted to either the cytosol-only (CPK17_{G2A}-NES-YA) or nucleus-only (NLS-YA) (Mehlmer *et al.*, 2012) were amplified with Q5 DNA polymerase (NEB) according to manufacturer's instructions. The promoter (1100 bp upstream of the ATG) of ubiquitin10 was amplified from the genome of *Lotus japonicus* (Gifu ecotype). Primers (listed in Table S1) were designed to be compatible with the GreenGate cloning system and cloning of the entry vectors was performed according to it (Lampropoulos *et al.*, 2013). Expression vectors were assembled via cut-ligation with BsaI (NEB) and T4-DNA ligase (NEB), following the GreenGate protocol. The selection and amplification of vectors were performed in DH5 α *E. coli* cells. The sequences were checked via Sanger sequencing at BMR Genomics (Padova, Italy) and by Primordium long-read DNA sequencing at Primordium Labs (Arcadia, CA, USA). The expression vectors were then transformed into *Agrobacterium rhizogenes* 1193 via the freeze & thaw method (Wise *et al.*, 2006). Expression vectors are listed in Table S2.

Generation of Lotus japonicus composite plants

L. japonicus ecotype Gifu seeds were scarified with sandpaper and sterilized in 0.5% (w/v) sodium hypochlorite for 11 min. Seeds were then rinsed and washed 5 times in sterile distilled water. For germination, seeds were placed into sterile Petri dishes with H₂O with 1% (w/v) plant agar and wrapped in aluminum foil. After 3 days at 23°C, young seedlings were transferred to square plates (12x12 cm) containing ½ strength B5 growth medium, supplemented with 0.8% (w/v) plant agar and adjusted to pH 5.5 with 1 M KOH. Plates were grown vertically under long-day conditions (23°C, 16 h light/8 h dark cycle). After 3 days, the seedlings were transformed via *A. rhizogenes* 1193 - mediated hairy root transformation (Boisson-Dernier *et al.*, 2001). The root was cut off with a blade and the wound was dipped into a fully grown plate of *A. rhizogenes* carrying the plasmid of interest. The infected shoots were then placed onto square plates (12x12) containing ½ strength B5 growth medium, 0.8% plant agar, pH 5.5. After 16 h in the

darkness, seedlings were co-cultivated with bacteria for 3 days. Afterward, the seedlings were transferred into new squared plates with the same medium supplemented with 300 mg/ml cefotaxime and 0.1% Plant Preservative Mixture (PPM, Duchefa) under long-day conditions (23°C, 16 h light/8 h dark cycle). After 3 weeks, transformed roots were checked for expression of the transformation marker (pAtUBQ10::mCherry) using the stereomicroscope MZ16F (Leica). The intracellular localization of the probe was confirmed by confocal microscopy observations (Zeiss LSM900 Airyscan2). Transformed plants were kept in the same growth medium under long-day conditions (23°C, 16 h light/8 h dark cycle).

Aequorin-based Ca²⁺ measurement assays

For Ca²⁺ measurement assays in *L. japonicus* composite plants, 5 mm segments of transformed roots expressing aequorin targeted to either the cytosol or nucleus were reconstituted overnight with 5 mM coelenterazine. On the following day, after extensive washing, each root piece was placed in the dark chamber of a custom-built luminometer (Electron Tubes) containing a 9893/350A photomultiplier (Thorn EMI). The root was placed in 50 µl H₂O and challenged by injection of an equal volume of a 2-fold concentrated solution for each tested stimulus: CO₄, CO₈ (IsoSep), mycLCOs (equimolar mix of both non-sulfated and sulfated C16:0 and C18:1). The stock solutions were 10⁻³ M in 50% ethanol for CO₄, 10⁻⁴ M in 50% ethanol for CO₈, 10⁻³ M in DMSO for mycLCOs. Controls were performed by injecting an equal volume of the solvents in which the compounds are dissolved at the working concentration. Ca²⁺ dynamics were recorded for a total of 30 min before the injection of 100 µl of the discharge solution (30%, v/v, ethanol, 1 M CaCl₂). The light signal was collected and converted offline into Ca²⁺ concentration values using a computer algorithm based on the Ca²⁺ response curve of aequorin (Brini *et al.*, 1995). All Ca²⁺ concentration values for each biological replicate are available (Table S3). For pharmacological analyses, the root pieces, before challenge with chito-oligomers, were pre-treated with the pharmacological agents for different time intervals: 1.5 mM LaCl₃ (Sigma) and 2 mM EGTA (Sigma) for 10 min,

50 μ M cyclopiazonic acid (CPA, stock solution 30 mM in DMSO) for 1 h, 10 μ M VAC1 (stock solution 10^{-3} M in DMSO) for 2.5 h (Dünser *et al.*, 2021).

Cameleon-based Ca^{2+} imaging assays

Medicago truncatula genotype Jemalong A17 and the *dmi2-2* mutant (Catoira *et al.*, 2000) were genetically transformed using *A. rhizogenes* to generate root organ cultures expressing the nuclear-localized 35S:NupYC2.1 cameleon construct (Sieberer *et al.*, 2009), as described in Chabaud *et al.* (2011). Ca^{2+} imaging was conducted on excised young lateral roots, placed in 2mm-thick microscope slide microchambers. The water in the microchamber was rapidly (< 30 s) substituted by 200 μ l of CO_4 solution before initiating confocal image acquisition within 1-3 minutes. FRET-based ratio imaging of the YFP and CFP cameleon fluorescence was used for the detection and plotting of relative changes in nuclear Ca^{2+} levels (Chabaud *et al.*, 2011).

Gene expression analysis

L. japonicus Gifu seeds were sterilized as described above and the seedlings were grown for 10 days (23°C, 16 h light/8 h dark cycle) in vertical square plates (12x12 cm) containing ½ strength B5 growth medium, 0.8% (w/v) agar, pH 5.5. Groups of 12 plants were treated in 4 ml solutions containing either 10^{-7} M CO_4 , 10^{-9} M CO_4 or the control treatment (50% ethanol diluted 1:1000). The grouped samples were harvested after 1 h of treatment. During harvesting, the roots were cut from the shoots and immediately frozen in liquid N_2 in a 2 ml tube containing two metal beads. The root material was homogenized with TissueLyser II (Qiagen) at 30 Hz for 45 seconds. Total RNA was extracted using the RNeasy Plant Mini Kit (Qiagen) following the manufacturer's instructions. RNA quantity and quality were checked by nanodrop and agarose gel electrophoresis. After DNase I (Invitrogen) treatment, cDNA synthesis was performed with random hexamers using the RevertAid RT Kit (Thermofisher). qRT-PCR was performed using the HOT FIREPOL EvaGreen qPCR mix plus (Solis Biodyne) on a 7500 real-time PCR system (Applied Biosystems). The *LjUbiquitin10* gene was used as an internal reference for analysis of the target gene expression. All the primers (Table

S1) used for the qRT-PCR analyses have been previously published (Nakagawa *et al.*, 2011; Giovannetti *et al.*, 2015; Bozsoki *et al.*, 2017).

Statistical analysis and data visualisation

Data were statistically analysed and presented graphically using R statistical environment and Rstudio (RStudio Team, 2020; R Core Team, 2022). When passing its assumptions, the Anova test and Tukey's post-hoc test was applied, in the other cases, Kruskal Wallis and Dunn's tests were performed (Table S3). R scripts (Supplementary Dataset S1) and raw data (Supplementary Dataset S2-S8) ensure full reproducibility of statistical analysis and plots.

Results

Different fungal signals activate apparently similar Ca²⁺ transients in both the cytosol and nucleus of L. japonicus roots

To monitor intracellular Ca²⁺ dynamics in *L. japonicus* roots, we assembled expression cassettes for YFP-tagged aequorin reporters specifically targeted to either the cytosol or the nucleus (Mehlmer *et al.*, 2012) under the control of the *LjUBI10* promoter (Supplementary Fig. S1). The constructs were inserted into *L. japonicus* Gifu background via *A. rhizogenes*-mediated hairy roots transformation and the correct localization of the Ca²⁺ probes was confirmed by confocal microscopy analyses (Supplementary Fig. S1). Root segments from *L. japonicus* composite plants were then challenged with the purified fungal signals CO4 (short-chain COs), CO8 (long-chain COs) and mycLCOs (sulfated and non-sulfated lipo-COs mixture), and the changes in intracellular [Ca²⁺] were measured. All categories of chitin-based oligomers were found to trigger stimulus-specific cytosolic Ca²⁺ signatures, varying according to the intensity and timing of the Ca²⁺ increase. In particular, CO4 and CO8 transiently induced cytosolic Ca²⁺ transients characterised by the highest magnitude of the peak (Figure 22A-C, Table S3 and Dataset S2). No Ca²⁺ changes were recorded upon administration of solvent controls (Figure 22A and Dataset S2).

Notably, the overall shape of the observed cytosolic Ca²⁺ dynamics is markedly biphasic, with an initial major peak recorded in the first 8 minutes after stimulation, followed by a broader shoulder. Such dynamics closely resembles those triggered by germinating spore exudates of *Gigaspora margarita* (Navazio *et al.*, 2007; Moscatiello *et al.*, 2018). CO4, mycLCOs, and CO8 were also found to induce Ca²⁺ transients in the nucleus (Figure 22B,D), in agreement with the activation of nuclear Ca²⁺ responses by short-chain (Genre *et al.*, 2013; Sun *et al.*, 2015) and long-chain COs (Feng *et al.*, 2019) monitored with cameleon probes. Interestingly, no significant differences could be detected in either the overall shape or peak intensity of the nuclear-induced Ca²⁺ transients triggered by the three categories of microbial signals (Figure 22 and Table S3).

Overall, the Ca^{2+} transients activated by the different fungal signals, and monitored via aequorin-based reporters, looked apparently similar, apart from the intensity of the early cytosolic Ca^{2+} peak.

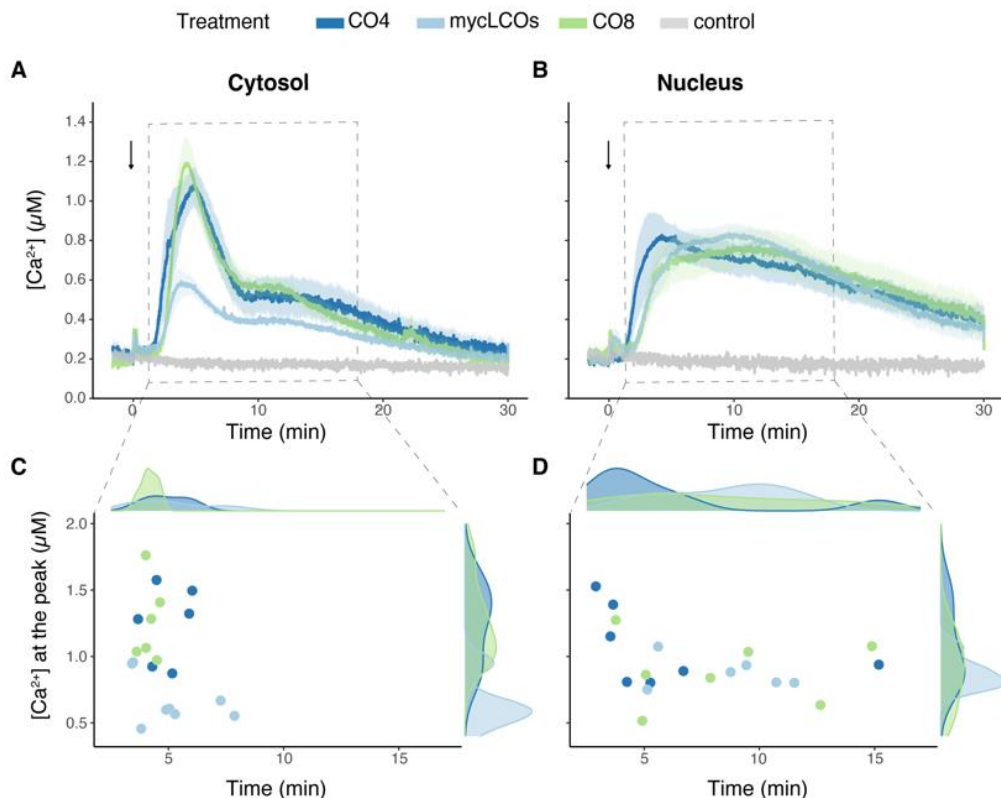


Figure 22. Monitoring of cytosolic and nuclear free $[\text{Ca}^{2+}]$ in 5 mm-long root segments from composite plants of *L. japonicus* in response to different chitin-based oligomers. *L. japonicus* roots were transformed via *A. rhizogenes* with constructs encoding aequorin chimeras targeted to either the cytosol (A,C) or nucleus (B,D) and subcellular Ca^{2+} dynamics were measured after challenge with 10^{-7} M CO4 (dark blue), 10^{-6} M CO8 (green), 10^{-7} M mycLCOs (light blue) or with the same concentration of the solvents in which the compounds were dissolved (grey). In A-B, data are presented as means \pm SE (shading) of $n \geq 6$ traces from at least 3 different composite plants (independent transformations). The arrow indicates the time of stimulus injection (time 0). In C-D, dots represent the maximum $[\text{Ca}^{2+}]$ value for each trace in the time range of 1-18 minutes. The frequency distributions of the dots are represented on top of the panel (time) and at the right of the panel ($[\text{Ca}^{2+}]$).

Origin and modulation of the CO4-induced intracellular Ca^{2+} fluxes

To elucidate the source of the observed nuclear and cytosolic Ca^{2+} fluxes activated by chitin oligomers we performed a pharmacological analysis, focusing on CO4, *i.e.* the symbiotic signals that triggered the strongest $[\text{Ca}^{2+}]$ changes in our experimental conditions. Firstly, in order to assess the contribution of extracellular Ca^{2+} to the generation of the observed Ca^{2+} responses, we pre-treated roots with either the Ca^{2+}

channel inhibitor LaCl_3 or the extracellular chelator EGTA. LaCl_3 treatment caused a complete abolishment of the Ca^{2+} response to CO4 in both the cytosol (Figure 23A,C, Table S3 and Supplementary Dataset S3) and nucleus (Figure 23B,D and Table S3). The cytosolic Ca^{2+} trace was almost completely flattened also in the presence of EGTA, where the main peak of the first phase (within 8 min after the stimulus, hereafter called phase 1) was replaced by a very limited elevation (Figure 23A,C and Table S3). EGTA only abolished the second part of the Ca^{2+} transient (8-30 min after the stimulus, hereafter phase 2) in the nucleus, while the phase 1 peak was maintained (Figure 23B,D and Table S3). These experiments suggested that Ca^{2+} in the external milieu can have a more relevant impact on phase 1 Ca^{2+} cytosolic signalling, rather than on the phase 1 peak in nuclear $[\text{Ca}^{2+}]$.

We then misregulated Ca^{2+} homeostasis in the plant cell endomembrane system, by applying drug treatments targeting the endoplasmic reticulum (ER) and the vacuole. The first drug we tested was cyclopiazonic acid (CPA), an inhibitor of ER-type Ca^{2+} ATPases present in the ER membrane, causing Ca^{2+} depletion of the ER lumen (De Vriese *et al.*, 2018; Cortese *et al.*, 2022). Pre-treatment with CPA did not alter the phase 1 peak in cytosolic Ca^{2+} elevation evoked by CO4 (Figure 23A,C and Table S3), suggesting that the ER to be acting as a Ca^{2+} sink, rather than a source, in this phase. By contrast, CPA completely abolished the Ca^{2+} transient in the nucleus (Figure 23B,D and Table S3); this is consistent with the predicted role played by the nuclear envelope - in continuity with the ER lumen - as a major source for nuclear and perinuclear Ca^{2+} spiking (Capoen *et al.*, 2011).

The second drug we used was VAC1, an inhibitor of SNARE-dependent vesicle fusions. VAC1 treatment is known to reduce cargo and membrane delivery to the vacuole, leading to an overall reduction in the vacuole size (Dünser *et al.*, 2022), thereby potentially affecting the Ca^{2+} homeostasis. After pre-treatment of *L. japonicus* roots with VAC1, the phase 1 Ca^{2+} peak in response to CO4 was strongly reinforced (Figure 23A,C and Supplementary Fig.S2), suggesting that VAC1- dependent alterations in vacuolar function reduced Ca^{2+} uptake from the cytosol. Nevertheless, the nuclear Ca^{2+} transient was largely unaffected in VAC1 pre-treated roots (Figure 23B,D and Table S3),

indicating that the vacuole has a minor (if any) role in the generation of symbiotic Ca^{2+} signals in the nucleus.

In short, our pharmacological analyses confirmed on the one hand the crucial role of the ER in the generation of nuclear Ca^{2+} signals in response to short-chain chitin oligomers (CO4). On the other hand, our data also demonstrated that the early and strong Ca^{2+} peak triggered by CO4 in the cytosol results from the combined action of a Ca^{2+} influx from the apoplast and sequestration in the vacuole.

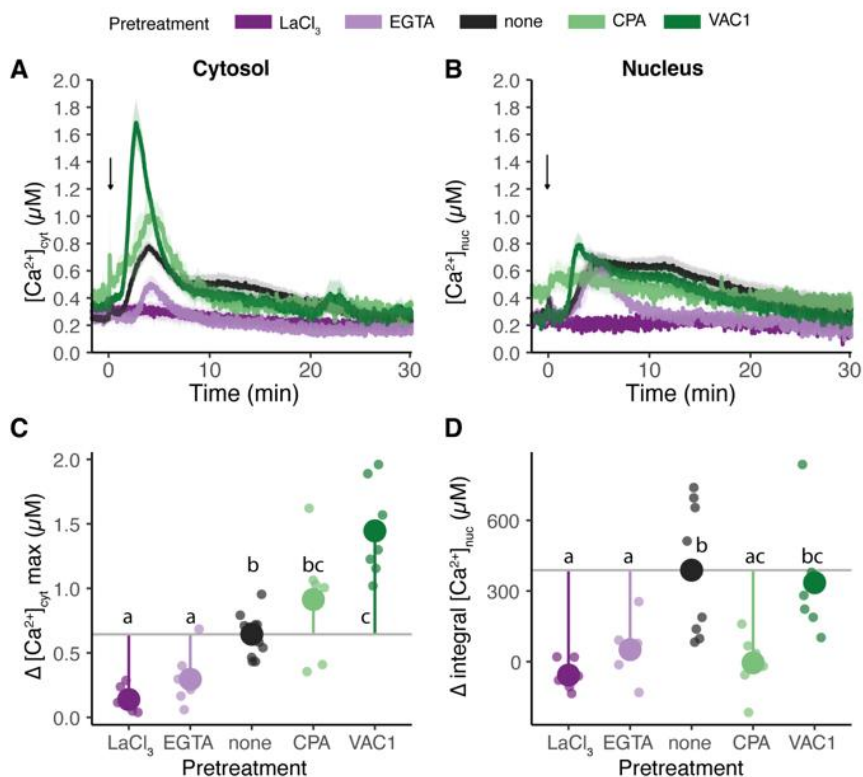


Figure 23. Pharmacological analyses of short-chain CO4-induced intracellular Ca^{2+} fluxes in *L. japonicus* roots. Cytosolic $[\text{Ca}^{2+}]_{\text{cyt}}$ (A,C) and nuclear $[\text{Ca}^{2+}]_{\text{nuc}}$ (B,D) dynamics were monitored in 5-mm long root segments from composite plants challenged with 10^{-7} M CO4 after pre-treatment with either 1.5 mM LaCl_3 (dark violet), 2 mM EGTA (light violet), 50 μM CPA (dark green), 10 μM VAC1 (light green) or none (grey, either H_2O or solvent control). In A-B, data are presented as means \pm SE (shading) of $n \geq 6$ traces obtained from at least 3 different composite plants (independent transformation). In C-D, small dots represent the delta maximum cytosolic $[\text{Ca}^{2+}]$ ($\Delta[\text{Ca}^{2+}]_{\text{cyt}}$) (C) and the delta integrated $[\text{Ca}^{2+}]$ ($\Delta[\text{Ca}^{2+}]_{\text{nuc}}$) (D) for each trace in the time range of 2-20 minutes, while the big circles represent the mean. $\Delta[\text{Ca}^{2+}]$ was calculated by subtracting the mean of the resting $[\text{Ca}^{2+}]$ in the pre-stimulus phase to each $[\text{Ca}^{2+}]$ measurement value following the stimulus injection (arrow). The coloured vertical line shows the difference between the mean of each treatment and the control (horizontal grey line). Different letters indicate statistically significant differences among groups, according to Kruskal-Wallis test followed by Dunn's post-hoc correction (p -value < 0.05).

Nuclear and cytosolic Ca²⁺ signatures triggered by chitin-derived oligomers differentially depend on the Common Symbiotic Signalling Pathway

To evaluate the role of the CSSP in triggering the observed Ca²⁺ signals in *L. japonicus* roots upon perception of chitin-derived molecules, we compared our analyses in wild-type *L. japonicus* and mutants for *LjSYMRK* and *LjCASTOR*, two well-characterised components of the CSSP (Oldroyd, 2013; Choi *et al.*, 2018; Radhakrishnan *et al.*, 2020). Phase 1 of the cytosolic Ca²⁺ transient was found to be maintained in the CSSP mutants, but with slight differences among stimuli and genotypes. Firstly, the CO4-induced cytosolic Ca²⁺ peak was significantly reduced in *castor* compared to both the wild-type and *symrk* (Supplementary Fig. S2A-B, Dataset S3 and Table S3). Secondly, the CO8-induced cytosolic Ca²⁺ peak showed a limited increase in both *symrk* and *castor*, compared to the wild-type (Supplementary Fig. S2E-F and Table S3). Lastly, no differences could be identified in the mycLCO-induced cytosolic Ca²⁺ peak in phase 1, which was anyway rather limited also in the wild-type (Supplementary Fig. S2I-J and Table S3). By contrast, a slight reduction was detected in the phase 2 Ca²⁺ elevation in response to both CO4 and mycLCOs in both the CSSP mutants in comparison with the wild-type, whereas the Ca²⁺ traces measured in response to CO8 were nearly superimposable (Supplementary Fig. S2 and Table S3).

The differences between genetic backgrounds became more apparent when focusing on nuclear Ca²⁺ transients (Figure 24). Indeed, the phase 2 broad dome-shaped Ca²⁺ elevation was absent in CO4- and mycLCO-treated mutants, but only weakly reduced upon CO8 application. This is further supported by the quantification of mobilised Ca²⁺ in terms of integral [Ca²⁺] and time duration of the response above an arbitrary [Ca²⁺] threshold (width) (Figure 24A-D, I-L and Table S3). Conversely, the initial and steep increase in nuclear [Ca²⁺] triggered by the three stimuli was retained in *symrk* and *castor* mutants. Together, these results suggest that a functional CSSP is not required for the cytosolic Ca²⁺ influx of phase 1, even if it appears to modulate it. The absence or reduction of the phase 2 nuclear and cytosolic Ca²⁺ elevation, respectively, in CSSP mutants were particularly intriguing because they mirrored the lack of nuclear and perinuclear Ca²⁺ spiking described in literature for mutants of the orthologous genes in

M. truncatula (Genre *et al.*, 2013; Feng *et al.*, 2019). We therefore hypothesised that the dome-shaped Ca^{2+} elevation recorded in phase 2 by our aequorin-based analyses of Ca^{2+} concentration in the whole root system may correspond to the sum of individual and non-synchronous Ca^{2+} -spiking events triggered in single root cells and previously described in studies based on fluorescent GECIs (Genre *et al.*, 2013; Kelner *et al.*, 2018; Feng *et al.*, 2019). Furthermore, by combining these observations with the results of our EGTA treatments, we concluded that the nuclear Ca^{2+} signalling triggered by CO4 and mycLCOs is composed of a CSSP-independent Ca^{2+} influx from the apoplast during phase 1 and a CSSP-dependent, nuclear-envelope generated Ca^{2+} elevation during phase 2, that we speculated to correspond to nuclear Ca^{2+} -spiking.

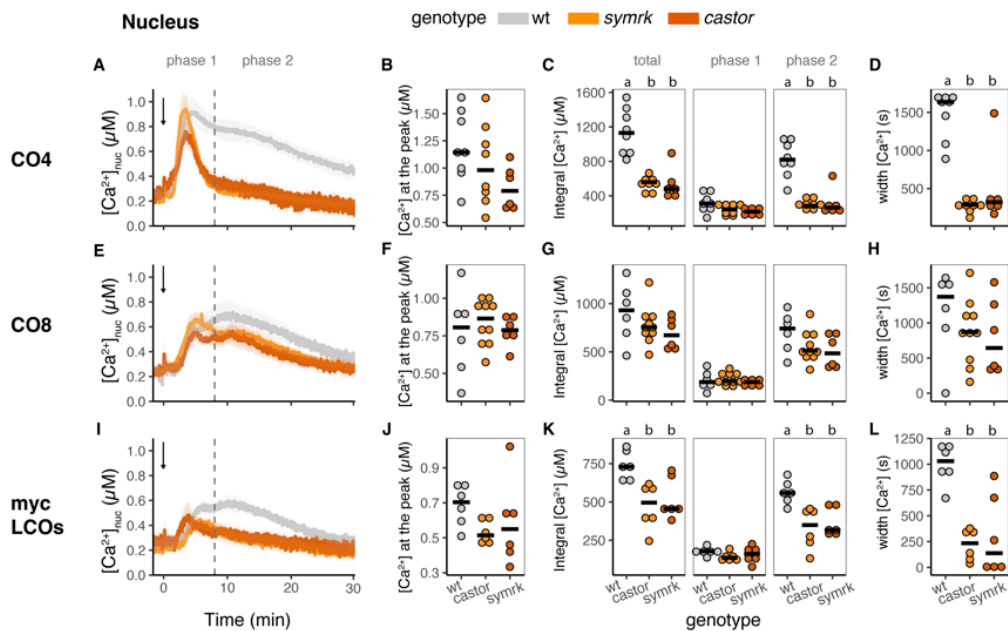


Figure 24. Monitoring of free nuclear $[\text{Ca}^{2+}]$ in 5 mm-long root segments from composite plants of *L. japonicus* Gifu wt (grey), *castor* (dark orange), *symrk* (light orange). Ca^{2+} measurements were conducted in response to 10^{-7} M CO4 (A-D), 10^{-6} M CO8 (E-H), 10^{-7} M mycLCOs (I-L). In A, E, I, data are presented as means \pm SE (shading) of $n \geq 6$ traces from at least 3 different composite plants (independent transformation). Arrows indicate the time of stimulus injection (time 0). The dashed line separates phase 1 (0-8 minutes after stimulus) and phase 2 (8-30 minutes after stimulus). In B, F, J, dots represent the maximum $[\text{Ca}^{2+}]$ for each trace in the whole run. In C, G, K, dots represent the integrated $[\text{Ca}^{2+}]$ for each trace in the whole run and in the two different phases. In D, H, L, dots represent the Ca^{2+} transient width, in terms of the time interval in which $[\text{Ca}^{2+}]$ exceeds the arbitrary threshold of 0.4 μM . The black line represents the median of each group. Different letters indicate statistically significant differences among groups, according to Kruskal-Wallis test followed by Dunn's post-hoc correction (p -value < 0.05).

Cameleon-based analyses of nuclear Ca^{2+} oscillations confirm a multiphasic response to CO_4

In order to test this hypothesis, we deployed an alternative set of experiments based on the fluorescent Ca^{2+} probe NupYC2.1, expressed in *Medicago truncatula* root organ cultures. When challenged with 10^{-7} M CO_4 , root atrichoblasts displayed a cell-autonomous range of Ca^{2+} -spiking signals (Figure 25A,B and Dataset S5), in line with literature data (Genre *et al.*, 2013). In more detail, we recorded 30-minute-long traces of at least 9 active atrichoblasts from 8 independent root samples, and the responding cells typically displayed an early elevation in $[\text{Ca}^{2+}]$ of variable height, shape and duration, but always embraced within the first 8 minutes from treatment. Subsequently, a series of peaks in $[\text{Ca}^{2+}]$ appeared, also in this case with a very broad variability in terms of peak number, frequency and regularity.

In order to compare this cameleon-based, single cell imaging of nuclear Ca^{2+} oscillations with aequorin-based whole-root analyses, we generated average traces combining the signals acquired from all responding cells for each root and a polynomial curve fitting data points of the resulting average trace for each root (Figure 25C,D and Dataset S1). The resulting Ca^{2+} curve showed an initial elevation during the first 8 minutes after treatment, followed by a second, broader shoulder, with a remarkable resemblance to the traces obtained with our aequorin-based analyses of nuclear $[\text{Ca}^{2+}]$. This provided convincing support to our hypothesis that whole-root records by the bioluminescence Ca^{2+} probe correspond to the summation of a population of Ca^{2+} signals from individual cells, as recorded using fluorescence-based Ca^{2+} reporters.

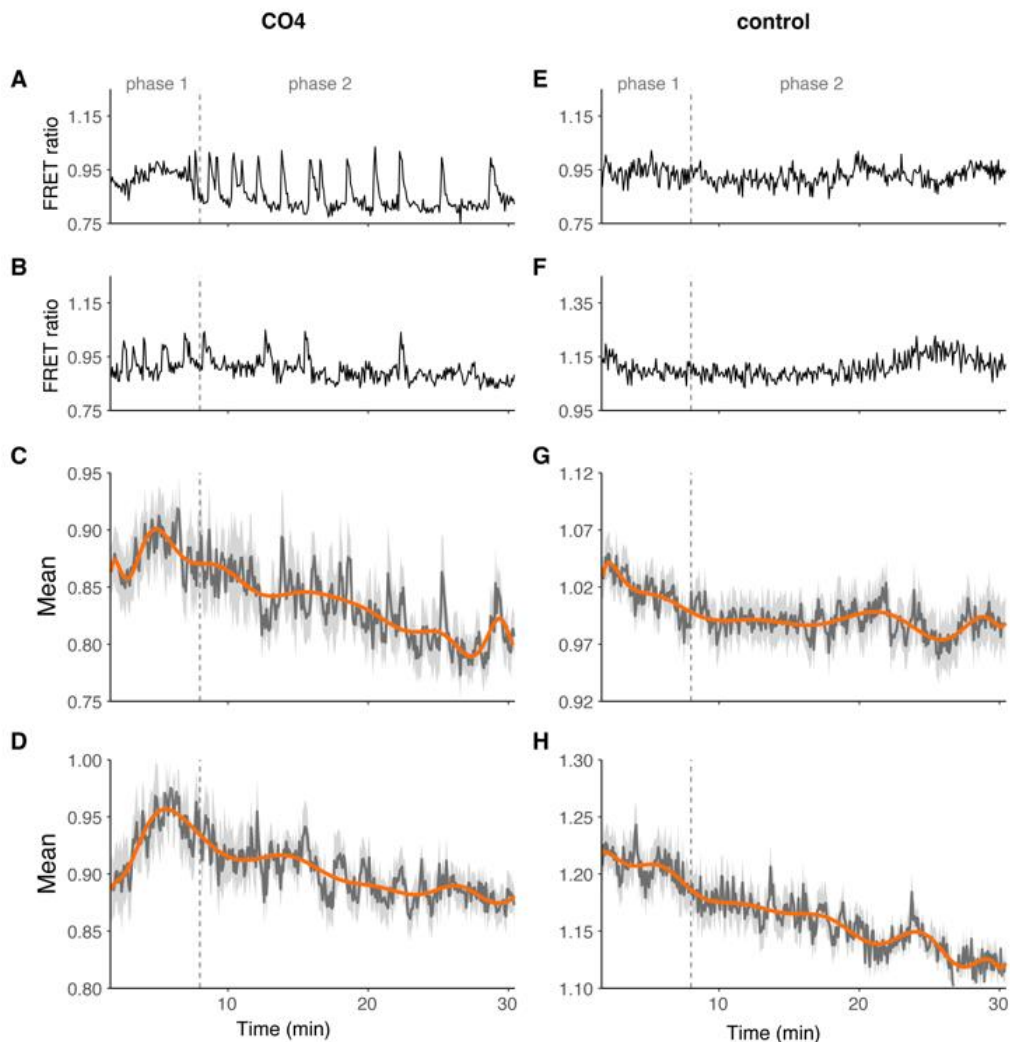


Figure 25. Traces of nuclear Ca^{2+} in root atrichoblasts of *M. truncatula*. A,B,E,F show representative nuclear Ca^{2+} profiles (expressed as YFP/CFP FRET ratio) of individual cells from treated (10^{-7} M CO4) and untreated (control) root segments. CO4 treatment triggered intense oscillations (spiking) in nuclear Ca^{2+} levels. C,D,G,H show polynomial curves (orange) fitting the average values (dark grey) of the FRET traces from the responding cells (light grey) of two independent roots, treated (C,D) or not (G,H) with CO4. The polynomial curves of CO4-treated roots display an initial maximum within the first 8 minutes and a second less pronounced elevation in the following period. A minimum of 9 nuclei were imaged for each root.

The initial phase of the CO4- and CO8-induced cytosolic and nuclear Ca²⁺ changes relies on the LysM receptor CERK6

The pharmacological approach and the use of CSSP mutants in the aequorin-based Ca²⁺ measurement assays in *L. japonicus* roots challenged with chitin-derived oligomers allowed to abolish either the whole Ca²⁺ response (Figure 23) or phase 2 only (Figure 24), but not phase 1 alone. Since phase 1 Ca²⁺ peak is particularly strong upon CO8 and CO4 treatment and a steep cytosolic Ca²⁺ influx is known to play a crucial role in plant immunity (Ranf *et al.*, 2012; Monaghan *et al.*, 2015; Kutschera *et al.*, 2019; Thor *et al.*, 2020), we analysed Ca²⁺ responses in the *L. japonicus cerk6* mutant background. CERK6 is a LysM-receptor kinase with high affinity for chitin oligomers and, according to previous reports, *cerk6* plants are unable to mount the immunity response against purified fungal molecules and show increased susceptibility to pathogen infection (Boszoki *et al.*, 2017 and 2020). In our hands, CO4 and CO8-induced cytosolic and nuclear Ca²⁺ responses were partially impaired in *cerk6* mutants compared to wild-type and *symrk* mutants (Figure 26 and Supplementary Dataset S4). Even if only about 30% of *cerk6* root fragments displayed Ca²⁺ signals in response to our treatments (compared to a responsiveness close to 100% in the other genetic backgrounds), all responding *cerk6* plants showed a very similar Ca²⁺ transient, whose timing was consistent with the maintenance of phase 2 only, as recorded in wild-type plants. This observation provided important additional insight into the biphasic nature of the Ca²⁺ responses that we recorded in the wild-type. We can in fact conclude that these include a CERK6-dependent, CSSP-independent phase 1, embracing a major Ca²⁺ influx from the apoplast, and a CERK6-independent, CSSP-dependent phase 2, corresponding to nuclear/perinuclear Ca²⁺-spiking.

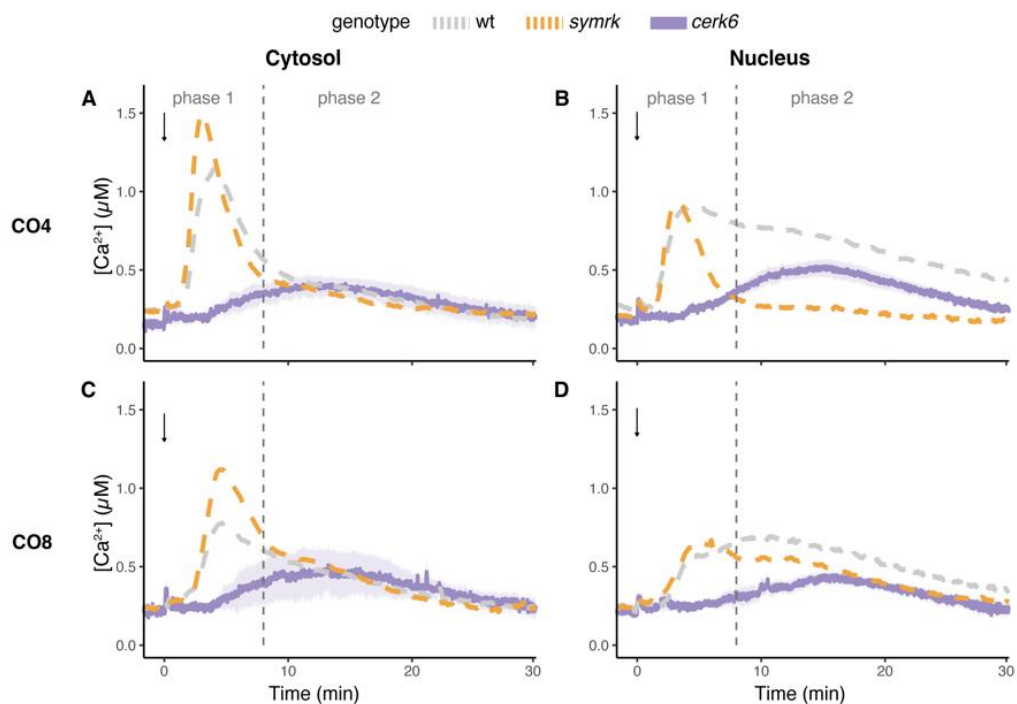


Figure 26. Monitoring of free cytosolic and nuclear $[Ca^{2+}]$ in 5 mm-long root segments from composite plants of *L. japonicus cerk6* (purple). Ca^{2+} measurements were conducted in the cytosol (A,C) and nucleus (B,D) in response to 10^{-7} M CO4 (A,C), 10^{-6} M CO8 (B,D). Data are presented as means \pm SE (shading) of $n \geq 3$ traces from at least 3 responsive composite plants (independent transformation). The Ca^{2+} responses measured in the Gifu wt (grey) and *symrk* (light orange) are shown as moving average (dashed line) for comparison. Arrows indicate the time of stimulus injection (time 0). The dashed line separates phase 1 (0-8 minutes after stimulus) and phase 2 (8-30 minutes after stimulus).

Fungal elicitor concentration affects the amplitude of the phase 1 Ca^{2+} elevation and the activation of immunity marker genes

It has previously been demonstrated that intracellular Ca^{2+} changes in response to rhizobial Nod-factors are concentration-dependent (Shaw et al, 2003). To test if this was also the case for fungal chitin oligomers, we monitored cytosolic and nuclear Ca^{2+} signals in *L. japonicus* roots challenged with serial dilutions of CO4 and CO8 (Figure 27, Supplementary Fig. S3 and Dataset S6). Intriguingly, we found that the amplitude of the phase 1 peak in $[Ca^{2+}]$ is strongly dependent on the concentration for both CO4 and CO8. Conversely, phase 2 was not apparently affected by the working dilutions. In more detail, 10^{-6} M and 10^{-7} M CO4 generated comparable Ca^{2+} signals, suggesting that the system is already saturated at 10^{-7} M. By contrast, the phase 1 Ca^{2+} peak triggered by 10^{-8} M CO4 was reduced in the cytosol, but unchanged in the nucleus. Moreover, 10^{-9} M CO4 did not trigger any response in the cytosol, while the nuclear phase 2 elevation

persisted (Figure 27A-B). In line with these observations, the treatment of NupYC2.1 *M. truncatula* ROCs with 10^{-9} M CO₄ resulted in nuclear Ca²⁺ traces that often lacked the phase 1 Ca²⁺ influx (Supplementary Fig. S4 and Dataset S7) but retained phase 2 Ca²⁺ spiking, albeit overall less pronounced than upon 10^{-7} M CO₄ treatments (Figure 25).

To investigate the physiological relevance of phase 1 Ca²⁺ peak and its possible link with plant defence system, we decided to test to what extent 10^{-7} M and 10^{-9} M CO₄ trigger the expression of the immunity marker genes *LjChitinase*, *LjRbohB-like*, *LjWRKY70-like*, *LjPRp27-like* (Bozsoki *et al.*, 2017). Indeed, our highest concentration of CO₄ triggered the expression of all four immunity markers as soon as 1 h after treatment. By contrast, 10^{-9} M CO₄ failed to activate the above-mentioned genes, with the only exception of a slight but significant induction of *PRp27-like* (Figure 27E and Supplementary Dataset S8). Intriguingly, according to LotusBase ExpressionAtlas (Mun *et al.*, 2016; Kamal *et al.*, 2020), *LjPRp27-like* shows a peculiar expression pattern with strong and specific gene activation in both *Ralstonia*-infected plants and AM-colonised roots (Supplementary Fig. S5). This expression profile is unique among the tested immunity marker genes (Lotus Base) and could provide an explanation for the activation of *LjPRp27-like* gene by the low concentration of CO₄.

Altogether, these results are consistent with our analysis of Ca²⁺ signals and indicate a dose-dependent regulation of both Ca²⁺-mediated signalling and immunity-related gene expression.

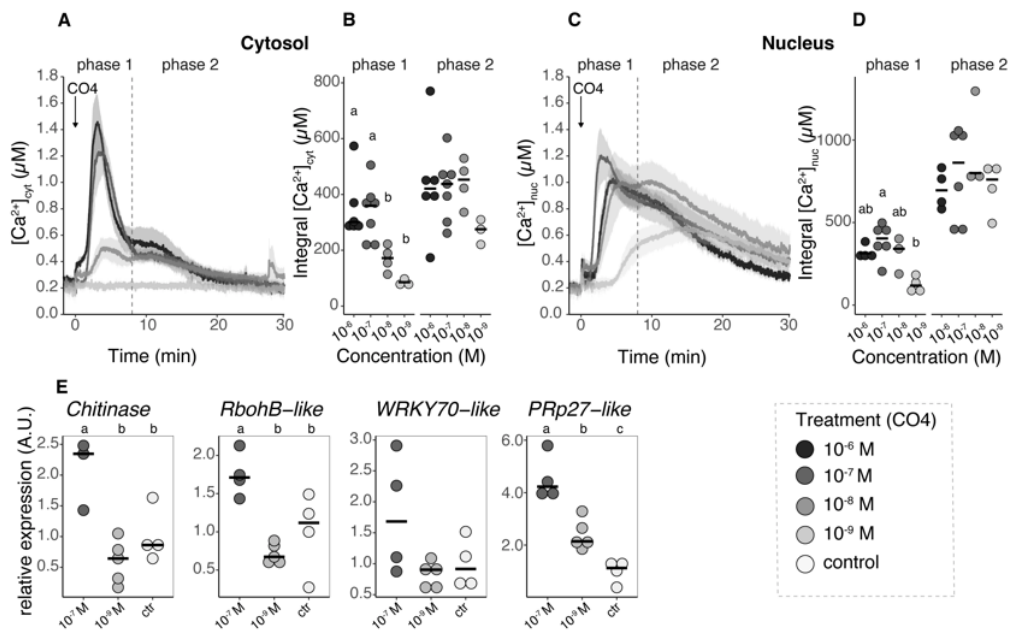


Figure 27. The effect of serial dilutions of CO4 on the induced intracellular Ca^{2+} changes (A-D) and on the activation of immunity marker genes (E). In A, changes in free cytosolic and nuclear $[Ca^{2+}]$ were measured in 5 mm-long root segments from composite plants of *L. japonicus* in Gifu wt in response to progressive dilutions of CO4 (10^{-6} M black trace, 10^{-7} M dark grey trace, 10^{-8} M grey trace, 10^{-9} M light grey trace). In A and C, data are presented as means \pm SE (shading) of $n \geq 3$ traces from at least 3 different composite plants (independent transformation). Arrows indicate the time of stimulus injection (time 0). The dashed line separates phase 1 (0-8 minutes after stimulus) and phase 2 (8-30 minutes after stimulus). In B and C, dots represent the integrated $[Ca^{2+}]$ for each trace in the two different phases. The black line represents the median of each group. In E, gene expression analysis by qRT-PCR of *LjChitinase* (Lj5g3v1961260), *LjRbohB-like* (Lj6g3v1549190), *LjWRKY70-like* (Lj1g3v1134110), *LjPRp27-like* (Lj5g3v2112200) relative to the reference gene *LjUbiquitin*. *L. japonicus* Gifu seedlings were treated for 1 h with solvent control (white), 10^{-9} M CO4 (light grey) or 10^{-7} M CO4 (dark grey) solutions. For each gene, expression is normalized to the control group average. Each dot represents a biological replicate, which is a pool of roots from 12 different plants. The black line represents the median. Different letters indicate statistically significant differences among groups according to Kruskal Wallis and Dunn's post hoc tests (B, D) or to ANOVA test followed by Tukey's post-hoc correction (E) (p-value < 0.05).

Discussion

In this work, we identified complex and multiphasic compartment-specific Ca^{2+} signatures activated in response to different fungal signals in *L. japonicus* roots. Aequorin-based Ca^{2+} measurement assays demonstrated that short-chain (CO4), long-chain (CO8) and lipidated (mycLCOs) chitooligosaccharides are all able to induce both cytosolic and nuclear Ca^{2+} transients, that we were able to dissect in two different temporal phases underpinning diverging signalling pathways.

Chitin oligomers trigger a rapid Ca^{2+} elevation (phase 1) dependent on their concentration and CERK6 activity

We found that all three tested fungal elicitors (CO4, CO8, mycLCOs) are able to induce an early and steep Ca^{2+} increase (phase 1) in both the cytosol and nucleus, independent of the CSSP and the CPA pre-treatment. These data confirm and extend previous reports in soybean and *L. japonicus* cell suspension cultures in response to germinating spore exudates (Navazio *et al.*, 2007; Francia *et al.*, 2011; Moscatiello *et al.*, 2018). The temporal dynamics and shapes of cytosolic phase 1 resemble the well-known Ca^{2+} influx activated by PAMPs that is crucial for mounting plant immunity (Ranf *et al.*, 2013, Zipfel and Oldroyd, 2017). We also characterised an analogous phase 1 in nuclear Ca^{2+} signals (and confirmed it at the single-cell level in *M. truncatula* root organ cultures), which appears to be associated with the cytosolic one, suggesting that the same signalling process may extend to the two cell compartments via diffusion of cytosolic Ca^{2+} into the nucleoplasm. The abolishment of the CO4-induced Ca^{2+} elevation in cytosolic phase 1 by EGTA and LaCl_3 confirms that a Ca^{2+} influx from the apoplast is at the origin of this process. Intriguingly, the use of VAC1, a recently developed drug affecting membrane delivery to the vacuole and thereby reducing vacuole size (Dünser *et al.*, 2022), hinted at the involvement of this extensive compartment in the dissipation of the Ca^{2+} rise in phase 1. The application of the newly designed aequorin-based (Cortese *et al.*, 2022) and GCaMP-based (Luo *et al.*, 2020; Resentini *et al.*, 2021) probes targeted to the plant ER, together with yet-to-develop GECIs for Ca^{2+}

measurement/imaging inside the vacuolar lumen, will help uncover the contribution of these Ca²⁺ pools to the generation and dissipation of this phase 1 Ca²⁺ response.

Our analyses of mutant backgrounds indicating the CERK6 dependence, but CSSP independence, of phase 1 signalling in response to chitin oligomers strongly suggests that the phase 1 Ca²⁺ influx is linked to a signal transduction pathway different from the CSSP, in line with previous indications that fungal elicitors may activate multiple parallel signalling cascades (Bonfante and Requena, 2011). Moreover, we observed phase 2 responses in absence of phase 1 under very low concentrations of the fungal elicitors or in the *cerk6* mutants. Similarly, Nod-factor-induced Ca²⁺ influx in *M. truncatula* root hairs has previously been shown to be independent of the CSSP but dependent on the Nod-factor dose (Shaw and Long, 2003) and chemical structure (Moriere *et al.*, 2013). Here, CERK6-dependence suggests that phase 1 Ca²⁺ signals are associated with plant immunity (Bozsoki *et al.*, 2017), and this is further supported by the activation of immunity marker genes by 10⁻⁷ M (but not 10⁻⁹ M) CO₄. However, we cannot exclude a role for phase 1 Ca²⁺ influx also in symbiotic signalling. Indeed, the absence of a mycorrhizal phenotype of *cerk6* was previously observed at a single time point (Bozsoki *et al.*, 2017), while a deeper analysis of AM colonisation in *MtLyk9* mutants (the putative CERK6 closest homolog in *M. truncatula*) showed a weak reduction compared to wild-type plants (Feng *et al.*, 2019; Gibelin-Viala *et al.*, 2019). Accordingly, about two-third of the *cerk6* root samples tested in our assays did not respond with a clear activation of phase 2 Ca²⁺ elevation.

Phase 2 of the Ca²⁺ change induced by chitin oligomers largely depends on the CSSP

By using pharmacological pre-treatments and different plant genetic backgrounds, we showed that the prolonged, phase 2-associated, Ca²⁺ elevations share several features with the Ca²⁺ spiking events induced by chitin oligomers and recorded with fluorescent GECIs (Genre *et al.*, 2013; Kelner *et al.*, 2018; Feng *et al.*, 2019). Such Ca²⁺ spiking events are acknowledged to depend on the CSSP and originate from the nuclear envelope, via the concerted activity of Ca²⁺-permeable channels and Ca²⁺ pumps (Zipfel and Oldroyd, 2017; Charpentier, 2018). Here, we showed that *symrk* and *castor* mutants

lack this nuclear Ca^{2+} response (phase 2), which is also abolished by the ER-type Ca^{2+} -ATPase inhibitor CPA, as previously shown for Nod factor-induced Ca^{2+} spiking (Capoen *et al.*, 2011).

We now hypothesise that perinuclear Ca^{2+} spiking, which is known to be simultaneous with nuclear Ca^{2+} spiking (Ehrhardt *et al.*, 1996; Kelner *et al.*, 2018), is represented in our aequorin-based analyses by the cytosolic phase 2 elevation. The low amplitude of this cytosolic Ca^{2+} transient may be due to the fact that the aequorin chimera (CPK17_{G2A}-NES-YA) used in this work measures $[\text{Ca}^{2+}]$ changes in the bulk cytosol, rather than at microdomains close to the nuclear envelope (Mehlmer *et al.*, 2012; Ottolini *et al.*, 2014). Despite being widely considered as canonical fungal PAMPs (Cao *et al.*, 2014; Bjornson *et al.*, 2021), CO8 have recently been suggested to also act as symbiotic molecules and activate both nuclear Ca^{2+} spiking and the expression of symbiotic genes (Feng *et al.*, 2019, Zhang *et al.*, 2021). In our experimental setup, CO8 activated a nuclear phase 2 Ca^{2+} response in the wild-type background, apparently similar to the CO4- and mycLCOs-induced ones. However, this response was only weakly dependent on SYMRK and CASTOR, highlighting that CO8-induced Ca^{2+} signalling also underlies transduction pathways unrelated to symbiosis.

Complementary approaches to measure and image intracellular Ca^{2+} can help disentangle the intertwined Ca^{2+} signalling events during plant root-fungus interaction

By comparing data coming from *L. japonicus* roots expressing nuclear aequorin and nuclear-targeted cameleon in *M. truncatula* root organ cultures, we depicted a precise correspondence between the two datasets, eventually leading to significant insights into plant symbiotic signalling. On the one hand, we confirmed the occurrence of a rapid Ca^{2+} change in response to CO4 perception during phase 1. This initial Ca^{2+} elevation induced by short-chain chitin oligomers is recognizable in published Ca^{2+} traces obtained with cameleon-based techniques but has been largely overlooked, most likely due to its quick and irregular appearance, and analogous Ca^{2+} elevations in response to Nod-factor perception have only been investigated in a couple of studies (Shaw *et al.*, 2003; Morieri

et al., 2013). In this frame, our results bring this elusive element of Ca²⁺-mediated symbiotic signalling back in the spotlight, hopefully fostering new research. Our present results show that a combination of cameleon-based Ca²⁺ traces from individual root epidermal cells does mimic the overall dynamics of this initial CO₂-induced Ca²⁺ transient as recorded using aequorin, but cannot fully reproduce its kinetic parameters, suggesting that additional cell layers (*e.g.* belonging to the root cortex), may contribute to the global root Ca²⁺ response to chitooligosaccharides. On the other hand, the combination of two investigation methods provided convincing support to our interpretation of the phase 2 elevation in Ca²⁺ concentration as the summation of individual nuclear Ca²⁺-spiking signals. This is a significant advance in our understanding of symbiotic signalling. In fact, the apparent similarity between aequorin-based and cameleon-based averaged traces of Ca²⁺ signals allows a direct comparison between the results obtained with these alternative and very common approaches. This possibility paves the way for high-throughput genetic screenings and will hopefully lead to fruitful synergies and novel intuitions on the way to disentangling the complexity of Ca²⁺-mediated symbiotic signalling in plants.

In conclusion, recent literature has suggested a cross-talk between immunity and symbiosis signalling pathways upon plant perception of root endosymbionts. In this scenario, the prevalence of either pathway depends on a combination of elicitors, receptor competition and cross-reactions among players of the activated signalling cascades (Feng *et al.*, 2019, Zhang *et al.*, 2021, Feng *et al.*, 2021). Here, we suggest that the boundaries between *bona-fide* pathogenic and symbiotic fungal signals are less clear-cut than previously thought, since all the tested molecules could activate parallel pathways that converge in a multi-phasic Ca²⁺ signal. In fact, we could dissect independent components of the Ca²⁺ responses based on the genetic background, time phase and elicitor concentration. Moreover, we correlated the activation of immunity marker genes with the presence of the phase 1 Ca²⁺ influx, via its critical dependence on the concentration of the elicitor, suggesting that the concentration of chitin-derived molecules plays a crucial role in the activation of different plant responses to root-

interacting microbes. Future research will be needed to further characterise the potential role of this Ca^{2+} influx in AM symbiosis.

Supplementary Data

Link to the supplementary material

https://drive.google.com/drive/folders/1NAqd6cBV_vkgJ2x4_M82wNhBtMCYATY4?usp=share_link

Fig. S1. Genetic map and intracellular localization of the cytosolic and nuclear YFP-aequorin chimeras in *L. japonicus* roots.

Fig. S2. CO₄-, CO₈- and mycLCOs-induced cytosolic Ca²⁺ responses in *L. japonicus* CSSP mutant backgrounds.

Fig. S3. Cytosolic and nuclear Ca²⁺ responses to serial dilutions of CO₈ in *L. japonicus* roots.

Fig. S4. Traces of nuclear Ca²⁺ concentration in root atrichoblasts of *M. truncatula* under 10⁻⁹M CO₄ treatment.

Fig. S5. Expression profile of the immunity marker genes retrieved from LotusBase ExpAt.

Table S1. List of primers used in this study.

Table S2. List of plasmids used in this study.

Table S3. Extended outcomes of the statistical analysis for all experiments in this manuscript.

Dataset S1. Script to reproduce all statistical analysis and figures in RStudio environment.

Dataset S2. Raw data for Figure 22.

Dataset S3. Raw data for Figure 23.

Dataset S4. Raw data for Figure 24, Figure 26 and Supplementary Fig. S5.

Dataset S5. Raw data for Figure 25.

Dataset S6. Raw data for Figure 27A-D and Supplementary Fig. S3.

Dataset S7. Raw data for Supplementary Fig. S4.

Dataset S8. Raw data for Figure 27E.

Acknowledgements

We thank Ute Vothknecht (University of Bonn, Germany) for the CPK17_{G2A}-NES-YA and NLS-YA plasmids, Marco Incarbone and Mattia Donà (Gregor Mendel Institute, Vienna, Austria) for the destination vector, and Sébastien Fort (CNRS, Paris, France) for the mycLCOs. We are grateful to Lene Heegaard Madsen, Simona Radutoiu and Jens Stougaard (Aarhus University, Denmark) for kindly providing *L. japonicus* *symrk*, *castor* and *cerk6-1* mutants, and to Myriam Charpentier (John Innes Centre, Norwich, UK) for fruitful discussions. The technical assistance of the Imaging Facility and the Plant Genome Editing Facility of the Department of Biology (University of Padova, Italy) is gratefully acknowledged.

Author contributions

LN and MG conceived the study and designed research; FB and MG conducted molecular cloning; FB performed intracellular localization studies and gene expression analysis; FB and EO performed aequorin-based Ca²⁺ measurements; AC and FB performed cameleon-based Ca²⁺ assays; MG and FB analysed data, conducted statistical analyses and data visualisation; AC, IS and FB conducted data analysis and modelling of Ca²⁺ imaging data; FB, MG and LN wrote the article; AG designed some experiments and contributed to the discussion and editing of the article; JKV provided materials and contributed to the discussion. All authors read and approved the final manuscript.

Conflict of interest

The authors declare that they have no conflicts of interest.

Funding

This work was supported by grants from the University of Padova, Italy (Progetti di Ricerca Dipartimentali (PRID) [grant number BIRD180317 to LN; grant number BIRD214519 to MG; PRID Seed Giovani to FB], from the European Union - NextGenerationEU [2021 STARS Grants@Unipd programme P-NICHE to MG]), from the Austrian Science Fund (FWF) ([grant number P 33044 to JK-V), and the German Science fund (DFG) [grant number 470007283 and CIBSS-EXC-2189 to JK-V).

Data availability

The datasets used in this study are available in the Supplementary data.

References

- Bjornson M, Pimprikar P, Nürnberger T, Zipfel C. 2021.** The transcriptional landscape of *Arabidopsis thaliana* pattern-triggered immunity. *Nature Plants* **7**, 579–586.
- Boisson-Dernier A, Chabaud M, Garcia F, Bécard G, Rosenberg C, Barker DG. 2001.** *Agrobacterium rhizogenes*-transformed roots of *Medicago truncatula* for the study of nitrogen-fixing and endomycorrhizal symbiotic associations. *Molecular Plant-Microbe Interactions: MPMI* **14**, 695–700.
- Bonfante P, Requena N. 2011.** Dating in the dark: how roots respond to fungal signals to establish arbuscular mycorrhizal symbiosis. *Current Opinion in Plant Biology* **14**, 451–457.
- Bonhomme M, Bensmihen S, André O, et al. 2021.** Distinct genetic basis for root responses to lipo-chitoooligosaccharide signal molecules from different microbial origins. *Journal of Experimental Botany* **72**, 4.
- Bozsoki Z, Cheng J, Feng F, Gysel K, Vinther M, Andersen KR, Oldroyd GED, Blaise M, Radutoiu S, Stougaard J. 2017.** Receptor-mediated chitin perception in legume roots is functionally separable from Nod factor perception. *Proceedings of the National Academy of Sciences, USA* **114**, 8118–8127.
- Bozsoki Z, Gysel K, Hansen SB, et al. 2020.** Ligand-recognizing motifs in plant LysM receptors are major determinants of specificity. *Science* **369**, 663–670.
- Brini M, Marsault R, Bastianutto C, Alvarez J, Pozzan T, Rizzuto R. 1995.** Transfected aequorin in the measurement of cytosolic Ca²⁺ concentration ([Ca²⁺]_c): a critical evaluation. *Journal of Biological Chemistry* **270**, 9896–9903.
- Cao Y, Liang Y, Tanaka K, Nguyen CT, Jedrzejczak RP, Joachimiak A, Stacey G. 2014.** The kinase LYK5 is a major chitin receptor in *Arabidopsis* and forms a chitin-induced complex with related kinase CERK1. *eLife* **3**.
- Capoen W, Sun J, Wysham D, et al. 2011.** Nuclear membranes control symbiotic calcium signaling of legumes. *Proceedings of the National Academy of Sciences* **108**, 14348–14353.
- Carotenuto G, Chabaud M, Miyata K, Capozzi M, Takeda N, Kaku H, Shibuya N, Nakagawa T, Barker DG, Genre A. 2017.** The rice LysM receptor-like kinase OsCERK1 is required for the perception of short-chain chitin oligomers in arbuscular mycorrhizal signaling. *New Phytologist* **214**, 1440–1446.
- Catoira R, Galera C, de Billy F, Penmetsa RV, Journet EP, Maillet F, Rosenberg C, Cook D, Gough C, Dénarié J. 2000** Four genes of *Medicago truncatula* controlling components of a nod factor transduction pathway. *The Plant Cell* **9**, 1647–66.
- Chabaud M, Genre A, Sieberer BJ, Faccio A, Fournier J, Novero M, Barker DG, Bonfante P. 2011.** Arbuscular mycorrhizal hyphopodia and germinated spore exudates trigger Ca²⁺ spiking in the legume and nonlegume root epidermis. *New Phytologist* **189**, 347–55.
- Charpentier M. 2018.** Calcium signals in the plant nucleus: origin and function. *Journal of Experimental Botany* **69**, 4165–4173.
- Chiu CH, Paszkowski U. 2020.** Receptor-like kinases sustain symbiotic scrutiny. *Plant Physiology* **182**, 1597–1612.
- Chiu CH, Roszak P, Orvošová M, Paszkowski U. 2022.** Arbuscular mycorrhizal fungi induce lateral root development in angiosperms via a conserved set of MAMP receptors. *Current Biology* **32**, 4428–4437.
- Choi J, Summers W, Paszkowski U. 2018.** Mechanisms underlying establishment of arbuscular mycorrhizal symbioses. *Annual Review of Phytopathology* **56**, 135–160.
- Cortese E, Moscaticello R, Pettiti F, et al. 2022.** Monitoring calcium handling by the plant endoplasmic reticulum with a low-Ca²⁺-affinity targeted aequorin reporter. *The Plant Journal* **109**, 1014–1027.
- Costa A, Navazio L, Szabo I. 2018.** The contribution of organelles to plant intracellular calcium signalling. *Journal of Experimental Botany* **17**, 4175–4193.

- De Vriese K, Costa A, Beeckman T, Vanneste S. 2018.** Pharmacological strategies for manipulating plant Ca^{2+} signalling. *International Journal of Molecular Sciences* **19**, 1506.
- Delaux PM, Schornack S. 2021.** Plant evolution driven by interactions with symbiotic and pathogenic microbes. *Science* **371**, eaba6605.
- Dünser K, Schöller M, Rößling AK, et al. 2022.** Endocytic trafficking promotes vacuolar enlargements for fast cell expansion rates in plants. *eLife* **11**, e75945.
- Ehrhardt DW, Wais R, Long SR. 1996.** Calcium spiking in plant root hairs responding to rhizobium nodulation signals. *Cell* **85**, 673–681.
- Feng F, Sun J, Radhakrishnan GV, et al. 2019.** A combination of chitoooligosaccharide and lipochitoooligosaccharide recognition promotes arbuscular mycorrhizal associations in *Medicago truncatula*. *Nature Communications* **10**, 5047.
- Feng Y, Wu P, Liu C, et al. 2021.** Suppression of LjBAK1-mediated immunity by SymRK promotes rhizobial infection in *Lotus japonicus*. *Molecular Plant* **14**, 1935–1950.
- Francia D, Chiltz A, Lo Schiavo F, Pugin A, Bonfante P, Cardinale F. 2011.** AM fungal exudates activate MAP kinases in plant cells in dependence from cytosolic Ca^{2+} increase. *Plant Physiology and Biochemistry* **49**, 963–969.
- Genre A, Chabaud M, Balzergue C, et al. 2013.** Short-chain chitin oligomers from arbuscular mycorrhizal fungi trigger nuclear Ca^{2+} spiking in *Medicago truncatula* roots and their production is enhanced by strigolactone. *New Phytologist* **198**, 190–202.
- Genre A, Lanfranco L, Perotto S, Bonfante P. 2020.** Unique and common traits in mycorrhizal symbioses. *Nature Reviews Microbiology* **18**, 649–660.
- Ghahremani M, MacLean AM. 2021.** Home sweet home: how mutualistic microbes modify root development to promote symbiosis. *Journal of Experimental Botany* **72**, 275–2287.
- Gibelin-Viala C, Amblard E, Puech-Pages V, et al. 2019.** The *Medicago truncatula* LysM receptor-like kinase LYK9 plays a dual role in immunity and the arbuscular mycorrhizal symbiosis. *New Phytologist* **223**, 1516–1529.
- Giovannetti M, Mari A, Novero M, Bonfante P. 2015.** Early *Lotus japonicus* root transcriptomic responses to symbiotic and pathogenic fungal exudates. *Frontiers in Plant Science* **6**, 480.
- Grenzi M, Resentini F, Vanneste S, Zottini M, Bassi A, Costa A. 2021.** Illuminating the hidden world of calcium ions in plants with a universe of indicators. *Plant Physiology* **187**: 550–571.
- Kamal N, Mun T, Reid D, et al. 2020.** Insights into the evolution of symbiosis gene copy number and distribution from a chromosome-scale *Lotus japonicus* Gifu genome sequence. *DNA Research* **27**, dsaa015.
- Keinath NF, Waadt R, Brugman R, Schroeder JI, Grossmann G, Schumacher K, Krebs M. 2015.** Live cell Imaging with R-GECO1 sheds light on flg22- and chitin-induced transient $[\text{Ca}^{2+}]_{\text{cyt}}$ patterns in *Arabidopsis*. *Molecular Plant* **8**, 1188–1200.
- Köster P, DeFalco T, Zipfel C. 2022.** Ca^{2+} signals in plant immunity. *The EMBO Journal* **41**, e110741.
- Kutschera A, Dawid C, Gisch N, et al. 2019.** Bacterial medium-chain 3-hydroxy fatty acid metabolites trigger immunity in *Arabidopsis* plants. *Science* **364**, 178–181.
- Lampropoulos A, Sutikovic Z, Wenzl C, Maegele I, Lohmann JU, Forner J. 2013.** GreenGate - a novel, versatile, and efficient cloning system for plant transgenesis. *PLoS One* **8**, e83043.
- Luo J, Chen L, Huang F, Gao P, Zhao H, Wang Y, Han S. 2020.** Intraorganellar calcium imaging in *Arabidopsis* seedling roots using the GCaMP variants GCaMP6m and R-CEPIA1er. *Journal of Plant Physiology* **246–247**, 153127.
- Maillet F, Poinso V, André O, et al. 2011.** Fungal lipochitoooligosaccharide symbiotic signals in arbuscular mycorrhiza. *Nature* **469**, 58–63.

- Mehlmer N, Parvin N, Hurst CH, Knight MR, Teige M, Vothknecht UC. 2012.** A toolset of aequorin expression vectors for in planta studies of subcellular calcium concentrations in *Arabidopsis thaliana*. *Journal of Experimental Botany* **63**, 1751–1761.
- Miwa H, Sun J, Oldroyd GED, Downie JA. 2006.** Analysis of Nod-factor-induced calcium signaling in root hairs of symbiotically defective mutants of *Lotus japonicus*. *Molecular Plant-Microbe Interactions* **19**, 914–923.
- Miyata K, Kozaki T, Kouzai Y, 2014.** The bifunctional plant receptor, OsCERK1, regulates both chitin-triggered immunity and arbuscular mycorrhizal symbiosis in rice. *Plant & Cell Physiology* **55**, 1864–1872.
- Monaghan J, Matschi S, Romeis T, Zipfel C. 2015.** The calcium-dependent protein kinase CPK28 negatively regulates the BIK1-mediated PAMP-induced calcium burst. *Plant Signaling & Behavior* **10**, e1018497.
- Morieri G, Martinez EA, Jarynowski A, Driguez H, Morris R, Oldroyd GED, Downie JA. 2013.** Host-specific Nod-factors associated with *Medicago truncatula* nodule infection differentially induce calcium influx and calcium spiking in root hairs. *New Phytologist* **200**, 656–662.
- Moscatiello R, Sello S, Ruocco M, et al. 2018.** The hydrophobin HYTLO1 secreted by the biocontrol fungus *Trichoderma longibrachiatum* triggers a NAADP-mediated calcium signalling pathway in *Lotus japonicus*. *International Journal of Molecular Sciences* **19**, 2596.
- Mun T, Bachmann A, Gupta V, et al. 2016.** Lotus Base: An integrated information portal for the model legume *Lotus japonicus*. *Scientific Reports* **6**, 39447.
- Nakagawa T, Kaku H, Shimoda Y, Sugiyama A, Shimamura M, Takanashi K, Yazaki K, Aoki T, Shibuya N, Kouchi H. 2011.** From defense to symbiosis: limited alterations in the kinase domain of LysM receptor-like kinases are crucial for evolution of legume–Rhizobium symbiosis. *The Plant Journal* **65**, 169–180.
- Nars A, Lafitte C, Chabaud M, et al. 2013.** Aphanomyces euteiches cell wall fractions containing novel glucan-chitosaccharides induce defense genes and nuclear calcium oscillations in the plant host *Medicago truncatula*. *PLoS One* **8**, e75039.
- Navazio L, Moscatiello R, Genre A, Novero M, Baldan B, Bonfante P, Mariani P. 2007.** A diffusible signal from arbuscular mycorrhizal fungi elicits a transient cytosolic calcium elevation in host plant cells. *Plant Physiology* **144**, 673–681.
- Oldroyd GED. 2013.** Speak, friend, and enter: signalling systems that promote beneficial symbiotic associations in plants. *Nature Reviews Microbiology* **11**, 252–263.
- Ottolini D, Cali T, Brini M. 2014.** Methods to measure intracellular Ca²⁺ fluxes with organelle-targeted aequorin-based probes. *Methods in Enzymology* **543**, 21–45.
- Platre MP, Satbhai SB, Brent L, et al. 2022.** The receptor kinase SRF3 coordinates iron-level and flagellin dependent defense and growth responses in plants. *Nature Communications* **13**, 4445.
- Radhakrishnan GV, Keller J, Rich MK, et al. 2020.** An ancestral signalling pathway is conserved in intracellular symbioses-forming plant lineages. *Nature Plants* **6**, 280–289.
- Ranf S, Eschen-Lippold L, Pecher P, Lee J, Scheel D. 2011.** Interplay between calcium signalling and early signalling elements during defence responses to microbe- or damage-associated molecular patterns. *The Plant Journal* **68**, 100–113.
- R Core Team. 2022.** R: A language and environment for statistical computing. R Foundation for Statistical Computing, Vienna, Austria. URL <https://www.R-project.org/>.
- Resentini F, Grenzi M, Ancora D, Cademartori M, Luoni L, Franco M, Bassi A, Bonza MC, Costa A. 2021.** Simultaneous imaging of ER and cytosolic Ca²⁺ dynamics reveals long-distance ER Ca²⁺ waves in plants. *Plant Physiology* **187**, 603–617.

- Ried MK, Banhara A, Hwu FY, Binder A, Gust AA, Höfle C, Hüchelhoven R, Nürnberger T, Parniske M. 2019.** A set of Arabidopsis genes involved in the accommodation of the downy mildew pathogen *Hyaloperonospora arabidopsidis*. *PLoS Pathogens* **15**, e1007747.
- RStudio Team. 2020.** RStudio: Integrated Development for R. RStudio, PBC, Boston, MA URL <http://www.rstudio.com/>.
- Shaw SL, Long SR. 2003.** Nod Factor elicits two separable calcium responses in *Medicago truncatula* root hair cells. *Plant Physiology* **131**, 976–984.
- Sieberer BJ, Chabaud M, Timmers AC, Monin A, Fournier J, Barker DG. 2009.** A nuclear-targeted cameleon demonstrates intranuclear Ca²⁺ spiking in *Medicago truncatula* root hairs in response to rhizobial nodulation factors. *Plant Physiol.* **151**, 1197–206.
- Sun J, Miller JB, Granqvist E, et al. 2015.** Activation of symbiosis signaling by arbuscular mycorrhizal fungi in legumes and rice. *The Plant Cell* **27**, 823–838.
- Thor K, Peiter E. 2014.** Cytosolic calcium signals elicited by the pathogen-associated molecular pattern flg22 in stomatal guard cells are of an oscillatory nature. *New Phytologist* **204**, 873–881.
- Thor K, Jiang S, Michard E, et al. 2020.** The calcium-permeable channel OSCA1.3 regulates plant stomatal immunity. *Nature* **585**, 569–573.
- Verbon EH, Liberman LM. 2016.** Beneficial microbes affect endogenous mechanisms controlling root development. *Trends in Plant Science* **21**, 218–229.
- Wan J, Tanaka K, Zhang X-C, Son GH, Brechenmacher L, Nguyen THN, Stacey G. 2012.** LYK4, a lysin motif receptor-like kinase, is important for chitin signaling and plant innate immunity in Arabidopsis. *Plant Physiology* **160**, 396–406.
- Wise AA, Liu Z, Binns AN. 2006.** Three methods for the introduction of foreign DNA into Agrobacterium. In: Wang K, ed. *Methods in Molecular Biology. Agrobacterium Protocols*. Totowa, NJ: Humana Press, 43–54.
- Wu F, Chi Y, Jiang Z, et al. 2020.** Hydrogen peroxide sensor HPCA1 is an LRR receptor kinase in *Arabidopsis*. *Nature* **578**, 577–581.
- Yu X, Feng B, He P, Shan L. 2017.** From chaos to harmony: responses and signaling upon microbial pattern recognition. *Annual Review of Phytopathology* **55**, 109–137.
- Zhang X, Dong W, Sun J, Feng F, Deng Y, He Z, Oldroyd GED, Wang E. 2015.** The receptor kinase CERK1 has dual functions in symbiosis and immunity signalling. *The Plant Journal* **81**, 258–267.
- Zhang C, He J, Dai H, Wang G, Zhang X, Wang C, Shi J, Chen X, Wang D, Wang E. 2021.** Discriminating symbiosis and immunity signals by receptor competition in rice. *Proceedings of the National Academy of Sciences* **118**, e2023738118.
- Zipfel C, Oldroyd GED. 2017.** Plant signalling in symbiosis and immunity. *Nature* **543**, 328–336.

CHAPTER 7

General conclusions

The main subject of my PhD dissertation and the research that went into it was the role of signal molecules in arbuscular mycorrhizas, with an emphasis on chito-oligosaccharides.

The evolutionary history of COs dates back to the early Neoproterozoic. In fact, spectroscopic investigations of a one billion year old sample of *Ourasphaira giraldae* revealed the presence of chitin and chitosan, indicating that the ability to synthesize chitin and generate COs may have arisen during that time, before the divergence into Dikarya and Glomeromycotina (Loron et al., 2019; Tedersoo et al., 2018). Concerning the ability of plants in perceiving COs, the first evidence of the genes needed for fungal colonization may be traced to the origin of freshwater charophyte algae (Delaux et al., 2015), where genes that are a part of the CSSP were discovered. Rush et al. (2020) demonstrated the generation of COs and LCOs by several fungi that currently associate with charophytes to support this theory, demonstrating the existence of AM symbiotic gene machinery even before plants began to colonize the planet. The discovery of CO function as PAMPs and in AM symbiosis (Wan et al., 2008; Lee et al., 2008; Genre et al., 2013) created a new scenario for their potential application as biostimulants and for crop protection in agriculture, in the context of regenerative and sustainable agricultural methods. Since then, numerous studies have been carried out that highlight the biological role of these molecules and their interactions with biotic and abiotic factors, emphasizing CO synthesis, structure, and effect on plants, and ecosystems (Guan et al., 2020; Feng et al., 2019; Tanaka et al., 2015; Zong et al., 2017). During my PhD, I contributed to the understanding of AM signaling, by clarifying a few aspects concerning CO extraction, their long-term impacts on the symbiosis, and cellular mechanisms of CO sensing.

Initially, we showed how CO application impacted on the transcriptome of both mycorrhizal and nonmycorrhizal roots over a period of weeks. This gave us a better understanding of some of the mechanisms behind the CO-dependent promotion of AM colonization: an increase in the biosynthesis of didehydroorobanchol and the enhancement of fungal accommodation responses in root epidermal cells. These promising results led us to investigate the possibility of CO production for large-scale

use in agronomic context. With the use of our protocol for CO extraction, we were able to successfully isolate short chain COs from lyophilized fungal biomass. Moreover, characterization studies and the application of extracted CO revealed how the degree of acetylation affected CO bioactivity and plant colonization. The involvement of CME on CO perception was suggested by a closer analysis of the cellular mechanisms underlying AM signaling. This was tested using a variety of CME inhibitors and our findings, albeit requiring further investigation, lead us to postulate that each cell layer can react to myc-factors differently in the presence of CME inhibition treatment and activate distinct molecular processes.

To measure AM colonization in *Solanum pennellii*, we developed two semi-automated image analysis methods based on pixel brightness thresholding and machine learning. These two techniques were contrasted with the manual quantification method developed by Trouvelot et al. (1986).

By combining a targeted aequorin-based Ca²⁺ reporter with cameleon-based bioassays, the examination of calcium signaling mechanisms was deepened, thanks to a collaboration with a research group from Padova, Italy. This investigation revealed the biphasic nature of cytoplasmic and nuclear oscillation in calcium concentration in both *Lotus japonicus* and *M. truncatula*. Plant immunity marker genes were shown to be activated during the quick initial phase, which was revealed to be significantly dependent on elicitor concentration. By contrast, the second phase resulted to correspond to the Ca²⁺ spiking previously described in response to symbiotic signals.

Overall, the work presented in this thesis demonstrated the role of COs in the development and maintenance of the arbuscular mycorrhizal symbiosis, illuminating the practical perspective of their use in agricultural contexts as biostimulants, with the aim of creating new procedures to lessen the adverse environmental effects of agrochemicals. Nonetheless, a number of aspects remain to be explored. Although the optimal CO extraction methodology produced promising results, both hydrolysis and extraction remain time-consuming and difficult processes. Additional trials will be necessary to cut down on time, lower overall costs, and increase the extraction yield. Lastly, in line with

the vision of Circular Economy, the use of industrial wastes as a substitute fungal growth medium should also be investigated further.

Since we had contrasting results about the role of CME in AM signaling, it will be important to further clarify the mechanisms underlying CO perception and the role of CME in symbiosis-related gene expression. To do this, additional research should be conducted that considers the responses of each root tissue (namely cortex and epidermis). Similarly, an appropriate experimental setup should be designed to investigate the possible role of phase 1 Ca^{2+} influx during AM signaling.

Finally, the development and testing of different image analysis algorithms may lead to a clearer discrimination of AM fungal structures, leading to a unique and highly reliable software for quantifying AM root colonization, a tool that would be of great use to a broad community of researcher.

References

- Delaux P-M, Radhakrishnan GV, Jayaraman D, Cheema J, Malbreil M, et al. 2015. Algal ancestor of land plants was preadapted for symbiosis. *PNAS* 112(43):13390–95.
- Feng F, Sun J, Radhakrishnan GV, Lee T, Bozsóki Z, et al. 2019. A combination of chitooligosaccharide and lipochitooligosaccharide recognition promotes arbuscular mycorrhizal associations in *Medicago truncatula*. *Nat. Commun.* 10(1):5047.
- Genre A, et al. 2013. Short chain chitin oligomers from arbuscular mycorrhizal fungi trigger nuclear Ca²⁺ spiking in *Medicago truncatula* roots and their production is enhanced by strigolactone. *New Phytol* 198:190–202. doi:10.1111/nph.12146.
- Guan F, et al. 2020. Highly efficient production of chitooligosaccharides by enzymes mined directly from the marine metagenome. *Carbohydr Polym.* 234:115909. doi:10.1016/j.carbpol.2020.115909.
- Lee CG, Da Silva CA, Lee J-Y, Hartl D, Elias JA. 2008. Chitin regulation of immune responses: an old molecule with new roles. *Curr. Opin. Immunol.* 20(6):684–89
- Loron CC, François C, Rainbird RH, Turner EC, Borensztajn S, Javaux EJ. 2019. Early fungi from the Proterozoic era in Arctic Canada. *Nature* 570(7760):232–35.
- Tanaka K, et al. 2015. Effect of lipo-chitooligosaccharide on early growth of C4 grass seedlings. *J Exp Bot* 66(19):5727–5738.
- Tedersoo L, Sánchez-Ramírez S, Kõljalg U, Bahram M, Döring M, et al. 2018. High-level classification of the fungi and a tool for evolutionary ecological analyses. *Fungal Divers.* 90(1):135–59.
- Trouvelot, A., Kough, J.L. & Gianinazzi-Pearson, V. Mesure du taux de mycorhization VA d'un système racinaire. Recherche de méthodes d'estimation ayant une signification fonctionnelle. in *Physiological and Genetical Aspects of Mycorrhizae* (eds Gianinazzi-Pearson, V. & Gianinazzi, S.), INRA edition, Paris (1986).
- Wan J, Zhang X-C, Neece D, Ramonell KM, Clough S, et al. 2008. A LysM receptor-like kinase plays a critical role in chitin signaling and fungal resistance in *Arabidopsis*. *Plant Cell* 20(2):471–81
- Zong H, et al. 2017. Improvement in cadmium tolerance of edible rape (*Brassica rapa* L.) with exogenous application of chitooligosaccharide. *Chemosphere.* 181:92–100.

Acknowledgements

First, I would like to thank Andrea Genre. He allowed me to explore a fascinating topic and has helped me in this learning journey with helpful suggestions and openness. A big thank goes to Veronica Volpe and Mara Novero, with whom I had the pleasure to share the totality of these PhD years, filled with interesting projects and engaging discussions. I would also like to thank Ivan Sciascia for the statistical support and the numerous running sessions. Thanks to all the members of the downstairs office for the different moments of break. I am also very grateful to all my PhD colleagues and friends for having shared with me “gioia e disagio”. Special thanks go to my friends of Cascine Ste, Anto, Soncio, Vins e GG for the fruitful and fruitless conversations, as well as funny moments. A big thank goes to Alessia. For all the support and for having been present when I needed. Finally, I want to thank my parents. Without their belief in me and all their efforts, nothing of this would have been possible. They provided the core of what I am, which keeps it all together.